Advanced Engineering Research

Theoretical and scientific-partical journal

Vol. 20
no. 3
2020

ISSN 2687-1653

1 Mechanics

2 Machine Building and Machine Science

3 Information Technology, Computer Science, and Management

DOI 10.23947/2687-1653

vestnik-donstu.ru

Advanced Engineering Research

Vol. 20, no. 3

Theoretical and scientific-practical journal

Published since 1999

4 issues a year
July-September 2020

ISSN 2687-1653
DOI: 10.23947/2687-1653

Founder and publisher – Federal State Budgetary Educational Institution of Higher Education Don State Technical University (DSTU)

The journal was known as Vestnik of Don State Technical University (until August 2020)

The journal is indexed and archived in the Russian Science Citation Index (RSCI), and in EBSCO International Database

The journal is a member of Directory of Open Access Journals (DOAJ), Association of Science Editors and Publishers (ASEP) and Cross Ref

Certificate of mass media registration ЭЛ № ФС 77 – 78854 of 07.08.2020 is issued by the Federal Service for Supervision of Communications, Information Technology, and Mass Media

The issue is prepared by:

Inna V. Boyko, Gennady I. Rassokhin, Marina P. Smirnova (English version)

Founder's, Publisher's and Printery Address:

Gagarin Sq. 1, Rostov-on-Don, 344003, Russia. Phone: +7 (863) 2-738-372

E-mail: vestnik@donstu.ru http://vestnik-donstu.ru/

CONTENTS

ANNIVERSARY OF THE SCIENTIST

Mikhail A. Tamarkin, Engineer, Teacher, Scientist, is 70

9 September, Mikhail Arkad'evich Tamarkin, Dr.Sci. (Engineering), professor, turned 70.

Mikhail A. Tamarkin graduated from the Rostov Institute of Agricultural Engineering majoring in 0501 “Engineering Technology, Cutting Machines and Tools”. Having gained experience in production (Rubin plant, from 1972 to 1975), he devoted his further career to the training of highly qualified personnel for machine-building enterprises.

Since 1998, he has been Head of one of the leading departments of the University, the Engineering Technology Department. He is Chairman of the Scientific and Methodological Council for the integrated group of research areas, 15.00.00 “Mechanical Engineering”. The scientist has made a significant contribution to the development and improvement of the educational process at the University under the preparation of bachelors, masters and postgraduates He is the author of more than 300 scientific and methodological publications, including 14 textbooks and 4 monographs, which are important educational and methodological literature majoring in “Design-Engineering Support of Machinery Productions”.

Mikhail A. Tamarkin is a well-known scientist in the area of vibration technologies in Russia and abroad. He has developed a basic procedure of calculating the optimal process variables of vibration treatment; theoretical foundations of the reliability of manufacturing systems for loose abrasive machining. The results of his scientific research have been implemented at many enterprises in the machine-building industry. He has trained 21 candidates of science. Under the supervision of M. Tamarkin, the research workshop “Perspectives of development of finishing and hardening processing and vibrowave technologies” is held annually on the basis of DSTU. It is dedicated to the memory of A.P. Babichev, Honored Worker of Science and Technology of the Russian Federation, Dr.Sci. (Engineering), Honorary Professor of DSTU. As well, M. Tamarkin supervises an international scientific symposium of mechanical engineering technologists “Fundamentals of physics, chemistry and mechanics of high-tech process systems for shaping and assembling products”.

The scientist is a member of three Dissertation Councils: D212.058.06, major in 05.26.01 “Labor protection (branch-wise)”; D212.058.02, major in 05.02.08 “Engineering Technology”, DSTU, and Council D 900.007.01, major in 05.02.08 “Engineering Technology”, on the basis of Sevastopol State University, as well as a member of the Board of Studies of DSTU.

Mikhail A. Tamarkin was awarded the badge “Honorary Worker of RF Higher Vocational Education”, 2011, and the Medal of the Russian Engineering Union “For Valorous Labor”, 2013. In 2015, he was awarded the title “Honorary Figure of Russian Higher Education”. In 2018, the Federation of Cosmonautics of Russia awarded M. A. Tamarkin with K. E. Tsiolkovsky medal. In 2020, the scientist was awarded the title “Honorary Professor of DSTU”.

MECHANICS

UDC 004.75 https://doi.org/10.23947/2687-1653-2020-20-3-205-215

Neural network technology for identifying defect sizes in half-plane based on time and positional scanning

A. N. Solov'ev[1,2], A. V. Cherpakov[1,2], P. V. Vasil'ev[1], I. A. Parinov[2], E. V. Kirillova[3]
[1] Don State Technical University (Rostov-on-Don, Russian Federation)
[2] Southern Federal University (Rostov-on-Don, Russian Federation)
[3] RheinMain University of Applied Sciences (Wiesbaden, Germany)

Introduction. The selected research topic urgency is due to the need for a quick assessment of the condition and reliability of materials used in various designs. The work objective was to study parameters of the influence of the defect on the response of the surface of the medium to the shock effect. The solution to the inverse problem of restoring the radius of a defect is based on the combination of a computational approach and the use of artificial neural networks (ANN). The authors have developed a technique for restoring the parameters of a defect based on the computational modeling and ANN.
Materials and Methods. The problem is solved in the flat setting through the finite element method (FEM). In this paper, we used the linear equations of the elasticity theory with allowance for energy dissipation. The finite element method implemented in the *ANSYS* package was used as a method for solving the boundary value problem. *MATLAB* complex was used as a simulation of the application process (ANN).
Results. A finite element model of a layered structure has been developed in a flat formulation of the problem in the *ANSYS* package. The problem of determining unsteady vibrations under pulsed loading for different radius variations of the defect is solved. Positional scanning of the research object is applied. Graphical dependences of the vibration amplitudes of points on the surface on the defect radius are plotted.
Discussion and Conclusions. As a result of studying the dependences of vibration responses on the defect radius, the authors have developed an approach to restore this parameter in a flat structure based on a combination of the FEM and ANN. The research has shown that the amount of data used is sufficient for successful training of the constructed ANN model and identification of a hidden defect in the structure.

Keywords: flat layered structure, defect, non-destructive diagnostics, *FE* modeling, impulse action, unsteady oscillations, surface waves, artificial neural networks, positional scanning, amplitude-time characteristics.

For citation: A.N. Solov'ev, A.V. Cherpakov, P.V. Vasil'ev, et al. Neural network technology for identifying defect sizes in half-plane based on time and positional scanning**.** Advanced Engineering Research, 2020, vol. 20, no. 3, p. 205–215. https://doi.org/10.23947/2687-1653-2020-20-3-205-215

Funding information: the research is supported by an internal grant from the Southern Federal University no. ВнГр-07/2020-04-ИМ (RF Ministry of Science and Higher Education)

Introduction. There is an extensive list of various building and bridge structures, premises, foundations, soils, composite materials that are used under different conditions. Structures can have a sufficiently long service life and defects of various configurations: cracks, cavities, inclusions, corrosive changes in the structure, dimples, etc. As a result, unforeseen pre-emergency conditions and structural failures may occur.

This fact determines the need for using various methods of non-destructive testing [1–2]. Some directions in the development of single methods for fault diagnosing defects in various objects are presented in [3–10]. The methods are based on the collection and analysis of certain structural parameters, which are the response to its loading. Vibration displacement of certain points of the surface under impulse loading of structure oscillations can be one of such parameters. In this case, a wave front propagates from the place of excitation of oscillations, exciting the displacement of points and oscillations of all structural elements. The problem can be reduced to considering measuring the velocity

constants of wave field propagation. Based on the analysis of publications in foreign literature, it can be stated that experimental studies show a clear tendency to operate with the "velocity measuring" technique [11–12].

The application of specialized devices, which are located at certain points of the object and collect information on various vibration parameters, are described in [13−14]. This technique assumes positional, time and frequency scanning of the study objects. The most attractive is using acoustic sensors and receivers installed on the outer surface of the structure. These sensors can record signals reflected from defects. The use of diagnostic systems and complexes requires the development of software, which provides the primary analysis of the signal. In the case of fine instrument tuning, for example, when using special processing algorithms for analyzing the reflected signal, the software identifies the region of imperfection of the structure. The corresponding software can be developed from using an artificial neural network (ANN) [15]. The application of ANN in problems of reconstruction of the damaged state of structural elements is described in [16–26]. The use of various architectures and ANN algorithms is described in [16–20]. The paper [21] considers the determination of defects in anisotropic plates using ANN. In [22], the authors pointed out the advantages of identification methods that do not require preliminary construction of a mathematical model of the research object.

In this paper, a method for reconstructing the diameter of a circular defect located in the half-plane of a layered structure is developed. Defects of this kind can often occur under the opening of the upper soil layers in the form of compaction of stone structures under the pavement layers. The elastic modulus and density of such structures can differ multi-fold from the basic parameters of the layer. In the mathematical setting, the problem is reduced to solving the inverse geometric problem of the elasticity theory [27]. The construction of an algorithm for recovering information on an object localized in a certain place is considered. For this, the application of the FE method, the analysis of the results of surface waves, and the correlation analysis of the dependence of the parameters of the defect on the wave field of the response using ANN, is considered.

Materials and Methods. An approach, whose purpose is to restore information on the parameters of the region of imperfection of the structure based on the analysis of the impact response of the surface of the medium, is proposed. The analysis is carried out on the basis of the developed algorithms with a combination of the computational approach and the use of ANN. A laminated material is considered as a sample.

Loading of the structure by impulse impact is carried out at a certain distance from the area under study, and the sensors recording vibrations are located in certain positions and sequences in the linear direction of this area. Lateral and longitudinal vibrations can be measured. Of interest is the period of time when waves reflected from the ends of the simulated section of the structure do not have time to reach the sensor. In this way, simulation of field operating conditions of a layered structure of the subgrade is simulated. The analysis of the measured amplitude-time characteristics (ATC) shows the possibility of their use in inverse problems of defect recovery.

As a tool for solving the inverse problem of reconstructing defect parameters, ANN are used, which were originally designed to solve the problems of determining nonlinear dependencies in multidimensional data arrays. Unlike other algorithms, ANNs are not programmed, but trained on a set of data for the investigated design parameters. Training samples are built through solving direct problems in the *ANSYS FE* package. The trained network, having received new, previously unknown analysis results, is able to correctly recognize the parameters of the defect.

Effective applications of analytical and numerical modeling, which correlate sufficiently well with the recoverable parameters of structural elements, are presented in [28–34].

Formulation of the problem. The problem is solved in a flat formulation using the finite element method (FEM). In this paper, we use linear equations of the elasticity theory with allowance for energy dissipation adopted in the *ANSYS* package [34−35].

For an elastic medium:

$$\rho\ddot{u}_\iota + \alpha\rho\dot{u}_\iota - \sigma_{ij,j} = f_i\,;$$

$$\sigma_{ij} = c_{ijkl}(\varepsilon_{kl} + \beta\dot{\varepsilon_{kl}})\,;$$

$$\varepsilon_{kl} = \frac{u_{k,l} + u_{l,k}}{2},$$

where ρ is material density; u_i — components of the vector-function of displacements; $\sigma_{i,j}$ — mechanical stress tensor components; f_i — components of the density vector of mass forces; ε_{kl} — strain tensor components; c_{ijkl} — components of the fourth-rank tensor of elastic moduli; α — nonnegative damping coefficients (in *ANSYS*).

Let us consider fully the mechanical boundary conditions. When defining mechanical boundary conditions, the body boundary is represented as a union of non-intersecting regions $S = S_u S_t S_{ut}$, on which the following conditions are set:

— the condition for fixing the border or specified displacements:

$$u_i|_{S_u} = u_i{}^0,$$

— the condition of force action, at which the components of the vector of mechanical stresses are given:

$$t_i = \sigma_{ij} n_j\big|_{S_t} = p_i,$$

— the condition of smooth contact with an absolutely rigid solid, the equality to zero of normal displacements and tangential stresses:

$$u_n = u_i n_i|_{S_{ut}} = 0, t_i{}^{(k)} = \sigma_{ij} n_j \tau_i{}^{(k)}\big|_{S_{ut}} = 0.$$

Description of the model. A layered construction is considered. The upper layer is rigidly linked to the underlying half-space (Fig. 1). Layer 1 contains a defect in the form of a circular configuration centered at a certain depth. The properties of the material are presented in Table 1. The defect is located at a depth of Y_{loc} = 1.5 m subsurface and at a distance of X_{loc} = 2 m from the point P_1 of application of a single pulsed P_t (Fig. 1) loading. Impulse loading depends linearly on the time of load application ($\tau = 0.003$ s), which corresponds to the parameters of real shock loading (Fig. 2). The field of surface displacements as a result of a short-term impulse action is considered as an input parameter. The radius of the defect varies in calculations as: R_i = 0; 0.25; 0.3; 0.35; 0.4; 0.45; 0.5 m. The basic objective is to determine the functional dependence of the defect radius on the oscillation responses measured at certain points of the structure based on the use of ANN.

Table 1

Layer options

No.	Name	Thickness, *m*	E, GPa	ρ, kg/m^3	*v*	Attenuation coefficient
1	Layer 1	5	0.1	2000	0.33	0.001
2	Underlying layer	0.1	0.1	2000	0.33	0.1
3	Defect R_i	X_{CENTER}=2 Y_{CENTER}= –1.5	1	2000	0.33	0.001

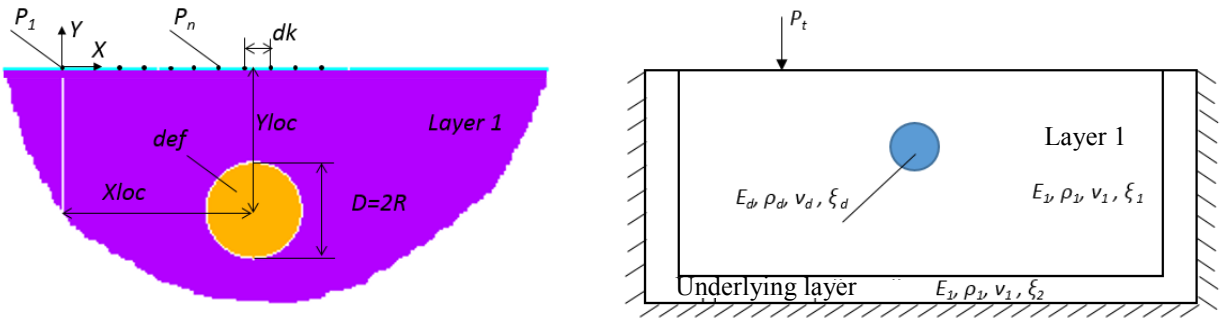

a) *b)*

Fig. 1. Layered construction model with inner circular defect:
(a) description of the region with imperfection; *(b)* layered structure model schematic

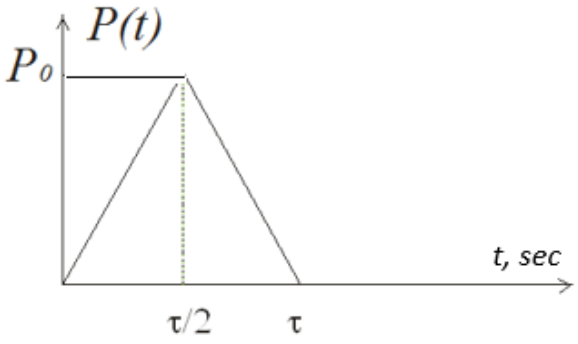

Fig. 2. Dependence of impulse load P on loading time

***FE* modeling.** Modeling of a flat structure (*10 m* wide) with a defect was carried out in the *ANSYS FE* complex: elements of the *PLANE82* type with triangular and quadrangular configurations with plane deformation (*3950* nodes and *1890* finite elements) were used for modeling. The outer layer of the structure (underlying) had high damping coefficients, but retained the basic properties of layer 1. The analyzed time was selected such that the impulse from the extreme boundaries of the structure did not return back. This was achieved by fixing the time of a sharp increase in the vibration amplitudes at the outer boundary of layer 1. The shock load was applied at the point P_t on the surface of the structure.

As a result of impulse loading, transverse and longitudinal wave displacements of points occur both on the surface of the structure and throughout its entire volume. An example of the form of transverse vibrations of the structure at time t = 0.01 s is shown in Fig. 3. Control points (40 points) are located on the surface at a distance of dk = *0.1 m* from each other (Fig. 1). The simulation of the distribution of points on the surface displays a true picture of measurements. The first measuring point is located at a distance of *0.1 m* from the place of impact.

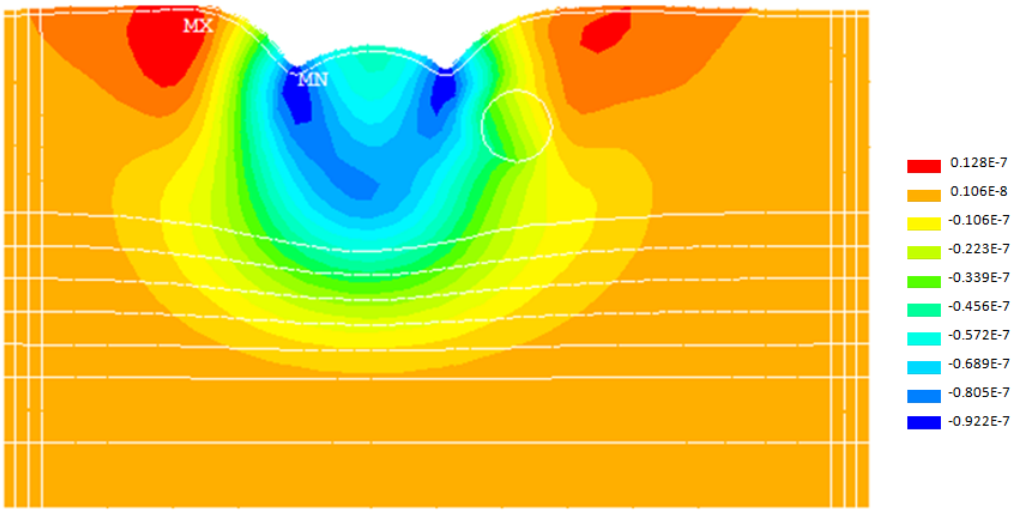

Fig. 3. Wave displacements along thickness of the structure at t = *0.01 s*

Fig. 4, 5 show the results of calculating the transverse displacements (direction OY) at various points of the surface. In the process of solving the problem, the transverse displacements were calculated at the control points of the structure in the time interval t = 0–0.1 s. Of special interest is the field of displacements of points of the surface layer in the time interval t = 0–0.04 s. At this time, the primary form of the layered structure deflections is formed, and there are no vibration responses from the excitation of the outer structure layers.

Fig. 5 shows the maximum values of vibration amplitudes depending on the time of their registration. The analysis shows that they have an exponential approximate trend. For the same measurement positions of the amplitude maxima, there are discrepancies in the vibration amplitudes depending on the value of the radius of the defect.

At the next stage, relative values of the displacement of amplitudes д ΔU_y (a), the velocity ΔV_y (b) and the acceleration ΔA_y (c) were calculated for the points N_p=1–40. These relative values were calculated as the difference between the current indicator of the maximum amplitude for the point at R_i (at i=2–7) and the amplitude of the vibration parameter at a defect size R_1=*0 (no defect in the structure):*

$$\Delta U_{yi}=U_{yi}-U_{y1};$$

$$\Delta V_{yi}=V_{yi}-V_{y1};$$

$$\Delta A_{yi}=A_{yi}-A_{y1}.$$

Fig. 6 shows three-dimensional graphs representing the dependences of the relative magnitudes of the displacement of the amplitudes ΔU_y (a), the velocity ΔV_y (b) and the acceleration ΔA_y (c) for points N_p=1–40 on the surface of the structure and a variant of the radius R_i of the defect.

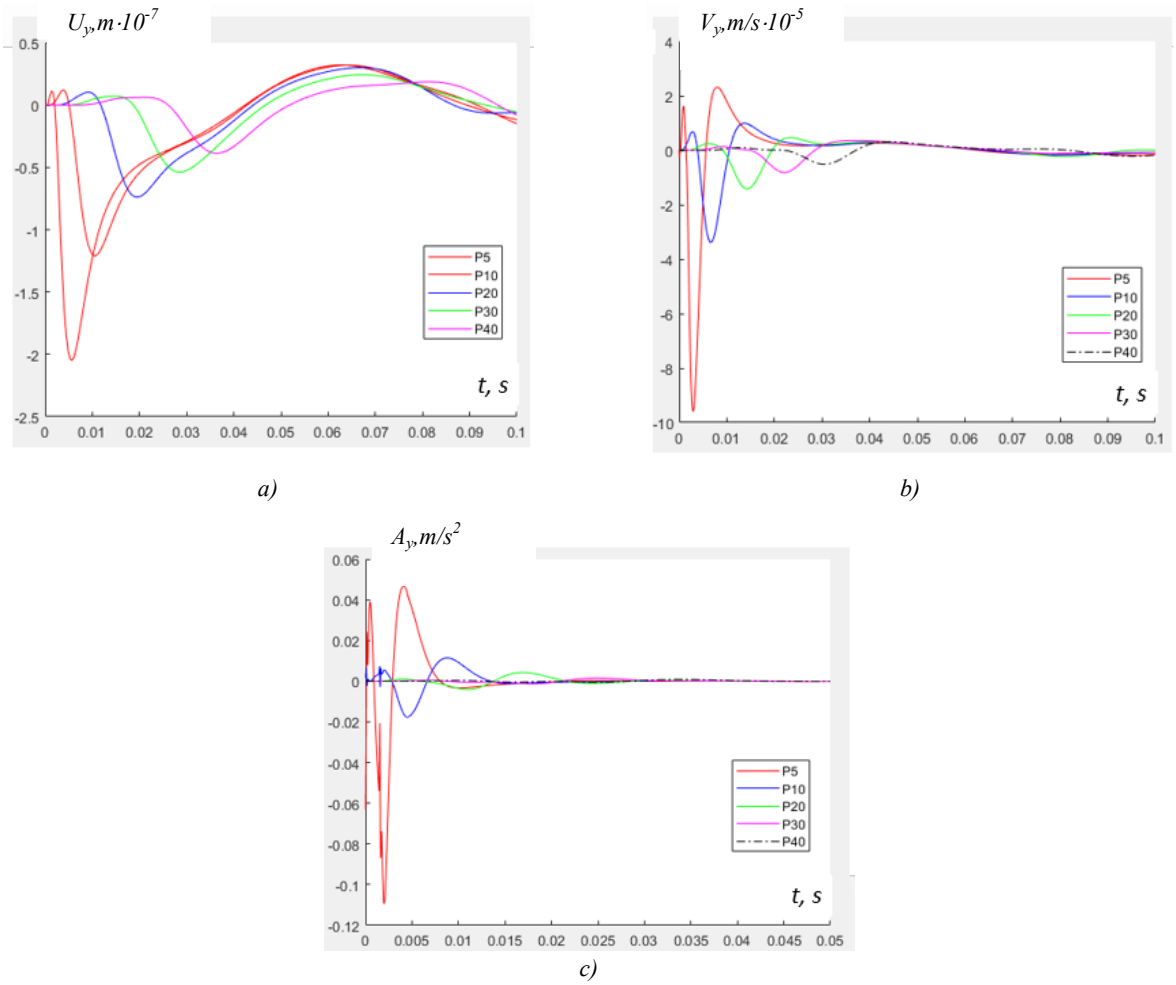

Fig. 4. Amplitudes of displacements U_y *(a)*, velocity V_y *(b)* and acceleration A_y *(c)* depending on time for points 1-40 on the surface of the structure

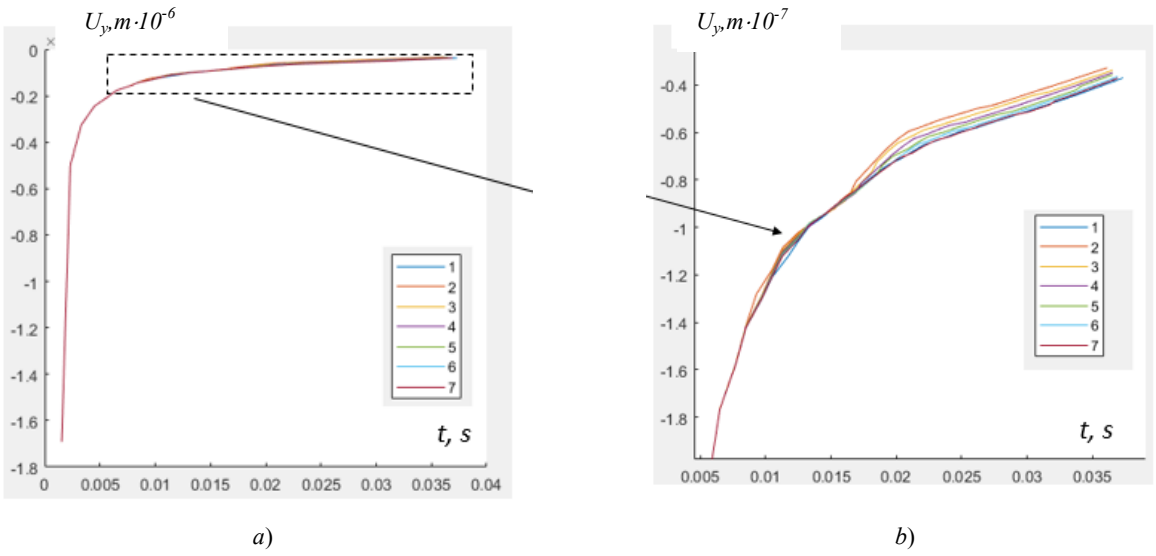

Fig. 5. Dependences of maximum displacements*: (a)* on time for points 1-40 on the surface of the structure for seven variants of the radius of the defect; *(b)* for the selected range of amplitudes

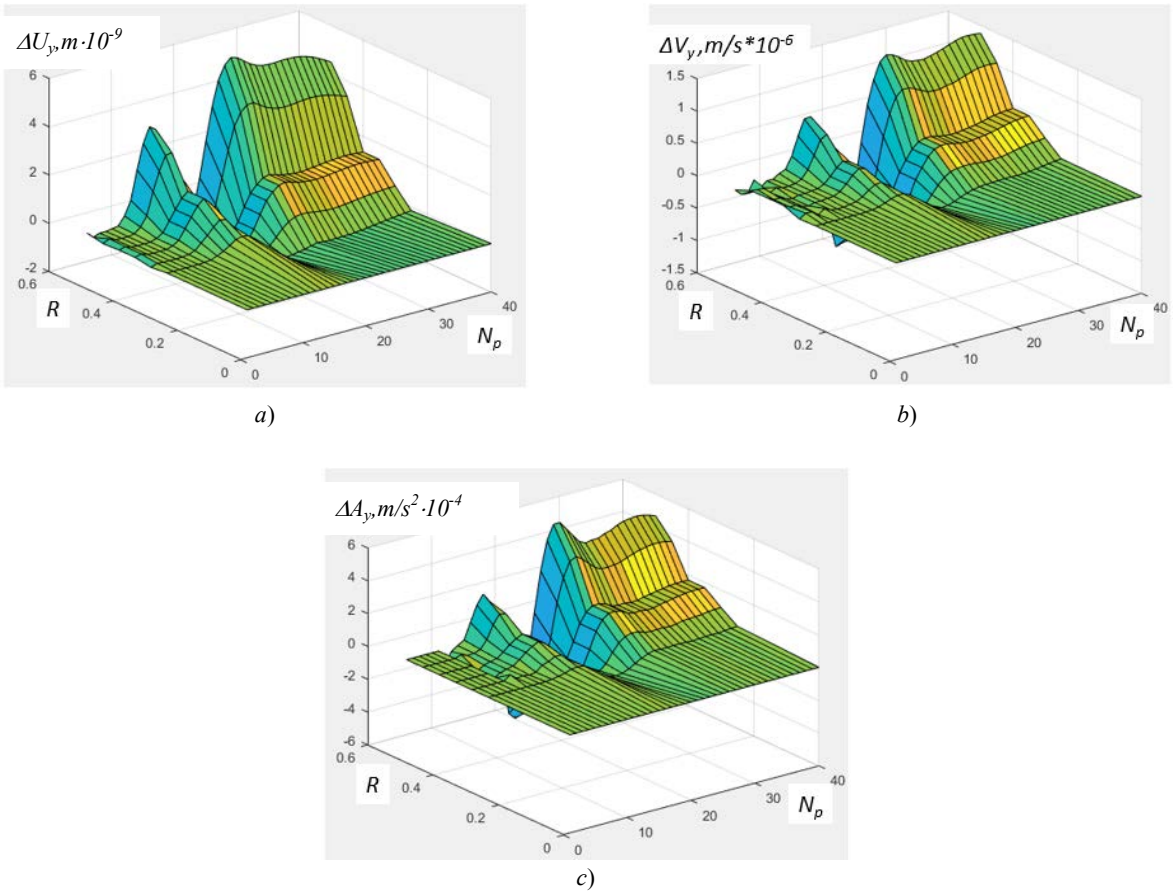

Fig. 6. Relative values of displacement amplitudes ΔU_y *(a)*, velocity ΔV_y *(b)* and acceleration ΔA_y *(c)* for points N_p = 1-40 on the surface of the structure and variant of radius R_i of the defect

The center of the defect was located under the point P_{20}. The analysis of these graphs shows that on the left and right in the vicinity of the defect, knees of the curves of the maximum oscillation amplitudes of the relative values of the displacement ΔU_y, velocity ΔV_y and acceleration ΔA_y occur. This tendency persists for all variations in the radius of the defect R_i. Thus, this sign can be an indicator of the location of the defect.

In practice, such effects can be achieved through positional scanning during registration and processing of vibration amplitudes. The curves of the relative indices of displacement, velocity and acceleration in the vicinity of the defect correlate sufficiently well with the size of the defect.

The use of neural network technologies in the problem of identifying the size of a hidden defect. Let us establish a connection between velocity, acceleration, and vibration amplitudes propagating in the layered structure, and the radius of the defect $R_{i.}$. Based on the data obtained at the *FE* modeling stage, a training set is formed with the help of which the constructed ANN model is trained.

As a result of the numerical solution to a number of direct problems in the *ANSYS FE* software package, data were obtained for 40 points on the surface of the layered structure with variations in the radius of the defect $R_{i.}$ with a calculation error within *3%*. For each set of 40 values, the corresponding defect radius was set. The prepared training vectors contained the relative values of the oscillation amplitudes $\Delta U_y(N_{pi})$, of the velocity $\Delta V_y(N_{pi}$, and acceleration $\Delta A_y(N_{pi})$ as the input values, and the defect radius as the output values.

A total of 100 numerical experiments were carried out. Thus, the training set consists of 100 vectors for each type of the investigated parameter ΔU_y, ΔV_y и ΔA_y. All data used in training the neural network are normalized and are on the interval [0, 1].

To identify the radius of a defective inclusion, a fully connected multilayered ANN model was used, simulated in the *Matlab* complex. The ANN model contained 1 layer, consisted of 40 input neurons and 1 output neuron. Sigmoid was chosen as the input activation function, and a linear dependence was established as the output activation function. The network was trained using an error backpropagation algorithm based on the Levenberg-Marquardt optimization [37].

The loss function was characterized by the mean square error (MSE). For the training and test set, 100 vectors were constructed from the indicators of the relative values of the oscillation amplitudes ΔU_y, velocity ΔV_y and acceleration ΔA_y. The correlation of these parameters to the radius of the defect is found. It was established that 8, 10

and 20 learning epochs for the corresponding indicators are sufficient to achieve the required level of the ANN performance. Fig. 7 shows the dependence of the root mean square error on the number of learning epochs of the ANN model. The analysis shows that when learning of more than 8 epochs is reached for all relative parameters of vibration amplitudes, the MSE changes insignificantly

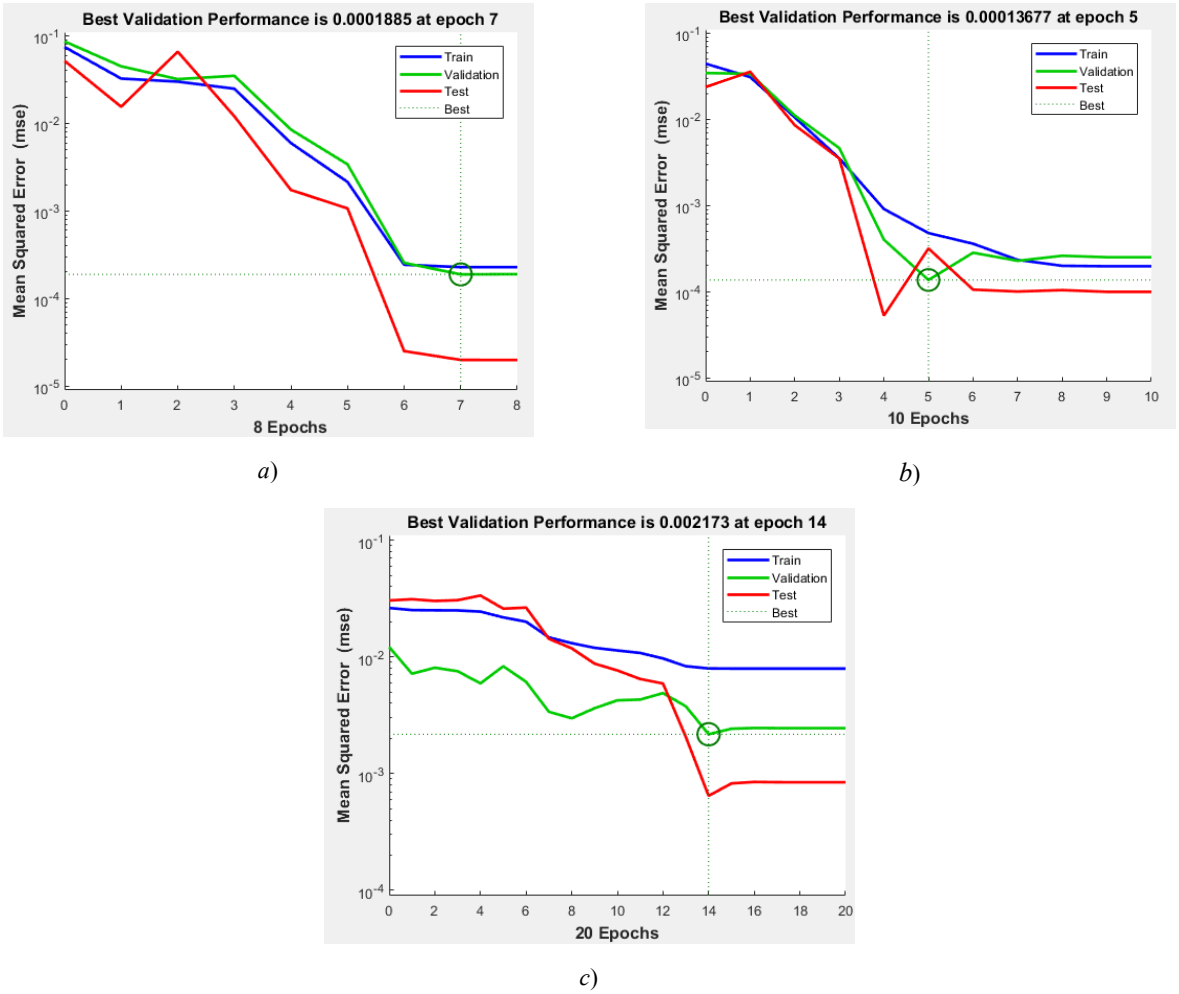

a) *b*)

c)

Fig. 7. Change in the MSE of the ANN operation under its training based on the relative values of the oscillations: *(a)* amplitudes ΔU_y, *(b)* velocity ΔV_y, and *(c)* acceleration ΔA_y

Table 2

Calculation accuracy evaluation

ANN applied	Relative error, %
ΔU_y	0.50
ΔV_y	3.03
ΔA_y	16.70

Testing the ANN dependences obtained. For a selective assessment of the restoration of the defect radius index R_i, sets of vibration amplitude parameters were performed, and their relative values were obtained. Graphical display of the results of three test sets for the relative values of vibration amplitudes ΔU_y *(a)*, velocity ΔV_y *(b)* and acceleration ΔA_y *(c)* are shown in Fig. 8. These indicators of the sets were substituted into the corresponding ANN, and the values of the radius of the defect were calculated. Table 2 shows the calculated error of the restored radius R of the defect. The analysis shows that the least accurate is the restoration of the radius from the acceleration parameters. At this, the average relative error in recovering the parameter of the radius R of the defect based on the data of the vibration amplitudes ΔU_y and the velocity ΔV_y does not exceed 5%.

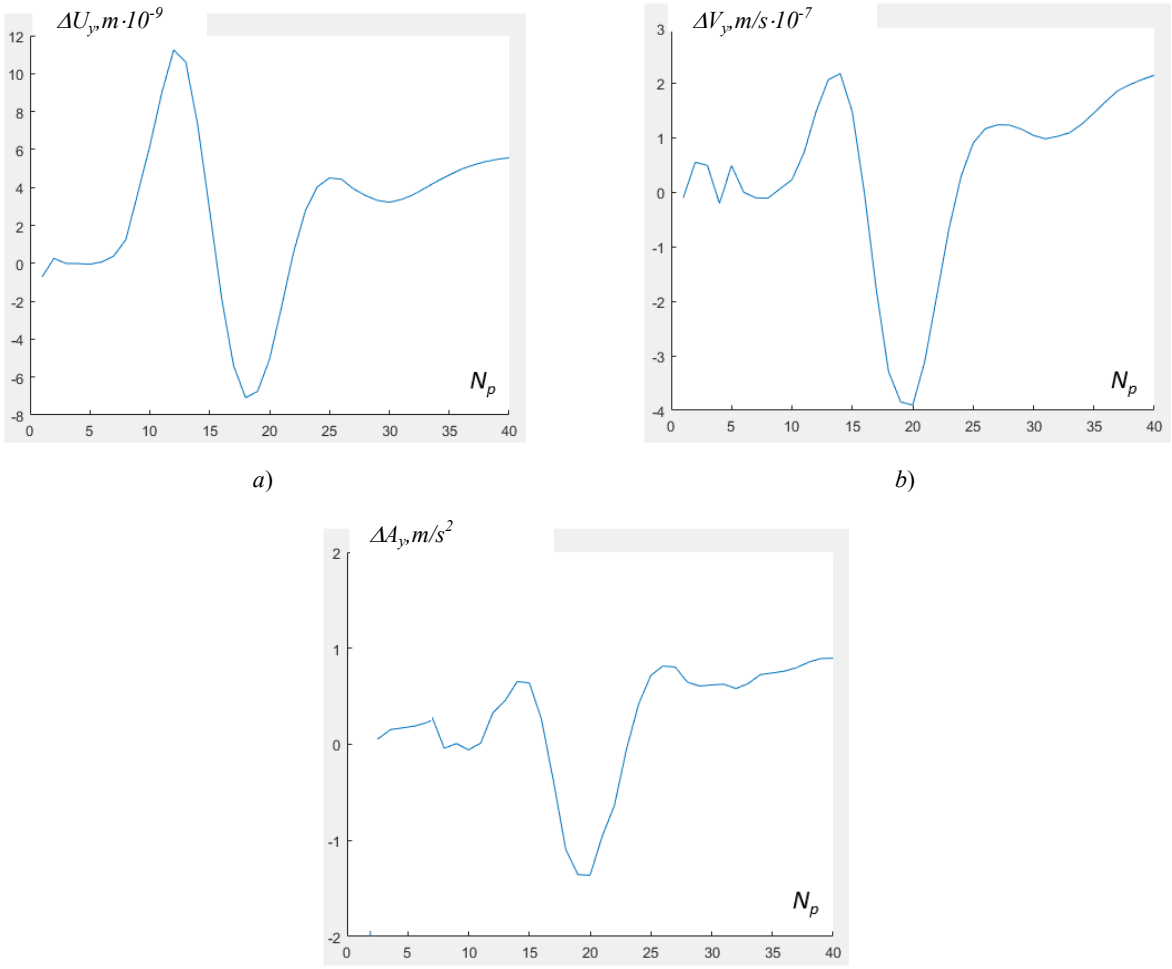

Fig. 8. Set of calculated relative values of vibration amplitudes ΔU_y *(a)*, velocity ΔV_y *(b)* and acceleration ΔA_y *(c)*

Discussion and Conclusions. The problem on reconstructing the radius of a defect based on the application of simulation modeling of oscillations in the *ANSYS* finite element complex and ANN in the *MATLAB* complex is considered. The results of unsteady oscillations of a half-plane with a circular internal defect are obtained. The transverse displacements are calculated at the control points of the structure during the propagation of a wave from a pulsed loading. As a result, an approach was developed to restore the radius of a defect in a structure based on a combination of the FEM and ANN. The best configuration of the ANN architecture consisting of 1 hidden and 1 output layers included 40 input neurons and 1 output neuron.

The study has shown that the amount of data used is sufficient for successful training of the constructed model and identification of a hidden defect in the structure. In addition, the relative accuracy of determining the radius of the defect inside layer 1, in the case of using the values of amplitudes of displacement oscillations and velocity, is more than 99%.

Thus, the constructed ANN algorithms can be successfully applied to assess the stratification of layered structures using temporal and positional scanning when oscillations are excited from a far zone.

References

1. Kershenbaum VYa, ed. Nerazrushayushchie metody kontrolya [Non-destructive control methods]. Moscow: Nauka i tekhnika; 1992. 656 p. (In Russ.)

2. Belokur IP. Defektologiya i nerazrushayushchii kontrol' [Defectology and non-destructive testing]. Kiev: Vyshcha shkola; 1990. 208 p. (In Russ.)

3. Akop'yan VA, Cherpakov AV, Rozhkov EV, et al. Integral'nyi diagnosticheskii priznak identifikatsii povrezhdenii v ehlementakh sterzhnevykh konstruktsii [Integral diagnostic sign of damage identification in elements of rod constructions]. Testing. Diagnostics. 2012;7:50–56. (In Russ.)

4. Kaptsov AV, Shifrin EI, Shushpannikov PS. Opredelenie parametrov ploskoi ehllipticheskoi treshchiny v izotropnom lineino uprugom tele po rezul'tatam odnogo ispytaniya na odnoosnoe rastyazhenie [Identification of parameters of a plane elliptic crack in an isotropic linearly elastic body from the results of a single uniaxial tension test]. Izvestia: Mechanics of Solids. 2012:4:71–88. (In Russ.)

5. Sedov AV, Kalinchuk VV, Bocharova OV. Adaptive-spectral method of monitoring and diagnostic observability of static stresses of elements of mechanical constructions. In: IOP Conference Series: Earth and Environmental Science. 2017;87(8):082043.

6. Solov'ev AN, Sobol' BV, Vasil'ev PV. Ul'trazvukovaya lokatsiya vnutrennikh treshchi nopodobnykh defektov v sostavnom uprugom tsilindre s primeneniem apparata iskusstvennykh neironnykh setei [Ultrasonic location of inner crack defects in a compound elastic cylinder using an artificial neural network apparatus]. Russian Journal of Nondestructive Testing. 2016;52(3):3–9. (In Russ.)

7. Xia J, Miller RD, Park CB. Estimation of near-surface shear-wave velocity by inversion of Rayleigh waves. Geophysics. 1999;64(3):691–700.

8. Esipov YV, Mukhortov VM, Pojda II. Criteria for identification of stress state of periodic rod construction based on ferroelectric sensors of deformation. In: Piezoelectrics and Related Materials: Investigations and Applications. 2012. P. 283-291.

9. Evtushenko SI, Lepikhova VA, Lyashenko NV, et al. Identification of soils, grounds and lands strata using the acoustic spectral analysis. In: IOP Conf. Series: Materials Science and Engineering. 2020;913:052043. DOI:10.1088/1757-899X/913/5/052043.

10. Il'gamov MA, Khakimov AG. Diagnostika povrezhdenii balki na sharnirnykh oporakh [Damage diagnosis of a hinge support beam]. Structural Mechanics of Engineering Constructions and Buildings. 2010;2:42–48. (In Russ.)

11. Park CB, Miller RD, Ryden N, et al. Combined use of active and passive surface waves. Journal of Environmental & Engineering Geophysics. 2005;10(3):323–334.

12. Brigante M, Sumbatyan MA. Acoustic Methods for the Nondestructive Testing of Concrete: A Review of Foreign Publications in the Experimental Field. Russian Journal of Nondestructive Testing. 2013;49(2):100–111.

13. Park CB, Miller RD. Roadside passive multichannel analysis of surface waves (MASW). Journal of Environmental & Engineering Geophysics. 2008;13(1):1–11.

14. Lyapin AA, Parinov IA, Buravchuk NI, et al. Improving Road Pavement Characteristics. Springer, Cham; 2020. 254 p. DOI: 10.1007 / 978-3-030-59230–1

15. Haykin S. Neural Networks: a comprehensive foundation. 2nd ed. Prentice Hall; 1998. 842 p.

16. Krasnoshchekov AA, Sobol BV, Solov'ev AN, et al. Identification of crack-like defects in elastic structural elements on the basis of evolution algorithms. Russian Journal of Nondestructive Testing. 2011;47(6):412–419.

17. Waszczyszyn Z, Ziemianski L. Neural networks in mechanics of structures and materials – new results and prospects of applications. Computers and Structures. 2001;79(22–25): 2261–2276.

18. Zinov'ev AYu. Vizualizatsiya mnogomernykh dannykh [Multidimensional data visualization]. Krasnoyarsk: Izd-vo Krasnoyarskogo gosudarstvennogo tekhnicheskogo universiteta; 2000. 180 p. (In Russ.)

19. Liu SW, Huang JH, Sung JC, et al. Detection of cracks using neural networks and computational mechanics. Computer Methods in Applied Mechanics and Engineering. 2002;191(25–26):2831–2845. DOI: 10.1016/S0045-7825(02)00221-9

20. Khandetsky V, Antonyuk I. Signal processing in defect detection using back-propagation neural networks. NDT&E International. 2002;35(7):483–488.

21. Xu YG, et al. Adaptive multilayer perceptron networks for detection of cracks in anisotropic laminated plates. International Journal of Solids and Structures. 2001;38:5625–5645.

22. Fang X, Luo H, Tang J. Structural damage detection using neural network with learning rate improvement. Computers and Structures. 2005;83:2150–2161.

23. Hernandez-Gomez LH, Durodola JF, Fellows NA, et al. Locating defects using dynamic strain analysis and artificial neural networks. Applied Mechanics and Materials. 2005;3-4:325–330.

24. Soloviev A, Sobol' B, Vasil'ev P. Identification of crack-like defect and investigation of stress concentration in coated bar. Springer Proceedings in Physics. 2019;4:165–174.

25. Pozharskii DA, Sobol' BV, Vasil'ev PV. Periodic crack system in a layered elastic wedge. Mechanics of Advanced Materials and Structures. 2020;27(4):318–324.

26. Cherpakov AV, Vasiliev PV, Soloviev AN, et al. The Study of Stratification of Multilayer Structures Based on Finite Element Modeling and Neural Network Technologies. In: Advanced Materials. In: Proc. Int. Conf. on Physics and Mechanics of New Materials and Their Applications, PHENMA 2019. 2020. P. 439–447. DOI: 10.1007/978-3-030-45120-2

27. Vatul'yan AO. Obratnye zadachi v mekhanike deformiruemogo tverdogo tela. [Inverse Problems in Solid Mechanics]. Moscow: Fizmatlit; 2007. 224 p. (In Russ.)

28. Boev NV, Ehl'-Marabi KhM, Vdovin VA, et al. Mnogokratnoe rasseyanie ul'trazvukovykh voln na sisteme prostranstvennykh defektov kanonicheskoi formy (teoriya i ehksperiment) [Multiple scattering of ultrasonic waves by system of 3D defects of canonical form (theory and experiment)]. Vestnik of DSTU. 2012;12(3):5–10. (In Russ.)

29. Lyapin A, Beskopylny A, Meskhi B. Structural Monitoring of Underground Structures in Multi-Layer Media by Dynamic Methods. Sensors. 2020;20(18):5241. DOI: 10.3390/s20185241.

30. Cherpakov AV, Akop'yan VA, Solov'ev AN, et al. Identifikatsiya parametrov povrezhdenii v uprugom sterzhne s ispol'zovaniem konechno-ehlementnogo i ehksperimental'nogo analiza mod izgibnykh kolebanii [Damage parameters identification in elastic rod using both finite elements and experimental analysis of flexural vibration modes]. Vestnik of DSTU. 2011;11(3):312–318. (In Russ.)

31. Cherpakov AV, Shilyaeva OV, Grigoryan MN, et al. Simulation of wave processes in the multilayer structure surface layer properties identification by the finite element method. In: IOP Conf. Ser.: Mater. Sci. Eng. 2019;698: 066021.

32. Cogranne R, Retraint F. Statistical detection of defects in radiographic images using an adaptive parametric model. Signal Processing. 2014;96(part B):173–189.

33. Vatul'yan AO, Osipov AV. Poperechnye kolebaniya balki s lokalizovannymi neodnorodnostyami [Transverse vibrations of beam with localized heterogeneities]. Vestnik of DSTU. 2012;12(8):34–40. (In Russ.)

34. Shevtsov SN, Soloviev AN, Parinov IA, et al. Piezoelectric Actuators and Generators for Energy Harvesting. Heidelberg, Springer; 2018. 182 p.

35. Vasil'chenko KE, Nasedkin AV, Solov'ev AN. K raschetu amplitudno-chastotnykh kharakteristik zadach ob ustanovivshikhsya kolebaniyakh na osnove klasternykh tekhnologii v ACELAN [A calculation of amplitude vs frequency characteristics for oscillations of permanent form using clusters technology in ACELAN]. Computational Technologies. 2005;10(1):10–20. (In Russ.)

36. Krasil'nikov VA, Krylov VV. Introduction to Physical Acoustics. Moscow: Nauka; 1984. 400 p.

37. Kingma D P, Ba J. Adam: A Method for Stochastic Optimization. Proc. 3rd International Conference for Learning Representation, San Diego. 2015.

Submitted 03.08.2020
Scheduled in the issue 14.09.2020

About the Authors:

Solov'ev, Arkadii N., Head of the Theoretical and Applied Mechanics Department, Don State Technical University (1, Gagarin sq., Rostov-on-Don, 344003, RF), Leading Research Scholar of the Laboratory for Computational Mechanics, Southern Federal University (105/42, Bolshaya Sadovaya St., Rostov-on-Don, 344006, RF), Dr.Sci. (Phys.-Math.), professor, ResearcherID H-7906-2016, ScopusID 55389991900, ORCID: http://orcid.org/0000-0001-8465-5554, Solovievarc@gmail.com

Vasil'ev, Pavel V., senior lecturer of the IT Department, Don State Technical University (1, Gagarin sq., Rostov-on-Don, 344000, RF), ORCID: http://orcid.org/0000-0003-4112-7449, liftzeigen@mail.ru

Cherpakov, Aleksandr V., Senior Research Scholar of the Vorovich Institute for Mathematics, Mechanics, and Computer Science, Southern Federal University (8a, Milchakova St., Rostov-on-Don, 344090, RF), associate professor of the Information Systems in Construction Department, Don State Technical University (1, Gagarin sq., Rostov-on-Don, 344000, RF), Cand.Sci. (Eng.), ORCID: https://orcid.org/0000-0003-3205-1577, alex837@yandex.ru

Parinov, Ivan A., Leading Research Scholar, Southern Federal University (8a, Milchakova St., Rostov-on-Don, 344090, RF), Dr.Sci. (Eng.), ORCID: https://orcid.org/0000-0003-3833-0331, parinov_ia@mail.ru

Kirillova, Evgeniya V., professor, RheinMain University of Applied Sciences, (18, Kurt-Schumacher-Ring, Wiesbaden, 65197, Germany), Cand.Sci. (Phys.-Math)., ScopusID: 24402885500.

Claimed contributorship

A. N. Solov'ev: basic concept formulation; research objectives and tasks setting. A. V. Cherpakov: calculations in the FE package; text preparation; formulation of conclusions. I. A. Parinov: academic advising; analysis of the research results. P. V. Vasil'ev: computational analysis; the text revision; correction of the conclusions. E. V. Kirillova: computational analysis; the text revision; correction of the conclusions.

All authors have read and approved the final manuscript.

MECHANICS

https://doi.org/10.23947/2687-1653-2020-20-3-216-224

Probabilistic design strategy for improved Austin-Moore stem used in artificial cementless hip prosthesis considering material property uncertainty

G. Kharmanda[1], I. R. Antypas[2]
[1]INSA Rouen Normandie (Saint-Etienne-du-Rouvary, France)
[2]Don State Technical University (Rostov-on-Don, Russian Federation)

Introduction. The use of probabilistic analysis is important when the input data are random, that leads to stochastic results. This paper describes the integration of a probabilistic design strategy of the solid and hollow stems implanted in a proximal femur in order to compare their advantages. The used hollow stem is called "Improved Austin-Moore" (IAM) model.
Materials and Methods. Probabilistic methods allow variations in factors which control the biomechanical effects of the implanted femur to be taken into account while determining its performance. Different material properties were generated randomly using Monte Carlo simulation (MCS). Monte Carlo sampling techniques were applied, and different von Mises stresses of the layers (bone and metal) were chosen as a performance indicator.
Results. A simple 2D implant-bone study of solid and IAM stem design was carried out with a high level of confidence, 99.87%, which corresponds to a target reliability index with regard to statistical uncertainties. The probabilistic design results show that the input and output parameters for the IAM stem are highly correlated relative to those for the solid stem.
Discussion and Conclusions. The sensitivity analysis shows that the input parameters for the IAM stem play a much larger part in the output parameters relative to the solid stem. The IAM stem is much more advantageous than the solid stem which causes an increase in the performance of the hip prosthesis.

Keywords: hip prosthesis, probabilistic analysis, finite element analysis, Monte Carlo simulation, IAM model.

For citation: G. Kharmanda, I.R. Antypas. Probabilistic design strategy for improved Austin-Moore stem used in artificial cementless hip prosthesis considering material property uncertainty. Advanced Engineering Research, 2020, vol. 20, no. 3, p. 216–224. https://doi.org/10.23947/2687-1653-2020-20-3-216-224

1. Introduction

In probabilistic studies on Total Hip Replacement (THR) models, several important random parameters may affect the hip performance, such as the geometrical description of the bone, the implant and the cement, the material properties of different layers, the magnitude and direction of the applied loads, and the position of the bone-implant [1–2]. In order to improve the stem design, several points have been considered. At the first stage, the rectangular section stem is considered more reliable than the circular section stem [3]. The rectangular section stem then provides a secure diaphyseal press-fit in the frontal plane of the femoral canal. This way it allows excellent rotational stability and improves the primary mechanical fixation [1]. In addition, wear as mentioned in Kharmanda and Albashi [4] can be reduced. At the second stage, the shouldered stem is considered more reliable than the non-shouldered one. It has been shown in the numerical results of Kharmanda, et al. [5], that, when considering the shouldered stem, there is an excellent decrease of the maximum values on von Mises stress in different bone layers compared to the non-shouldered one. At the third stage, the hollow stems are considered. In Kharmanda [6], a multi-objective structural optimization strategy has been integrated into Austin-Moore prosthesis in order to improve its performance. The resulting model was called Improved Austin-Moore (IAM). The topology optimization was considered as a conceptual design stage to sketch the IAM stem according to the daily loading cases. The shape optimization presented the detailed design stage considering several objectives. A new multiplicative formulation has been proposed as a performance scale to define the best compromise between several requirements. In this paper, a probabilistic design strategy is applied on two kinds of

stems (solid and IAM stems) to determine the mechanical effects, the response sensitivities with respect to input parameters, and the correlation of the used material properties with different output parameters. A numerical application on a 2D problem is carried out to show the advantages of the IAM stem relative to the solid one.

2. Material and Methods

2.1 Model description and material properties

Fig. 1*a* and *b* show 2D sections for the studied solid and IAM stems implanted in bone layers (cortical bone and cancellous bone). The bone materials are generally anisotropic [7]. In the current study, the material properties of bone have been for simplicity considered as linearly elastic and isotropic. In Fig. 1, the cortical bone material is considered to be homogeneous and isotropic with Young's modulus $E = 17$ GPa and Poisson's ratio $\nu = 0.33$. The corresponding number of elements for the cortical region is 605 elements for the solid stem model, while it is 545 elements for the IAM stem model. The cancellous bone material is also considered to be homogeneous and isotropic with Young's modulus $E = 386$ MPa and Poisson's ratio $\nu = 0.33$ [8]. The corresponding number of elements for the cancellous region is 417 elements for the solid stem model, while it is 418 elements for the IAM stem model. The modulus of titanium alloy of stem is considered to be: $E = 110$ GPa with Poisson's ratio: $\nu = 0.3$ [9]. The corresponding number of elements for the metal region is 529 elements for the solid stem model, while it is 861 elements for the IAM stem model. The used element is PLANE82 (8-node, nonlinear). The number of the total nodes is 5048 nodes for the solid stem model, while it is 6094 nodes for the IAM stem model.

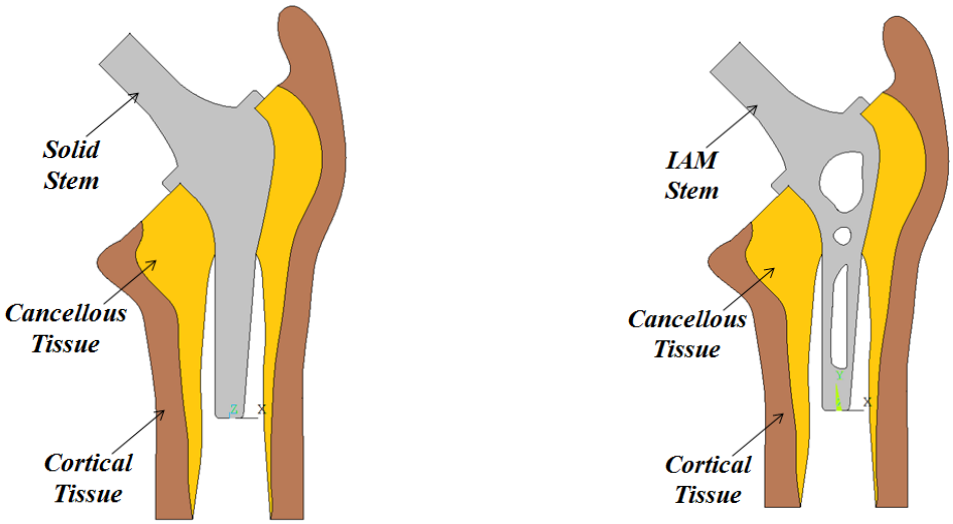

Fig 1. Geometry models for: *(a)* solid stem and; *(b)* IAM one

2.2 Boundary conditions

The loading cases are considered as daily loading conditions [10]: one-legged stance (L1), extreme ranges of motion of abduction (L2), and adduction (L3) as shown in Fig. 2.

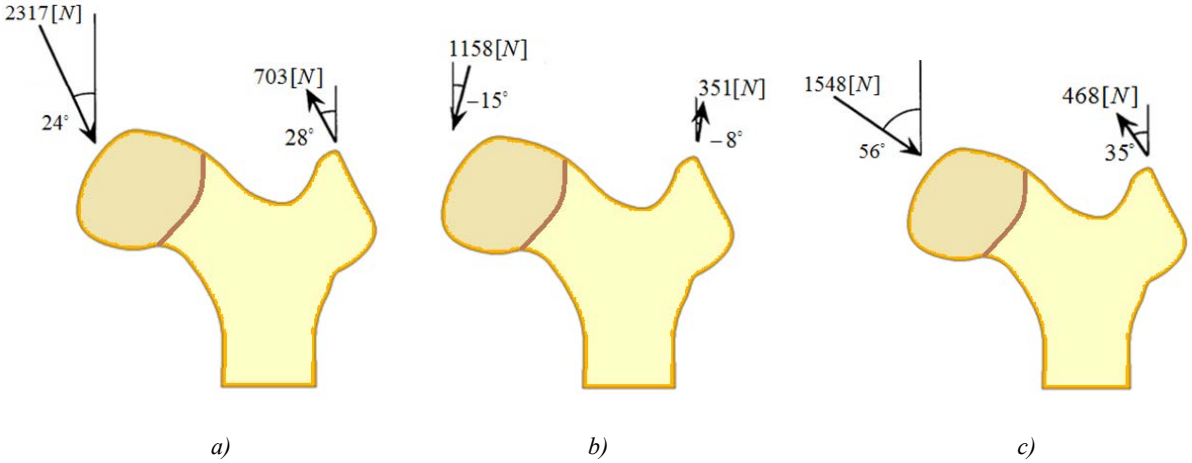

Fig. 2. Loading cases: *a*) One-legged stance case (L1); *b*) Abduction case (L2); and *c*) Adduction case (L3)

Table 1 presents different components of the three loading cases (L1, L2 and L3) which are illustrated in Fig. 1.

Table 1

Force components

Loading Case	Body Forces		Muscle Forces	
	F_x^B [N]	F_y^B [N]	F_x^M [N]	F_y^M [N]
L1	942.41	-2116.68	-330.04	620.71
L2	-299.71	-1118.54	48.85	347.58
L3	1283.35	-865.63	-268.43	383.36

According to the results of Kharmanda [6], the third loading case (L3) leads to the highest von Mises stress values in the bone tissues. Thus, in this work, a probabilistic design strategy is performed considering the third loading case L3.

2.3 Probabilistic design strategy

2.3.1 Failure probability

The design of structures and the prediction of their good performance lead to the confirmation of a certain number of rules depending on the knowledge of physical and mechanical experience of designers. Thus, there are several events leading to a failure mode. It is the objective to evaluate the probability of failure corresponding to the occurrence of critical failure scenarios. The probability of failure is then given by:

$$P_f = \Pr\left[G(\mathrm{x},\mathrm{y})\right] = \int_{G(\mathrm{x},\mathrm{y})\le 0} f_Y(\mathrm{y})dy_1...dy_n \tag{1}$$

where $G(\mathrm{x},\mathrm{y})$ is a limit state surface (curve) that is defined by the condition of good structural performance [11]. The limit state surface (curve) $G(\mathrm{x},\mathrm{y})=0$ is located between the failure part $G(\mathrm{x},\mathrm{y})<0$ and the safety part $G(\mathrm{x},\mathrm{y})>0$. $f_Y(\mathrm{y})$ is the density function of the random parameter Y. Several techniques can be used to compute the probability of failure. Monte Carlo Simulation (MCS) is the most conservative probability technique [12]. Here, the parameters are sampled at random from their underlying distributions and the probability of failure which is estimated by solving the model repeatedly. For all time, the MCS gives the correct solution if a sufficient number of trials is computed, but it requires a high computing time. In order to decrease this expense, and avoid overlapping of samples and/or lack of samples in some regions of the domain, another technique called Latin Hypercube Sampling (LHS) can be applied [13]. The MCS based approach divides the sample space into separate intervals with equal probabilities, and one sample is randomly taken from each interval. When considering implicit models, finite element analysis has been combined with probabilistic design methods in order to allow uncertainty in the system parameters to be taken into account. Several types of uncertainties can be distinguished:

- Physical uncertainty: For example: material properties, dimensions, loading, etc.;
- Statistical uncertainty: Due to limited sample sizes, probabilistic model is considered uncertain;
- Model uncertainty: For example, mathematical models, numerical approaches due to simplifying assumptions, unknown boundary conditions, and unknown effects of other variables that are not included in the model.

2.3.2 Reliability index

The reliability is the inverse of failure probability. The relationship between the reliability R is related with the failure probability, it can be written as follows:

$$P_f = 1 - R \tag{2}$$

To estimate the reliability index, several techniques have been developed during the last five decades, namely FORM (First Order Reliability Methods), SORM (Second Order Reliability Method) and simulation techniques [11, 14]. In FORM approximation, the probability failure is simply evaluated by

$$P_f \approx \Phi(-\beta) \tag{3}$$

where $\Phi(\bullet)$ is the standard Gaussian cumulated function calculated through the following integral:

$$\Phi(Z) = \frac{1}{\sqrt{2\pi}} \int_{-\infty}^{Z} e^{-\frac{z^2}{2}} dz, \tag{4}$$

For practical engineering applications, Eq. (3) gives sufficiently accurate estimation of the failure probability. In general, the nuclear and spatial studies necessitate very small values of failure probability, the failure probability should be: $P_f \in [10^{-6} - 10^{-8}]$ that corresponds to a reliability index $\beta \in [4.75 - 5.6]$ when using equations 3 and 4; while in structural engineering studies, the failure probability should be: $P_f \in [10^{-3} - 10^{-5}]$ that corresponds to a reliability index $\beta \in [3 - 4.25]$ (A detailed study on target safety indices can be found in Jeppsson [15]. In the next section, a simple 2D implant-bone study of solid and IAM stem designs is presented with account for statistical uncertainties.

3. Results

The Probabilistic Design System in ANSYS software analyzes a component or a system involving uncertain input parameters. The input parameters concerning geometry, material properties, boundary conditions, etc., are defined in ANSYS software. The variation of these input parameters is considered as random input variables and is characterized by their distribution type (normal, lognormal, etc.), as well as their distribution parameters (mean values, standard deviation, etc.). The important responses are defined as random output parameters. During a probabilistic study, the software executes multiple analysis loops to compute random output parameters as a function of a set of random input variables. The values for the input variables are generated randomly using Monte Carlo simulation.

The studied model has six parameters that are regarded as random input parameters. Thus, six sources of uncertainty were considered in the present investigation: E_{Can}, E_{Cor}, E_M, ν_{Can}, ν_{Cor} and ν_M. These sources are Young's modulus and Poisson's Ratio for the three studied layers (cortical, cancellous and metal layers). According to several references in the literature [16, 17], the maximum and the minimum values of Young's modulus are respectively 19.7 GPa and 10.4 GPa for the cortical tissue, 5.6 GPa and 192 MPa for the cancellous tissue, and 120 GPa and 100 GPa for the titanium alloy. And the maximum and the minimum values of Poisson's ratio are respectively 0.33 GPa and 0.3 GPa for the cortical tissue and for the cancellous tissue, while they are: 0.36 and 0.3 for the titanium alloy. It is considered that the input parameters follow the uniform distribution law. To assess the accuracy of the results, it is performed with a high confidence interval of 99.87% (reliability level). The failure probability is noted to be 0.13% which corresponds to a reliability index equal to $\beta = 3$ (Equations 3 and 4). Using Sampling Method, Monte Carlo based simulations were run, with 30000 simulations for the third loading case (L3) on the solid and IAM stems. A sensitivity analysis was performed to assess the influence of each parameter on the maximum von Mises stress values for the cortical and cancellous bone, and for the metal (σ^1_{max}, σ^2_{max} and σ^M_{max}). The evaluation of the sensitivities was based on both Rank-order correlation coefficients between the input parameters and the output parameters.

Table 2

Statistics of the random input and output parameters for solid stem

Parameter	Mean	Standard Deviation	Skewness	Kurtosis	Minimum	Maximum
E_{Can} (MPa)	2896	1561	-1.73×10^{-7}	6.65×10^{4}	192.1	5600.
E_{Cor} (MPa)	1.51×10^{4}	2685	2.06×10^{-7}	6.65×10^{4}	1.04×10^{4}	1.97×10^{4}
E_M (MPa)	1.10×10^{5}	5774	2.36×10^{-7}	6.65×10^{4}	1.00×10^{5}	1.20×10^{5}
ν_{Can}	0.3150	8.66×10^{-3}	-5.96×10^{-7}	6.65×10^{4}	0.3000	0.3300
ν_{Cor}	0.3150	8.66×10^{-3}	1.39×10^{-6}	6.65×10^{4}	0.3000	0.3300
ν_M	0.3300	1.73×10^{-2}	5.56×10^{-7}	6.65×10^{4}	0.3000	0.3600
σ^1_{max} (MPa)	16.93	1.783	1.992	2.49×10^{5}	14.81	25.06
σ^2_{max} (MPa)	7.057	0.7837	2.311	3.34×10^{5}	6.333	11.24
σ^M_{max} (MPa)	11.28	1.44×10^{-2}	-1.42×10^{-2}	6.65×10^{4}	11.26	11.31

Tables 2 and 3 show the statistical results of the random input and output parameters for the solid stem and for the IAM stem, respectively.

Table 3

Statistics of the random input and output parameters for the IAM stem

Parameter	Mean	Standard Deviation	Skewness	Kurtosis	Minimum	Maximum
E_{Can} (MPa)	2896	1561	-1.57×10^{-7}	6.65×10^{4}	192.0	5600.
E_{Cor} (MPa)	1.51×10^{4}	2685	1.71×10^{-7}	6.65×10^{4}	1.04×10^{4}	1.97×10^{4}
E_{M} (MPa)	1.10×10^{5}	5774	3.08×10^{-7}	6.65×10^{4}	1.00×10^{5}	1.20×10^{5}
ν_{Can}	0.3150	8.66×10^{-3}	5.64×10^{-7}	6.65×10^{4}	0.3000	0.3300
ν_{Cor}	0.3150	8.66×10^{-3}	-5.93×10^{-7}	6.65×10^{4}	0.3000	0.3300
ν_{M}	0.3300	1.73×10^{-2}	3.34×10^{-8}	6.65×10^{4}	0.3000	0.3600
$\sigma^{1}_{\max}$ (MPa)	16.92	1.822	1.963	2.43×10^{5}	14.76	25.18
$\sigma^{2}_{\max}$ (MPa)	7.081	0.7954	2.295	3.28×10^{5}	6.345	11.33
$\sigma^{M}_{\max}$ (MPa)	11.30	1.18×10^{-2}	-1.78×10^{-2}	6.65×10^{4}	11.28	11.32

Fig. 3 shows the probability density function histograms of output parameters. Fig. 3 *a* and *b* show the histograms of the maximum von Mises stress value ($\sigma^{1}_{\max}$) for the solid stem, and the IAM stem, respectively. Fig. 3 *c* and *d* show the histograms of the maximum von Mises stress value ($\sigma^{2}_{\max}$) for the solid stem, and the IAM stem, respectively. Fig. 3 *e* and *f* show the histograms of the maximum von Mises stress value ($\sigma^{M}_{\max}$) for the solid stem, and the IAM stem, respectively. The probability density function calculates an appropriate number of classes based on the number of samples. The number of classes is equal to the number of bars which are presented in the histogram. The distance between the smallest and largest sample value is divided into classes of equal width. A histogram is modeled by counting the number of hits in the individual classes and dividing this number by the total number of samples. Thus, a histogram represents the relative frequencies of the random quantity that is drawn for.

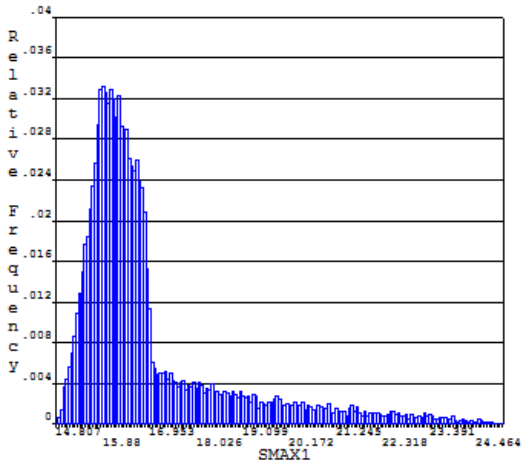

a)

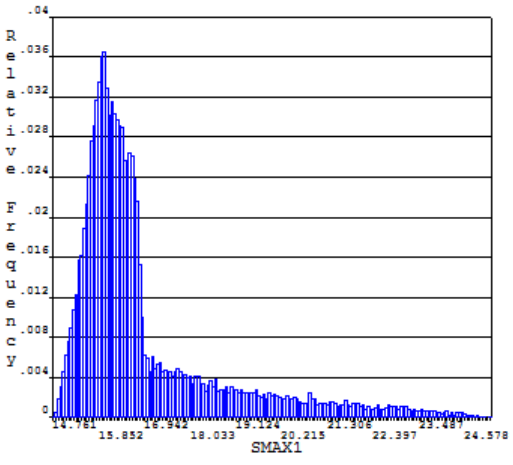

b)

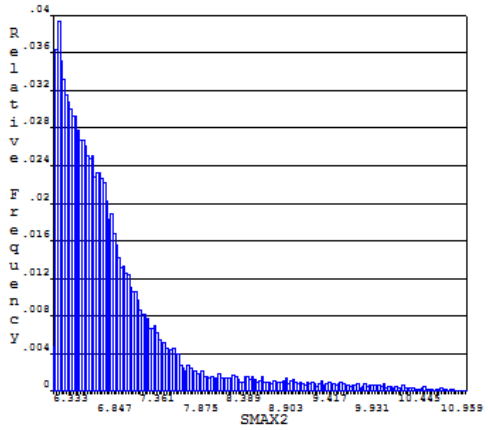

c)

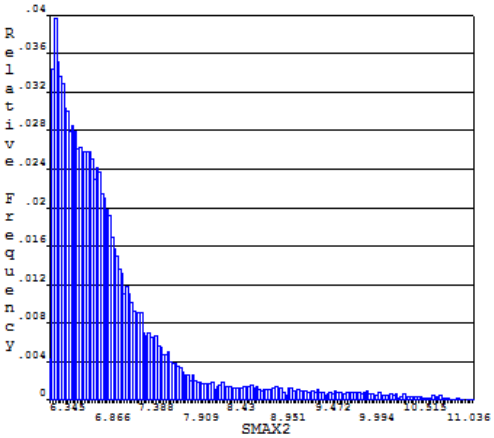

d)

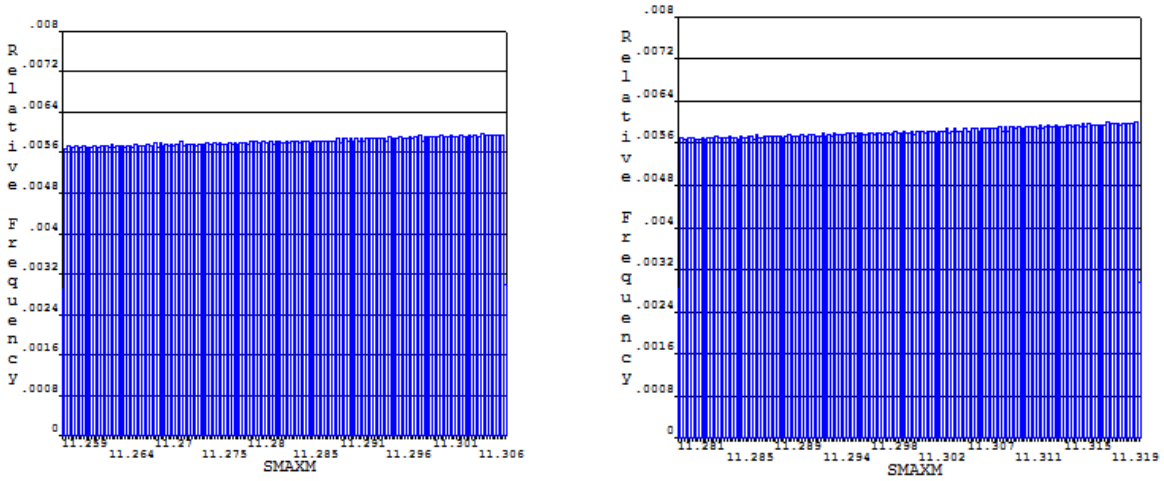

e) *f)*

Fig. 3. Histograms of the output parameters: σ^1_{max} for *(a)* solid stem; *(b)* IAM stem; σ^2_{max} for; *(c)* solid stem; *(d)* IAM stem; σ^M_{max} *(e)* solid stem, and *(f)* IAM stem.

Fig. 4 shows the sensitivity evaluation of the output parameter with respect to the input random variables: Fig. 4 *a* and *b* show the sensitivities of the maximum von Mises stress value (σ^1_{max}) for the solid stem, and the IAM stem, respectively. Fig. 4*c* and *d* show the sensitivities of the maximum von Mises stress value (σ^2_{max}) for the solid stem, and the IAM stem, respectively. Fig. 4 *e* and *f* show the sensitivities of the maximum von Mises stress value (σ^M_{max}) for the solid stem, and the IAM stem, respectively. The sensitivities of a certain random output parameter are modeled. The random input parameters are separated into two types: significant parameters and insignificant parameters. The sensitivity plots include only the significant random input parameters.

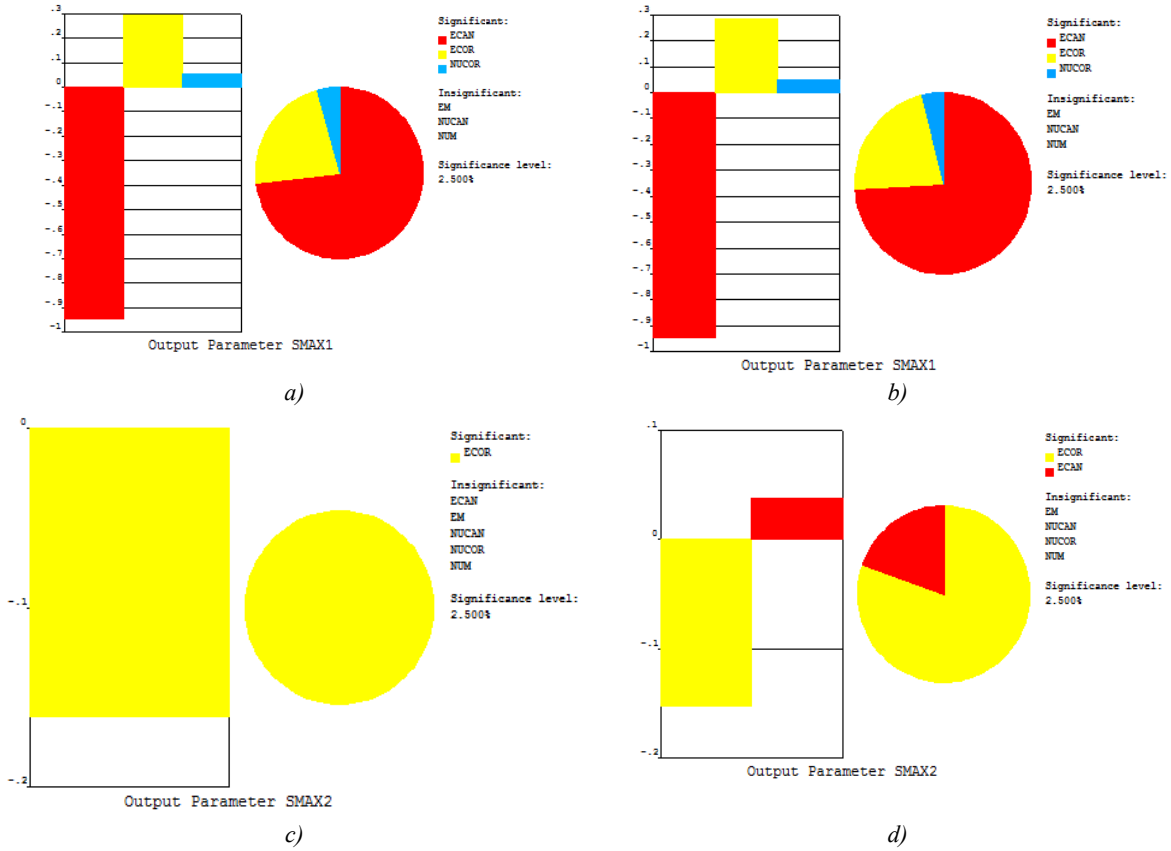

a) *b)*

c) *d)*

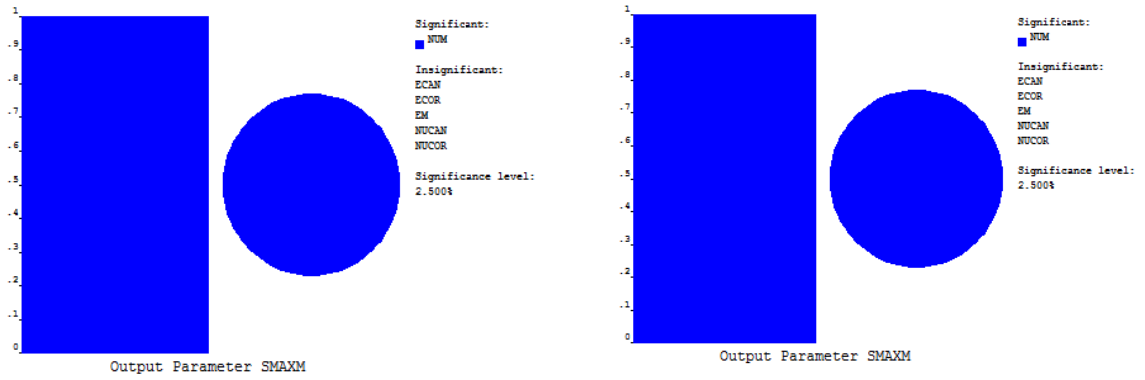

e) *f)*

Fig. 4. Sensitivities of the output parameters: σ^1_{max} for *(a)* solid stem; *(b)* IAM stem; σ^2_{max}; *(c)* solid stem; *(d)* IAM stem; and σ^M_{max} for *(e)* solid stem; *(f)* IAM stem

Table 4 shows the correlation coefficients between the input and output parameters for the solid and IAM stems. Here, it is shown the statistical interdependence between the input and output parameters. The values being closer to zero show that the two parameters are weakly correlated. However, the values being closer to 1 or -1, show that the two variables are highly correlated either in positive or negative sense, respectively.

Table 4

Correlation coefficients between the input and output parameters for solid and IAM stems

Parameters	Solid stem			IAM stem		
	σ^1_{max} (MPa)	σ^2_{max} (MPa)	σ^M_{max} (MPa)	σ^1_{max} (MPa)	σ^2_{max} (MPa)	σ^M_{max} (MPa)
E_{Can} (MPa)	-0.799	-0.320	---	-0.801	-0.304	0.010
E_{Cor} (MPa)	0.191	-0.038	-0.002	0.187	-0.036	0.003
E_M (MPa)	0.002	0.004	0.007	0.001	-0.001	0.010
ν_{Can}	-0.006	---	0.004	-0.006	-0.002	-0.008
ν_{Cor}	0.025	---	-0.011	0.025	0.004	-0.004
ν_M	-0.004	-0.006	1.000	-0.007	-0.003	1.000

4. Discussion. In this work, a probabilistic design strategy is established to compare in details the role of different input and output parameters considered when designing the solid and hollow (IAM) stems. Monte Carlo technique is used as a robust tool with a big number of simulations to provide with accurate results. The histograms of the probability density function of three output parameters are presented. The three output parameters have three different distribution forms: The maximum von Mises stress values for the cortical tissue (σ^1_{max}) has the lognormal distribution form. The maximum von Mises stress values for the cancellous tissue (σ^2_{max}) has the exponential distribution form. The maximum von Mises stress values for the metal (σ^M_{max}) has the uniform distribution form. The skewness values of the input values (asymmetry) for the IAM stem differ from those for the solid stem, while there is no big difference when considering the output parameters. The sensitivity analysis for the output parameters with respect to the input random variables is next carried out in order to determine the input parameter influence. Three input parameters (E_{Can}, E_{Cor} and ν_{Cor}) have different roles on the maximum von Mises stress values for the cortical tissue (σ^1_{max}). Here, there is a small difference when comparing the diagram for the solid and IAM stems. For the maximum von Mises stress values for the cancellous tissue (σ^2_{max}), two input parameters (E_{Cor} and E_{Can}) play significant roles when considering the IAM stem, while only one input parameter (E_{Cor}) when considering the solid stem. For the maximum von Mises stress values for the metal (σ^M_{max}), only one input parameter (ν_M) has a significant influence for the solid and IAM stems. According to the correlation study, the correlation coefficients between the input parameters and the output ones for the IAM stem are much higher than those for the solid stem where several values are closer to zero. According to the presented probabilistic design strategy, the IAM stem has several advantages relative to the solid one.

5 Conclusion. A probabilistic design strategy is applied to find different probabilistic bounds with high reliability (confidence) levels. The results show that the IAM stem is much more advantageous than the solid stem especially. This study was limited to a 2D modeling in order to reduce the computing time since 30000 simulations were performed. However, in future work, it is recommended to perform a 3D modeling and to deal with anisotropy behavior for bone tissues.

References

1. Gonzalez CD. Probabilistic Finite Element Analysis of Un-cemented Total Hip Replacement, PhD thesis. School of Engineering Sciences, Bioengineering Sciences Research Group: University of Southampton; March 2009.

2. Kharmanda G, Antypas I. Reliability-based design algorithm for artificially replaced hip prosthesis considering material property uncertainty. Journal of Advances in Engineering Research, AER. 2018. Advances in Engineering Research (AER). 2018;157:44−50. https://www.atlantis-press.com/proceedings/aime-18/25901891

3. Kharmanda G, El-Hami A, Ibrahim MH. Integration of reliability and optimization concepts into orthopedic prosthesis design: Application on hip prosthesis design. Journal of Uncertainties and Reliability of Multiphysical Systems. 2017. DOI: 10.21494.ISTE.OP.2017.0120

4. Kharmanda G, Albashi L. Numerical Study for Increasing Efficiency of Artificially Un-cemented Hip Joint. Research Journal of Aleppo University, Engineering Science Series. 2011;101:47−64.

5. Kharmanda G, Mulki S, Sabsabi Y. Computer-Aided Design of Internal Replacement Models in Orthopedics Surgery. Research Journal of Aleppo University, Engineering Science Series. 2012;105:312−328.

6. Kharmanda G. Integration of multi-objective structural optimization into cementless hip prosthesis design: Improved Austin-Moore model, Computer Methods. Biomechanics and Biomedical Engineering. 2016;19(14):1557–1566. DOI: 10.1080/10255842.2016.1170121

7. Mackerle J. Finite element modeling and simulations in orthopedics. Bibliography 1998–2005, J. Computer Methods in Biomechanics and Biomedical Engineering. 2006; 9(3):149–199. DOI: 10.1080/10255840600751523

8. Senapati S-K, Pal S. UHMWPE-alumina Ceramic Composite. A Proposed Metal Substitute for Artificially Replaced Hip Joint. IE (I) Journal MC. 2005;85:157−162. https://www.researchgate.net/scientificcontributions/2092553592_SK_Senapati.

9. Shaik SA, Bose K, Cherukuri HP. A study of durability of hip implants. Materials and Design. 2012;42:230–237. DOI: 10.1016/j.matdes.2012.05.049

10. Beaupré GS, Orr TE, Carter DR. An approach for time-dependent bone modeling and remodelingapplication: a preliminary remodeling simulation. Journal of Orthopaedic Research. 1990;8(5):662–670. DOI: http://dx.doi.org/10.1002/jor.1100080507

11. Kharmanda G, El-Hami A. Reliability Concept. Reliability in Biomechanics. 2016:63−112. DOI: 10.1002/9781119370840.ch2 P.

12. Haldar A, Mahadevan S. Probability, reliability and statistical methods. Engineering design. New York, USA: John Willey & Sons; 2000. P. 304. https://books.google.ru/books?id=wZNRAAAAMAAJ&redir_esc=y

13. McKay MD, Beckman RJ, Conover WJ. A comparison of three methods for selecting values of input variables. The analysis of output from a computer code. Technometrics. 1979;42:55–61. DOI: 10.1080/00401706.1979.10489755

14. Kharmanda G, Antypas I. Integration of Reliability Concept into Soil Tillage Machine Design. Vestnik of Don State Technical University. 2015;15(2):22−31. DOI: https://doi.org/10.12737/11610

15.Jeppsson J. Reliability-based assessment procedures for existing concrete structures: PhD dissertation. Division of Structural Engineering, Lund University. 2003. P. 199.

16. Cheal E, Spector M, Hayes W. Role of loads and prosthesis material properties on the mechanics of the proximal femur after total hip arthroplasty. Journal of Orthopaedic Research. 1992;10(3):405−422. DOI: http://dx.doi.org/10.1002/jor.1100100314

17. Kayabasi O, Ekici B. Probabilistic design of a newly designed cemented hip prosthesis using finite element method. Materials and Design. 2008;9(5):963−971. DOI: 10.1016/j.matdes.2007.03.024

Submitted 18.05.2020
Scheduled in the issue 20.07.2020

About the Authors:

Ghais Kharmanda, Guest Researcher, LMN, INSA Rouen Normandie (St. 685 avenue de l universite BP08, 76801 Saint-Etienne-du-Rouvary, LMN, INSA Rouen Nomandie, France), Cand.Sci. (Eng.)., ResearcherID: O-6690-2018, ORCID: https://orcid.org/0000-0002-8344-9270, g.kharmanda@gmail.com

Imad R. Antypas, associate professor of the Machine Design Principles Department, Don State Technical University (1, Gagarin Square, Rostov-on-Don, 344000, RF), Cand.Sci. (Eng.), ResearcherID: O-4789-2018, ORCID: https://orcid.org/0000-0002-8141-9529, Imad.antypas@mail.ru

Claimed contributorship

G. Kharmanda: scientific guidance, statement of the problem, definition of research methodology; collection and analysis of analytical and practical materials on the research topic, critical analysis and finalization of the solution; computer realization of the solution of the problem. I.R. Antypas: analysis of analytical and practical materials on the research topic and analysis of scientific sources on the topic of research, critical analysis and revision of the text.

All authors have read and approved the final version of the manuscript.

MECHANICS

UDC 621.791.05:620.17 https://doi.org/10.23947/2687-1653-2020-20-3-225-234

Analytical model for assessing fatigue limit of welded joints of ferritic-pearlitic steels

K. A. Molokov, V. V. Novikov, A. P. German
Far Eastern Federal University (Vladivostok, Russian Federation)

Introduction. Microdefects and zones with stress concentration in welded joints cause fatigue macrocracks. Such damage is potentially dangerous, especially if the fatigue life of the structure is almost exhausted. In this case, the crack size is close to the critical value, and it is crucial to determine its length. The paper considers the development of an engineering analytical model for assessing the critical crack length and endurance limit of weld joints with the formed grain in the structure of ferrite-pearlitic steels after welding.

Materials and Methods. The theory and methods of fracture mechanics at the mesoscale are used. A simple analytical dependence is obtained, which provides determining the critical dimensions of a macrocrack for ferrite-pearlite steels without using the Griffiths formula. . The calculation results of the critical crack lengths of various steels depending on their yield strength are presented. An analytical dependence of the endurance limit calculation for the most dangerous symmetric loading cycle, according to the standard set of mechanical characteristics and the average grain diameter of ferrite-pearlite steel, is presented.

Results. Structural deformation analysis of the crack propagation process has been performed. On its basis, an engineering technique for assessing the endurance limit is developed. A mathematical model that enables to calculate the endurance limit and the critical crack length in the components of welded assemblies of large-sized facilities, considering periodic loads of a symmetrical cycle, is developed. Using this model, it is possible to estimate the degree of metal sensitivity to the original characteristics (yield stress, Poisson's ratio, grain diameter, relative constriction, Young's modulus, power-law hardening coefficient, etc.).

Discussion and Conclusion. Under stresses corresponding to the steel endurance limit, the critical crack opening rates of the tip and edges approach each other. Energetically, this moment approximately corresponds to the transition of the crack to an unstable state. The accumulation of one-sided plastic deformations causes the limiting state of plasticity of the region adjacent to the crack tip and its avalanche-like or sharply accelerated motion. This critical area is interrelated with the grain diameter of the material, the characteristic of critical plasticity and the critical opening at the crack tip at the fatigue limit. The proposed analytical dependences can be used to assess the residual life and the fatigue limit of welded structures, the influence of various factors on the fatigue limit of welded joints of ferrite-pearlitic steels used in mechanical engineering, shipbuilding, pipeline transport, etc.

Keywords: welded joint, ferritic-pearlitic steel, crack length, endurance limit, critical deformation, mathematical model, structural damage.

For citation: K. A. Molokov, V.V. Novikov, A. P. German. Analytical model for assessing fatigue limit of welded joints of ferritic-pearlitic steels. Advanced Engineering Research, 2020, vol. 20, no. 3, p. 225–234. https://doi.org/10.23947/2687-1653-2020-20-3-225-234

Introduction. Microdefects and stress concentration zones in welded joints cause fatigue macrocracks. Such damage is potentially dangerous, especially if the fatigue life of the structure is practically exhausted. In this case, the

crack size is close to the critical value, and it is crucially important to determine its length. The paper considers the development of an engineering analytical model for assessing the critical crack length and endurance limit of weld joints with the formed grain in the structure of ferrite-pearlitic steels after welding.

It should be noted that an equally-strength weld joint for static loading does not guarantee its reliability under cyclic loads. This is due to local plastic deformations in stress points in discontinuities of the structures subjected to cyclic loads [1]. It can be assumed that for plastic materials, the maximum stresses in these zones will be constant and equal to the yield point if we neglect some strengthening of the material in the stress points and assume that the regions of disturbed stresses are relatively small compared to the material thickness [2].

Materials and Methods. The fatigue strength of structural steels corresponds approximately to the values of $\sigma_{-1} = 0.5 \ldots 0.7\sigma_{т}$, and destruction under cyclic stresses, as a rule, occurs locally in the form of cracks originating from stress concentrators or defects in the weld joint (Fig. 1).

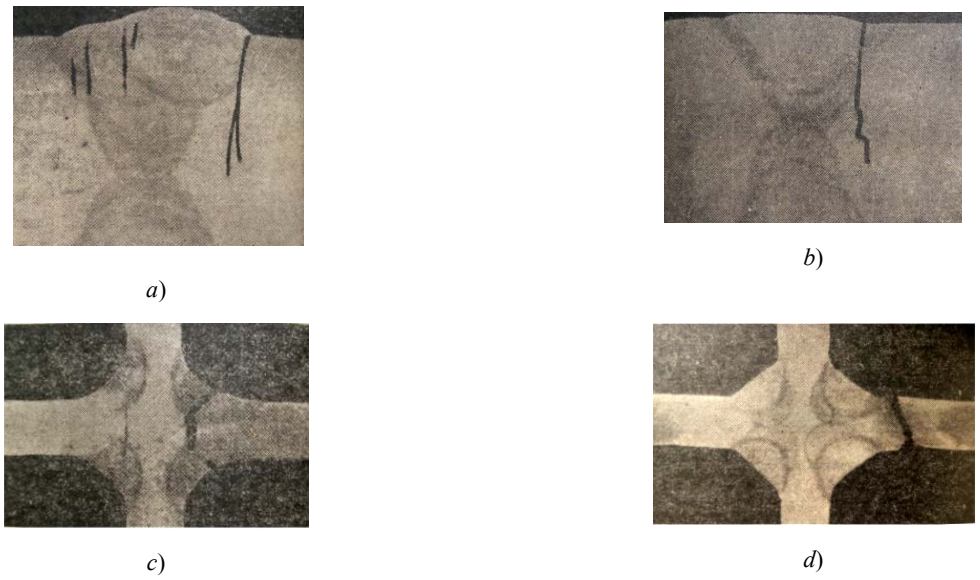

a) *b*) *c*) *d*)

Fig. 1. Cracks at undercut and in seam (*a, b*), destruction of cross joints from crack under incomplete penetration (*c*) and in heat-affected zone (HAZ) with full penetration (*d*) [2]

The stress concentration resulting from partial penetration during the formation of a weld joint can also play a decisive role in the formation of weak zones. This is facilitated by significant inhomogeneity of mechanical characteristics, major defects in the seam and near-weld zone.

In the corner and T-joints (with or without grooving), in most cases, the crack originates from the stress concentrator (see Fig. 1*c,d*). If the seam is convex, destruction can occur along the fusion zone or near it, along the base metal in the HAZ, whose structure has undergone changes [3].

Over time, microdefects cause fatigue cracks [4, 5]. Such cracks in the weld joints of some elements propagate slowly, so they may not be particularly dangerous. This is evident from the practice of using modern steel grades for ship hulls [6]. At the same time, fatigue cracks are potentially dangerous in two cases.

1. If the resource provided by the static indeterminacy of the structure and other factors is practically exhausted.

2. If the crack size corresponds to the Griffiths critical length in an infinite plate $L|_{\sigma_{-1}} = L_c$, determined from the dependence:

$$L = (K_{1c}/\sigma_{-1})^2/\pi, \quad (1)$$

where K_{1c} is critical stress intensity factor under plane deformation at the crack tip; σ_{-1} is stress of material endurance limit; L is half the length of the through-crack.

The coefficient K_{1c} can be calculated on the basis of a standard set of mechanical characteristics and average grain diameter of ferrite-pearlitic steel according to [7] for plane deformation and according to [8] for the planar stress state. However, to find the critical crack length of the fatigue limit, it is required to know value σ_{-1}.

The mechanism of the influence of the average diameter of steel grain at the moment of initiation of the transition of a crack into an avalanche-like advance is likely to differ from the mechanism that controls its movement at the stage of its formation. Such assumptions, based on the results of the studies [7, 9–11], motivate a more detailed consideration of the processes that control the end of the stage of stable development of macrocracks at stresses equal to the fatigue limit. It is not difficult to determine it at the critical crack size according to (1), if we find the pattern of the influence of the structure, plastic properties and mechanical characteristics of the material on the critical crack size.

The study objective is to develop analytical dependences that make it possible to establish the relationship between the critical crack length at stresses σ_{-1}, mechanical characteristics of ferrite-pearlite steel and the average grain diameter in the metal structure. The task is to bring the obtained dependencies to engineering formulas to estimate the endurance limit of ferrite-pearlitic steels.

The results of studying the cracking process at high nominal stresses indicate their discrete, jump-like development [12]. This character of growth is demonstrated through modeling at the final stage of fracture [7] under the load corresponding to the endurance limit. This suggests that, after the accumulation of one-sided plastic deformation, plastic deformation is restrained if large volumes of material with a fragmented structure are adjacent to the crack tip.

Results. At a high density of dislocations that create a fragmented structure, we will accept the conditions of plane deformation at the crack tip. Additional conditions will be provided due to constraint and accumulated one-sided plastic deformation under cyclic loads. Let us write the postulates for the moment when $L = L_{\text{кр}}$, $\sigma = \sigma_{-1}$.

1. One-sided plastic deformation reaches a critical value at the crack tip.

2. Fragmentation (cellularity) of the structure of the ferrite-pearlite material is limiting (located at the second level).

3. The function of the difference between the opening of the crack edges and the crack tip has an inflection at a point close to the state when $L = L_{\text{кр}}$, $\sigma = \sigma_{-1}$.

The experimental data shows that the cyclic loading of metals causes a significant change in the structure, substructure, and affects all sensitive characteristics. For example, an increase in the number of loading cycles of cyclically hardening (or softening) metals contributes to an increase (or decrease) in hardness (primarily on the surface of the samples under study) [13, 14].

The results of the elastoplastic analysis of the plastic zones at the crack tip determined by the Panasyuk-Dugdale model [15], differ significantly from the real ones for materials with a hardening index $m > 0.05$. Nevertheless, we will assume that at low nominal stresses $\sigma_{\text{н}} = \sigma_{-1}$, the opening at the crack tip δ and the ratio δ/r_p can be determined quite accurately for the case of plane deformation from the formulas [16]:

$$\delta = 8\sigma_{\text{т}} \cdot L/pi/E \cdot \ln\sec[\pi\sigma_{\text{н}}/2/\sigma_{\text{т}}], \quad (1)$$

$$\delta/r_p = \frac{8e_{\text{т}} \ln\sec(\pi\sigma_{\text{н}}/2)}{\pi(\sec(\pi\sigma_{\text{н}}/2)-1)} \quad (2)$$

where r_p is the linear size of the plastic zone along the crack extension from its tip (Fig. 2); $e_{\text{т}}$ is deformation of the yield point.

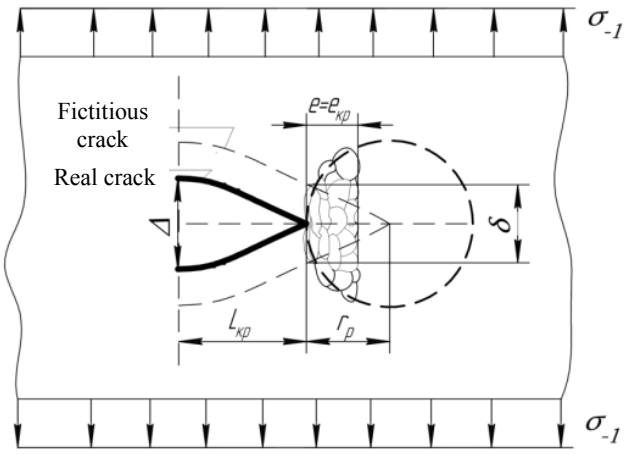

Fig. 2. State of metal at the tip of a critical opening mode crack under stresses of fatigue limit

Let us estimate the opening of the edges of this crack at rated stresses below the proportionality limit, allowing for some error [16]:

$$\Delta = \frac{4\sigma_н L}{E} \quad (3)$$

After derivation of the difference between δ and Δ, we find that the voltages corresponding to the moment of accelerated convergence δ and Δ will correspond to the nominal ones determined from the expression:

$$\sigma_н = \sigma_т/2. \quad (4)$$

With significant plastic deformations, the structure of the material undergoes fragmentation at the crack tip; therefore, the value $e_{кр}$ is associated with the staging and deformability of the fragmented structure. According to A.M. Glezer [17], the boundary between macroplastic and mega plastic deformations is conventional; it is at the level of relative deformation, equal to one hundred percent, or true. In this case, the critical deformation value:

$$e_{кр} \approx 1. \quad (5)$$

A. N. Balakhnin[1] notes that self-organization of the structure with the cell formation (Fig. 3) starts already under the deformation of ferrite of 09G2S steel and with an average value of the degree of cold deformation ε 15–35%.

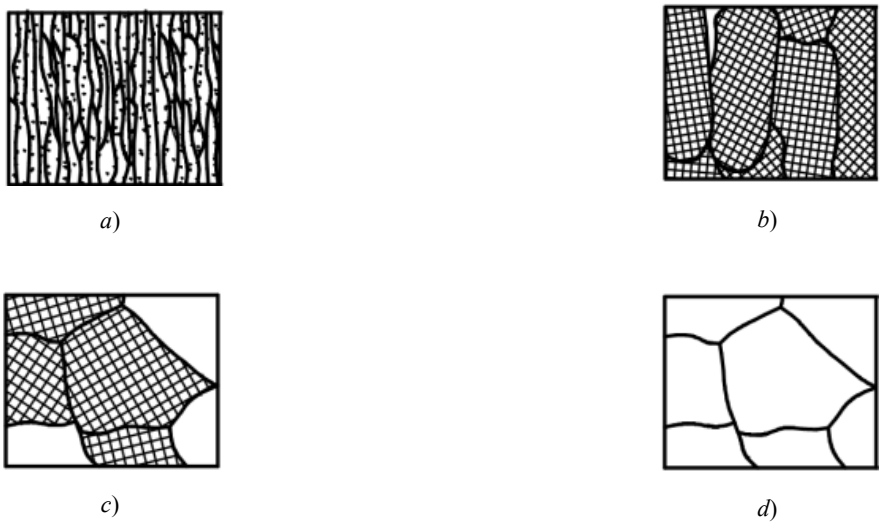

a) *b*) *c*) *d*)

Fig. 3. Microstructure under plastic deformation: ε = 80 % (*a*), ε = 40 % (*b*), ε = 1 % (*c*), ε = 0 % (*d*) [11]

With a further increase in deformation, the cell walls become thinner, and their size decreases. The fragments acquire an elongated shape, and the grains stretch in the direction of the plastic flow (Fig. 3).

At critical crack opening in the region adjacent to the tip, the grain structure in the fictitious crack model should expand and pass into the pre-cleavage state (Fig. 3*a*). It is likely to be formed due to the containment of the influx of new dislocations and their transition across grain boundaries. The material in this area should be in a state of extreme critical plasticity, and the linear characteristics of its fragments should be at the second fragmentary level. Obviously, in the adjacent plasticity zone, the crack should also have a certain number of grains in their ultimate plastic state.

Thus, the zone can be formed due to the accumulation of a part of one-sided plastic deformation, covering practically all stages of crack propagation. However, the most significant contribution to the increase in such deformation is made at the final stage of fracture, when the plasticity region is large not only in relation to the crack length, but also to the linear characteristic of the metal structure. In this zone, the grains have a prolate shape in the form of an oblong grain of rice with a cross-sectional size $d_к$.

Let us refer the average grain diameter of the undeformed material d_z to $d_к$. Then, for the second fragmentary level:

$$d_z/d_к \cong 1/0{,}618/0{,}618 = 2{,}618, \quad (6)$$

where $d_к$ is the fragment diameter.

[1] Balakhnin A N. Formation of the structure and properties of hardened sectional low-carbon steels under cold radial forging and subsequent thermal exposure: Cand.Sci. (Eng.) diss. Perm, 2015. 158 p. (In Russ.)

It is not hard to conclude that for this state, plastic deformation can be determined from the dependence of the maximum uniform elongation [3, 14]:

$$e_{\text{кр}} = 2\,ln(d_z/d_{\text{к}}) \cong 2. \quad (7)$$

For the same state, critical plastic deformation on the test specimen in the neck under rupture is expressed by the well-known dependence:

$$e_{\text{кр}} = k_{\text{н}} \cdot ln\left(\frac{1}{1-\varphi_{\text{к}}}\right), \quad (8)$$

where $k_{\text{н}}$ is the normalization factor introduced by the authors for the transition from the structure in the critical plastic state to the value of the critical plastic deformation of the sample under rupture.

Let us find this coefficient through the relative (critical) contraction of the sample under rupture, equating (9) to (8). Then, considering (6), the critical plastic deformation is determined by the expression:

$$e_{\text{кр}} = 2 = ln\frac{1}{1-\varphi_{\text{к}}} + ln\frac{1}{1-\varphi_{\text{к}}} = 2\,ln\frac{1}{1-\varphi_{\text{к}}} \quad (9)$$

For the critical opening at the crack tip, the structural-deformation criterion can be expressed:

$$\delta_{\text{кр}} = d_{\text{з}} e_{\text{кр}} = 2d_z\,ln\left(\frac{1}{1-\varphi_{\text{к}}}\right). \quad (10)$$

As a result of the effect of the critical transverse narrowing $\varphi_{\text{к}}$ on the stress intensity factor at plane deformation K_{1c} for high-strength steels, the following is indicated [18]:

— significant spread of values K_{1c} and $\varphi_{\text{к}}$;

— satisfactory correlation between them.

At the same time, it is concluded that the relationship between K_{1c} and $\varphi_{\text{к}}$ can be applied only as a qualitative one. We can agree with such conclusions, but only if we discard the relationship with some other structural characteristics, for example, the average grain diameter of steel, etc.

To find the required dependence, we substitute (5) into (2). We equate the resulting expression to (11) and write it with respect to L. As a result of calculations, we obtain the critical length of a macrocrack for nominal stresses equal to the endurance limit at the most dangerous asymmetry of the cycle:

$$L_{\text{кр}}\big|_{\sigma_{\text{н}}=\sigma_{-1}} = 0{,}3607\frac{\pi\cdot E}{\sigma_{\text{т}}}2d_z\ln\left(\frac{1}{1-\varphi_{\text{к}}}\right). \quad (11)$$

It follows from this that the length of the critical crack is directly proportional to the value of the critical logarithmic plastic deformation $e_{\text{кр}}$ of steel and is inversely proportional to the yield strain $\sigma_{\text{т}}/E$. Having transformed the numerical constant, (12) we can write in the form:

$$L_{\text{кр}}\big|_{\sigma_{\text{н}}=\sigma_{-1}} = 0{,}7214\frac{\pi\cdot d_z\cdot e_{\text{кр}}}{\varepsilon_{\text{т}}} \quad (12)$$

Using the empirical dependence of the resistance to micro cleavage of grain $R_{\text{Mc}} = \sigma_{\text{в}}/(1-\varphi_{\text{к}}^2)$, which is valid for the group of ferrite-pearlitic low-carbon steels, we find the average grain diameter:

$$d_z = [5{,}7(1-\varphi_{\text{к}}^2)/\sigma_{\text{в}}]^2. \quad (13)$$

Here, $\sigma_{\text{в}}$ is tensile strength of steel. Substituting d_z in (13), we can obtain the desired simple formula for estimating $L_{\text{кр}}$, which includes only the key characteristics of the material.

To calculate the endurance limit of a symmetric cycle, it is sufficient to equate (12) to (1). To find K_{1c}, we use the conclusion obtained in [7]. The final formula for calculating K_{1c} under the conditions of plane deformation at the crack tip, with mathematical rigor, has the form:

$$K_{1c} = \sqrt{\frac{\pi\,0{,}618\,d_z}{[\sigma_{\text{т}}{}^{1/m-1}\cdot(1-2\mu)^2\,]/2}\left(\frac{R_{Mce}\cdot D}{q}\right)^{1/m+1}} \quad (14)$$

Here, R_{Mce} is resistance to micro cleavage of deformed metal, which for the class of ferrite-pearlitic steels $R_{Mce} = 1.618R_{Mc}$; R_{Mc} is resistance to micro cleavage of ferrite grain; m is the coefficient (indicator) of the power-law hardening of the material; q is the overvoltage factor equal for this case $1 - 2D/\sqrt{3}$; μ is Poisson's ratio. D is the coefficient that takes into account the increase in the first principal e $(1 + m)(1 - 2\mu)/2$.

The resistance of grain micro cleavage is calculated according to the classical relationship $R_{Mc} = 5.7/\sqrt{d_z}$ for cleavage of ferrite or ferrite-pearlite grains. Substituting (15) with all components from (12) into (1), we obtain the final value of the fatigue limit depending on the standard set of mechanical characteristics of the material and the average grain diameter:

$$\sigma_{-1} = \sqrt{\frac{1{,}091\left(\frac{4{,}611\cdot(1-2\mu)(m+1)}{\sqrt{d_z}}\right)^{1/m+1}\cdot\sigma_т{}^{2-1/m}}{E(2\mu-1)^2\cdot e_{кр}\left(\frac{\sqrt{3}\cdot(2\mu-1)(m+1)}{3}+1\right)^{1/m+1}}} \qquad (15)$$

If the value of the average grain diameter d_z is unknown, it can be calculated using (14).

The results of numerical testing of the endurance limit show that the dependence (16) is “sensitive” to some characteristics of the material. For example, varying the value of Poisson's ratio in hundredths can change the result by $\sqrt{2}$ times. Probably, such an error in calculations is associated with the unique features of the models used and the assumptions made when deriving (16).

Let us check the adequacy of the proposed analytical model through the example of a group of ferrite-pearlitic steels (Table 1).

Table 1

Basic experimental and calculated characteristics of steels

Steel grade	$\sigma_т, MPaa$	$\sigma_в, MPa$	μ	m	$\varphi_к$	$d_з, \mu m$	K_{1c}, MPa	σ_{-1}, MPa
10 steel	190	320	0.3	0.17	0.73	66	103.6	135.4[1]
St3sp	270	450	0.3	0.16	0.71	37	101	192[1]
22K	310	540	0.3	0.16	0.69	30	97	220[1]
50 steel	350	680	0.3	0.16	0.62	25	78	247[1]
37KHN3A	743	1014	0.26	0.12	0.6	14[3]	73	480[1]
15G	280	490	0.29	0.156[1]	0.65	45[4]	–	230
09G2	300	440	0.29	0.16	0.69	33	–	235
30KHGSA	1360	1750	0.26	0.13[2]	0.44	7[4]	–	490
16G2AF	417	600	0.29	0.16	0.5	22	–	255
10KHSND	390	540	0.29	0.132[2]	0.71	27[4]	–	284

[1] Values obtained by calculation [7].

[2] Dependency calculation $m = \{0.75 \cdot lg[\sigma_в(1 + 1.4\varphi_к)/\sigma_{0,2}]\}/lg\left[10^5 \cdot ln\left(\frac{1}{1-\varphi_к}\right)/(200 + 0.5\sigma_{0,2})\right]$ [2].

[3] Calculated from the data on the resistance of micro-cleavage of an undeformed material.

[4] Dependency calculation (14).

To compare the results obtained by (12), we find the critical crack lengths from the experimental data and with account for the formula (1). The endurance limits are calculated under the condition of plane deformation by the method [7], which considers the average grain diameter, the hardening rate m and other mechanical characteristics that significantly affect the endurance limit.

Fig. 4 *a* shows the values of the critical lengths of through-cracks at the fatigue limit for steels with different yield strengths. The calculated values according to (12) are compared to the experimental data. The comparison has shown a reasonably good agreement for ferrite-pearlitic steels of different strength, despite the numerous assumptions made (Fig.4 *b*).

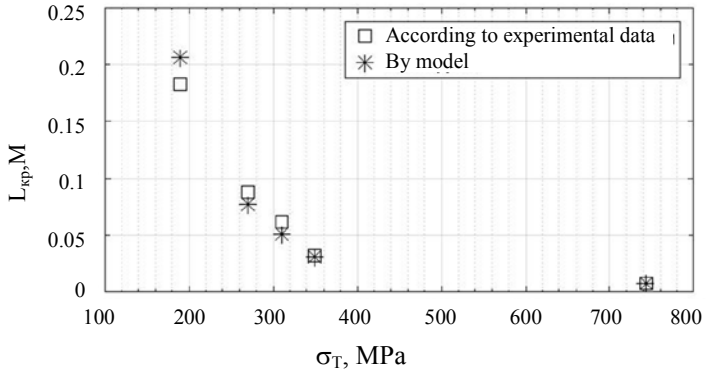

a)

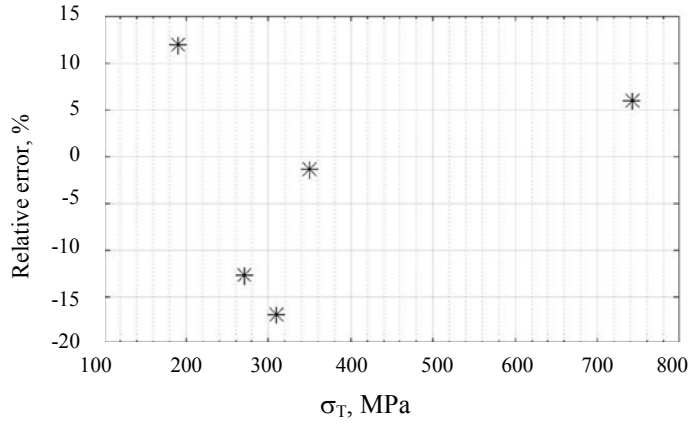

b)

Fig. 4. Values of critical crack lengths of steels depending on yield point (*a*), and relative error of the model (*b*)

Fig. 5 shows the results of comparing the fatigue limit of a symmetric cycle according to (16) for a group of steels (Table 1) to the experimental and known calculated values.

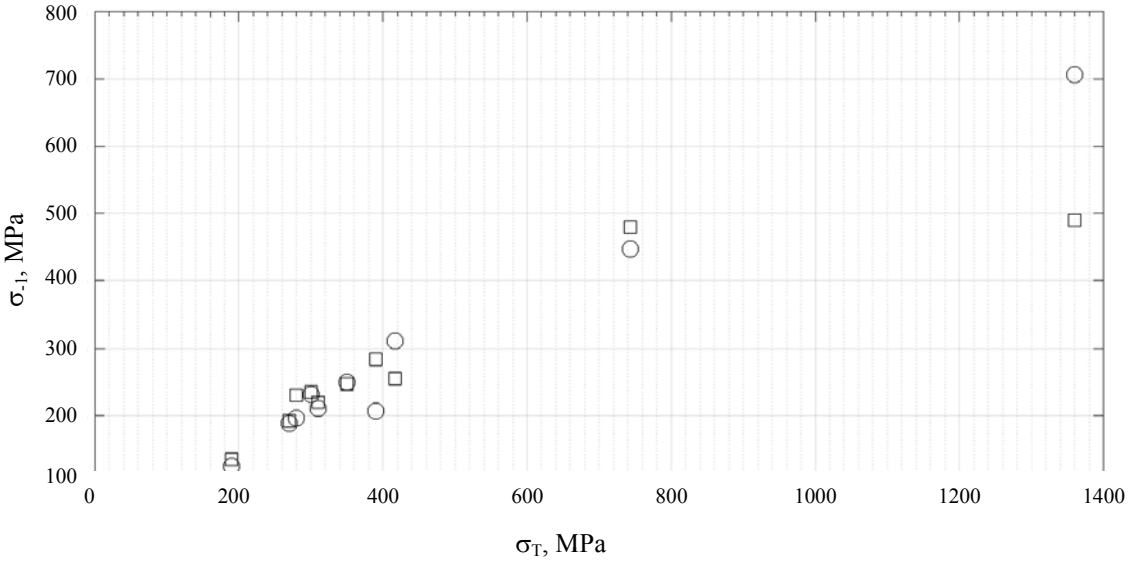

Fig. 5. Comparison of endurance limits of symmetric cycle and yield strength: ○ is calculation according to the model (16); □ is known data (Table 1)

Based on the comparative analysis results, conclusions can be drawn.

1. The stronger the steel, the more the "sensitivity" (16) affects the initial data, and the calculation error grows.

2. For ferrite-pearlite steels with $\sigma_т < 400$ MPa, the results of calculating the fatigue limits are in satisfactory agreement with the initial data in Table 1.

The dependence (16) has high "sensitivity" to some initial parameters, so, at this stage of the study, it is

impossible to more accurately assess the results.

When the crack length approaches the critical value $L_{кр}$, it starts to grow stepwise. Therefore, the deterministic model cannot accurately determine the number of cycles after which this crack propagation will end and it will propagate at the speed of sound. The average grain diameter of a material can vary significantly in areas of welded structures, for example, in the HAZ and the material that is not affected by welding.

It should be noted that the stage of the macrocrack development in air for elements of large-sized parts without stress concentrators takes almost 20% in time.

In this regard, when determining $L_{кр}$, the relative error up to ~15% can be considered a positive result. The period of the so-called "cyclic breakdown" [11] falls within the framework of this error, where for low cyclic fatigue stresses, ~1/10 a part of the residual life corresponds to an increase in the crack length about two fold.

Thus, the analytical dependences proposed on the basis of the structural-deformation analysis criteria can be used in calculating the endurance limit of the ship and other large-sized structures.

Discussion and Conclusions. A safe operation of ships requires up-to-date and adequate information on the condition of the hull structures including metallurgical defects and structural stress concentrators. It is important to assess the residual life and, accordingly, to determine the critical dimensions of fatigue cracks. At the top of a critical developing macrocrack under stresses corresponding to the endurance limit, one-sided plastic deformation, which reduces the plasticity of the highly fragmented zone, is accumulated. At the same time, the number of residual life cycles remains insignificant and strongly depends on the yield point, defects, grain diameter of the steel of the structure in which the crack develops.

The study results show that under stresses corresponding to the endurance limit of steel, the rates of the critical crack opening of the tip and the edges approach. Energetically, this moment corresponds approximately to the transition of the crack to an unstable state. The accumulation of one-sided plastic deformations causes the limiting state of plasticity of the region adjacent to the crack tip and its avalanche-like or sharply accelerated motion. This critical area is related to the material grain diameter, critical plasticity characteristic and critical opening at the crack tip at the fatigue limit.

The analytical dependences obtained allow us, with account for the average grain diameter of ferrite-pearlite steel and critical narrowing, to calculate the endurance limit of the most dangerous loading cycle according to the classic Griffith relationship between the crack length, stresses and the stress intensity factor.

The proposed mathematical model and the approach based on structural-deformation analysis criteria can be used in engineering calculations of machine-building, ship structures and their connections to assess the service life.

References

1. Kazanov GT, Novikov VV, Turmov GP. Kontsentratsiya napryazhenii i drugie osobennosti napryazhennogo sostoyaniya sudovykh korpusnykh konstruktsii [Stress concentration and other features of the stress state of ship hull structures]. Vladivostok: Izd-vo DVFU; 2014. 178 p. (In Russ.)

2. Kazanov GT, Novikov VV, Turmov GP. Osnovy raschetnogo proektirovaniya svarnykh konstruktsii. Tom 1. Napryazhennoe sostoyanie i osnovy konstruirovaniya [Fundamentals of computational design of welded structures. Vol. 1. Stress State and Design Basics]. Vladivostok: Izd-vo DVFU; 2019. 204 p. (In Russ.)

3. Yamaleev KM, Gumerova LR. Strukturnye aspekty razrusheniya metalla nefteprovodov [Structural aspects of the metal destruction of the oil pipelines]. Ufa: Gilem; 2011. 144 p. (In Russ.)

4. Jordan C, Cochran C. In-Service Performance of Structural Details. Washington: Ship Structure Committee; 1978. 188 p.

5. Akita Y. Statistical Trend of Ship Hall Failure. In: Proc. 2nd International Symposium on Practical Design in Shipbuilding in Tokyo and Seoul, October 17–22, PRADS, 83. Tokyo: Society of Naval Architects of Japan; 1983. P. 619–624.

6. Novikov VV, Turmov GP, Surov OEh, et al. Povrezhdeniya i raschetnyi analiz prochnosti korabel'nykh konstruktsii [Damage and design analysis of the strength of ship structures]. Vladivostok: Izd-vo DVFU; 2020. 266 p. (In Russ.)

7. Matokhin GV, Gorbachev KP. Osnovy raschetnykh metodov lineinoi mekhaniki razrusheniya [Fundamentals of computational methods of linear fracture mechanics]. Vladivostok: Izd-vo DVGTU; 2008. 304 p. (In Russ.)

8. Molokov KA. Otsenka vynoslivosti svarnykh soedinenii s uchetom obshchego plasticheskogo deformirovaniya materiala pri ploskom napryazhennom sostoyanii [Evaluation of the fatigue limit of welded joints, taking into account the total plastic deformation of the material in the state of plane stress]. FEFU: School of Engineering Bulletin. 2019;1(38):19–26. (In Russ.)

9. Faivisovich AV, Bereza IG. Kinetika geometrii makrotreshchiny [Kinetics of macrocrack geometry]. Ehkspluatatsiya morskogo transporta. 2019;1(90):77–83. (In Russ.)

10. Fedotov SN. Kvazikhrupkoe razrushenie kak razrushenie ierarkhicheskoi struktury [Quasi-brittle fracture as failure of hierarchical structure]. Physical Mesomechanics. 2015;18(6):24–31. (In Russ.)

11. Terent'ev VF, Korableva SA. Ustalost' metallov [Fatigue of metals]. Moscow: Nauka; 2015. 479 p. (In Russ.)

12. Ivanova VS. Sinergetika i fraktaly. Universal'nost' mekhanicheskogo povedeniya materialov [Synergetics and fractals. Versatility of mechanical behavior of materials]. Ufa: Izd-vo UGNTU; 1998. 363 p. (In Russ.)

13. Ivanova VS, Terent'ev VF. Priroda ustalosti metallov [Nature of metal fatigue]. Moscow: Metallurgiya; 1975. 454 p. (In Russ.)

14. Krokha VA. Uprochnenie metallov pri kholodnoi plasticheskoi deformatsii [Hardening of metals during cold plastic deformation]. Moscow: Mashinostroenie; 1980. 157 p. (In Russ.)

15. Sergisen SS, Shneidorovich RM, Makhutov NA, et al. Polya deformatsii pri malotsiklovom nagruzhenii [Deformation fields under low-cycle loading]. Moscow: Nauka; 1979. 277 p. (In Russ.)

16. Kurkin SA. Prochnost' svarnykh tonkostennykh sosudov, rabotayushchikh pod davleniem [Strength of welded thin-walled pressure vessels]. Moscow: Mashinostroenie; 1976. 184 p. (In Russ.)

17. Glezer AM. (ed.) Osnovy plasticheskoi deformatsii nanostrukturnykh materialov [Fundamentals of plastic deformation of nanostructured materials]. Moscow: Fizmatlit; 2016. 304 p. (In Russ.)

18. Smirnov AN, Murav'ev VV, Ababkov NV. Razrushenie i diagnostika metallov [Destruction and diagnostics of metals]. Moscow; Kemerovo: Innovatsionnoe mashinostroenie; 2016. 479 p. (In Russ.)

Submitted 20.04.2020
Scheduled in the issue 01.07.2020

About the Authors:

Molokov, Konstantin A., associate professor of the Welding Engineering Department, School of Engineering, Far Eastern Federal University (8, Sukhanova St., Vladivostok, 690090, RF), Cand.Sci. (Eng.), ResearcherID AAH-6348-2019, ORCID: https://orcid.org/0000-0002-9764-9329, ScopusID: 57197836777, Spektrum011277@gmail.com.

Novikov, Valerii V., associate professor of the Shipbuilding and Ocean Engineering Department, School of Engineering, Far Eastern Federal University (8, Sukhanova St., Vladivostok, 690090, RF), Cand.Sci. (Eng.), ORCID: https://orcid.org/0000-0001-5892-815X, ScopusID: 5641710410, leka1551@rambler.ru.

German, Andrei P., associate professor of the Shipbuilding and Ocean Engineering Department, School of Engineering, Far Eastern Federal University (8, Sukhanova St., Vladivostok, 690090, RF), ResearcherID D-1725-2014, ORCID: https://orcid.org/0000-0002-9530-5258, ScopusID: 56417290300, gerand1@yandex.ru.

Claimed contributorship

K. A. Molokov: basic concept formulation; research objectives and tasks setting; computational analysis; text preparation; formulation of conclusions. V. V. Novikov: academic advising; analysis of the research results; finalization of conclusions; the text revision. A. P. German: work with sources; the text correction; execution and preparation of supporting papers.

All authors have read and approved the final manuscript.

MACHINE BUILDING AND MACHINE SCIENCE

UDC 621.01 https://doi.org/10.23947/2687-1653-2020-20-3-235-242

Formation of surface layer quality under abrasive treatment of polymer-composite materials

M. A. Tamarkin, E. E. Tishchenko, A. V. Verchenko, V. M. Troitsky
Don State Technical University (Rostov-on-Don, Russian Federation)

Introduction. The study results of the abrasive processing of parts made of polymer-composite materials are presented. The features of processing polymer composites and the technology of preforming through waterjet cutting are described. The stages of preparation of a part made of polymer-composite material for the "glueing" operation are investigated.

Materials and Methods. Dependences for determining the surface roughness under waterjet cutting of polymer-composite material are considered. Research is carried out to achieve the required surface roughness under adhesive bonding of workpieces. The dependence is given that describes the roughness that is required for a reliable adhesive bond.

Results. The theoretical and experimental studies of the waterjet cutting process are resulted. Their implementation technique, the tool and equipment used are described. The results of theoretical and experimental studies are compared. Their high convergence is established. The results of experimental studies on the preparation of parts made of polymer-composite materials for glueing are shown. The abrasive tools and processing modes are selected.

Discussions and Conclusions. The process design procedure of abrasive treatment of workpieces from polymer-composite materials is proposed.

Keywords: treatment of polymer composites, waterjet cutting, treatment by petal wheels, surface roughness.

For citation: M. A. Tamarkin, E. E. Tishchenko, A. V. Verchenko, et al. Formation of surface layer quality under abrasive treatment of polymer-composite materials. Advanced Engineering Research, 2020, vol. 20, no. 3, p. 235−242. https://doi.org/10.23947/2687-1653-2020-20-3-235-242

Introduction. Increase in labor productivity in modern engineering production is possible through the use of new technologies and materials. For the manufacture of machine parts, polymer composite materials (PCM) are increasingly used. This is a composition of two or more materials, a base and a binder. Compared to metal products, products made of polymer composites have better physical and mechanical properties and, as a rule, weigh much less. The anisotropic structure of the polymer composite material allows the workload to be distributed throughout the product structure, which increases its performance properties. PCM is formed in a certain way. The base layers are laid in directions mutually opposite to each other. And the binder plays the role of filler, that is, it provides immobility and filling the space between the base layers. A special layer, formed by a hardened binder, is created on the surface of the polymer composite.

This layer may not match the ideal surface shape. Its adhesion properties provide:

— substances that are on the workpiece surface and contain a hardener,

— chemical reaction products occurring during curing.

The anti-adhesive layer of the polymer composite should be removed through mechanical treatment. This provides optimum surface roughness of the machined part. Mechanical processing of PCM has a number of features:

— delamination occurs,

— fibers close to the processing site loosen,

— a large amount of heat is generated during cutting,

— burns are formed,

— the material is destroyed.-.

In this case, it is not always possible to use lubricating coolants since their effect causes delamination, swelling, and the PCM loses the required physical and mechanical properties. This is due to the fact that polymer composites absorb moisture abundantly. The use of fluid in PCM processing requires further study.

At the majority of enterprises where parts are made from polymer composites, the technological process consists of cutting a sheet and further machining the workpiece. Polymer-composite parts are often glued together, which requires careful preparation of the surface layer. Within the framework of this work, the formation of surface quality under waterjet cutting of PCM, as well as during preparation of the surface for further bonding is studied.

Materials and Methods. In modern mechanical engineering, cutting of materials through water-jet cutting is on rise. Its advantages are as follows: a wide variety of processed materials, high productivity, good quality of the cut surface and the ability to obtain profiled surfaces. When using this method, significant internal stresses do not arise due to the low-temperature nature of the process.

In addition, waterjet cutting is characterized by a small allowance and high cutting accuracy. This is in contrast to edge cutting and fixed-abrasive machining. The process of cutting a material with water jet is rather complicated, underexplored. Its result is influenced by many technological factors: jet velocity, jet travel speed along the part, characteristics of the abrasive powder, distance from the jet to the surface to be treated, as well as physical and mechanical properties of the processed polymer composite materials. Some difficulties arise when designing cutting technology. They are primarily associated with the selection of optimal cutting conditions: it is necessary to provide the given workpiece surface quality under the lowest processing costs. The use of waterjet cutting for PCM processing also requires a study of the effect of water on the state of the cut surface. Preliminary investigations have allowed establishing the power of the energy of a supersonic jet of water with an abrasive. It is so great that when it interacts with the surface to be treated, destruction is comparable in intensity to damage from a hard abrasive tool. Under cutting, water does not deviate from the motion trajectory, the effect on the workpiece material is minimal, i.e. water is not absorbed [1–4].

As you know, under deep cutting of materials (including polymer composites) in the contact zone of the abrasive jet and the cut material, two clearly traceable zones appear:

— with low surface roughness (smooth cut zone),

— with higher roughness (wavy cut zone) [1, 2].

Their occurrence is due to the fact that, upon contact of the jet with the lower part of the cut, the angle of attack of the embedded particles grows. A significant number of them do not participate in an effective collision and are reflected from the material. In this case, new interacting particles encounter an obstacle, are reflected and cause blocking of particles entering the treatment zone. The result is a wavy cut zone with high surface roughness. In the upper part of the cut, there is nothing to prevent particles from collision; therefore, a smoother surface with lower roughness is formed. Under present-day conditions, when designing technological processes for waterjet cutting, it is difficult to determine not only the surface roughness of various cutting zones, but also the dimensions of the smooth and wavy cutting zones. The forecast of obtaining the required roughness at the stage of technology design will provide determining the feasibility of finishing and the required allowances in this case.

Theoretical studies of the formation of the roughness profile of various cutting zones of the PCM clearly show regularities that describe the abrasive particle - workpiece surface interaction process. It has been established that the cut surface roughness depends on the process parameters of the treatment. The cut layer of the material is conventionally divided into two cutting zones: wavy and smooth. The mechanism of the formation of these zones is described. The range of penetration depths of particles is specified [1–2]:

$$h_{\max} = DK_L \sin\alpha \sqrt{\frac{2P_{дин}\rho_ч}{3c\rho_{см}k_s\sigma_s}}, \quad (1)$$

where $\rho_ч$ is particle material density; k_s is the coefficient that considers the effect of the workpiece surface roughness on the real contact area; K is the volume concentration of particles in the process fluid; $P_{дин}$ is dynamic pressure of the mixture; $\rho_{см}$ is the density of the working mixture of liquid and particles; σ_s is the yield point of the workpiece material; D is the particle diameter; K_L is the coefficient of energy losses to overcome the distance from the jet to the workpiece surface; c is the bearing capacity factor of the contact surface; α is the impact angle of an abrasive particle with a processed surface.

Let us describe the flow of abrasive particles as an event stream corresponding to the Poisson distribution: the particles of the medium perform microcutting in a fixed time interval, which does not depend either on its origin or on possible realizations of previous or subsequent similar acts. The parameter λ in Poisson's law is the intensity of the flow of events. Let us assume for waterjet cutting that λ is the number of possible interactions per unit time on the square of the abrasive particles packing. Then, $\sqrt{\lambda}$ particles will pass through each side of the packing square 2*R,* and $\frac{L_{ед}}{2R}$ particles will pass through the unit length. With this in view, a formula has been proposed that provides the determination of the arithmetic mean deviation of the profile of the steady-state surface roughness under the waterjet cutting of PCM [1, 2]:

$$Ra = 13.01K_\alpha^{Ra} \cdot R\sqrt{K_L \cdot \sin\alpha \cdot \sqrt{\frac{P_{дин} \cdot \rho_ч}{\lambda \cdot c \cdot \rho_{см} \cdot k_S \cdot \sigma_S}}}, \quad (2)$$

where K_α^{Ra} is the coefficient considering the abrasive particles – workpiece surface impact angle; R is the average radius of particles.

The number of effective interactions λ functionally depends on the amount of feed, the pressure of the abrasive jet, and the depth of roughness measurement $\lambda = f(S, Q, h)$. A theoretical description of the value λ is difficult. Therefore, λ has been determined on the basis of experimental studies, which made it possible to propose a set of regression dependences.

The experiments were carried out on the basis of the Rostvertol, Russian Helicopters JSC. A *Flow* 5-axis waterjet cutting machine was used. Garnet was used as an abrasive medium. The samples were made of VPS-7 fiberglass reinforced with titanium foil (OT4-0-0.1 × 220 marking). This fiberglass is used at Rostvertol for full-scale parts of Mi-28 helicopter.

Surface roughness was measured using a *Surtronic* 25 digital profilometer from *Taylor Hobson*. The effect of water on PCM cutting was investigated on a *NETZSCH* DSC 200 F3 *Maia* differential scanning calorimeter. The results were processed by the method of mathematical statistics in the *MathCad* program.

Research Results. The cut surface roughness grows with the jet rate increase. At the same time, the relative height of the wavy cut zone increases. The intervals of surface roughness values and processing modes required for waterjet cutting of PCM with specified properties are determined. When studying the influence of the jet feed, its speed was varied in the range from 5 to 480 mm/min. The material is characterized by a layered structure and anisotropy. In this regard, the cut surface roughness was measured in two directions: perpendicular to the feed and along it.

The experimental results analysis of the waterjet cutting process allows obtaining models of the cut surface formation:

— one-factor that describes the change in roughness across the cut section;

— two-factor – for calculating the change in roughness along the cut section and varying the depth of roughness measurement (4) based on the regression analysis:

$$Ra = 3,538 \cdot 10^{-6} + 4,721 \cdot 10^{-6} \cdot S, \quad (3)$$

$$Ra = 2.706 \cdot 10^{-13} \cdot S \cdot h - 3.157 \cdot 10^{-10} \cdot h + 1.886 \cdot 10^{-8} \cdot h^2 - \\ - 3.062 \cdot 10^{-7} \cdot h - 1.301 \cdot 10^{-10} \cdot S \cdot h + 1.469 \cdot 10^{-12} \cdot S^2 \cdot h + \\ + 4.288 \cdot 10^{-6} + 1.324 \cdot 10^{-8} \cdot S - 5.142 \cdot 10^{-11} \cdot S^2 + 7.308 \cdot 10^{-14} \cdot S^3. \quad (4)$$

The effect of water on the thermophysical properties of a polymer composite under the waterjet cutting has been studied. The investigation was carried out by the method of differential scanning calorimetry. As a result, the possibility of using this processing technique for cutting parts from PCM was established.

The cut surface roughness was determined using a theoretical model (2) and was compared with the results obtained experimentally. It is found that the discrepancy does not exceed 15%. This indicates that the resulting set of theoretical models can be used in the technological design of processing parts from PCM.

At many machine-building enterprises, manual processing with coated abrasive is used to prepare the surface for gluing (GOST 13344-79, GOST 5009-82 and GOST 10054-82). As a rule, the sample is sanded to gloss remove, which cleans a thin layer of binder from the part and does not damage the fibers. At the same time, the manual labor content is very high, and the costs for it are high. The coated abrasive wears out quickly and has to be replaced. In addition, the quality of sanding depends directly on the qualifications of the employee, his ability to create a certain pressing force and remove the surface layer without destroying the fibers of the composite [4–8]. It is required to reduce the labor content of the operation in question, to eliminate hand work while maintaining the quality of processing. In this regard, two approaches to solving the problem have been proposed. The first one is based on a comprehensive study of the processes of providing the roughness specified for PCM parts. It is assumed that the resulting roughness will provide adhesion strength without having to be limited by the minimum possible roughness. You can select a tool for mechanizing the processing of PCM parts. Such studies were carried out at Rostvertol with full-scale parts made of polymer-composite materials. The processing with grinding elastic tools, which provides mechanizing the process, was considered. The grains move in the direction of the normal component of the cutting force reducing the intensity of the heat flux and increasing the tool life [7]. A feature of this process is the absence of microcracks typical for processing with a hard grinding tool [8]. In addition, lack of the required rigidity is characteristic of many PCM parts: casings, shells, caps, etc. For their processing, it is much more reasonable to use an elastic grinding tool. Due to its elastic properties, such a tool (in contrast to a tool on a rigid base) quenches vibrations and oscillations, and also absorbs shocks under processing [4–8]. The hygroscopicity of polymer composite materials makes it difficult or does not allow the use of a coolant during processing. A flexible abrasive tool is well suited for such cases. It provides high quality grinding without cooling and without wetting the workpiece surface.

The formation of the surface quality of a PCM part intended for further bonding is theoretically investigated.

When calculating the surface roughness parameters, the technique developed by Prof. A.V. Korolev [9] was applied. It is used to describe the formation of a roughness profile when machining with a rigidly bound abrasive:

$$Ra = 0.9\sqrt{\frac{t_c \cdot v_S \cdot l_\phi^3 \cdot L_{e\partial}}{60 \cdot v_K \cdot L_K}}, \quad (5)$$

where t_c is the thickness of the material layer removed in one pass; v_s is the feed rate; $l_ф$ is the actual distance between the contact grains; $L_{ед}$ is the width of the treated area; $v_к$ is the wheel speed; $L_к$ is the total length of the petals.

To check the adequacy of the dependence obtained, a set of experiments was carried out to prepare polymer-composite parts for further bonding. Specimens made of VPS-7 fiberglass, having a significant area (80 × 200 mm), were processed by flexible abrasive flap wheels from *Klingspor* (MM 630 model with dissected lamellae, Fig. 1).

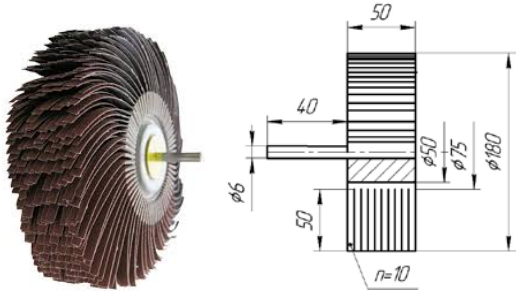

Fig. 1. Scheme of abrasive flap disc from *Klingspor* (MM 630 model): diameter is 180 mm, width is 50 mm, abrasive material is electrocorundum, binding material is synthetic resin

The sanding pads are fixed on a mandrel with a diameter of 6 mm and are cut in the radial direction into ten equal segments, which, in turn, are wrapped in the same direction. The length of such a segment is 50 mm. The tool has high elasticity and can be made of abrasive materials of various grain sizes.

The stability of the processing modes is achieved by the constancy of the centrifugal and elastic forces created by the sanding cloth petals. The quality of the surface layer of the processed parts is significantly affected by the feed rate and the specific pressure of the petals. Also of great importance is the dynamic radius of the wheel $r_Д$, the distance from its axis to the contact surface of the petal with the workpiece [7, 9].

The grinding wheel selected in this way was fixed in the spindle of the vertical mill. The wheel rotation speed was 450–1400 rpm, the feed was 100–800 mm/min. The dynamic radius was chosen from the sizes: 55 mm, 60 mm, 65 mm, which created a different contact area of the petals with the workpiece surface. The samples were fixed on the machine in a special device.

The experiments have proven the possibility of obtaining a uniform matte surface, devoid of gloss, using flexible petal discs. After processing, the integrity of the fibers was not compromised. The surface roughness of the samples was measured on a *Tailor Hobson* profilometer. For the above modes, the arithmetic mean value of the roughness Ra = 1.22 μm was obtained (Fig. 2).

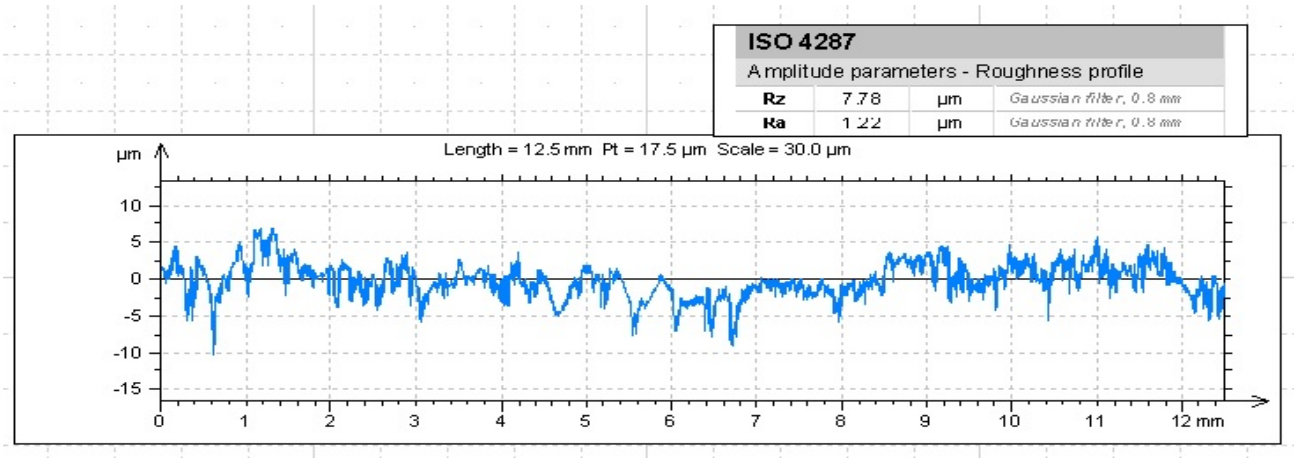

Fig. 2. Profilogram of the sample surface processed by the flap wheel: rotation speed is 1400 rpm, feed is 315 mm/min, and dynamic radius of the circle ($r_Д$) is 55 mm

As a result of the experiments on processing PCM samples with flexible petal wheels, a uniform matte surface devoid of gloss was obtained. In this case, the integrity of the fibers is not compromised. The finished surface was examined, and the roughness was measured on a *Tailor Hobson* profilometer. The roughness Ra = 1.22 μm was obtained under the selected processing modes, which is shown on the profilogram (Fig. 2).

Statistical processing of the experimental data has shown their high convergence with the results of theoretical calculations.

Discussion and Conclusion. The issues of design and optimization of the PCM waterjet cutting processes and preparation of their surface for gluing are considered. A technique has been developed that takes into account the specified roughness of the cut surface and the surface to be glued and provides the minimum cost of the product [1, 2, 10–13]. The cut surface roughness e is calculated from the formula (2). Taking into account the initial processing parameters ($P_{дин}$, R, $\rho_ч$, h, L, S, Q), the number of effective collisions λ is calculated. Then the roughness value Ra is determined. Variants of technological processes, in which the condition $Ra \le Ra_{зад}$ is not met, are eliminated, and the cost of the cut is calculated. The combination of processing parameters is considered optimal, at which the cost of the cut will be minimal.

Designing the preparation of a PCM part for gluing starts with a technological assessment of the part design and the glued joint in which this part is involved. For each type of adhesive and of adhesive bond to be made, the developer should indicate the required roughness class of the surface to be bonded. Taking this into account, the technologist chooses the grain size of the grinding tool and processing modes. The resulting PCM part surface should be

homogeneous and uniformly processed over the entire bonding surface. The machining quality describes the arithmetic mean deviation of the roughness profile *Ra*. Measurements of this parameter are carried out using a probe-type profilometer. At this, a correct assignment of processing modes and an adequate tool selection provide the required surface roughness.

The part, whose surface is being prepared for gluing, should be cleaned and free from residues of crimping materials (separating materials, vacuum bag materials, sealants, etc.). Technological allowances that are not needed in subsequent operations are removed. The sanded surface is visually checked for runs, pebbles and other defects to be removed.

The roughness, which will provide the required strength of the adhesive bond, is determined. Depending on it, the grain size of the abrasive wheel is selected. To process thin-walled products with insufficient rigidity when preparing their surfaces for bonding, it is recommended to use grinding wheels of 240, 220, 180 and 150 grit according to FEPA (Federation of the European Producers of Abrasives).

To process PCM parts with a thickish surface epoxy layer (0.01 mm or more), the grain size 40, 80, 100, 120 (according to FEPA) is suitable. For sanding runs, pebbles, gradients, etc., with simultaneous preparation of the surface for bonding, it is recommended to use flap discs with grain size 80, 100, 120 (according to FEPA). The productivity of this process is increased (when compared to the use of wheels with smaller grit).

Processing modes are selected. Based on the surface area to be sanded, the number of tool passes is calculated. Separately, it should be mentioned about the odd-shaped parts with surfaces located at an angle, with spherical radii and curved sections of structural components. They are processed first and only then you move on to flat areas. Parts with curved surfaces can be treated on high-end machine tools and software-controlled installations. In this case, the tool moves in accordance with the control program, and its path follows the theoretical contour of the part.

Table 1 gives recommendations on the selection of processing modes for parts made of fiberglass, which will be glued further on. The equipment is flap discs from *Klingspor*. The grinding process parameters that provide the required roughness are as follows: wheel rotation speed n (rpm), feed S (mm/min) and $r_Д$ (mm).

Table 1

Recommendations for selection of cutting conditions for final abrasive processing of PCM parts

Required roughness	Material grain size		*Rc**, mm	*S*, mm/min	*n*, rpm
	of petal wheel, recommended by FEPA	of abrasive according to GOST 3647-80			
4.5–5.0	P40	40	55	200–350	1400–1600
4.2–4.5	P80	20	55	200–350	1400–1600
3.7–4.2	P100	16	55	200–350	1400–1600
3.0–3.7	P120	12	50	200–400	1100–1400
2.6–3.0	P150	10	50	200–400	1100–1400
1.6–2.5	P180	8	50	200–400	1100–1400
1.2–1.6	P220	6	48	200–350	1100–1200
1.0–1.2	P240	5; M63	48	350–500	1100–1200
0.6–1.0	P320	5; M50	46	350–500	1100–1200
**Rc* is specified for petal wheels of the model considered in this study.					

After finishing the treatment, the workpiece surface is cleaned of sanding products using a clean cotton cloth or a sweep brush with soft bristles. In this case, fiberglass dust should not rise into the air.

Visual inspection will reveal untreated areas (gloss on the surface), as well as exposure and destruction of polymer composite fibers.

References

1. Tamarkin MA, Verchenko AV, Kishko AA. Povyshenie kachestva gidroabrazivnoi rezki detalei iz aviatsionnykh materialov [Improving the quality of waterjet cutting of parts made of aircraft materials]. Vestnik of P. A. Solovyov Rybinsk State Aviation Technical University. 2017;2(41):88–96. (In Russ.)
2. Verchenko AV, Tamarkin MA, Kishko AA. Issledovanie sherokhovatosti poverkhnosti reza pri gidroabrazivnoi rezke [Cut face roughness analysis under waterjet cutting]. Vestnik of DSTU. 2017;17(2):116–130. DOI: https://doi.org/10.23947/1992-5980-2017-17-2-116-130. (In Russ.)
3. Shchegolev VA, Ulanova ME. Ehlastichnye abrazivnye i almaznye instrumenty (teoriya, konstruktsiya, primenenie) [Elastic abrasive and diamond tools (theory, design, application)]. Leningrad: Mashinostroenie; 1977. 184 p. (In Russ.)
4. Novoselov YuK. Dinamika formirovaniya poverkhnostei pri abrazivnoi obrabotke [Dynamics of surface formation under abrasive processing]. Sevastopol: Izd-vo SeVNTU; 2012. 304 p. (In Russ.)
5. Gdalevich AI. Finishnaya obrabotka lepestkovymi krugami [Finishing with flap wheels]. Moscow: Mashinostroenie; 1990. 112 p. (In Russ.)
6. Kozul'ko NV. Mekhanizatsiya abrazivnoi obrabotki detalei iz polimernykh kompozitnykh materialov pod operatsiyu «skleivanie» [Abrasive processing mechanization of parts from polymeric composite materials for paste operation]. Vestnik of DSTU. 2018;18(2):179–189. DOI: https://doi.org/10.23947/1992-5980-2018-18-2-179-189. (In Russ.)
7. Kozul'ko NV, Seminichenko KV. Issledovanie protsessa okonchatel'noi abrazivnoi obrabotki detalei iz polimernykh kompozitsionnykh materialov (PKM) [Research of process of final abrasive processing of details from the polymeric composite materials (PCM)]. Scientific and Technical Volga region Bulletin. 2019;1:55–59. (In Russ.)
8. Korolev AV, Novoselov YuK. Teoretiko-veroyatnostnye osnovy abrazivnoi obrabotki [Theoretical and probabilistic foundations of abrasive processing]. Saratov: Izd-vo Saratov. un-ta; 1989. 320 p. (In Russ.)
9. Tamarkin MA, Tishchenko EE, Shvedova AS. Optimization of Dynamic Surface Plastic Deformation in Machining. Russian Engineering Research. 2018;38(9):726–727.
10. Tamarkin MA, Butenko VI, Isaev AN, et al. Optimization of the flat stock cutting process by hydroabrasive jet. MATEC Web of Conferences. 2018;226:232–235. DOI: https://doi.org/10.1051/matecconf/201822601025
11. Hamouda K, Bournine H, Amrou HE, et al. Effect of the velocity of rotation in the process of vibration grinding on the surface state. Materials Science. 2016;52(2):216–221.

Submitted 01.06.2020
Scheduled in the issue 31.08.2020

About the Authors:

Tamarkin, Mikhail A., Head of the Engineering Technology Department, Don State Technical University (1, Gagarin sq., Rostov-on-Don, 344003, RF), Dr.Sci. (Eng.), professor, ORCID: http://orcid.org/0000-0001-9558-8625, Scopus ID 6603762604, tehn_rostov@mail.ru.

Tishchenko, Ehlina Eh., associate professor of the Engineering Technology Department, Don State Technical University (1, Gagarin sq., Rostov-on-Don, 344003, RF), Cand.Sci. (Eng.), associate professor, ORCID: https://orcid.org/0000-0001-5156-5544 , ScopusID: 26640675300, lina_tishenko@mail.ru.

Verchenko, Aleksei V., senior lecturer of the Engineering Technology Department, Don State Technical University (1, Gagarin sq., Rostov-on-Don, 344003, RF), Cand.Sci. (Eng.), ORCID: https://orcid.org/0000-0003-2898-039X, Alex290292@mail.ru.

Troitsky, Viktor M., postgraduate student of the Engineering Technology Department, Don State Technical University (1, Gagarin sq., Rostov-on-Don, 344003, RF), ORCID: https://orcid.org/0000-0002-8545-8816, mihailovich2313@mail.ru.

Claimed contributorship

M. A. Tamarkin: academic advising; formulation of the research objectives and tasks; correction of the conclusions. E. E. Tishchenko: analysis of the research results; text preparation; formulation of conclusions. A. V. Verchenko: formulation of the basic research concept; conducting experiments. V. M. Troitsky: experimentation and computational analysis; the text revision.

All authors have read and approved the final manuscript.

MACHINE BUILDING AND MACHINE SCIENCE

UDC 625.54, 625.57, 621.86 https://doi.org/10.23947/2687-1653-2020-20-3-243-251

Methods of creating and using a digital twin of a mobile transport and transshipment rope complex

I. A. Lagerev[1], V. I. Tarichko[2], A. V. Panfilov[3]

[1] Ivan Petrovsky Bryansk State University (Bryansk, Russian Federation)

[2] Bryansk Automobile Plant JSC (Bryansk, Russian Federation)

[3] Don State Technical University (Rostov-on-Don, Russian Federation)

Introduction. The paper considers the creation and application of digital twins at various stages of the life cycle of mobile transport and transshipment rope complexes (mobile ropeways), the equipment of which is mounted on the basis of wheeled or tracked chassis of high load capacity. The work objective is to improve safety in using such transport systems based on real-time forecasting of potential failures. This will prevent the occurrence of emergencies in a timely manner.

Materials and Methods. The structure of the digital twin of the mobile transport and transshipment rope complex is proposed. Approaches to the analysis of ongoing work processes in order to prevent accidents have been developed. They are based on simulation modeling of the system dynamics using new complex mathematical models built through the system approach.

Results. The developed method was tested on a large-scale layout of a mobile transport and transshipment rope complex created by 3D printing methods. A mathematical model of this system was developed; it was used to construct a digital double of the experimental model. The possibility of predicting failures in the layout is shown experimentally through the example of a rope slipping case. To do this, the actual value of the load suspension point coordinate obtained through the video stream processing method was compared to the predicted value calculated using a digital twin.

Discussion and Conclusions. The research results provide the creation of an industrial digital twin of a mobile transport and transshipment rope complex mounted on cross-country wheeled chassis.

Keywords: ropeway, mobile complex, suspension of load, digital twin, creation, applying.

For citation: I.A. Lagerev, V.I. Tarichko, A.V. Panfilov. Methods of creating and using a digital twin of a mobile transport and transshipment rope complex. Advanced Engineering Research, 2020, vol. 20, no. 3, p. 243−251. https://doi.org/10.23947/2687-1653-2020-20-3-243-251

Funding information: the research is done with the financial support from the Grant of President of the Russian Federation no. МД-422.2020.8 for young Russian scientists — Doctors of Sciences.

Introduction. Concepts for creating a new generation of ropeway transport systems are proposed. These include urban passenger ropeway transport systems based on the “Rope Metro” technology [1, 2], and mobile transport and reloading ropeway complexes (MTRRC) [2-5]. The complex (Fig. 1) represents several base stations of the cable way whose equipment is mounted on mobile chassis.

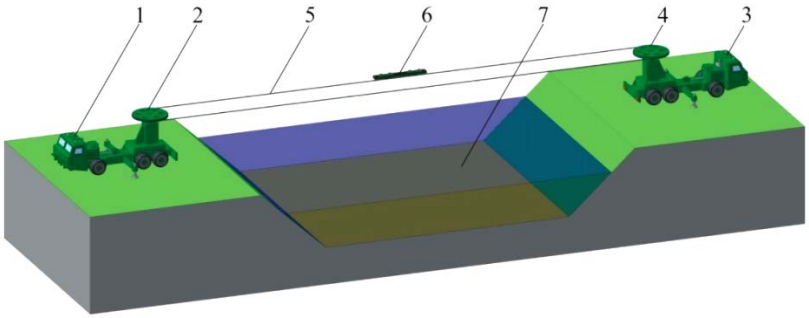

Fig. 1. Conception of mobile transport and reloading cable system [2, 6]:
1 – drive base station on the basis of wheeled chassis; 2 – drive pulley; 3 – non-drive base station; 4 – non-drive pulley with cable rope tensioner; 5 – ring traction and drive rope; 6 – carriage for suspension of cargo; 7 – overcome barrier

For successful implementation of this idea, it is required to develop a scientific basis for studying work processes and design of MTRRC. At the same time, it is necessary to solve scientific and technical problems of providing the overall stability of base stations, installation and tension of the rope system, loading and unloading of the ropeway [2].

In the context of digitalization of the industrial production, it is required to develop high-precision digital twins of the MTRRC, which enable to create effective and globally competitive product samples.

Materials and Methods. Active development of system digital models, which can be considered the prototype of digital twins, started with the introduction of computer-aided design systems that support the basic stages of the life cycle of an industrial product. The relationship between the stages of the life cycle and the main types of computer-aided design systems is widely known (Fig. 2) [7].

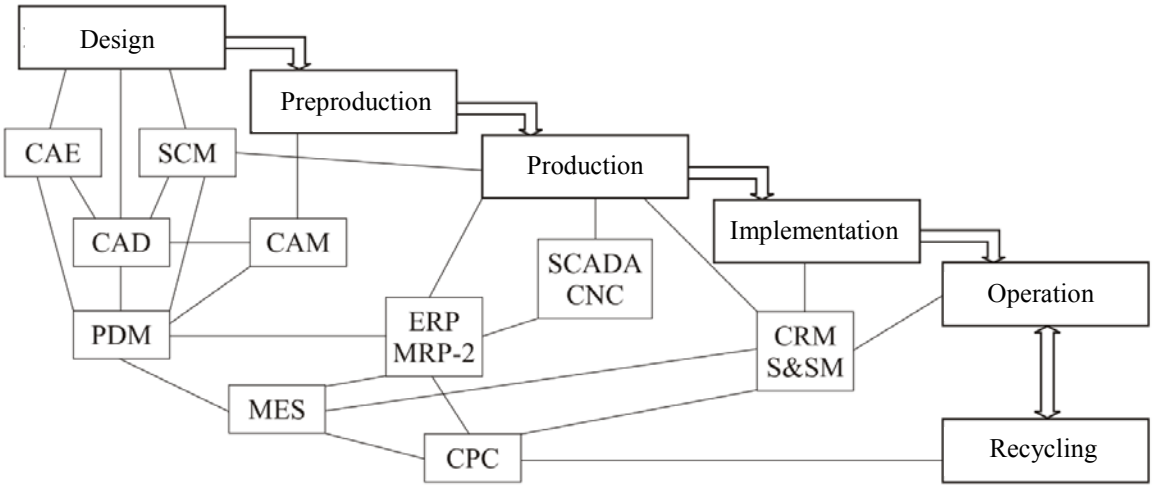

Fig. 2. Relationship between stages of industrial product life cycle and main computer-aided design systems

The creation of a system digital model starts with the definition of the configuration (geometry) of the object in the CAD system. Then, the required calculations of the dynamics, strength, stability, performance of the designed object, are performed in CAE systems; while process documentation is developed, and programs for machine tools with numerical control are prepared in CAM systems. SCM systems allow us to consider the possibility of using purchased products during design and to provide their timely delivery at the production stage. The indicated CAD systems are integrated at the level of PDM systems that control the design and preproduction processes. In the production shops, SCADA systems provide operation dispatching, and CNC systems control technological equipment including numerically controlled machines. The last two systems are integrated at the level of the MES-system that controls production processes. ERP and MRP-2 systems provide the enterprise with the desired resources. At the stage of implementation and operation, interaction with consumers is carried out using CRM-systems of sales and S&SM-

systems of maintenance and repair. Integration of all of these systems forms the basis of digital business (CPC), which is also called digital enterprise [7].

The analysis of the circuit (Fig. 2) shows that existing digital twins of industrial products have the greatest refinement when used at the design and production stages. At this, the work processes occurring at the stage of operation of an industrial product are considered in the design in terms of initial data presented in the form of numerical values or distribution laws. Foremost, such data include external loads and other influences, sequences of working operations. Under this approach [7], after manufacturing, an industrial product becomes a commodity for which not technical, but economic properties are more important: sales volumes, price, quantity and nature of claims for warranty service, customer reviews, and parameters of purchase and sale documents. Therefore, during the operation phase, detailed digital twins developed during design and production are usually not used. They can be used for overhaul or modernization of an industrial product, but in this case, it is taken out of service and returned to the manufacturer or a specialized repair company. This conclusion is also confirmed by the fact that 11 out of 14 computer-aided design systems presented in Fig. 2 are related to design and manufacture.

In the context of digitalization of the industrial production, such an approach is insufficient since the manufacturer of industrial products does not have the needed data to improve the design, control algorithms and technology for manufacturing competitive products and the consumer does not have complete information on the product in use. At the same time, mainstreaming of digital twins at the stage of operation of an industrial product will allow solving two main problems:

— operational challenge is to take into account possible abnormal and emergency conditions that should be avoided under the operation of the finished product;

— project designing task is focused on the creation of new structures and algorithms for program control considering the array of statistical data and mathematical models formed under the operation of industrial products.

At the same time, constant updating of the digital twin of the object under operation plays a key role. Thus, it is required to use the developed high-precision digital twins at all stages of the life cycle of an industrial product [8, 9].

For this, the developed mathematical models that underlie the digital twin are processed in real time on high-speed computers. Signals from sensors installed on a real object are used as initial data for the calculation (Fig. 3). The digital twin is linked to a real object through a cloud service.

This approach enables to increase the efficiency and safety of the industrial product operation, reveal hidden phenomena and effects, collect material for further modernization and improve consumer qualities, and prevent emergencies [8, 9].

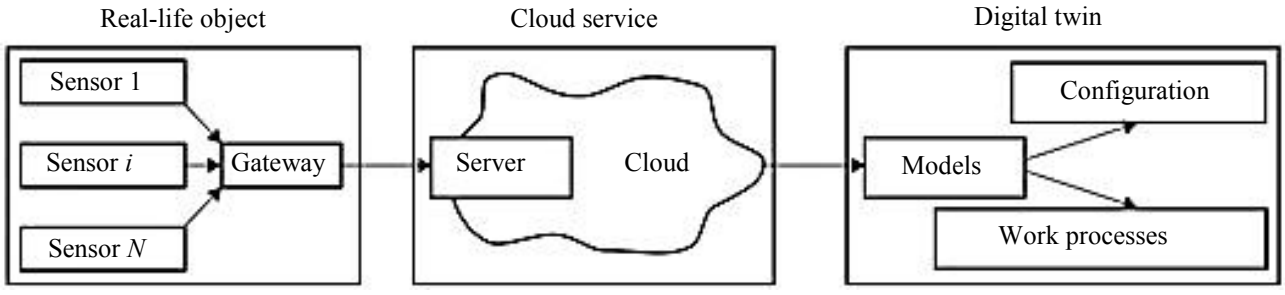

Fig. 3. Relationship between an industrial product and its digital twin

Thus, a digital twin is a software analogue of a physical device (industrial product) that simulates in real time the internal processes, technical characteristics and behavior of the device under the impact of random actions and the environment whose parameters are transmitted from the sensors of a real device operating in parallel [8, 9]. The digital

twin contains mathematical models of the object's configuration and workflows. In this case, the dimensions and characteristics of the configuration are used to calculate the initial parameters of mathematical models that describe work processes. For example, the inertia moment of a mechanism element is calculated on the basis of its geometric model. Then, the obtained value of the moment of inertia is translated into the differential equation of motion of the element.

To construct mathematical models of the industrial product workflows, it is recommended to use a systematic approach [10], according to which each significant element of the system is associated with a mathematical submodel assigned to submodels of other elements through joint parameters and communication equations. This approach provides the creation of easy-to-use modular mathematical models with account for the feedbacks between system elements.

This paper considers the creation and use of a digital twin of a mobile transport and transshipment rope complex at the stage of operation. Other stages of the MTRRC life cycle are not considered since they use general approaches that are applied for any machinery and equipment. It is believed that for the development of a digital twin, there are complete sets of three-dimensional computer geometric models of the MTRRC and design-engineering documentation developed at the design and preproduction stage.

Let us consider the options for using a digital twin to prevent emergencies under the operation of a mobile transport and transshipment rope complex. Let $\{a\}$ be the vector of parameters of a real-life object obtained by means of objective control means (sensors connected to measuring systems). These parameters describe the current state of the MTRRC and the nature of the ongoing work processes at the current time moment t_i. The values of the parameters $\{a\}$ are determined periodically, within a given period Δt. The parameters obtained from the physical object correspond to the parameters $\{x\}$ calculated using the mathematical model. The results of modeling work processes are written into the matrix [X], which contains information on the change in the simulated parameters over time. The parameters are simulated using various step-by-step numerical methods while the size of the computation step by the model time t_m is equal to Δt_m.

The parameters $\{a\}$ at each current moment of time t_i are transferred to the mathematical model input, with the help of which the modeling of the MTRRC work processes for a given period of time T is carried out. Besides, information on the configuration (structure) of a real-time object is used in the calculation. As a result of the calculation in real time, the values [X] are obtained, and according to the results of their analysis, an assessment (forecast) of the possibility of an emergency occurs. If the onset of an emergency is predicted according to the simulation results, the MTRRC immediately stops, or other measures are taken to prevent the accident.

The relationship between a real-time object and a digital twin is clearly illustrated in Fig. 4.

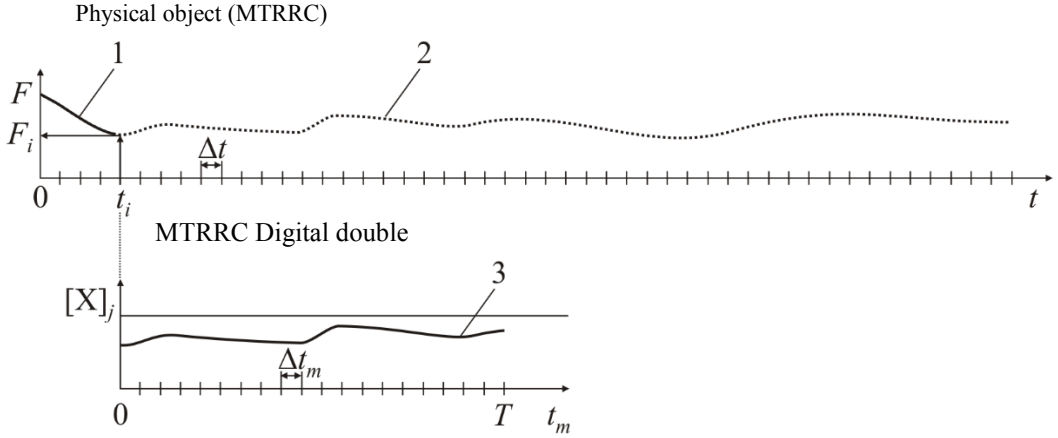

Fig. 4. Implementation of workflow parameter change obtained using objective control of real-time object and digital double: 1 – actual parameter change before t_i, 2 – actual parameter change of real-time object in future; 3 – result of modeling parameter change in future using digital double

One of the parameters of the vector $\{a\}$, for example, the tension force of the carrying rope F, is determined using a force-measuring transducer at intervals Δt. In real time, the tensile force is F_i. Similarly, other components a_i of the vector $\{a\}$, which are transferred for analysis through a digital twin, are determined.

The j-th row of the matrix [X] corresponds to the tension force. If, according to the results of modeling the working processes of MTRRC, the possibility of an emergency is not established, then the work of MTRRC does not

stop. At the next iteration, at time $t_i + \Delta t$, new values of the vector $\{a\}$ are determined, after which a new simulation session is performed. In the event of a negative forecast, for example, if the calculated tensile force exceeds the permissible value, then the operation of the MTRRC stops until the reasons are identified and the threat of an emergency is eliminated.

To improve the accuracy of the forecast, it is required to use adequate mathematical models. The deviation of the simulation result (section 3 in Fig. 4) from the actual behavior of the object (section 2 in Fig. 4) can serve as an accuracy criterion. Ideally, the forecast for changes in parameters should fully coincide with the actual change in parameters in future.

In the course of the study, a complex mathematical model being the basis for the MTRRC digital twin [10] was used. The equations of motion included in this model can be written in general form as follows:

$$\begin{cases} [M]\{\ddot{x}\} + [B]\{\dot{x}\} + [C]\{x\} = \{P\}, \\ [Y] = \{0\}, \end{cases}$$

where $\{x\}$ is the vector of laws of motion of system elements (changes in their coordinates in time); $\{\dot{x}\}$ is the velocity vector of system elements; $\{\ddot{x}\}$ is the vector of accelerations of system elements; $[M]$ is the matrix of inertial parameters depending on the masses and moments of inertia of the system elements; $[B]$ is the matrix of dissipation coefficients; $[C]$ is the elastic matrix depending on the rigidity of the system elements; $\{P\}$ is the vector of external loads on the system elements; $[Y]$ is the matrix of algebraic equations for the system parameters association:

$$F_i = F\left(\{x\}, \{\dot{x}\}, \{\ddot{x}\}\right) \text{ [10].}$$

The considered approach enables to predict and prevent the onset of emergencies:

— cable break due to excess driving force;

— rope coming off the pulley;

— fall of the base station due to loss of overall stability;

—the cable car drive stop with self-swinging;

— detachment of the ropeway cab with rolling down the rope and collision with another cab or support;

— impact of the cab on the support or base station equipment;

— heavy side roll when exposed to wind

Research Results. As discussed, the digital twin should interact with a physical object. However, mobile transport and transshipping rope complexes are a promising type of transport systems; so, there are no full-scale experimental prototypes nowadays. At this stage of research, a full-scale model of the MTRRC was created to work out the technique for creating a digital twin. Data on its operation was transmitted to the input of the digital twin. The prototype version of the complex made on the basis of the Engineering Research and Educational Center of Digital Technologies “Industry 4.0” of Ivan Petrovsky Bryansk State University is shown in Fig. 5.

The coordinate of the load suspension point *z* was chosen as the controlled parameter. The coordinate center is located on the axis of rotation of the drive pulley, and the coordinate axis connects the centers of the ropeway pulleys. The current coordinate value on a real-time object was determined using the Kinovea software, which provides analyzing video data.

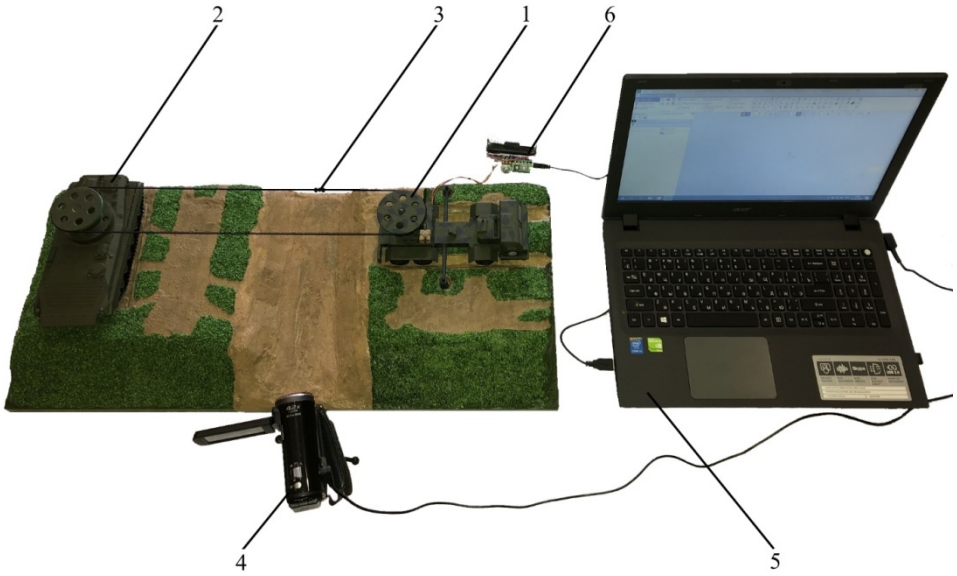

Fig. 5. Full scale mock-up of mobile ropeway complex: 1 – drive base station; 2 – non-drive base station; 3 – suspended load; 4 – videocamera; 5 – laptop computer for signal processing and simulation; 6 – control module based on a microcontroller

The predicted coordinate of the load suspension point was calculated using the model shown in Fig. 6.

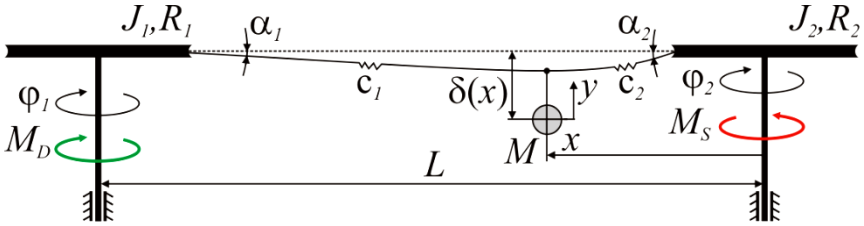

Fig. 6. Computational model to study work processes of the mock-up

At the stage of the rope system acceleration, when the speed of the load $\dot{x}$ is less than the nominal value load $x_{ном} = 0.013$ m/s corresponding to steady motion, the equations of motion of the elements of the system are as follows:

$$\begin{cases} J_1\ddot{\phi}_1 + c_1\left(\phi_1 - \dfrac{x}{R_1\cos\alpha_1} + (\delta(x)-y)\dfrac{\sin\alpha_1}{R_1}\right)\cos\alpha_1 = M_D(\dot{\phi}_1); \\ J_2\ddot{\phi}_2 - c_2\left(\phi_2 - \dfrac{x}{R_2\cos\alpha_2} + (\delta(x)-y)\dfrac{\sin\alpha_2}{R_2}\right)\cos\phi_2 = -M_S(\dot{\phi}_2); \\ M\ddot{x} - c_1\left(R_1\phi_1 - \dfrac{x}{\cos\alpha_1} + (\delta(x)-y)\sin\alpha_1\right)\cos\alpha_1 - \\ -c_2\left(R_2\phi_2 - \dfrac{x}{\cos\alpha_2} + (\delta(x)-y)\sin\alpha_2\right)\cos\alpha_2 = 0; \\ M\ddot{y} + c_1\left(R_1\phi_1 - \dfrac{x}{\cos\alpha_1} + (\delta(x)-y)\sin\alpha_1\right)\sin\alpha_1 - \\ -c_2\left(R_2\phi_2 - \dfrac{x}{\cos\alpha_2} + (\delta(x)-y)\sin\alpha_2\right)\sin\alpha_2 = -9{,}81M, \end{cases}$$

where ϕ_1, J_1 angle of rotation, inertia moment of the head pulley, respectively; ϕ_2, J_2 are angle of rotation, inertia moment of the tail pulley, respectively; x, y are horizontal, vertical coordinates of the load, respectively; M is load weight; c_1 and c_2 is rigidity of the rope in the area of the head and tail pulley, respectively; α_1 and α_2 are angles of inclination of the rope in the area of the head and tail pulley, respectively; R_1 and R_2 are radii of the head and tail pulley, respectively; L is the distance between the axes of rotation of the pulleys (a span of the ropeway).

Inclination angles of rope branches:

$$\alpha_1 = \alpha_1(x) = a\sin\left(\frac{\delta(x)}{x}\right) \text{ at } x \neq 0,\ \alpha_1 = 0 \text{ at } x = 0;$$

$$\alpha_2 = \alpha_2(x) = a\sin\left(\frac{\delta(x)}{L-x}\right) \text{ at } x \neq 0,\ \alpha_2 = 0 \text{ at } x = L,$$

where the dependence of the rope curve on the position of the load in the span of the ropeway is determined on a full-scale model and has the following form:

$$\delta(x) = 0.003\sin(\pi x / L) \text{ м}.$$

Stiffness of the model elements are determined as follows:

$$c_{x1} = c_{x2} = 100 \text{ N/m};\ c_1 = c_{x1} / R_1;\ c_2 = c_{x2} / R_2.$$

Here are the values of other parameters of the model: $J_1 = J_2 = 0.059$ kgm; $M = 0.025$ kg; $L = 0.395$ m; $R_1 = R_2 = 0.03$ m; $M_D = 34.3 \cdot 10^{-3}$ Nm; $M_S = 0.15 \cdot 10^{-3}$ Nm.

At the stage of steady motion, the law of motion is used:

$$x = x_0 + x_{ном} t,$$

where x_0 is the coordinate of the position of the load corresponding to the end of the transient process and the beginning of the steady motion.

Fig. 7 shows the real-time motion path of the load suspension point and the results of its simulation using a digital twin. In the case of a forced stop of the rope system by keeping the load, the actual position of the load deviated from the predicted one using the digital twin. This fact was recorded by the control system of the mock-up, while the deviation ε was determined, which made it possible to identify an emergency, such as “the rope slipping”.

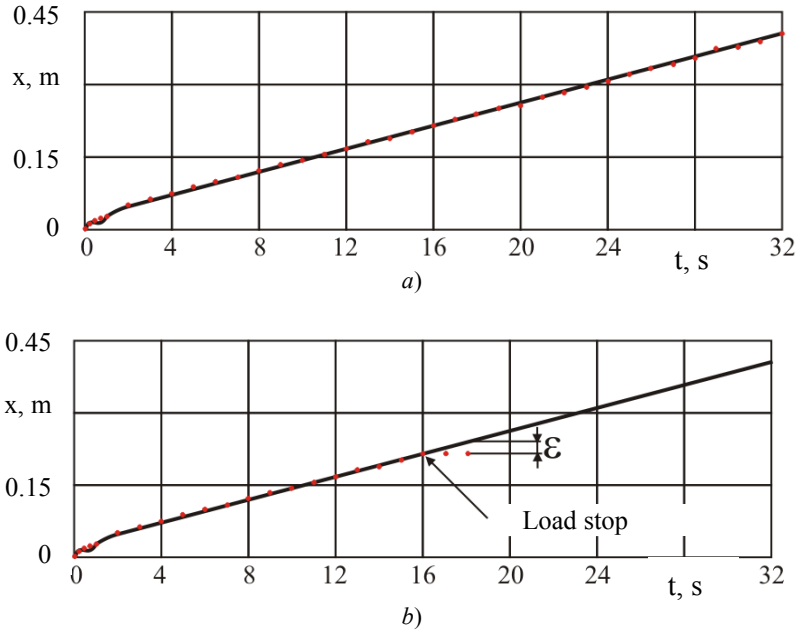

Fig. 7. Simulation results using a digital twin: *(a)* normal movement; *(b)* case of forced rope stop; —— is simulation results; ■ is experimental values

Discussion and Conclusions. The application of the considered methodology for creating digital twins has provided the identification of deviations from correct operation to prevent non-routine events and emergencies as in the case of a full-scale ropeway model. In the course of further research, an industrial digital twin of a mobile transport and transshipment rope complex based on the considered methodology will be created. In this case, of emergency situation models will be built.

References

1. Lagerev AV, Lagerev IA, Korotkii AA, et al. Kontseptsiya innovatsionnoi sistemy gorodskogo transporta «Kanatnoe metro goroda Bryanska» [Concept of the innovative system of urban transport "Cable metro of Bryansk city"]. The Bryansk State University Herald. 2012;3:12–15. (In Russ.)

2. Korotkii AA, Lagerev AV, Meskhi BCh, et al. Transportno-logisticheskie tekhnologii i mashiny dlya tsifrovoi urbanizirovannoi sredy [Transport and logistics technologies and machines for digital urbanized environment]; Lagerev AV (ed.). Rostov-on-Don: DSTU Publ. Centre; 2019. 268 p. (In Russ.)

3. Korotkii AA, Lagerev AV, Meskhi BCh, et al. Razvitie transportnoi infrastruktury krupnykh gorodov i territorii na osnove tekhnologii kanatnogo metro [Development of transport infrastructure of large cities and territories on the basis of cableway technology]. Rostov-on-Don: DSTU Publ. Centre; 2017. 344 p. (In Russ.)

4. Kudakaev TZ. Ispol'zovanie gruzovykh kabel'-kranov dlya raboty v slozhnykh usloviyakh. Opyt primeneniya v Rossii [Use of cargo cable cranes for operation under close conditions. Application experience in Russia]. Territory Engineering. 2014;5:62–67. (In Russ.)

5. D'yachkova OM, Volod'kin PP. Sfery primeneniya gorodskogo passazhirskogo transporta [The scope of application of urban passenger transport]. Uchenye Zametki TOGU. 2013;4(4):1492–1501. URL: http://pnu.edu.ru/ejournal/pub/issues/14/ (accessed: 29.08.2020). (In Russ.)

6. Lagerev AV, Tarichko VI, Soldatchenkov SP. Obespechenie obshchei ustoichivosti bazovykh kolesnykh stantsii mobil'nykh kanatnykh dorog [General stability of a base vehicle of a mobile ropeway]. Scientific and Technical Journal of Bryansk State University. 2019;2:210–220. (In Russ.)

7. Norenkov IP. Avtomatizirovannye informatsionnye sistemy: uchebnik dlya vuzov [Automated information systems]. Moscow: Bauman University Publ. House; 2011. 344 p. (In Russ.)

8. Kokorev DS, Yurin AA. Tsifrovye dvoiniki: Ponyatie, tipy i preimushchestva dlya biznesa [Digital twins: concept, types and benefits for business]. Colloquium-journal. 2019;10-2:101–104. (In Russ.)

9. Vasil'ev AN, Tarkhov DA, Malykhina GF. Metody sozdaniya tsifrovykh dvoinikov na osnove neirosetevogo modelirovaniya [Methods of creating digital twins based on neural network modeling]. Modern Information Technologies and IT-Education. 2018;14(3):521–532. (In Russ.)

10. Tarichko VI, Khimich AV. Kompleksnaya matematicheskaya model' mobil'nogo transportno-peregruzochnogo kanatnogo kompleksa [Comprehensive model of the mobile transport and overloading ropes complex]. Scientific and Technical Journal of Bryansk State University. 2019;4:523–532. (In Russ.)

Submitted 08.06.2020
Scheduled in the issue 20.08.2020

About the Authors:

Lagerev, Igor' A., Pro-rector of Innovation, Ivan Petrovsky Bryansk State University (14, Bezhitskaya St., Bryansk, 241036, RF), Dr.Sci. (Eng.), associate professor, ResearcherID: W-3063-2018, ScopusID: 56436754400, ORCID: http://orcid.org/0000-0002-0921-6831, lagerev-bgu@yandex.ru

Tarichko, Vadim I., Deputy General Director, chief designer, Bryansk Automobile Plant JSC (1, Staleliteynaya St., Bryansk, 241038, Russia), Cand.Sci. (Eng.), ScopusID: 57212305096, ORCID: https://orcid.org/0000-0003-0286-725X, 32.6909@mail.ru

Panfilov, Aleksei V., associate professor of the Transport Systems Operation and Logistics Department, Don State Technical University (88, Troitskaya St., Novocherkassk, Rostov Region, 346428, RF), Cand.Sci. (Eng.), associate professor, ResearcherID: A-5035-2014, ScopusID: 57216301201, ORCID: https://orcid.org/0000-0001-7211-1824, panfilov@ikcmysl.ru

Claimed contributorship

I. A. Lagerev: general concept development; scientific editing; the text revision; the text layout. V. I. Tarichko: creation of a 3D model of the mobile ropeways and a full-scale experiment; preparation of materials for the manuscript. A. V. Panfilov: development of a mathematical model of a digital twin of the mobile ropeways; preparation of materials for the manuscript.

All authors have read and approved the final manuscript.

MACHINE BUILDING AND MACHINE SCIENCE

UDC 621.791.052:539.015 https://doi.org/10.23947/2687-1653-2020-20-3-252-258

Methods and technologies of electroslag welding with controlled thermal cycle

Yu. V. Poletaev, V. Yu. Poletaev, A. N. Gritsyna, R. B. Aguliev
Don State Technical University (Rostov-on-Don, Russian Federation)

Introduction. Improving the quality and operational reliability of welded structures of power equipment is an urgent task of welding production. Its solution is possible on the basis of the development or selection of advanced methods and technologies of electroslag welding (ESW), which eliminate the causes of the formation of tempering cracks (TC) in thick-plate welds. This paper considers a comparative assessment and recommendations on the selection of such advanced ESW methods. The work objectives are to solve the problem of forming a fine-grained, uniform, crack-resistant metal structure of a welded joint with high mechanical characteristics and to reduce the negative impact of the ESW thermal cycle on the base metal. The solution to this problem is possible on the basis of a reasonable choice of methods and technologies for ESW with regulated (controlled) thermal cycle.

Materials and Methods. A comparative analysis of advanced methods and technologies of ESW with a controlled thermal cycle is carried out; a comparison of their pros and cons is provided; practical recommendations on the selection of advanced methods for controlling the thermal cycle parameters are offered.

Results. It is shown that moderate heat input at high-speed ESW in a narrow gap provides a single pass to form a welded joint with a finer-grained structure and high mechanical properties compared to the in-house technologies of ESW and automatic submerged-arc welding. Recommendations for practical use of the method in welding production are given.

Discussion and Conclusions. The results obtained are recommended to be used in the development of ESW technology for thick-sheet welded structures of nuclear and thermal power equipment that enables to abandon post-welding heat treatment (normalization and high tempering).

Keywords: ESW, electroslag welding, slag welding method, thermal cycle of welding, welding joint, narrow-gap welding, structure, properties.

For citation: Yu.V. Poletaev, V.Yu. Poletaev, et al. Methods and technologies of electroslag welding with controlled thermal cycle. Advanced Engineering Research, 2020, vol. 20, no. 3, p. 252–258. https://doi.org/10.23947/2687-1653-2020-20-3-252-258

Introduction. Electroslag welding is a high-performance process for the production of thick-walled welded structures for the power equipment. However, obtaining a homogeneous structure providing high mechanical properties of weld joints is achieved only after complete heat treatment in the form of normalization and high tempering. Moreover, coarse-grained weld metal and heat-affected zone (HAZ) metal has low resistance to cracking during welding and heat treatment in the form of tempering.

The problem urgency is determined by the fact that TC (Fig. 1) are detected unexpectedly at the stage of manufacturing and operation of a welded structure causing emergency situations and significant material costs [1].

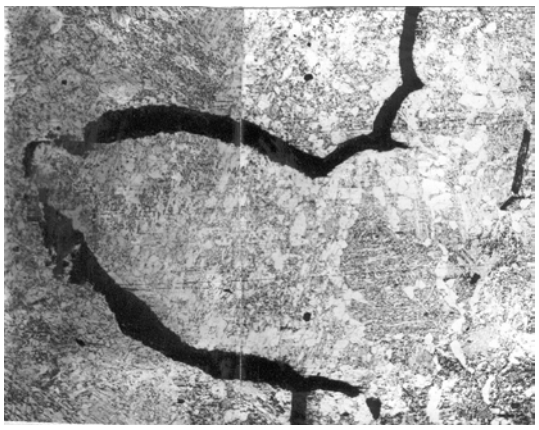

Fig. 1. TC nature in the electroslag weld joint of low-alloy steel, × 100

Studies of national and foreign scientists Eh.L. Makarov, V.N. Zemzin, Yu.V. Poletaev, A.S. Zubchenko, I. Grivnyak, F. Muller, R. Cadman, J. Tanaka, H. Nakamura and others show [2–9] that the tendency to the formation of cracks under welding increases significantly as a result of the combined effect of the unfavorable thermal cycle of ESW and embrittlement of the structure.

Materials and Methods. The developed methods of affecting the ESW thermal regime are based on the regulation of the key parameters of the thermal welding cycle: maximum heating temperature, the metal residence time at a temperature above the temperature of the grain intensive starting, cooling rate, etc. For example, an increase in the cooling rate to form a fine-grained structure of a weld joint can be achieved through introducing additional filler materials into the weld pool: wire, wire bundle, consumable tip, granular metal filler, metal powder, etc. A similar effect can be achieved under concomitant heating of the weld metal and HAZ for local continuous normalization. An increase in the quality and technological strength of the weld metal under ESW is achieved with the use of fluxes with reduced basicity index [10−11]. The method of weld metal exposure to external magnetic fields should be considered efficient.

The solution to a wide range of problems, of which the ESW technology is summarized, is associated with the properties of the slag and metal baths, as well as with the possibilities of controlling the crystallization of the weld using the magnetic hydrodynamic (MHD) flows generated in it. The nature of MHD flows depends mainly on the electric current passing through the melt, and the magnetic fields interacting with this current. The application of controlled MHD flows provides improving the quality, mechanical properties and technological strength of weld joints through optimizing the shape of the metal bath, refining the metal structure and increasing the resistance against the formation of TC. Higher values of plasticity and impact toughness of the metal obtained using controlled MHD flows made it possible, in a number of cases, to exclude post weld heat treatment.

Research Results. Electromagnetic stirring of liquid metal is carried out using magnetic fields generated by a solenoid or electromagnets (Fig. 2). This field interacts with the molten weld pool and regulates the thermal regime of the weld metal. In this case, a decrease in the heat input under welding, the residence time of the crystallizing metal above the temperature of the grain intensive starting, the size of dendrites.

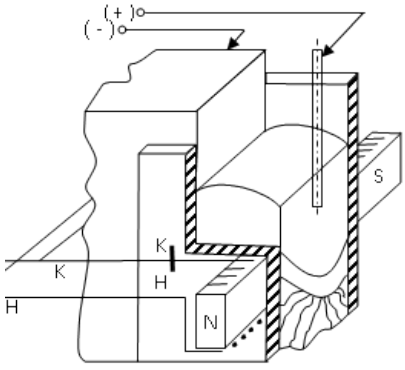

Fig. 2. Scheme of ESW with electromagnets mounted on formers [1]

[1] Poletaev VYu. Methods for improving quality of weld joints made by electroslag welding (review) In: Proc. 5th Int. Sci.-Pract. Conf. on Actual problems of science of the 21st century. St.Petersburg: Cognitio. 2015;2:131–139. (In Russ.)

In Fig. 3, you can see the difference in the macrostructure of weld joints made according to the standard ESW technology and under the magnetic field effect. It should be noted that in the case of standard technology (Fig. 3 a), the average thickness of the weld and its width are much smaller than when exposed to a magnetic field. The area of large overheated grain in the HAZ is the largest and reaches 5−7 mm. For comparison, its surface size does not exceed 1–2 mm, and the zone of large columnar crystals reaches almost the middle of the seam. Therefore, in the central part of the seam, the area of relatively small equiaxed grains has a length of only 3−4 mm.

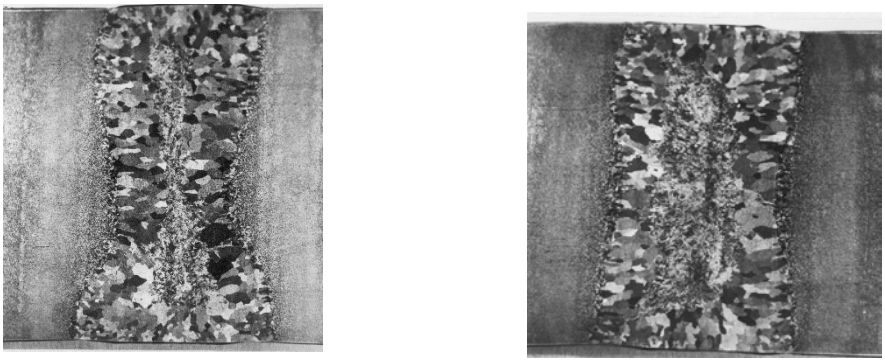

a) *b*)

Fig. 3. Macrostructure of electroslag weld joint made according to standard technology (a) and under impact of magnetic field (b), × 100

Under the magnetic field impact, there is a noticeable improvement in the macrostructure and, first of all, a decrease in the zone of large columnar crystals (Fig. 3 b); the zone of relatively small equiaxed crystals in the center of the weld has a length of 25−30 mm, which is more than 50% of the weld width. For an AN-8 submerged-arc weld joint, this zone is somewhat smaller and amounts to 16−20 mm. In all samples, the size of large columnar crystals of the weld metal reaches 10−11 mm. A decrease in the size of the zone of large columnar crystals should contribute to an increase in mechanical and, above all, plastic properties[2].

The principle of the high-speed ESW method is to programmatically change the current lead points to the electrodes and welded edges with a specified frequency (Fig. 4).

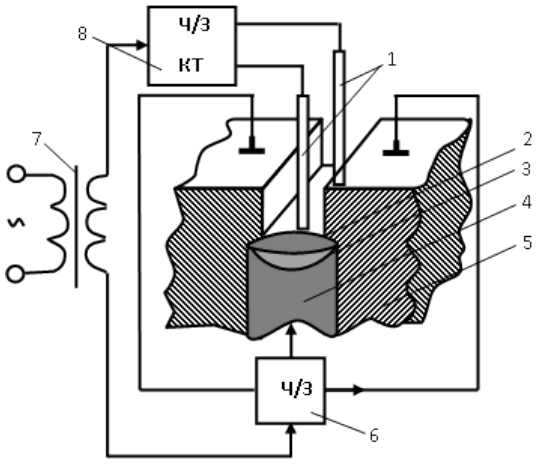

Fig. 4. ESW circuit with switching current leads: 1 — electrodes; 2 — slag bath; 3 — metal bath; 4 — weld seam; 5 — product; 6 — three-channel current changer; 7 — power supply; 8 — two-channel current switch

Switching current leads during welding causes periodic changes in the direction of the electric current lines in the weld pool [12]. At the same time, the motion pattern of the slag-metal melt and, accordingly, the temperature balance in the bath changes sharply. Most of the energy is used to melt the electrodes, while less is transferred to the base metal. All this increases the rate of melting of electrodes by 3−4 times and minimizes the degree of heat removal to the walls of the base metal. Fluctuations of the liquid phase relative to the solid one reduce the temperature gradient at the interface, stop the growth of crystals, and disrupt the frequency and direction of the

[2] Poletaev VYu. Increase in crack resistance under tempering of weld joints of 15Kh2NMFA-VRV thick plate steel based on development of a single-pass automatic arc welding technology: Cand.Sci. (Eng.) diss. Rostov-on-Don, 2017. 162 p. (In Russ.)

dendritical crystallization. The development of these processes contributes to the formation of a finer-grained structure with high mechanical properties without high-temperature heat treatment.

A.N. Khakimov and his colleagues proposed the ESW method without subsequent heat treatment (normalization). With regard to low-alloy heat-hardened steels, the efficiency of regulating the parameters of the thermal welding cycle through reducing the heating time $t_н$ and increasing the cooling rate w_0 is shown. When welding, the parameters of the thermal cycle are controlled by accompanying cooling according to the optimal program. Special technological equipment provides the supply of a cooling water-air mixture to the weld seam and HAZ of the joint using slotted air-hydraulic nozzles installed inside the welding machine at the level of the molten metal pool. Intensive heat dissipation to provide the required parameters of the thermal cycle over the thickness of the metal is carried out from one surface of the weld joint.

Studies on the weld joint metal microstructure have shown that under ESW at a cooling rate of 0.7−1.0° C/s, a ferrite-pearlite structure of the weld and HAZ metal is formed, such as Widmanstätt. Significant precipitation of ferrite along the boundaries of primary austenite grains is observed. The grain size corresponds to a score of 0−1. The ferrite content in the weld metal structure is about 60%, and in the HAZ metal structure – 40%. At a cooling rate of 6 − 8° C/s, the residence time above the temperature of the critical point Ac3 is reduced from 140 to 40−45 s. This contributes to a decrease in ferrite the content in the structure of the weld joint and an increase in mechanical properties.

All of the above welding methods do not completely solve the main problem of overheating and a decrease in the technological strength of thick-plate welded joints in ESW. One of the methods that reduce heat input, and, as a consequence, the grain size and the length of the heat-affected zone, is the method of single-pass electric-arc narrow-gap welding with PF constraint shaping of the weld (Fig. 5). The method is developed by a group led by Yu. V. Poletaev. The thermal welding cycle is regulated through changing the parameters of the electric arc process mode. This is where the proposed method is fundamentally different from ESW.

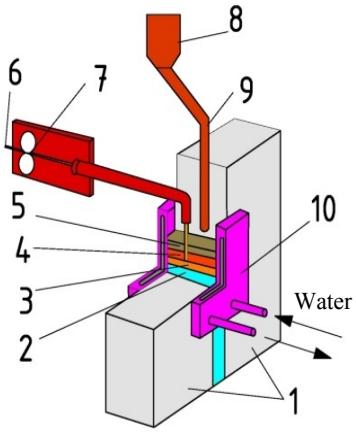

Fig. 5. Basic diagram of the welding technique: 1 — parts to be welded; 2 — weld metal; 3 — welding pool; 4 — liquid slag; 5 — flux envelope; 6 — welding wire; 7 — wire feeder; 8 — flux dispenser; 9 — supply of flux to the welding zone; 10 — copper water-coiled dam

The arc process provides the required heat input, high-quality penetration of the welded edges and a “soft” thermal cycle of metal welding in the HAZ. For this, the height of the liquid slag layer covering the welding arc is maintained equal to the width of the welding gap of slotted cutting, which is 14−18 mm. This completely eliminates slag splashing, provides the process stability and the formation of a high-quality weld joint. The height of the slag layer is controlled and maintained by an automatic flux control device. The optimal welding gap depends on the thickness and length of the weldments and is set experimentally with account for the possibility of welding and high-quality fusion of the edges. For welding sheets of heavy thickness, two or more electrode wires of small diameter (2 mm) are simultaneously fed into the gap located one after the other along the cutting axis. Small-diameter wire feed into a narrow gap provides a high welding speed – up to 5 m/h, while under the traditional ESW method, this speed is no more than 0.9−1.0 m/h. The proposed technique increases the weld metal solidification rate, which contributes to the formation of a fine-grained structure and the required level of mechanical properties of the joint (Fig. 6). It is found that

weld joints of carbon and low-alloy steels, made through the electric arc slot welding with a heat input $Q_{св}$ up to 15 MJ/m, a favorable macro- and microstructure without large columnar crystals with a minimum length of the area of overheated large grains near the fusion zone (no more 1 mm) is formed. The quality and mechanical properties of such structures meet regulatory requirements.

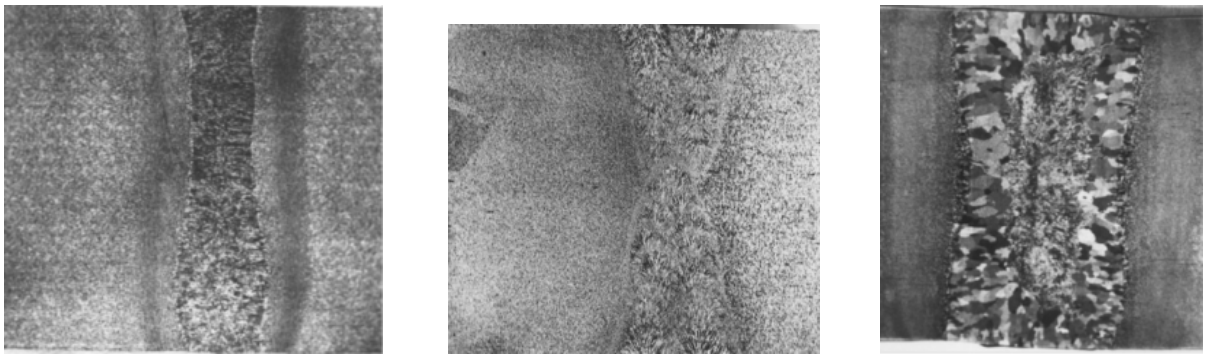

a) *b*) *c*)

Fig. 6. Macrostructure of weld joint made by the following method:
(a) slot welding; *(b)* automatic submerged arc welding; *(c)* ESW, × 100

In the course of the experimental study, the following advantages of the electric arc slot welding method were established:

— weld joints undergo only high tempering;

— high welding speed (up to 5 m/h);

— fabricability and high quality of joints;

— minimum angular deformations during welding;

— no mechanical processing of preweld edges;

— welding is performed without preliminary and concomitant heating;

— low flux consumption;

— the formation of joints with high resistance to the formation of intergranular fracture under welding and heat treatment (tempering);

— low costs for heat treatment and subsequent mechanical descaling the joints.

Discussion and conclusions:

1. Advanced methods and technologies of electroslag welding with controlled thermal cycle are studied. It is shown that the optimization of heat input (the thermal cycle parameters) under welding provides the control of structural, mechanical homogeneity of the weld joint and its process through.

2. It is shown that the implementation of ESW methods with a controlled thermal cycle is associated with the complication of technology and equipment.

3. Single-pass electric arc slot welding enables to abandon the multi-pass automatic submerged arc welding technique and single-pass ESW, which significantly increases the production cost of the weldments.

4. Directions for further research are associated with the development of competitive, alternative methods of ESW, single-pass electric arc slot welding of thick-walled structures of the power engineering providing a noticeable decrease in heat input during the formation of joints.

References

1. Poletaev YuV, Poletaev VYu. Svarka teploustoichivykh stalei bol'shoi tolshchiny [Welding of thick heat-resistant steels]. Rostov-on-Don: DSTU Publ. Centre; 2017. 167 p. (In Russ.)

2. Makarov EhL, Yakushin BF. Teoriya svarivaemosti stalei i splavov [Theory of weldability of steels and alloys]. Moscow: Bauman University Publ. House; 2014. 487 p. (In Russ.)

3. Poletaev YuV, Poletaev VYu. Vliyanie sposoba vyplavki stali Cr-Ni-Mo-V na sklonnost' k mezhzerennomu razrusheniyu pri ehlektroshlakovom pereplave [Effect of the method of smelting steel Cr-Ni-Mo-V on the tendency to intergranular destruction under electroslag remelting]. Tekhnologiya Mashinostroeniya. 2016;8:5–10. (In Russ.)

4. Poletaev YuV, Poletaev VYu. Vliyanie termicheskogo tsikla svarki i povtornogo nagreva na strukturno-fazovye izmeneniya nizkolegirovannoi stali Cr-Ni-Mo-V [Effect of thermal cycle of welding and reheating on structural-constitutional changes of low-alloyed Cr-Ni-Mo-V steel]. Vestnik of DSTU. 2016;16(4):96–103. (In Russ.)

5. Zubchenko AS, Fedorov AV, Suslova EA. Issledovanie vliyaniya povtornogo nagreva na uprochnenie i rastreskivanie svarnykh soedinenii perlitnykh stalei [Study on the reheating effect on hardening and cracking of welded joints of pearlitic steels]. Welding and Diagnostics. 2009;4:2–5. (In Russ.)

6. Zubchenko AS, Fedorov AV, Nechaev YuV. Issledovanie prichin rastreskivaniya svarnykh soedinenii tolstostennykh sosudov davleniya pri posleduyushchei termicheskoi obrabotke [Investigation of the causes of cracking of welded joints of thick-walled pressure vessels during subsequent heat treatment]. Welding and Diagnostics. 2009;2:21–25. (In Russ.)

7. Krishna K. Narrow-gap improved electroslag welding for bridges. Welding in the World. 1996;38(11):325−335.

8. FHWA Memorandum: Narrow-gap electroslag welding for bridges. March 20, 2000. P. 76−83.

9. Zemzin VN, Shron RZ. Termicheskaya obrabotka i svoistva svarnykh soedinenii [Heat treatment and properties of welded joints]. Leningrad: Mashinostroenie; 1978. 367 p. (In Russ.)

10. Potapov NN, Rymkevich AI, Roshchin MB. Osobennosti metallurgicheskikh protsessov pri EHSHS konstruktsionnykh stalei s ispol'zovaniem flyusov ponizhennoi osnovnosti [Features of metallurgical processes under ESW of structural steels using low basicity fluxes]. Svarochnoe Proizvodstvo. 2011;1:27–32. (In Russ.)

11. Rymkevich AI, Potapov NN, Roshchin MB. Vliyanie khimicheskoi aktivnosti flyusa na svoistva naplavlennogo metalla pri ehlektroshlakovoi svarke i ehlektroshlakovom pereplave [Effect of the flux chemical activity on properties of deposited metal under electroslag welding and electroslag remelting]. Svarochnoe Proizvodstvo. 2011;3:3–8. (In Russ.)

Submitted 27.07.2020
Scheduled in the issue 02.09.2020

About the Authors:

Poletaev, Yurii V., professor of the Machines and Welding Fabrication Automation Department, Don State Technical University (1, Gagarin sq., Rostov-on-Don, 344003, RF), Dr.Sci. (Eng.), professor, ORCID: https://orcid.org/0000-0001-5465-1886, anclav51@mail.ru

Poletaev, Valerii Yu., General Director, AVALON VIDEO LLC (14, pr. Kurchatova, Volgodonsk, Rostov Region, 347380, RF), Cand.Sci. (Eng.), ORCID: https://orcid.org/0000-0003-3677-7500, afshor@mail.ru

Gritsyna, Aleksandr N., associate professor of the Machines and Welding Fabrication Automation Department, Don State Technical University (1, Gagarin sq., Rostov-on-Don, 344003, RF), Cand.Sci. (Eng.), ORCID: https://orcid.org/0000-0002-9936-7712, svarka.dstu@mail.ru

Aguliev, Ruslan B., engineer of the Machines and Welding Fabrication Automation Department, Don State Technical University (1, Gagarin sq., Rostov-on-Don, 344003, RF), ORCID: https://orcid.org/0000-0002-7092-495X, rus.aguliev@mail.ru

Claimed contributorship

Yu. V. Poletaev: academic advising; basic research concept and the paper structure formulation; definition of research methodology; task setting. V. Yu. Poletaev: organizing and conducting the experimental research. A. N. Gritsyna: collection and analysis of literature data; participation in the research; critical analysis; editing. R. B. Aguliev: literature and patent analysis; participation in the theoretical research; text editing.

All authors have read and approved the final manuscript.

MACHINE BUILDING AND MACHINE SCIENCE

УДК 621.791.75:004.942 https://doi.org/10.23947/2687-1653-2020-20-3-259-268

Physicomathematical modeling of the formation features of fillet welds of bridge metal structures under submerged-arc welding

A. A. Mosin[1], V. A. Erofeev[2], M. A. Sholokhov[3]
[1] "Kurganstalmost" CJSC (Kurgan, Russian Federation)
[2] Tula State University (Tula, Russian Federation)
[3] Ural Federal University named after the First President of Russia B.N. Yeltsin (Ekaterinburg, Russian Federation)

Introduction. The weld formation under the submerged-arc welding of bridge metal structures is investigated. The work objective is to study possibilities to increase the welding performance during the arc welding of fillet seams.
Materials and Methods. Methods of computer analysis are used to optimize the technology. With their help, a physicomathematical model of fillet weld formation under the submerged-arc welding has been developed. It is based on a system of equations for thermal conductivity and equilibrium of the weld pool surface. In this system, the formation of an arc cavern is determined through the flux boiling isotherm under the action of the arc column radiation; heat transfer by the flux vapor inside the arc cavern and the influence of the spatial position on the formation of the weld pool are taken into account.
Results. New mathematical relationships that describe physical phenomena under the submerged-arc welding of fillet welds are proposed. The key feature of the proposed model is in the fundamental difference between the submerged-arc welding and the gas-shielded arc welding, i.e., during submerged-arc welding, the arc burns in a gas-vapor cavern that appears due to the melting and evaporation of flux. Numerical simulation of the temperature distribution during production of the fillet welds in 1F and 2F positions is carried out. The process constraints under the single-run welding of the fillet welds are specified. It was determined that the single-run submerged-arc welding of fillet welds in 1F position exhibits high-quality formation of welds for almost the entire range of metal sheet thicknesses. During production of fillet welds in 2F position, high-quality formation is provided only for sheet thicknesses up to 8 mm. At heavy thicknesses, the formation of the seam is disrupted due to the melt flow from the vertical wall. In this case, the leg length decreases; a typical undercut is formed; so the weld will be asymmetric and less strong.
Discussion and Conclusions. Comparison of the numerical analysis results with actual data on welding modes under the production of bridge metal structures shows that the existing fillet welding technologies have already reached their maximum efficiency rate. Further productivity gain is possible by forming oversized legs only with multiarc or multielectrode welding methods.

Keywords: fillet weld, submerged-arc welding, physicomathematical model, numerical simulation, arc cavern.

For citation: A.A. Mosin, V.A. Erofeev, M.A. Sholokhov. Physicomathematical modeling of the formation features of fillet welds of bridge metal structures under submerged arc welding. Advanced Engineering Research, 2020, vol. 20, no. 3, p. 259−268. https://doi.org/10.23947/2687-1653-2020-20-3-259-268

Introduction. Traditional methods of bridge construction provide for the enlarged assembly of bulk welded metal structures at the construction site [1]. Therefore, at the facility itself, welding work is carried out to a minimum. They are performed mainly at the factories of bridge metal structures [2], and most of them are associated with the welding of elongated seams. Of these, corner welds account for 40% to 70%. Fillet welding with small thickness is carried out without grooving. For thicknesses up to 50 mm, asymmetric and symmetrical grooves with an included angle of 45-60 ° are used. Fillet welds with a flat surface in cross section and smooth transitions to the base metal along the fusion zones without sagging and undercuts, gas cavities and slag inclusions are optimal. In addition, weld joints should have high ductility and impact toughness at low temperatures. Defects in the formation of seams are unacceptable. Sound reproduction of the maximum possible leg, when welding fillet seams, is the main capacity for increasing productivity [3].

To minimize defects and increase the productivity of welding processes for bridge metal structures, it is advisable to weld fillet seams with the largest possible leg size in one pass. Therefore, an urgent task is to increase the leg welded in one pass [4]. This can be achieved through the following:

— optimization of the parameters of welding processes,
— using new sources of heating,
— reduction of auxiliary time,
— increasing the fusibility of the electrode wire.

In our opinion, first of all, one should consider the possibility of a sound shop reproduction of the maximum possible leg using the traditional submerged-arc consumable-electrode welding technology.

This work objective is to study the possibilities of increasing the productivity of the arc welding process of fillet welds with account of the characteristic properties of their formation.

Materials and Methods. As noted in [5], in addition to the well-known parameters of the welding mode (arc current, welding speed), the performance of the submerged-arc welding process is influenced by the arc voltage and the diameter of the electrode wire. The spatial position during welding and the positioning of the electrode in the groove also affect significantly the formation of fillet welds [6]. It is a highly time-consuming task to consider the influence of the entire set of the listed factors on the productivity of the welding process and the quality of fillet welds without using modern research methods.

For a significant reduction in the volume of experimental studies of fillet welding, physicomathematical modeling of stresses and features of shaping and penetration is used [7–9]. Let us consider the sequence of computer simulation of the features of the formation of fillet welds — from creating a model to its visualization. The principle difference between the submerged-arc welding method and gas shielded arc welding is that the arc burns in a vapor-gas cavity arising from the melting and evaporation of the flux. The second important feature is that physical phenomena determining the formation of the weld pool and seam occur in different environments [9]. This should be taken into account in the physicomathematical model of the seam formation under the submerged-arc welding.

Modeling space coordinates. When modeling, the space in which fillet welding is performed, and the geometric dimensions of high-quality welds are specified. In Fig. 1*a,* an area of space covering the welded edges and zones of arc burning, melting of the flux and metal is highlighted; and in Fig. 1*b,* geometric dimensions of fillet welds, which can be used to assess the quality of their formation in accordance with the recommendations, are shown [5].

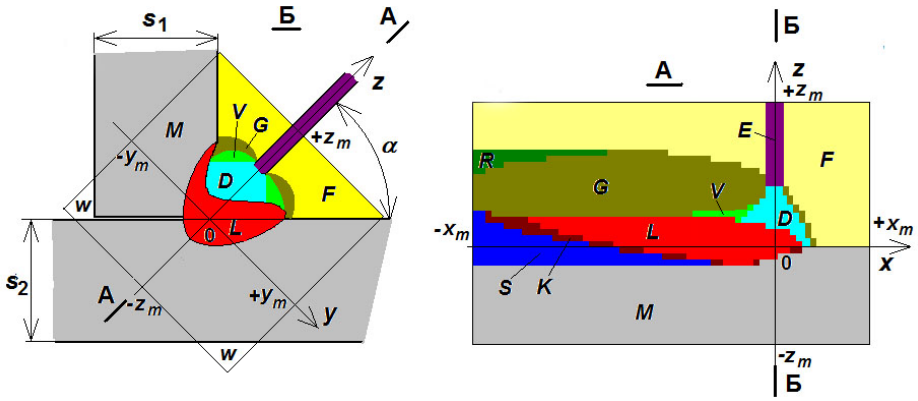

a)

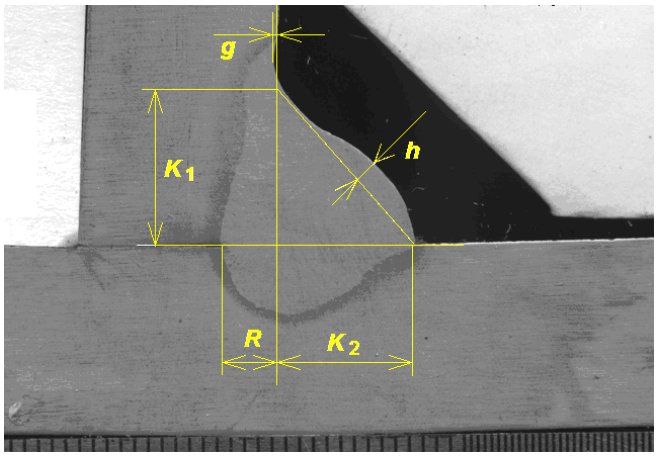

b)

Fig. 1. Structure of the simulation space for the welding process (*a*), and the geometric dimensions of fillet welds (*b*), which determine the quality of their formation

The simulation space includes the following zones: *M* — parent metal, *E* — electrode, *D* — welding arc, *F* — free flow flux, *V* — flux vapor, *G* — molten flux, *R* — solidified flux, *L* — liquid metal, *K* — solid-liquid metal, *S* — weld metal, *W* — air. Internal interzone surfaces are designated as intersections of sets of points belonging to the corresponding zones.

For example, the surface of the weld pool Z_L (x, y) is designated $L \cap (D \cup V \cup G)$. It separates the weld pool *L* from the welding arc *D*, the vaporous *V* and liquid *G* flux. The sizes of the *V, G, L, K* zones and the location of the interfaces between them are unknown. They need to be defined under the simulation. These indicators depend on the results of solving the system of equations describing physical phenomena of the submerged-arc welding. It is more convenient to solve such a problem in a fixed Cartesian coordinate system, in which the metal of the welded joint is stationary, and the electrode and arc move at the welding speed v_w in the direction of the *x* coordinate. Accordingly, the coordinates of the electrode axis x_f and y_f are determined:

$$H_{i,j,k}(t) = H_{i+1,j,k}(t - \tau), \tag{1}$$

where *t* is time since excitation.

When welding, the surfaces of fillets and interface zone are oriented mainly in the plane connecting the fillet weld legs. It is convenient to describe such surfaces as a deviation from this plane. Therefore, the *z* coordinate is directed along the bisector α of the angle between the sheets (or the groove angle).

Heat transfer is a common process for all designated areas. The simulation considers the thermodynamic state of media with different thermophysical properties, in which several internal local distributed heat sources operate. The rate of change and distribution of enthalpy should be described from the equation [10]:

$$\frac{\partial H}{\partial t} = \frac{\partial}{\partial x}\left(\lambda \frac{\partial T}{\partial x}\right) + \frac{\partial}{\partial y}\left(\lambda \frac{\partial T}{\partial y}\right) + \frac{\partial}{\partial z}\left(\lambda \frac{\partial T}{\partial z}\right) + q\,(x, y, z, t). \tag{2}$$

Here, $H = H\,(x, y, z, t)$ is volumetric enthalpy, J/cm^3; $\lambda = \lambda(T)$ is heat conductivity factor dependent on temperature and material of the medium, W/(cm·°C); q is volumetric heat source. The temperature $T\,(x, y, z, t)$ is related to the enthalpy $H\,(x, y, z, t)$ by the nonlinear function $T(H)$, which takes into account the dependence of the heat capacity on the temperature and heat of phase and aggregate transformations. At the initial moment of time, the weld pool is absent, the flux is in a free flow state, the temperature at all points in space is the same and equal to the ambient temperature. Taking this into account, the heat exchange between the simulation zone and the external space can be described by the boundary conditions:

$$\frac{\partial^2 T}{\partial x^2} = 0,\ x = \pm x_m, \tag{3}$$

$$\frac{\partial^2 T}{\partial y^2} = 0,\ y = \pm y_m, \tag{4}$$

$$\frac{\partial^2 T}{\partial z^2} = 0,\ z = \pm z_m. \tag{5}$$

Heat sources. The main heat sources are the electric arc q_{arc} acting in zone *D*, and the heat released under the electrode stickout [11, 12]. Heat release in the liquid flux is close to non-existent, since it has no direct contact with the electrode whose temperature is lower than the melting point of the flux, and the electrical resistance of the powder flux is very high. Taking these circumstances into account, the heating rate of the metal in the electrode stickout (in zone *E*) can be described by the relation:

$$\frac{\mathrm{d}T_f}{\mathrm{d}z} = \frac{\rho_e j^2}{c\rho_f} \frac{z_m - z}{v_f} \tag{6}$$

where T_f is temperature of the stickout; $\rho_e = \rho_e(T_f)$ is electrical resistivity; $j = \frac{4I}{\pi d_f^2}$ is current density *I* in the electrode of diameter d_f; $c\rho_f$ is volumetric heat capacity of the electrode material; v_f is the wire feed speed.

Heat release in the anodic region of the arc on the surface $E \cap D$ is described as the heat flux:

$$\frac{dq}{dz} = jU_a, \tag{7}$$

where U_a is voltage drop in the anode region of the arc.

Heat release in the plasma arc flame is considered as the distribution of the arc column radiation over the surface of the arc cavern $L \cap (D \cup V)$:

$$\frac{\partial^2 T}{\partial y^2} = 0, y = \pm y_{n'}. \tag{8}$$

The heat flux created by heat release in the cathode region of the arc on the surface $L \cap D$ is:

$$\frac{dq}{dn} = \frac{IU_k}{\pi R^2} \exp\left(\frac{-r_0^2}{R^2}\right), \tag{9}$$

where U_k is cathode arc voltage, *R* is effective radius of the arc, r_0 is the distance between the surface point $L \cap D$ and the point of intersection of the arc axis and this surface.

Heat transfer by drops of electrode metal is considered by the heat flux through the surface $L \cap D$ [13]:

$$\frac{dq}{dn} = \frac{IT_k}{\pi R^2} \exp\left(\frac{-r_0^2}{R^2}\right), \tag{10}$$

where T_k is droplet temperature taken equal to the half-sum of the melting and boiling temperatures of the electrode material.

Heat transfer by flux vapor is described as heat flux through the surface of the weld pool $L \cap V$ and flux $G \cap V$: $\frac{\partial^2 T}{\partial z^2} = 0, z = \pm z_m$. The heat transfer coefficient is determined from the balance of the capacities of evaporation and condensation of steam:

$$\int_{S_Z} \frac{dq}{dn} dS_Z \overrightarrow{p\,\mathrm{vap} = \mathrm{var}} 0, \tag{11}$$

where S_z is the area of specified surfaces $L \cap V \cup G \cap V$.

Equilibrium equation of the weld pool surface. The location of the weld pool surface $Z(x, y)$, delimiting the zones $L \cap (D \cup V \cup G)$, is determined by solving the pressure equilibrium equation on it:

— capillary p_σ,

— gravitational p_g,

— stream of electrode metal drops p_f,

— hydrodynamic pressure of the weld pool metal flow p_v,

— electrodynamic pressure of the arc p_a,

— internal pressure of liquid metal p_m.

$$\frac{dT_f}{dz} = \frac{\rho_e j^2}{c\rho_f} \frac{z_m - z}{v_f}. \tag{12}$$

Capillary pressure is determined by the curvature of the surface $Z(x, y)$, and for small deflections, it is calculated:

$$p_\sigma = -\sigma \left(\frac{\partial^2 Z}{\partial x^2} + \frac{\partial^2 Z}{\partial y^2} \right), \tag{13}$$

where σ is the surface tension constant.

Gravitational pressure is determined by the weight of a column of substance above a point on the surface of the weld pool:

$$p_g = \mathrm{g}(\rho(Z - z_{\max}) + \rho_h Z_h), \tag{14}$$

where g is acceleration of gravity; ρ, ρ_h are densities of metal and slag; z_{max} is maximum height of the weld pool surface; Z_h is thickness of the liquid slag layer.

Electrodynamic pressure of the welding arc is determined by the arc current:

$$p_a = \frac{k_a I^2}{\pi R_p^2} \exp\left[-\frac{(x_0 + v_w t)^2 + y^2}{R_p^2} \right], \tag{15}$$

where k_a is the electrodynamic coefficient, R_p is force radius of the arc.

Flow pressure of electrode metal droplets is determined by the flow rate and mass:

$$p_f = \rho \frac{v_f^2}{2} \exp\left[\frac{-(x_0 + v_w t)^2 + y^2}{R_f^2} \right]. \tag{16}$$

Hydrodynamic pressure of the weld pool metal flow is determined by the rate of change in the weld pool section area S_L:

$$p_v = -\rho v_x^2 \frac{dS_L}{dx}. \tag{17}$$

This component increases the pressure in front of the arc and decreases it behind the arc.

Internal pressure in the melt p_m is determined from the equality of the deposited metal area to the amount of consumed electrode metal:

$$S_{S \cup M}(-x_m) - S_M(+x_m) \overrightarrow{p_m = var} \pi r_f \frac{v_f}{v_w}, \tag{18}$$

where $S_{S \cup M}(-x_m)$ is the cross-sectional area of the metal at the end of the simulation area at $x = -x_m$; $S_M(x)$ is the initial groove cross-sectional area at $x = x_m$.

Current and location of the welding arc. The welding arc current I is set by the feed rate v_f and the diameter d_f of the electrode:

$$I = v_f \frac{\pi d_f^2}{4} \left(c\rho_f (T_k - T_f) + H_{LS} \right), \tag{19}$$

where T_k is temperature of the electrode metal droplets; H_{LS} is the volumetric specific heat of fusion.

The length l of the welding arc is set by the voltage U_0 of the power source and depends on the electrical resistance of the current-carrying elements R_0 and the stickout of the electrode R_f:

$$l = 1/E\,(U_0 - U_a - U_k - I\,(R_0 + R_f)). \tag{20}$$

The arc length l is determined by the potential gradient E in the arc column whose value depends on the properties of the flux vapor. With curved surface $L \cap D$ of the cathode spot, the concept of arc length needs to be clarified. If we consider the arc column as a set of parallel conductors, then the current density will be the greater, the smaller the distance from the electrode tip to the point of the metal surface. The average length l of the set of such conductors can be determined by solving the equation:

$$\sqrt{\frac{1}{S}\int_0^S \frac{1}{r^2}\,dS} = \frac{1}{l}. \quad (21)$$

Here, r is the distance from the electrode tip to the considered point of the weld pool surface; S is the cross-sectional area of the column determined by the effective radius R of the arc. The radius depends on the current I of the arc [13]:

$$R = \sqrt{\frac{I}{\pi j} + R_f^2},$$

where j is the current density in the arc in flux vapors.

Electrical resistance of the stickout depends on its length L_f and temperature T_f distributed along the length:

$$R_f = \frac{4}{\pi d_f^2}\int_0^{L_f} \rho_e\big(T_f(z)\,dz\big). \quad (22)$$

Algorithm for the numerical solution to the system of equations of the physicomathematical model. Initially, the geometric structure of the weld pool formation zone is unknown. This requires continuous adjustment of the location of the interzone surfaces depending on the results of solving the equations of thermal conductivity and equilibrium of the weld pool. The location of the surfaces delimiting the solid, liquid and gaseous state of the flux and metal is specified by the position of the corresponding isotherms as a result of solving the heat conduction equation. To correct the location of the weld pool surface, the equation of pressure equilibrium on the given surface $Z(x, y)$ is solved. In this case, it is required to change the sizes of the zones *L, V, G, D*. It is assumed that the temperatures of the metal and slag in the displacement zone are equal to the surface temperature at the time of the solution, and their enthalpies change in accordance with this temperature. During the transformation, errors arise, which are defined as the rate of change in enthalpy when changing the volumes v_L, v_G of zones L and G:

$$\Lambda_L = \frac{d}{dt}\Big(\int_{v_L} H dv_L\Big) \text{ и } \Lambda_G = \frac{d}{dt}\Big(\int_{v_G} H dv_G\Big). \quad (23)$$

These errors are compensated for a change in the enthalpy of the L and G zones depending on the temperature distribution in them:

$$\frac{d}{dt}H\big((x, y, z) \in L\big) = \Lambda_L \frac{T(x, y, z) - T_L}{\frac{1}{v_L}\int_{v_L}(T(x, y, z) - T_L)\,dv_L}, \quad (24)$$

where T_L is the liquidus temperature.

As the thermodynamic state approaches the steady state, the transformation error is $\Lambda_L \to 0$. The condition for the simulation termination is stabilization of the solidus isotherm length:

$$\frac{d}{dt}(\max x \in S) \to 0. \quad (25)$$

The model system of equations is solved by the temperature distribution $T(x, y, z, t)$ and the geometric structure of the simulation zone. This provides reproducing the initial stage of the process from the arc starting moment until the established dimensions of the weld pool are reached. To solve the equations of thermal conductivity and equilibrium of the weld pool surface, the finite-difference method on conjugate meshes was used. On the interphase surfaces, the thermal conductivity coefficient was determined as the average harmonic value of the thermal conductivity of adjacent phases.

An algorithm for the numerical simulation of the welding process is schematically presented below.

Initial data: groove geometry after the previous pass, thermophysical properties of steel and flux, welding parameters
Determination of the initial geometry of the numerical solution domain Calculation of melting parameters of the electrode wire and energy characteristics of the welding arc
Cycle of unsteady numerical simulation of the thermodynamic state of the weld pool formation region
Determination of the distribution of heat fluxes over the surfaces of metal and slag Solving the heat equation
Solution to the variational problem on the location of welding arc in the groove
Solution to the equilibrium equation of the weld pool surface under the action of capillary, gravitational, electrodynamic, hydrodynamic and internal pressures
Calculation of the weld pool internal pressure by the condition of the balance of seam masses and electrode feed
to equal masses of surfacing and electrode feed
Correction of the location of the interphase boundaries of "vapor - slag – free flow flux - solid slag", "solid - liquid metal" according to the solutions to the equation of thermal conductivity and equilibrium of the surface of the weld pool
until the length of the solidus temperature isotherm stabilizes
Formation of a protocol of simulation results on temperature distribution, geometry of the weld pool formation area, energy characteristics of the welding process

Fig. 2. Algorithm for numerical simulation of the weld formation under the submerged-arc welding

Research Results. For a virtual study, we took information on the thermophysical properties of steels from [13]. In addition, we used the data of the Transstroiinvest corporate group on the specific steel grades and technological materials used, the modes of submerged-arc fillet welding of bridge metal structures[1].

Virtual reproduction of the welding process in 1F position. To test the developed model, we performed computer simulation of the T-joint welding of 15KHSND T1steel sheets 12 mm thick. The welding mode was chosen according to the recommendations [14]: Sv08GA wire with a diameter of 5 mm, arc voltage — 34 V, welding speed — 18 m/h (5 mm/s), electrode stickout — 25 mm. The electrode feed rate, calculated in the model, is 10 mm/s. This corresponds to the data of [14], which recommends these values in the range of 55–61 m/h.

Fig. 3 shows the results of welding simulation when the sheets are tilted 45° (1F position).

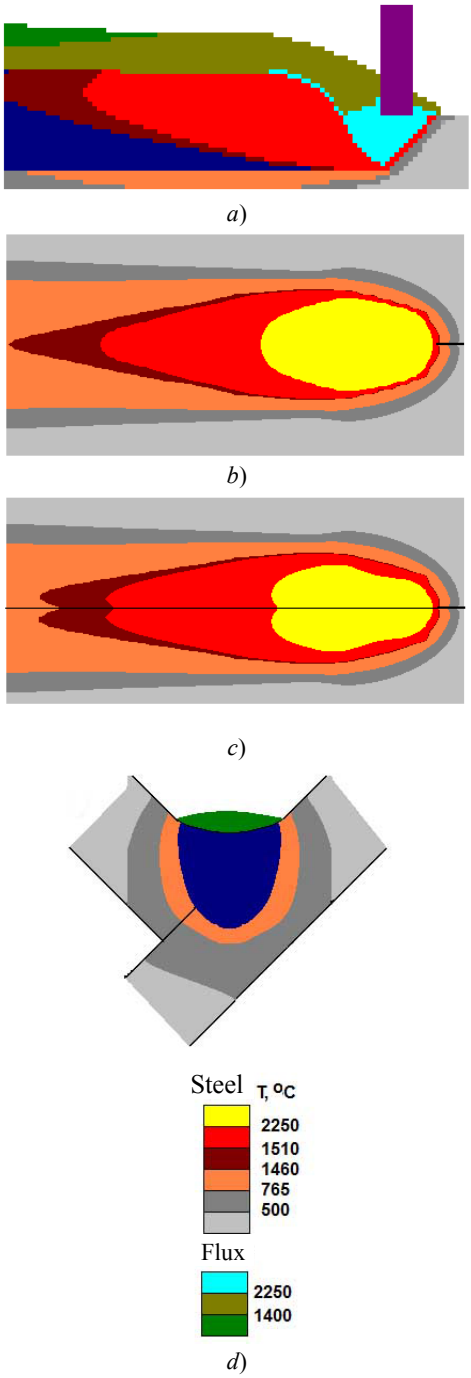

Fig. 3. Temperature distribution under submerged-arc fillet welding simulation when the sheets are tilted at 45° (1F position):
(a) longitudinal section of the weld pool in the plane of joint symmetry;
(b) submerged metal surface); (c) surface of the sheets to be welded;
(d) calculated cross-sectional profile of the seam

[1] STO-GK “Transstroi” -012-2007. Steel structures of bridges. Factory production. Moscow: Transstroy; 2007. 174 p. (In Russ.)

As a result, the following values were obtained: arc length — 6.8 mm; effective drop of anode voltage — 5.9 V, that of cathode voltage — 8.5 V; potential gradient in the arc column — 4.4 V/mm; arc column diameter — 18 mm. The total power of the process is 23 kW, of which 12.9 kW is radiation. The arc emits 4.3 kW at the electrode; 5.8 kW — at the joint surface. Heat dissipation power at the electrode stickout is 0.2 kW; the temperature of its heating by the arc current is 152°C. The area of the arc cavern plan is 135 mm^2; cavern volume is 519 mm^3. The crater depth under the arc is 16 mm. The length of the weld pool on the surface along the liquidus is 38 mm, along the solidus — 52 mm. The welding pool weight is 150 g. Seam width is 15 mm; the leg is 10.7 mm; the joint penetration depth is 6 mm; the cross-sectional area is158 mm^2. The weld is formed with a meniscus up to 1.3 mm.

Virtual simulation of the corner welding process. When welding large structures, it is impossible to use rotators. In this case, corner welding is performed. The simulation result of the formation of a weld at this position and under the same conditions is shown in Fig. 4.

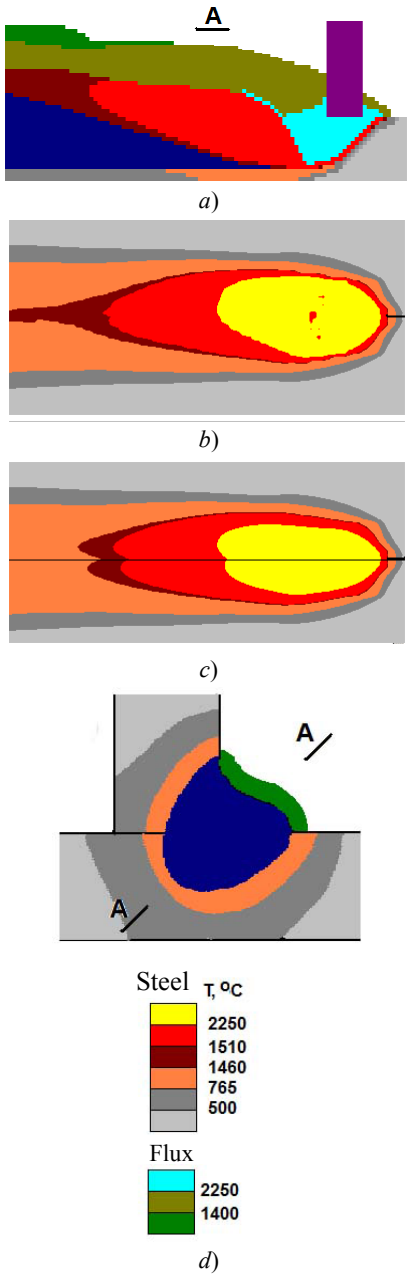

Fig. 4. The computer simulation result of the fillet weld formation under corner welding with welding of a vertical wall to a horizontal base: (*a*) longitudinal section of the weld pool in the symmetry plane of the joint; (*b*) submerged metal surface; (c) surface of weld sheets; (*d*) design weld cross-sectional profile

A noticeable melt flow from the butt wall to the flange under the corner welding is due to large mass of the weld pool. The deviation of the seam surface from the plane connecting the walls is ± 1.5 mm. The melt flows from the vertical wall to the horizontal base, so the weld is asymmetric, and the melt in the upper part of the weld is reduced by 2 mm.

The largest possible leg size. It needs to be specified at what maximum leg size ("1F position" and "corner"

welding) a high-quality seam is formed. For this purpose, we simulated fillet welding of 8 mm thick sheets with a 2 mm diameter wire at an arc current of 350 A. The welding speed and arc voltage were varied. The results are shown in Fig. 5.

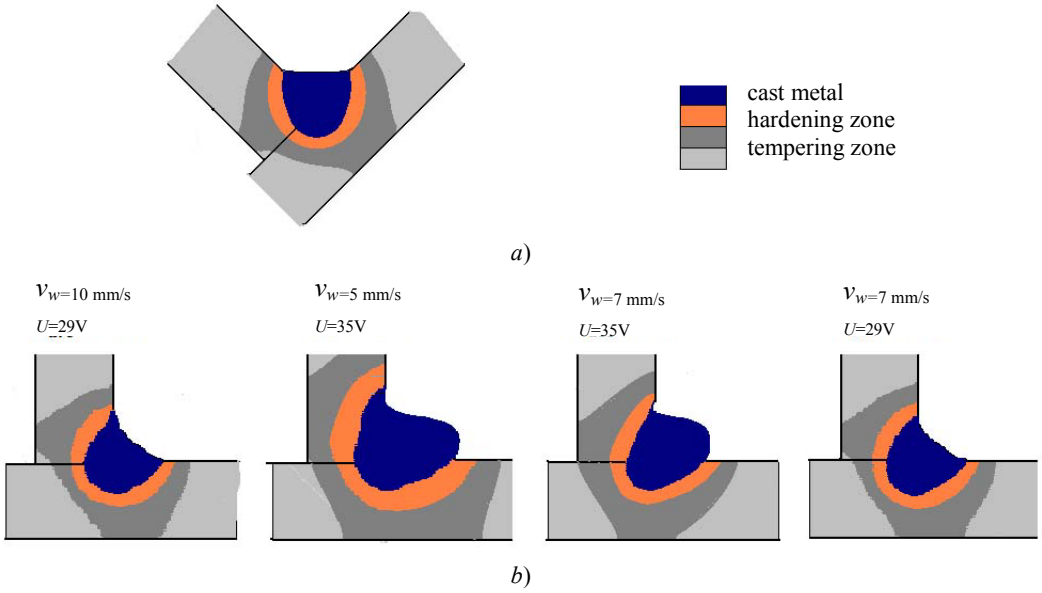

Fig. 5. Result of computer simulation of seam formation:
(*a*) 1F position, (*b*) corner

If the recommended 1F position welding speed is observed (Fig. 5*a*), a seam with equal legs of 6 mm is formed. This is less than required, but without collaring and meniscus. Under the corner welding in the same mode (Fig. 5*b*), a seam with meniscus is formed. To increase the leg, simulations were performed at a lower welding speed and a higher arc voltage value. At a speed of 5 mm/s and a voltage of 35 V, the cross-sectional area of the cast zone and its dimensions increase dramatically, but a seam is formed with an undercut and collar. Increasing the welding speed up to 7 mm/s reduces collaring. If the tension is reduced, an acceptable seam is formed with the legs of about 7 mm.

These results show that the recommended submerged arc welding modes are the most productive for obtaining legs of a given size. To obtain larger legs under single-arc welding, additional passes are required. However, in this case, the overall welding performance is significantly reduced.

Discussion and Conclusions. Labor intensity of manufacturing elements of bridge structures is largely determined by labor intensity of welding. A rational way to increase productivity is to use automatic submerged-arc welding. To optimize the technology using computer analysis methods, a physicomathematical model of forming fillet welds under submerged-arc welding has been developed. The model is based on a system of equations for heat conductivity and equilibrium of the weld pool surface. In this system, the formation of an arc cavern is determined by the boiling isotherm of the flux under the action of radiation from the arc column. Heat transfer by flux vapors inside the arc cavity and the influence of the spatial position on the formation of the weld pool are taken into account. The equations of the model of submerged-arc welding of fillet joint with metal thickness typical for bridge structures are solved numerically. The solution shows that when performing 1F position welding, the joint is formed in one pass. According to the simulation data, when welding a fillet weld “into a corner”, unsatisfactory formation is possible due to the flow of liquid metal from the vertical wall. In this case, additional backing passes are required to obtain a high-quality seam.

The studies have shown that the traditional technology of single-arc submerged-arc fillet welding with the formation of oversized legs has already reached its maximum productivity. To further increase it, it is required to use more complex advanced techniques. Such unconventional technologies include:

— multi-arc and multi-electrode welding methods [14, 15],

— introduction of non-conducting filler wire (cold wire feed welding) [16], granular metal additive (grit) or metal powder into the weld pool [17].

References

1. Kurlyand VG, Kurlyand VV. Stroitel'stvo mostov: ucheb. posob. dlya vuzov [Bridge Engineering]. Moscow: MADI; 2012. 176 p. (In Russ.)

2. Poloskov SS, Zheltenkov AV. Organizatsionno-upravlencheskii mekhanizm upravleniya innovatsionnym potentsialom vysokotekhnologichnykh naukoemkikh predpriyatii [Organizational and economic mechanism of management of innovative potential for high-tech knowledge intensive enterprises]. Economy and Entrepreneurship. 2019;2(103):1051–1057. (In Russ.)

3. Votinova EB, Shalimov MP, Fiveiskii AM. Osnovy tekhnologicheskoi podgotovki proizvodstva [Basics of technological preparation of production]. Ekaterinburg: URFU; 2017. 168 p. (In Russ.)

4. Mosin AA. Vozmozhnosti povysheniya proizvoditel'nosti svarki protyazhennykh uglovykh shvov mostovykh metallokonstruktsii [Ways to solve problems of increasing the efficiency of welding long corner seams of three-dimensional metal structures]. Welding and Diagnostics. 2020;1:50–54. (In Russ.)

5. Artemov AO, Karatysh VV, Yazovskikh VM, et al. Issledovanie vliyaniya rezhimov svarki pod sloem flyusa na formu i proplavlenie uglovykh shvov [Investigation of the effect of submerged-arc welding modes on the shape and penetration of fillet welds]. Bulletin of Perm University. Machine Building, Materials Sciences. 2010;12(5):130–142. (In Russ.)

6. Tomas KI, Il'yashchenko DP. Tekhnologiya svarochnogo proizvodstva [Welding technology]. Tomsk: Izd-vo TPU; 2011. 247 p. (In Russ.)

7. Shen J, Chen Z. Welding simulation of fillet-welded joint using shell elements with section integration. Journal of Materials Processing Technology. 2014;214(11):2529–2536.

8. Cho D-W, Song W-H, Cho M-H, et al. Analysis of submerged arc welding process by three-dimensional computational fluid dynamics simulations. Journal of Materials Processing Technology. 2013;213(12):2278–2291.

9. Sudnik VA, Erofeev VA, Maslennikov AV, et al. Matematicheskaya model' protsessa svarki pod flyusom i yavlenii v dugovoi kaverne [Mathematical model of the submerged-arc welding process and phenomena in the arc cavern]. Svarochnoe Proizvodstvo. 2012;7:3–12. (In Russ.)

10. Sudnik VA, Erofeev VA, Maslennikov AV. Matematicheskaya model' formirovaniya svarochnoi vanny pri dugovoi svarke pod flyusom i analiz protsessa perenosa metalla [Mathematical model of the weld pool formation in the saw-process and analysis of the electrode metal transfer]. Izvestiya TulGU. 2015;6(2):21–31. (In Russ.)

11. Ghosh A, Chattopadhyay H. Mathematical modeling of moving heat source shape for submerged arc welding process. The International Journal of Advanced Manufacturing Technology. 2013;6:2691–2701.

12. Leskov GI. Ehlektricheskaya svarochnaya duga [Electric welding arc]. Moscow: Mashinostroenie; 1970. 355 p. (In Russ.)

13. Taits NYu. Tekhnologiya nagreva stali [Steel heating technology]. Moscow: Metallurgizdat; 1962. 568 p. (In Russ.)

14. Mel'nikov AYu, Fiveiskii AM, Sholokhov MA, et al. Inzhenernaya metodika rascheta parametrov rezhima dvukhdugovoi svarki uglovykh shvov [Engineering method for calculating the parameters of the mode of double-arc welding of fillet welds]. Welding and Diagnostics. 2016;3:46–48. (In Russ.)

15. Kiran DV, Cho D-W, Song W-H, et al. Arc interaction and molten pool behavior in the three wire submerged arc welding process. International Journal of Heat and Mass Transfer. 2015;87:327–340.

16. Ribeiro RA, Dos Santos EBF, Assunção PDC, et al. Predicting weld bead geometry in the novel CW-GMAW process. Welding Journal. 2015;94(9):301–311.

17. Ivochkin II, Malyshev BD. Svarka pod flyusom s dopolnitel'noi prisadkoi [Submerged arc welding with additional additive]. Moscow: Stroiizdat; 1981. 176 p. (In Russ.)

Submitted 30.04.2020
Scheduled in the issue 06.07.2020

About the Authors:

Mosin, Aleksei A., Deputy Director for Production, "Kurganstalmost" CJSC (3, Zagorodnaya St., Kurgan, 640023, RF), ORCID: https://orcid.org/0000-0002-5809-5423, Mosinaa@kurganstalmost.ru.

Erofeev, Vladimir A., professor of the Welding, Casting and Construction Materials Technology Department, Tula State University (92, Lenin Pr., Tula, 300012, RF), Cand.Sci. (Eng.), ORCID: https://orcid.org/0000-0003-3756-2640, Va_erofeev@mail.ru.

Sholokhov, Mikhail A., Head of the Automation and Robotization of Welding Production Department, Yeltsin Ural Federal University (UrFU) (19, Mira St., Ekaterinburg, 620002, RF), Cand.Sci. (Eng.), ORCID: https://orcid.org/0000-0002-7666-5645, M.a.sholokhov@urfu.ru.

Claimed contributorship

A. A. Mosin: research objectives and task setting; determination of the modeling area and boundary conditions; analysis of the research results; text preparation; formulation of conclusions. V. A. Erofeev: building of the physicomathematical model; analysis of the research results. M. A. Sholokhov: academic advising; the text revision; correction of the conclusions.

All authors have read and approved the final manuscript.

MACHINE BUILDING AND MACHINE SCIENCE

UDC 621.793.1(620.18) https://doi.org/10.23947/2687-1653-2020-20-3-269-279

Morphology and genealogy of structural defects in vacuum ion-plasma coatings

O. V. Kudryakov, V. N. Varavka, I. Yu. Zabiyaka, E. A. Yadrets, V. P. Karavaev
Don State Technical University (Rostov-on-Don, Russian Federation)

Introduction. The main work objective is systematization and analysis of structural defects of vacuum ion-plasma coatings; on this basis, their classification principles are developed and given in the paper. Another important part of the work is the experimental study on one of the specific defects of coatings, which the authors propose to call "defect of substructural origin".

Materials and Methods. PVD coatings of various nitride and metal systems 1.5–9.0 μm thick were used as an object of the research. Coatings were applied in vacuum installations using arc and magnetron evaporators. The research results were obtained by high resolution electron microscopy, energy dispersive analysis and indentation.

Results. Various types of defects in ion-vacuum coatings are presented as the research results. They include discontinuities, deformation of crystallites, and structural inhomogeneity. The principles of their systematization are validated. It is proposed to classify defects into droplet, substructural, and growth defects (depending on the causes of their nucleation), as well as regular and stochastic ones (depending on their distribution in the coating volume). The study of "substructural defects", classified by the authors as stochastic, is given special consideration. These micrometric defects are shaped like a cylinder with a conical "head". Their main axle is oriented perpendicular to the surface of the coating. They can be "extruded" (tore away) by the coating. The paper validates the dislocation mechanism of their nucleation and the helicoid growth principle.

Conclusions. The inference is summarized that the proposed systematization of defects in ion-plasma coatings has the character of an intermediate result of research in this scientific area. At this, the "substructural defects" do not have a fatal effect on the structure and properties of the coating due to a small size.

Keywords: metal ceramic coatings, vacuum ion-plasma deposition, microstructure, structure defects, scanning electron microscopy.

For citation: O.V. Kudryakov, V.N. Varavka, I.Yu. Zabiyaka, et al. Morphology and genealogy of structural defects in vacuum ion-plasma coatings. Advanced Engineering Research, 2020, vol. 20, no. 3, p. 269–279. https://doi.org/10.23947/2687-1653-2020-20-3-269-279

Funding information: the research is done with the financial support from RFFI (grant no. 18-08-00546).

Introduction and Problem Statement. Obtaining ion-plasma coatings is one of the most rapidly developing research areas. Despite the high publication activity of scientists working in this area, the authors failed to find thorough fundamental studies on the defects of ion-plasma coatings. The problem of defects is usually rated as technological, and, in this case, it is considered not in the content-related part of a scientific publication, but only in the methodological one. In this regard, when performing this work devoted to the problem of defects in ion-plasma coatings, two objectives have been set:

— to suggest classification principles for defects of this type of coating on the basis of a small review;

— to conduct a study on one of the specific types of such defects, which we propose to call “defects of substructural origin”.

Materials and Methods. To obtain coatings, vacuum ion-plasma spraying units were used: two-cathode system PLATIT π^{80} equipped with two arc evaporators; modernized TINA-900 unit equipped with magnetron evaporators. The operating modes of coating deposition were as follows: deposition temperature — 300−450ºC; pressure in the vacuum chamber — $(1.3−4.7)\times10^{-2}$ mbar; bias voltage — 100−150 V. In accordance with the given parameters of the vacuum ion-plasma technology, the resulting coatings are classified as PVD. The coatings of various nitride and metal systems with a thickness of 1.5−9.0 μm have been investigated. The basic results on the study of substructural defects were obtained on Ti-Al-N coatings. The coating hardness of the selected systems exceeded 12−15 GPa, which allows them to fall into the category of wear-resistant.

Samples from various structural steels were used as a substrate. The impact of the composition, structure, and properties of the substrate on the parameters of the coatings was not taken into account. Before coating deposition, the sample surface was cleaned in a vacuum chamber by a continuous flow of Ar ions for 5 min. To provide high adhesion of the coatings, a sublayer of the first metal in the system was applied to the sample surface cleaned by the ion beam.

To study the microstructure of the coatings and their surface relief with high resolution, we used a scanning dual beam (electron/ion, SEM/FIB) microscope ZEISS CrossBeam 340 with an integral energy-dispersive X-ray detector X-Max EDAX (Oxford Instruments).

Results and Discussion. One of the basic conditions for zero-defect coatings obtained using the ion-plasma technology is the minimum branching of the substrate surface relief. To implement the procedure, according to the normative requirement to the surface relief, roughness should have the parameters not lower than $R_a \le 0.12$ μm; $R_z \le 0.6$ μm. Failure to comply with these conditions can cause the formation of “regular growth defects” in the coating during deposition in the form of porosity, deformation of crystallites and lattice, internal stresses, etc. Microroughnesses located separately on a tolerably smooth substrate relief cause disorientation of the axes of growing crystallites, which induces their deformation and forms incoherent, often porous, intercrystalline boundaries. High density of microroughnesses causes the formation of a large volume of porosity near the coating and substrate interface. Large waviness of the substrate surface, for example, during rough grinding, forms high stresses in the coating, which, under weak cohesive bonds in the coating, can induce its delamination, and under poor adhesion — complete delamination of the coating. Coatings with such defects, as a rule, do not meet even the most moderate operating requirements in terms of protecting products from wear, corrosion and similar actions.

If the specified requirements for the substrate surface roughness are met and the coating is uniform in density and structure, this does not exclude the appearance of random defects in it: those of substructural origin and due to the presence of a droplet phase.

Since the appearance of both types of defects in a specific microvolume of the coating is of a random nature, then, in contrast to “regular growth defects”, it is logical to combine them into a class of “stochastic defects”. Among them, “droplet defects” are mainly formed when using powerful thermal evaporators of a vacuum installation, as well as during the deposition of fusible coating elements. “Droplet defects” can be almost completely eliminated through magnetron evaporation. Examples of “drop stochastic defects” of ion-plasma coatings are shown in Fig. 1. On the surface, they have a characteristic shape with a flaky configuration, which is marked in Fig. 1 a with dark arrows. Getting on the surface of the coating during its application, the droplet phase violates the laminar dynamics of the normal growth of the coating, which manifests itself in the form of irregular pores in the cross section of the coating (Fig. 1 b). In multilayer coatings, pores and structural inhomogeneity formed in the droplet phase zones can have an elongated shape at the boundaries of the coating layers during the transition from a layer with refractory components to a layer with a fusible element (Fig. 1 c).

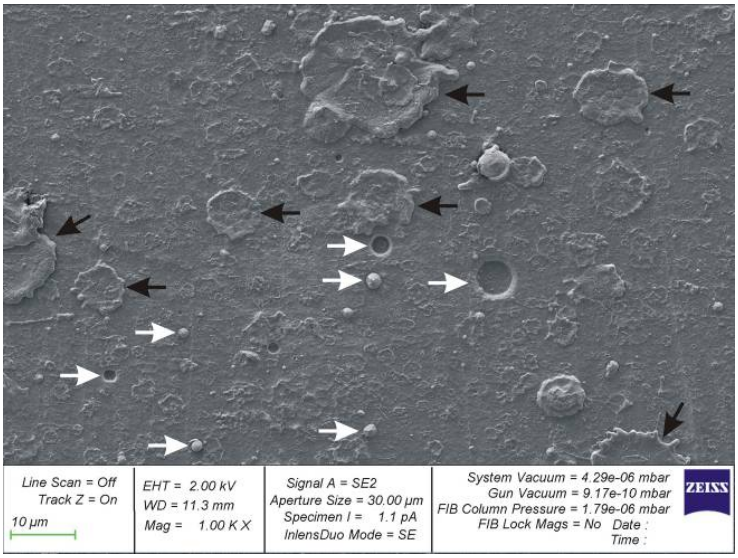

a)

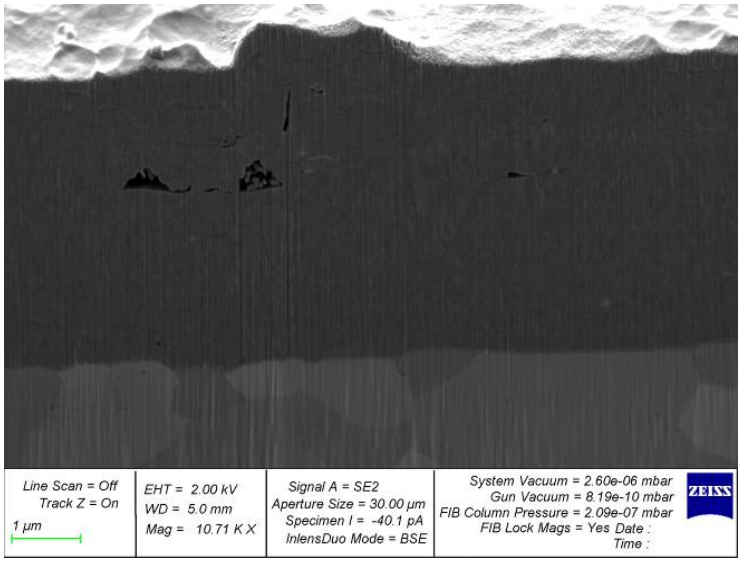

b)

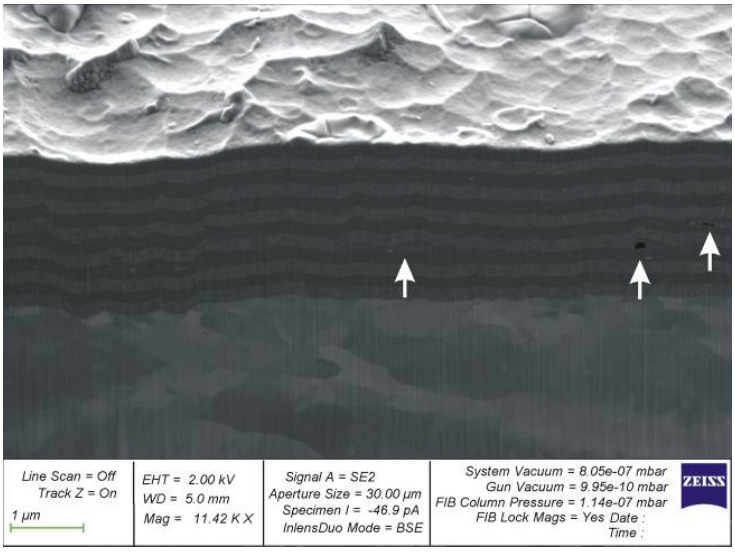

c)

Fig. 1. Examples of droplet defects in TiAlN coatings, SEM: *(a)* on the coating surface (marked with dark arrows); *(b)* in the cross section of a monolayer coating; *(c)* in the cross section of a multilayer coating (marked with light arrows)

In general, all of the coating defects discussed above are of technological origin. Their appearance can be excluded or limited through optimization of the process variables of the ion-plasma method and equipment. With regard to defects of substructural origin, the regulation or exclusion of their appearance in the coating seems unlikely since they are due to the very nature of the actual coating material. The results of studying such defects are the subject matter of this work.

Examples of the studied defects of substructural origin are shown in Fig. 1 *a* (marked with light arrows) and in Fig. 2. They have a characteristic geometric shape. In the body of the coating, there is a cylindrical part of the defect, and a conical part protrudes above the surface of the coating. Under certain conditions, the formed defect is rejected through undergoing extrusion, i.e., extrusion by the coating, leaving cylindrical depressions of the correct geometric configuration in place of its localization. If the coating process continues, the cavity is filled with the deposited ions of the coating material at a higher rate than the rest of the flat surface. This is probably due to the "edge effects" of the electromagnetic field formed by the bias voltage on the substrate. As a result, the cylindrical depressions are "healed" during the application process, and the coating is sufficiently uniform in this area. If the considered defects are extruded from the coating immediately before the end of the process of its application, then the remaining cylindrical niches are clearly visible on the surface (Fig. 1 *a*, and 2 *a* – 2 *d*).

Fig. 2 shows a complete microscopic picture of various stages of the life cycle of substructural defects in the PVD coating of the Ti-Al-N system. Normal projection shows three defects of different sizes located at a distance of several micrometers from each other (marked with arrows). The conical shape of the protruding part of localized defects and the cylindrical niche of the extruded defect are clearly visible. In Fig. 2 *b* – 2 *d*, these stages of the existence of defects are presented in a three-dimensional picture. Conical "heads" protruding from the coating are designated by number 1, cylindrical niches — by number 2; and number 3 in Fig. 2 *d*, shows the place of the niche at the stage of "healing". The volumetric image was obtained through preparing the FIB cross-section, perpendicular to the coating surface, and then tilting the sample towards the detector by 15–28°. Fig. 2 *b*, 2 *c*, show only the cross section of the coating and its surface, and Fig. 2 *d* — the entire cross-section in block. The preparation of cross-sections provided obtaining a cross section of the investigated defects (Fig. 2 *b*, 2 *c*). It is clearly seen that their lower base is flat, being located inside the coating at different depths, and morphologically not related to the coating structure or to the substrate relief. Almost all visible in Fig. 2 defects have different diameters and heights, while the angle at the apex of the conical "head", i.e., the ratio of its diameter to height, changes insignificantly. This suggests that defects grow as the coating grows. Defects originate at a certain point on the surface of an already existing "growing" coating and subsequently increase their diameter and height further on with time. The growth of the coating and the defect occurs simultaneously and at the same rate, with the exception of the advanced growth of the "head" of the defect, since until the moment of extrusion, the "head" has to always be above the level of the coating surface.

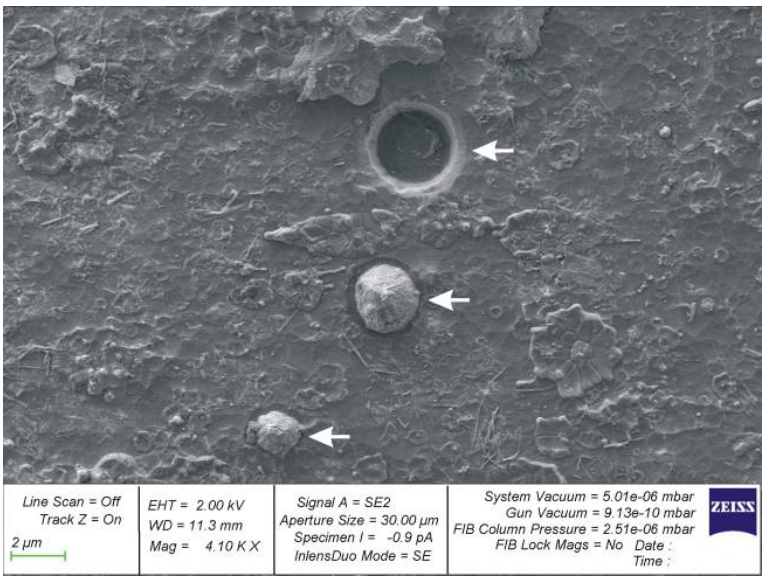
Line Scan = Off
Track Z = On
2 µm
EHT = 2.00 kV
WD = 11.3 mm
Mag = 4.10 K X
Signal A = SE2
Aperture Size = 30.00 µm
Specimen I = -0.9 pA
InlensDuo Mode = SE
System Vacuum = 5.01e-06 mbar
Gun Vacuum = 9.13e-10 mbar
FIB Column Pressure = 2.51e-06 mbar
FIB Lock Mags = No Date :
Time :
ZEISS

a)

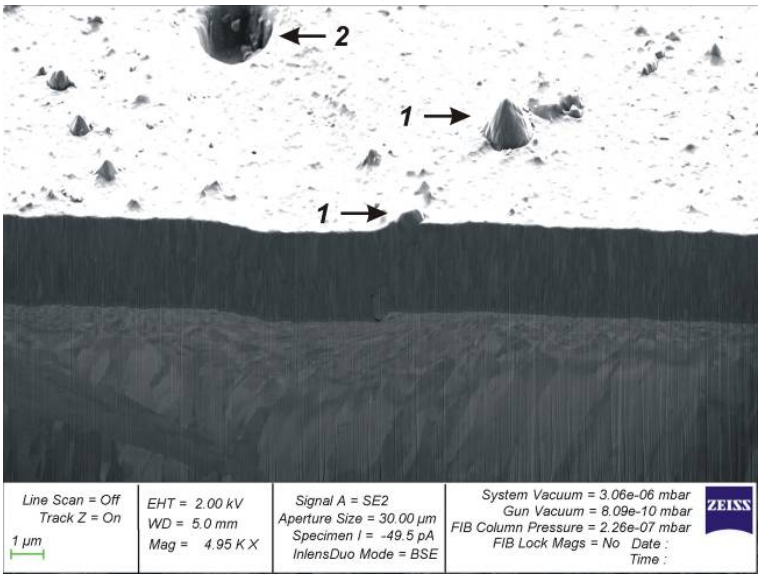
2
1
1
Line Scan = Off
Track Z = On
1 µm
EHT = 2.00 kV
WD = 5.0 mm
Mag = 4.95 K X
Signal A = SE2
Aperture Size = 30.00 µm
Specimen I = -49.5 pA
InlensDuo Mode = BSE
System Vacuum = 3.06e-06 mbar
Gun Vacuum = 8.09e-10 mbar
FIB Column Pressure = 2.26e-07 mbar
FIB Lock Mags = No Date :
Time :
ZEISS

b)

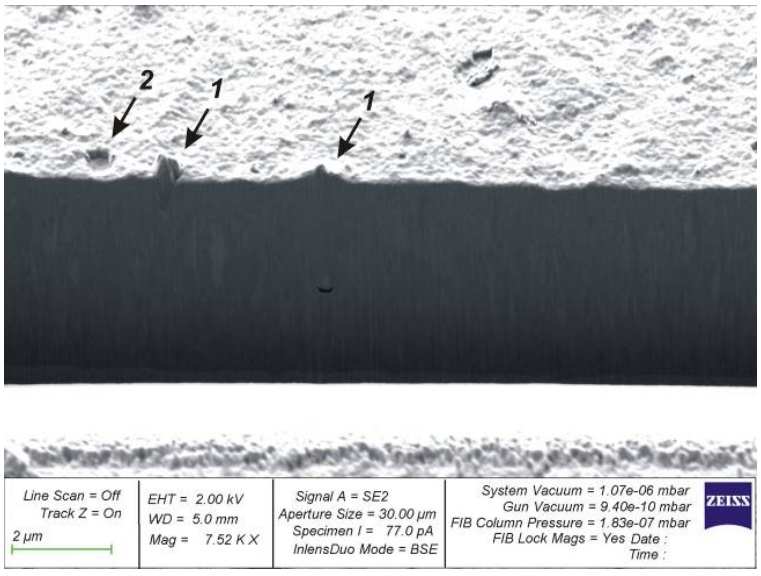
2
1
1
Line Scan = Off
Track Z = On
2 µm
EHT = 2.00 kV
WD = 5.0 mm
Mag = 7.52 K X
Signal A = SE2
Aperture Size = 30.00 µm
Specimen I = 77.0 pA
InlensDuo Mode = BSE
System Vacuum = 1.07e-06 mbar
Gun Vacuum = 9.40e-10 mbar
FIB Column Pressure = 1.83e-07 mbar
FIB Lock Mags = Yes Date :
Time :
ZEISS

c)

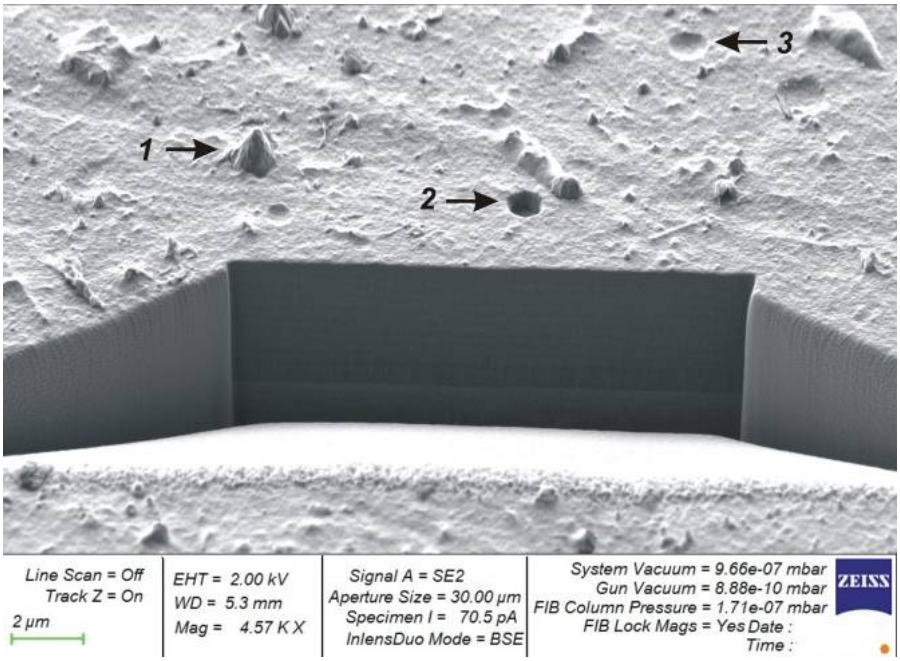

d)

Fig. 2. Substructural defects of ion-plasma TiAlN coatings, SEM: (*a*) on the coating surface in normal projection (marked with arrows); (*b*)–(*d*) on the surface of the coating and in cross-sections FIB

In the literature, both scientific and technological, concerning the formation of ion-plasma coatings, the substructural defects under discussion are often attributed to a droplet origin. It is assumed that the droplet phase formed in the chamber, when getting on the coating surface, burns it through and is fixed in the surface layer. When a drop crystallizes, its volume decreases, and it falls out leaving a cylindrical niche. This mechanism of formation of the defects under consideration contradicts the kinetics of their growth described above, based on the presented micrographs, and is also refuted by the experimental fact that defects of such geometry are observed not only during thermal evaporation, when the presence of a droplet phase cannot be avoided, but also during magnetron evaporation, whose regime eliminates the formation of drops in the chamber. Moreover, the morphology of the described defects under the arc and magnetron evaporators is identical. In addition, in the coatings obtained through the magnetron evaporation, these defects occur also in the case when all the components of the coating are infusible and temperature of their transition to the liquid state cannot be obtained under the applied coating modes [1, 2].

On the basis of the experimental data presented in [3], the authors put forward and validated a hypothesis on the endogenous (internal with respect to the coating) origin of the defects considered. Its physical essence is as follows. As you know, there are no real defect-free materials including coatings. In the process of formation of the crystal structure of the coating, inherent defects of various geometries are also formed: point, linear, surface, volumetric. Even the densest PVD coatings with an ordered structure, for example, monolayer thin films, contain various defects in the crystal structure [4–8]. The formation of dislocations under the growth of coatings, as in any crystallization process, is natural. Taking into account the nature of the deposition of ion-plasma coatings, when the modes of shear stresses in the coating are practically absent, the formation of screw dislocations is most likely. If such a dislocation reaches the coating surface, it forms a helical step. During deposition, as a result of the attachment of ions to a non-growing step,

the latter will move along the surface rotating around a fixed axis. This is how the well-known mechanism of spiral (helical) crystal growth in the direction of the dislocation axis is implemented [9]. The dislocation growth mechanism is also used to explain the formation of "crystal whiskers".

At a high density of screw dislocations on the surface, the distance between them is small, and the atomic layers formed on adjacent steps merge. In this case, the growth of the surface occurs in a cohesive way and gives a tolerably flat coating plane [10–12]. Dislocations distant wide apart form single cones. This is due to the fact that the portions of the step located closer to the dislocation axis rotate around it faster and require a smaller amount of deposited ions per unit time for growth than the distant portions. Thus, the twisting of the spiral under the screw growth occurs from the periphery to the dislocation axis, which determines the conical shape of the protruding part ("head") of the growing crystal (Fig. 2). The shape of the helicoid spirals, that is, the size of the steps, is determined by the rate of their growth, which, in turn, depends on the concentration of the components in the growing crystallite. The shape of the areas of growing spirals at a fast growth rate and, accordingly, high over-saturations, is close to circular; at a lower growth rate and, accordingly, low over-saturations, it is polygonal. With an increase in the growth rate (with an increase in over-saturation), the angle of the growth cone becomes steeper, and the height of the steps in such spirals is large [13–16].

These features of helical growth suggest that the considered defects of ion-plasma coatings (Fig. 2) are formed at a high growth rate. This is indicated by the cylindrical shape of their "base" recessed into the coating, and a sharp conical shape of the "head" protruding above the coating surface. These geometric features also assume enrichment of conical crystallites in one of the coating components. Apparently, the higher growth rate of the spiral faces of the considered defect in comparison with the surrounding volume of the coating is the key reason for the isolation of the considered substructural defects in the coating and their subsequent extrusion.

Thus, from the terminological point of view, the defects of PVD coatings considered by us are substructural in origin, since:

— they originate at dislocations;

— for the place of localization, they are stochastic since the occurrence of dislocations in the coating is a random process;

— by morphology, they are helicoid since they are formed on screw dislocations and develop according to the mechanism of spiral growth.

Statistical data on the geometric characteristics of substructural defects in the Ti-Mo coating are shown in Fig. 3. Under the statistical analysis, the maximum diameter of the "head" measured over the coating surface was considered as the diameter of the defect *d*.

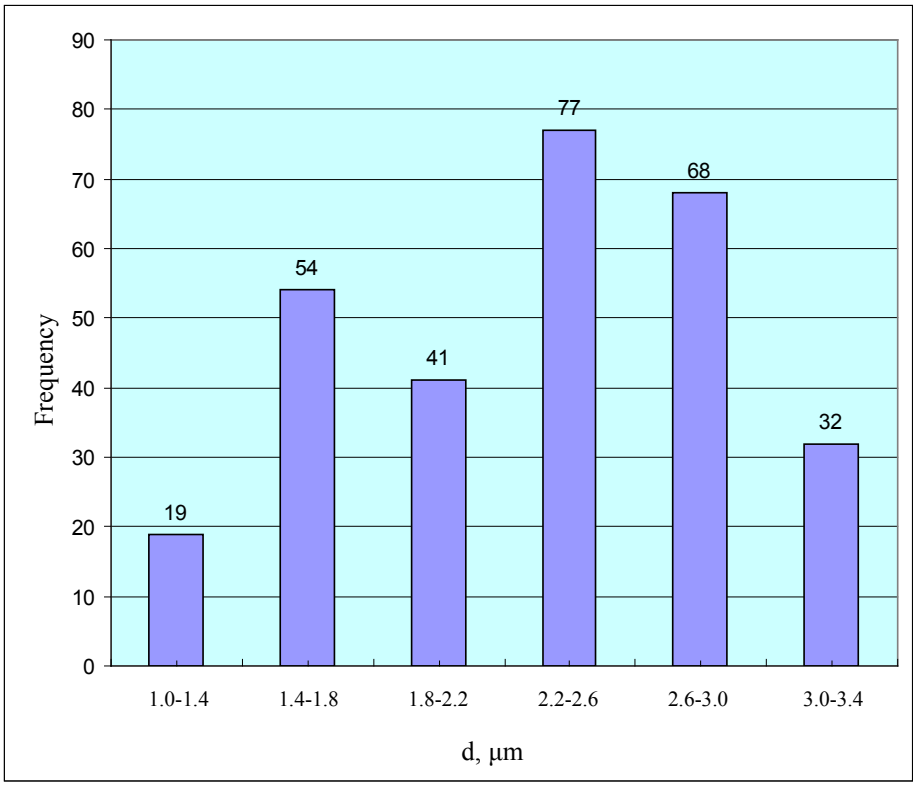

Fig. 3. Diameter d distribution of substructural defects in Ti-Mo coatings

The scatter of d values is quite significant and amounts to 0.95 – 3.3 μm, the average value is $d_{cp.} = 2.26$ μm. For coatings of the Ti-Al-N system, the values of similar statistical parameters are: $d = 1.2 – 4.0$ μm; $d_{cp} = 1.91$ μm. The average statistical value of the parameter d/h_0, where h_0 is the height of the conical "head" of the defect protruding above the coating surface; for all studied coating compositions was 1.48, which corresponds to the angle at the apex of the "head" cone — 73°.

A similar statistical analysis based on the results of electron microscopic studies of the diameters of extruded defects (niches) d_e, has shown that the spread in d_e values is too large to assert that the extrusion of a defect occurs when a certain fixed critical value d_e is attained. Fig. 4 shows that in the coating of the Ti-Al-N system there are extrusions of various diameters, whose range of values is $d_e = 1.3 – 4.6$ μm. This interval overlaps with the interval of d values, and average values of the compared parameters are also close: $d_{cp} = 1.91$ μm and $d_{ecp} = 2.17$ μm.

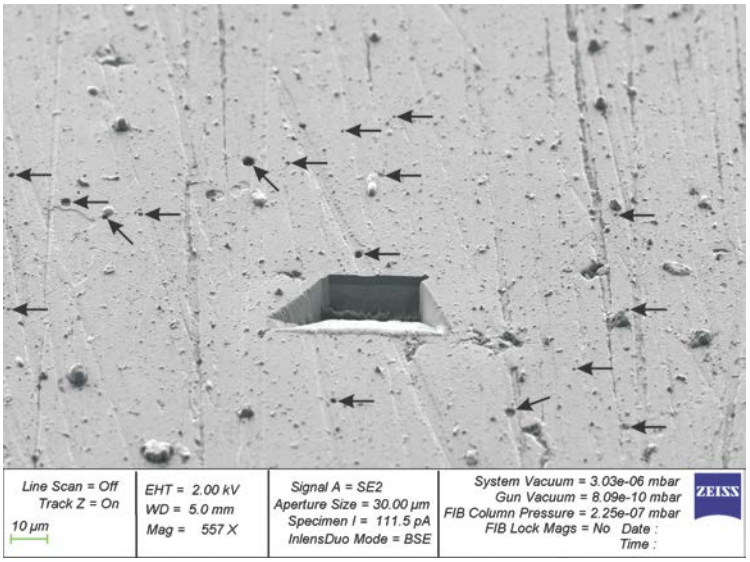

Fig. 4. Surface of TiAlN coating with substructural defects, SEM: arrows indicate extrusion defects; in the center there is rectangular FIB cross-section

The available experimental data do not explain at what geometrical parameters of a growing substructural defect it is extruded from the coating, but they establish the baseline for further theoretical study on this aspect, for example, based on the classical theories of dislocation and nucleation.

Conclusion. Within the framework of the objectives set by the authors, the study gives certain intermediate results both on the classification characteristics of defects in ion-plasma coatings and on the investigation of defects of substructural origin. The substructural defects considered by the authors are found in coatings of various compositions and structures. Therefore, they can, despite their stochastic nature, claim to be a "systemic error of technology", which, however, does not have a fatal effect on the structure and properties of the coating due to the smallness of its size. Thus, they can, despite their stochastic nature, pretend to be a "systemic error of technology," which, however, does not have a fatal effect on the structure and properties of the coating due to the smallness of its size. More or less fully, the authors have studied this type of defects only in coatings of the Ti-Al-N system; therefore, the logical development of this research area involves expanding the range of coating composition.

References

1. Varavka VN, Kudryakov OV, Ryzhenkov AV. Multilayered Nanocomposite Coatings for Anti-Erosive Protection. Chapter 5. In: "Piezoelectrics and Nanomaterials: Fundamentals, Developments and Applications", I. A. Parinov (ed.). USA, NY: Nova Science Publishers; 2015. P. 105−132.

2. Kudryakov OV, Varavka VN, Zabiyaka IYu, et al. Structure and properties of multilayered nanocomposite coatings. Int. J. Res. 2016;46(4-2):117−120.

3. Varavka VN, Kudryakov OV, Zabiyaka IYu, et al. Conditions and mechanisms of the defects formation in vacuum ion-plasma coatings. IOP Conference Series: Materials Science and Engineering. 2019;680:012021. DOI: 10.1088/1757-899X/680/1/012021

4. Cavaleiro A, de Hosson JT (eds.). Nanostrukturnye pokrytiya: sbornik; per. s angl. [Nanostructured coatings]. Moscow: Tekhnosfera; 2011. 752 p. (In Russ., transl. from Eng.)

5. Freund LB, Suresh S. Thin film materials: stress, defect formation and surface evolution. Boston Cambridge University: Press; 2003. 750 p.

6. Cleland AN. Foundations of Nanomechanics. Berlin: Springer-Verlag; 2003. 436 p.

7. Sapunov SYu, Kudryakov OV, Fartushnyi NI. Stroenie i svoistva nikel'-tsinkovogo pokrytiya na stali [Structure and properties of nickel-zinc coatings on steel]. Steel. 2003;11:94–96. (In Russ.)

8. Il'in AA, Plikhunov VV, Petrov LM, et al. Vakuumnaya ionno-plazmennaya obrabotka [Vacuum ion-plasma treatment]. Moscow: INFRA-M; 2014. 160 p. (In Russ.)

9. Burton WK, Cabrera N, Frank FC. The growth of crystals and the equilibrium structure of their surfaces. Phil. Trans. R. Soc. Lond. 1951;A243:299–358.

10. Chernov AA. Protsessy kristallizatsii: T. 3 Sovremennaya kristallografiya [Crystallization Processes: Vol. 3. Modern Crystallography], BK Vainshtein (ed.). Moscow: Nauka; 1980. 408 p. (In Russ.)

11. Kudryakov OV, Pustovoit VN. Strukturnyi kriterii korrozionnoi stoikosti «belykh sloev» [Structural criterion of corrosion resistance of "white layers"]. Materialovedenie. 1998;7:33–40. (In Russ.)

12. Kudryakov OV, Varavka VN. Fenomenologiya martensitnogo prevrashcheniya i struktury stali [Phenomenology of martensitic transformation and steel structure]. Rostov-on-Don: DSTU Publ. House; 2004. 200 p. (In Russ.)

13. Rashkovich LN, Petrova EV, Shustin OA, et al. Formirovanie dislokatsionnoi spirali na grani (010) kristalla biftalata kaliya (BFK) [Formation of a dislocation spiral on the (010) face of a potassium hydrogen phthalate crystal]. Physics of the Solid State. 2003;45(2):377–383. (In Russ.)

14. Ester GR, Price R, Halfpenny PJ. The relationship between crystal growth and defect structure: a study of potassium hydrogen phthalate using x-ray topography and atomic force microscopy. JOP: Applied Physics. 1999;32(10A):128–133.

15. Ester GR, Halfpenny PJ. Observation of two-dimensional nucleation on the {010} face of potassium hydrogen phthalate (KAP) crystals using ex situ atomic force microscopy. J. Cryst. Growth. 1998;187(1):111–117.

16. Murugakoothan P, Kumar RM, Ushasree PM, et al. Habit modification of potassium acid phthalate (KAP) single crystals by impurities. J. Cryst. Growth. 1999;207(4):325–329.

Submitted 02.06.2020

Scheduled in the issue 31.08.2020

About the Authors:

Kudryakov, Oleg V., professor of the Physical and Applied Materials Science Department, Don State Technical University (1, Gagarin sq., Rostov-on-Don, 344003, RF), Dr.Sci. (Eng.), professor, ResearcherID: AAM-3486-2020, ScopusID 6602455202, ORCID: http://orcid.org/0000-0002-1462-4389, kudryakov@mail.ru

Varavka, Valerii N., professor of the Physical and Applied Materials Science Department, Don State Technical University (1, Gagarin sq., Rostov-on-Don, 344003, RF), Dr.Sci. (Eng.), associate professor, ResearcherID: K-8387-2017., ScopusID 6602988833, ORCID: http://orcid.org/0000-0003-4703-7372, varavkavn@gmail.com

Zabiyaka, Igor' Yu., postgraduate student of the Physical and Applied Materials Science Department, Don State Technical University (1, Gagarin sq., Rostov-on-Don, 344003, RF), ResearcherID: AAN-7230-2020, ScopusID 57195480998, ORCID: http://orcid.org/0000-0001-6759-549X, zabiyakaigor@gmail.com

Yadrets, Ehduard A., graduate student of the Physical and Applied Materials Science Department, Don State Technical University (1, Gagarin sq., Rostov-on-Don, 344003, RF), ORCID: http://orcid.org/0000-0002-2943-2160, xperia1058@gmail.com

Karavaev, Vadim P., graduate student of the Physical and Applied Materials Science Department, Don State Technical University (1, Gagarin sq., Rostov-on-Don, 344003, RF), ORCID: http://orcid.org/0000-0002-7376-6408, super.vud2015@yandex.ru

Claimed contributorship

O. V. Kudryakov: underlying concept and research plan; development of conceptual classification principles for defects in vacuum ion-plasma coatings; analysis of the experimental data; theoretical underpinning of the hypothesis

of the formation of "substructural defects" of coatings; academic advising; editing of the text of the paper. V. N. Varavka: formulation of the research objectives and tasks; organization and support of the methodological and experimental part of the research; preparation and formation of the text of the paper, results and conclusions. I. Yu. Zabiyaka: experimental studies using scanning electron microscopy, energy dispersive analysis and nanoindentation. Eh. A. Yadrets: sample preparation for research; participation in the application of experimental ion-plasma coatings; participation in obtaining the required experimental data. V. P. Karavaev: analysis of literary sources and own data on the subject area of the work; recordation and textualisation of the experimental data; preparation of illustrations for the paper.

All authors have read and approved the final manuscript.

MACHINE BUILDING AND MACHINE SCIENCE

UDC 621.793.182 https://doi.org/10.23947/2687-1653-2020-20-3-280-288

Selection of technologies for metal film application using physical deposition techniques

S. P. Glushko
Kuban State Technological University (Krasnodar, Russian Federation)

Introduction. Obtaining high-quality thin metal films is important for advances in the technologies of applying antifriction and wear-resistant coatings on cutting tools or parts of friction pairs. Various techniques of physical film deposition are applied using technologies of cathode (ion), magnetron and ion beam assisted sputtering. The work objective is to analyze, compare and determine the feasibility of techniques for the physical deposition of thin metal films when applying antifriction and wear-resistant coatings on cutting tools or parts of friction pairs.

Materials and Methods. Technologies of cathode (ionic), magnetron and ion-beam sputtering are considered. Schematic diagrams, conditions and parameters of the considered processes are presented.

Results. An advanced technology for the deposition of thin films, alloying and hardening of the surfaces of metal parts is magnetron sputtering. Continuous wave (cw) magnetrons are used to apply coatings of complex composition or multilayer coatings on flat substrates. Ion beam sputtering is considered as slow sputtering of the target surface by bombardment with a high-energy ion beam and deposition on the substrate surface. Under the ion implantation, the surface of metals is doped with recoil atoms, which receive high energy from accelerated ions and move a few nanometers deeper. This enables to obtain ultra-thin doped layers. Low temperature of ion implantation, the possibility of sufficiently accurate control of the depth and the impurity distribution profile create the prerequisites for the process automation. Wear tracks are more acidified under the same wear conditions on implanted steel compared to non-implanted steel. The nonequilibrium process under ion implantation causes the formation of such alloys in the surface layers that cannot be obtained under normal conditions due to diffusion of components or limited solubility. Ion implantation makes it possible to obtain alloys of a certain composition in the surface layer. Surface properties can be optimized without reference to the bulk properties of the material. Implantation is possible at low temperatures without a noticeable change in the size of the product.

Discussion and Conclusion. Cathode (ion), magnetron and ion-beam sputtering have common advantages: due to the relatively low temperature, the substrate does not overheat; it is possible to obtain uniform coatings; the chemical composition of the deposited coatings is accurately reproduced. The rest of the advantages and disadvantages of the considered methods are individual. The results can be used to create thin films through alternating magnetron and then ion-beam deposition processes, which enables to obtain films uniformly modified in depth. This is important in the production of parts of friction pairs and cutting tools to improve their quality.

***Keywords*:** metal film, physical deposition, anti-friction coating, wear-resistant coating, ion sputtering, magnetron sputtering, ion-beam sputtering.

For citation: Glushko, S.P. Selection of technologies for metal film application using physical deposition techniques. Advanced Engineering Research, 2020, vol. 20, no. 3, p. 280–288. https://doi.org/10.23947/2687-1653-2020-20-3-280-288

Introduction. Obtaining high-quality thin metal films is important for advances in the technologies of applying antifriction and wear-resistant coatings on cutting tools or components of friction pairs [1–6].

The thermal vacuum method, which was used earlier, did not provide the reproducibility of the properties of the films, especially during the deposition of materials of complex composition. The transition to continuous processing contributed to the development of ion-plasma deposition of thin films.

Currently, various methods of physical film deposition are utilized using cathode (ion) sputtering, magnetron sputtering, and assisted ion-beam sputtering. This creates thin films that cannot be obtained by other techniques (for example, films of refractory or multicomponent materials). The work objective is to analyze and compare the feasibility of methods for the physical deposition of thin metal films when applying antifriction and wear-resistant coatings on cutting tools or parts of friction pairs.

The use of cathode (ion), magnetron and ion-beam sputtering provides fully automation of the production of film coatings in the continuous technological installations.

Materials and Methods. In cathode (ion) sputtering, ions of the discharged gas bombard and destroy the cathode material [1]. Its atoms evaporate and condense on the substrate.

A schematic diagram of the thin films deposition through cathode sputtering is shown in Fig. 1.

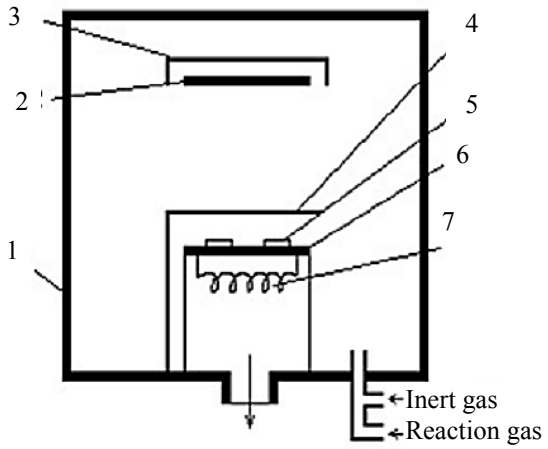

Fig. 1. Schematic diagram of the process of applying thin films by cathode sputtering: 1 — chamber, 2 — cathode, 3 — ground shield, 4 — shutter, 5 — substrate, 6 — ground anode, 7 — substrate resistive heater

Under this spraying, air is pumped out from the chamber in which the anode and cathode are installed to a vacuum state with pressure of 10^{-4} Pa. Then, an inert gas (e.g., argon) with pressure of 1–10 Pa is fed into the chamber [1]. When constant high potential difference of 1–5 kV is applied to the cathode and anode, glow discharge arises between them, in which positively charged ions of the inert gas are formed. Ions are accelerated by an electric field and bombard the cathode causing evaporation and sputtering of material atoms, which are deposited on the substrate in the form of a thin film [1, 3].

The initial ideas on the cathode sputtering were based on the predominant role of chemical processes. It was believed that the transfer of the cathode material to the substrate to be coated consists of:

a) the formation of fragile compounds with the cathode material on the substrate surface,

b) the evaporation of compounds of the substrate and cathode materials,

c) the partial decay of these compounds.

Inert gases in an ionized state (as opposed to a normal state) can exhibit some chemical activity.

However, it is not possible to explain all cases of such sputtering through chemical processes since there is cathode sputtering of weakly volatile compounds (for example, Al_2O_3), which practically cannot evaporate at cathode heating temperatures.

Therefore, not a chemical but a physical mechanism of cathode sputtering was proposed. According to this approach, material particles leave the cathode surface because the cathode material atoms receive energy directly from the bombarding atoms or molecules. There are two ideas on such energy transfer.

1. Impacts of bombarding atoms cause a strong local increase in the temperature of microscopic areas of the cathode material surface resulting in its evaporation.

2. The bombarding atom transfers kinetic energy to the atom on the cathode surface. As a result, the bonds of the cathode atom with neighboring atoms are destroyed, and it escapes from the cathode surface.

Such a mechanism better represents physical sputtering, especially in accordance with studies on ionic and neutral emission (i.e., emission of neutral atoms) of solids under ion bombardment.

Research Results. When considering cathodic sputtering in general, both physical and chemical mechanisms should be kept in mind. One of them may prevail depending on the actual process conditions.

The advantages of the cathode sputtering method are listed below.

1. The process runs at a relatively low temperature, the substrate does not overheat.

2. Uniform in thickness coatings can be obtained.

3. The chemical composition of the deposited coatings is accurately reproduced.

4. The areas of the coatings are quite large since the material is applied to the substrate not from a point source.

5. The resulting coatings have high adhesion to the substrate material due to high energy of the condensing atoms.

6. It is possible to achieve a high utilization rate of the coating material.

Let us list the disadvantages of the cathode sputtering method.

1. Films are characterized by a high level of mechanical stress.

2. The deposition rate is low (0.3–2 nm/s).

3. In some cases, working pressure in the chamber is 1–10 Pa; therefore, the films are contaminated by the working gas.

Magnetron sputtering is an advanced technology for the deposition of thin films, alloying and hardening of the surfaces of metal parts. Its advantages:

— high speed of obtaining film coatings;

— low level of contamination by foreign inclusions counting gases;

— low heating temperature of the substrate material;

— availability of spraying conducting and dielectric materials;

— availability of ultrathin films (<20 nm) with small defects;

— laglessness of the process

Magnetron sputtering is used to deposit ultra-thin films of chromium, aluminum (and its alloys) and various refractory metals.

The pattern of the sprayed particles motion in the magnetron sputtering system (MSD) is shown in Fig. 2.

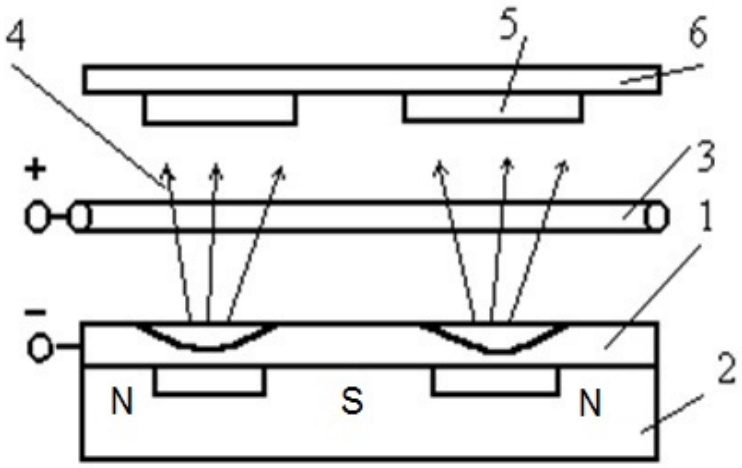

Fig. 2. Motion pattern of sputtered particles in MSD:
1 — target cathode, 2 — permanent magnet, 3 — anode, 4 — flux of sputtered particles, 5 — substrate, 6 — substrate holder

The MSD is mounted in a vacuum spray chamber from which air is evacuated. Argon or a mixture of inert gases is used as a working gas. The total pressure is kept constant with an accuracy of ± 5%. Through selecting the partial pressure of the gas mixture components, it is possible to change the coating characteristics in a wide range, including electrical.

The working environment in the chamber changes through varying the amount of oxygen, nitrogen, carbon dioxide, sulfurous gas compounds. This provides the creation of thin films of oxides, nitrides, carbides, sulfites of various materials, which cannot, for example, be obtained by thermal evaporation.

The composition of compounds in film coatings containing oxides, carbides, nitrides directly depends on the purity of materials and gases. Therefore, chemically pure materials should be used for spraying. To control the partial pressure, the vacuum units should be equipped with pumps that provide a constant pumping speed in the required pressure range.

MSDs use direct current sources. A constant electric field above the cathode target forms a glow discharge, creates plasma, and causes ion bombardment of the target (cathode). The MSD closed magnetic field concentrates plasma at the surface of the target cathode.

Under the action of ion bombardment, electrons are emitted from the target cathode. They are collected and held by the magnetic field. The electrons perform a complex cyclic motion over the surface of the target cathode. Before reaching the anode, the electrons collide with the atoms of the working gas (argon) and spend a significant part of their energy under the collision on ionizing the working gas (argon). This increases the number of ions at the surface of the target cathode, enhances bombardment, and increases the rate of material sputtering, deposition and film formation.

In the MSD, electric and magnetic fields intersect, which creates a magnetic trap at the sputtered target surface and increases the sputtering rate. The magnetic trap captures high-energy secondary electrons. They do not participate in the bombardment of the substrate, and this explains its insignificant heating.

The deposition rate of the coating material under magnetron sputtering depends on the pressure of the working gas in the installation chamber, the current strength, and the discharge power, which sets strict requirements for energy sources. To provide the process stability, it is required to maintain the discharge current with an accuracy of ± 2%. If the process is stabilized by the discharge power, it should be maintained with an accuracy of ± 20 W in the control range of 0–10 kW.

The average deposition rate of molybdenum is 12–37 nm/s under the following setup parameters:

— cobalt target in the form of a flat disk 150 mm in diameter,

— 4 kW power supply,

—molybdenum substrate is located at a distance of 60 mm from the power source [7].

In this case, the temperature of heating the substrate is approximately equal to the temperature of thermal evaporation in vacuum of low-melting metals, but much lower than the temperature of evaporation of refractory metals. This provides applying thin films to materials with low heat resistance (e.g., plastics).

Stability of film deposition on a substrate is provided by correctly selected parameters of the MSD:

— supply voltage of electrodes,

— discharge current,

— current density on the target,

— specific power,

— magnetic field induction,

— working gas pressure in the chamber.

The cathode — anode potential difference does not exceed 1000 V. The current of the electric discharge is established empirically. The current density on the target is about 200 mA/cm², but it can be higher in the central spray zone. The specific power of the electric discharge is from 40 to 100 W/cm². It is specified by the thermal conductivity of the deposited material and the cooling conditions.

The current-voltage characteristic of the electric discharge between the anode and cathode depends on the working gas pressure and the magnetic induction. With a decrease in the pressure and the magnetic field induction in the chamber, the current-voltage characteristics of the discharge shift to the region of high operating voltages.

The deposition rate of the film material is almost linearly dependent on the discharge power. With an increase in the discharge power, the deposition rate increases.

The discharge power reaches its maximum with an increase in the magnetic field induction to 0.08–0.1 T and a low working gas pressure (from 1 to 10 Pa). If the working gas pressure is high, the maximum discharge power is reached at a magnetic field induction of 0.04–0.06 T.

It should be noted that despite these advantages, as well as direct deposition of dielectrics with a high-frequency magnetron, this method is characterized by a low rate of film deposition, i.e., low productivity. There are also difficulties in matching the power supply of the magnetron sputtering set with the load when operating at high frequencies. In addition, the power source should have an arc discharge quenching system, as arc discharges cause instability of the parameters of the MSD.

In the batch-type MSDs, spraying means are located along the axis of the cylindrical chamber or along its generatrix. In the first case, cylindrical sputters are used, in the second, planar ones. Substrates move through the plasma region.

According to the operation principle, magnetron vacuum installations with ion-plasma sputtering sources are divided into two types — batch-type and continuous.

Batch-type magnetrons are used for coating dielectrics. In this case, to lower the substrate temperature, one should:

— improve the thermal contact of the substrate with the cooling system;

— make parts of the cooling system from materials with high thermal conductivity; or to increase the thermal conductivity of the gas layer between the cooling system and the film;

— cool the units of the cooling system to temperature of 243–253 ºK;

— expand the coverage area and increase the size of the cooling system.

High rate of release of substrate gases liberation, as well as the possible interaction of ionized gases with the deposited material, causes the use of condensation vacuum traps.

Continuous magnetrons are used to apply coatings of complex composition or multilayer coatings on flat substrates [8]. Typically, continuous installations consist of a chain of flat rectangular chambers separated by locks and gates. Continuous installations use either top-down spraying or vertical movement of substrates and lateral placement of sputters.

When operating a magnetron sputtering system, as a rule, one parameter is controlled. The rest ones are fixed at the optimal value through adjusting the thickness of the films, changing the deposition time, etc.

The advantages of magnetron sputtering are listed below.

1. The process runs at a relatively low temperature, the substrate does not overheat.

2. Uniform in thickness coatings can be obtained.

3. The chemical composition of the deposited coatings is accurately reproduced.

4. The process is fast. High sputtering speed of materials at low working voltages (600–800 V) and low pressure of the working gas ($5 \cdot 10^{-1}$ – 10 Pa) are marked.

The disadvantages of magnetron sputtering are as follows:

1. High requirements for the purity and dryness of the protective gas (argon).

2. Requirement for locks in front of the discharge chamber for protection against oxidation. The chamber should be supplied with shielding gas.

3. Probability of breakdowns between anode and cathode.

4. High requirements for the accuracy of positioning the substrates relative to the evaporators to provide uniformity of the films in thickness and in composition.

Ion-beam sputtering is used for deposition of thin films in vacuum, as well as for modification and doping of surface layers of metals through implantation of ions from separated beams.

Fig. 3 shows a diagram of an ion-beam sputtering tool.

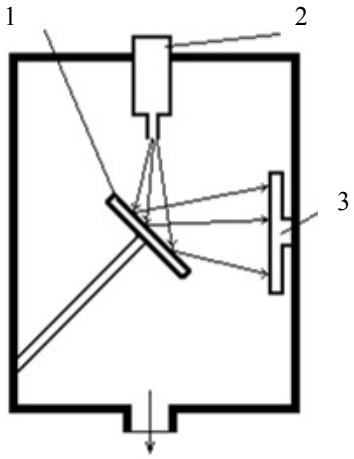

Fig. 3. Ion-beam sputtering tool diagram: 1 — target, 2 — ion source, 3 — substrate

Ion beam sputtering is considered a slow sputtering of a target surface under bombardment with a high energy ion beam and deposition on a substrate surface. This process is physical, not chemical in nature. An impulse is transmitted to the surface atoms from the incident ion:

— directed away from the surface,

— strong enough for the atoms to leave the surface.

Under ion implantation, the surface of metals is doped with recoil atoms, which receive high energy from accelerated ions and move deeper by several nanometers. This provides obtaining ultra-thin doped layers. Low tempera-

ture of ion implantation, the possibility of sufficiently accurate control of the depth and profile of impurity distribution create the prerequisites for the process automation.

Ion implantation is also used to modify the surface properties of metals: increase in hardness, increase in wear resistance, corrosion and radiation resistance, increase in resistance to fatigue failure, and reduction of the friction factor. Ion implantation is used to obtain anti-friction wear-resistant surfaces. For machine parts, the wear resistance of a material is, as a rule, a more important characteristic than its hardness or friction factor [4–8].

It has been noted that, e.g., a large dose of implanted nitrogen can significantly reduce the wear rate [9]. In addition, it was found that the implantation of ions of inert gases (e.g., neon, argon), which creates compressive stresses in the surface layer, does not cause a decrease in the wear rate. However, the implantation of interstitial atoms (boron, carbon, and nitrogen) at ion irradiation doses of 10^{17} cm^{-2} ions was very effective, and this effect exceeded considerably the penetration depth of the implanted ions in thickness of the wear layer.

The implanted interstitial atoms segregate even at normal temperatures under ion-beam sputtering (for example, nitrogen, carbon or boron). This blocks their motion in the deposited material, hardens the surface layer, and increases wear resistance.

During friction wear, two processes occur, whose action explains the effect of ion implantation on a layer deeper than the depth of ion penetration.

The first is the nucleation and development of new dislocations under the action of high local loads on the contact spots of the surface microroughness. Impurity atoms diffuse deep into the solution under the action of a stress field arising around a pileup of dislocations.

The second is local heating of the surface at the contact points. For example, when testing materials for wear resistance, the temperature at microroughnesses reaches 600–700° C. The motion of impurities occurs under the influence of large temperature gradients. Diffusion along dislocation lines is the most probable transport mechanism.

The friction factor in steels is also reduced under ion implantation due to two effects.

1. Welding bridges at the contact of two surfaces become brittle due to hindered dislocation motion.

2. The oxide film is more stable under these conditions, and its presence reduces adhesion.

The analysis confirmed that the wear marks are more oxidized under the same wear conditions on the implanted steel compared to the non-implanted steel.

When considering a composite material (for example, tungsten carbide on a cobalt bond), a more complex situation occurs. At high temperatures, wear is accompanied by diffusion, cobalt is carried to the surface, and substances such as iron (from the metal being processed) diffuse into the bulk, causing the carbide grain breakdown. At low temperatures, adhesion and abrasion of cobalt are more likely, and the process is intensified if the shear forces reach values sufficient to squeeze out the cobalt soft bond between the carbide grains.

Implanted nitrogen or carbon ions can be displaced to dislocations in cobalt, as in iron alloys. Cobalt, unlike iron, does not form stable nitrides or carbides, so the implanted atoms remain in the hard alloy. Using an electron microscope, martensitic transformations were detected in the cobalt bond of the implanted hard alloy based on tungsten carbide, which indicates a distortion of the crystal lattice and possible hardening upon dissolution of nitrogen in the hard alloy.

In addition, nitrogen can segregate to the interfaces between carbide grains and cobalt binder enhancing chemical bonds on these surfaces and hardening the composite.

Under ion implantation in tungsten hard alloys (tungsten carbide on a cobalt bond), the implanted nitrogen or carbon migrates along the insertion sites of the cobalt bond. It is accelerated by large thermal gradients under the surface microroughnesses. For this reason, if the wear conditions are relatively mild and the cooling is intense, the implanted atoms are inactive, and the process should be less intense.

The advantages of ion implantation are listed below.

1. The process runs at a relatively low temperature, the substrate does not overheat.

2. Uniform in thickness coatings can be obtained.

3. The chemical composition of the deposited coatings is accurately reproduced.

4. The process runs fast.

5. The process is recommended for doping with impurities with low solubility in the solid phase or with low diffusion coefficients.

The nonequilibrium process during ion implantation causes the formation of such alloys in the surface layers that cannot be obtained under normal conditions due to diffusion of components or limited solubility.

Ion implantation provides obtaining alloys of a certain composition in the surface layer. Surface properties can be optimized without reference to the bulk properties of the material. Implantation is possible at low temperatures without a noticeable change in the size of the product.

The disadvantages of ion implantation should be noted.

1. Implantation is a surface treatment process only in the area of direct action of the ion beam due to defocusing of the beam at large deviations. Therefore, it cannot be used to process substrates with complex surface geometry.

2. The shallow depth of penetration of the ion beam does not allow the deposition of coatings of sufficient thickness (> 1 μm) on the parts of friction pairs and the cutting tool.

3. Rather sophisticated equipment is used.

Discussion and Conclusions. A comparative analysis of the methods of physical deposition of films has shown their pros and cons.

Cathode (ion), magnetron, and ion-beam sputtering have common advantages.

1. The processes run at a relatively low temperature, the substrate does not overheat.

2. It is possible to obtain coatings uniform in thickness.

3. The chemical composition of the deposited coatings is accurately reproduced.

The rest of the advantages and disadvantages of the considered methods are individual.

The process of cathode (ion) sputtering allows for the deposition of films on sufficiently large areas with high utilization rate of the sprayed material, but it has the lowest deposition rate (0.3–2 nm/s). Films have high adhesion to the substrate, but are characterized by a high level of mechanical stress. In addition, films are contaminated by the working gas since the working pressure in the chamber can be 1–10 Pa. Nevertheless, cathode (ion) sputtering provides using refractory materials as targets and synthesizing multicomponent compounds.

Versatility is the major advantage of magnetron sputtering systems. They can use DC sputtering, RF sputtering and reactive ion plasma film deposition.

Advantages of magnetron sputtering systems are as follows.

— high deposition rate of film coatings (several microns/min) and its adjustability in a fairly wide range;

— high chemical purity of film coatings;

— low thermal effect on the substrate and the deposited film coating;

— possibility of applying films uniform in thickness to fixed substrates.

Ion sputtering has the following advantages over magnetron:

— low working gas pressure (10^{-3} – 10^{-2} Pa);

— integrity of the chemical composition of the target material (cathode);

— energy-handling of the ions bombarding the target;

— increase in the rate of sputtering the target through ion bombardment at an angle to its surface (impossible under magnetron sputtering).

For the deposition of thin films of dielectric and composite materials under ion-beam sputtering, cold cathode ion sources are proposed, which create radially directed converging or radially diverging ion beams [3, 8].

Ion sources for ion-beam sputtering with a cold cathode have the following advantages:

— promote the formation of ion beams of both inert and chemically active gases (e.g., O_2);

— have long life of the cold cathode;

— provide uniformity of the chemical composition of film coatings with large areas on stationary substrates;

— allow for automating the deposition of films of dielectric and composite materials with specified properties.

To obtain thin films, using the technique of alternating magnetron and then ion-beam sputtering processes is effective. This is how film coatings uniformly modified in depth are obtained [10]. This is important in the production of parts of friction pairs [5–7] and cutting tools to improve their quality [11

References

1. Petukhov GG, Gumarov VYu. Ionno-luchevye metody polucheniya tonkikh plenok [Ion beam techniques for producing thin films]. Kazan': Izd-vo Kazan. un-ta; 2010. 87 p. (In Russ.)

2. Levichev VV. Ehlektronnye i fotonnye ustroistva: printsip raboty, tekhnologii izgotovleniya [Electronic and photonic devices: principle of operation, manufacturing technologies]. St.Petersburg: ITMO University; 2015. 65 p. (In Russ.)

3. Grigor'ev FI. Osazhdenie tonkikh plenok iz nizkotemperaturnoi plazmy i ionnykh puchkov v tekhnologii mikroehlektroniki [Deposition of thin films from low-temperature plasma and ion beams in microelectronic technology]. Moscow: MIEM; 2006. 35 p. (In Russ.)

4. Belyi AV, Karpenko GD, Myshkin NK. Struktura i metody formirovaniya iznosostoikikh poverkhnostnykh sloev [Structure and methods of formation of wear-resistant surface layers]. Moscow: Mashinostroenie; 1991. 208 p. (In Russ.)

5. Glushko SP, Denisenko SG. Sintez kriteriya kachestva bimetallicheskikh podshipnikov skol'zheniya [Synthesis of the quality criterion for bimetallic plain bearings]. In: Structural strength, durability, hardening of materials and machine parts: Proc. All-Union. Sci. Conf. Volgograd: Dom nauki i tekhniki; 1990. P. 202–204. (In Russ.)

6. Denisenko SG, Glushko SP. Optimizatsiya tekhnologii proizvodstva podshipnikov skol'zheniya iz bimetalla stal'-bronza [Optimization of the production technology of plain bearings made of steel-bronze bimetal]. In: Modern surfacing methods, hardening coatings and materials used: Proc. IV Ukrainian Republican Sci.-Tech. Conf. Khar'kov: KHADI; 1990. P. 70–71. (In Russ.)

7. Astsilene DL. Tekhnika magnetronnogo raspyleniya tonkikh plenok. Gazofaznoe osazhdenie tonkikh plenok [Magnetron sputtering technique of thin films. Gas-phase deposition of thin films]. In: Modern technologies in education: Proc. Int. Sci.-Pract. Conf. in 2 pt. B.M. Khrustalev (ed.). Minsk: BNTU; 2016. Pt. 2. P. 17–20. (In Russ.)

8. Belyi AV, Karpenko SD, Myshkin NK. Struktura i metody formirovaniya iznosostoikikh poverkhnostnykh sloev [Structure and methods of formation of wear-resistant surface layers]. Moscow: Mashinostroenie; 1991. 208 p. (In Russ.)

9. Vityaz' PA, Belyi AV, Kukarenko VA, et al. Soprotivlenie kontaktnomu i ustalostnomu razrusheniyu modifitsi-rovannykh ionami azota khromistykh stalei [Resistance to contact and fatigue fracture of modified chromium steels ion-implanted by nitrogen]. Physical Mesomechanics. 2004. Special Iss. 7, part 2. P. 149–152. (In Russ.)

10. Fomin AA, Fomina MA, Rodionov IV, et al. Sverkhtverdye oksidnye pokrytiya, poluchaemye na titane pri obrabotke tokami vysokoi chastoty [Superhard oxide coatings obtained on titanium through treatment by high frequency currents]. Technical Physics Letters. 2015:41(18):89–95. (In Russ.)

11. Grigor'ev SN, Volosova MA. Nanesenie pokrytii i poverkhnostnaya modifikatsiya instrumenta [Coating and surface modification of the tool]. Moscow: Yanus-K; 2007. 324 p. (In Russ.)

Submitted 18.05.2020
Scheduled in the issue 01.07.2020

About the Author:

Glushko, Sergei P., associate professor of the Control Systems and Technological Complexes Department, Kuban State Technological University (2, Moskovskaya St., Krasnodar, 350072, RF), Cand. Sci. (Eng.), associate professor, ORCID: https://orcid.org/0000-0002-7087-6572, sputnik_s7@mail.ru

The author has read and approved the final manuscript.

MACHINE BUILDING AND MACHINE SCIENCE

UDC 621.78.015:620.1 https://doi.org/10.23947/2687-1653-2020-20-3-289-294

Contact potential difference of alloy steel after heat treatment

L. P. Aref'eva, A. G. Sukiyazov, Yu. V. Dolgachev, L. S. Shakhova
Don State Technical University (Rostov-on-Don, Russian Federation)

Introduction. The paper considers an actual issue of the development and application of a non-destructive method for controlling the quality of surfaces of steel products (Kelvin probe method). The work objective is to establish the magnitude of the contact potential difference (CPD) of 107WCR5 (KHVG) steel after heat treatment.
Materials and Methods. The object of study is 107WCR5 alloy tool steel. The chemical composition of the samples was refined through the optical emission analysis method. To carry out the statistical processing, there were three samples in three series. We chose different heat treatment modes for each series, i.e., quenching with low tempering, strengthening and normalization. The end surfaces of the samples were polished and then one of them was treated with a solution of nitric acid. Further, the measurement of the contact potential difference and statistical data processing were carried out.
Results. The data obtained show that the CPD value of 107WCR5 steel samples changes after heat treatment. With an increase in tempering temperature, the contact potential difference of the polished surface and the hardness, decrease almost linearly. Exposure to acid causes a significant decrease and equalization of the contact potential difference for all structures. The contact potential difference of steels 107WCR5 and CT105 (U10) is compared. Alloying steel by the elements with the work function values of the electron higher than that of iron causes a decrease in the CPD between the standard and the sample. The CPD behavior under a change in the composition of the steel depends strongly on the presence of alloying elements. The dependence of CPD on the dispersion of the structure is seen in both cases; however, it is more pronounced for 107WCR5 steel. The electron work function of the martensite, troostite, and sorbitol structures obtained as a result of heat treatment of steels 107WCR5 and CT105 is calculated.
Discussion and Conclusions. The dependence of the contact potential difference on the structure, chemical and phase composition was experimentally established; the electron work function of 107WCR5 and CT105 steels was calculated. This technique is more sensitive to alloy steel samples than to carbon steel. It seems possible to conclude that the measurement of the contact potential difference can be used to control surfaces exposed to active media or elevated temperatures as a non-destructive express diagnostic method.

Keywords: contact potential difference, electron work function, alloy steel, heat treatment, Kelvin probe method, nondestructive testing.

For citation: L.P. Aref'eva, A.G. Sukiyazov, Yu.V. Dolgachev, et al. Contact potential difference of alloyed steel after heat treatment. Advanced Engineering Research, 2020, vol. 20, no. 3, p. 289–294. https://doi.org/10.23947/2687-1653-2020-20-3-289-294

Introduction. The review [1] describes in detail the change in the concept of the electron work function (EWF) and understanding of its nature from the discovery of the photoelectric effect in 1895 by G. Hertz to the consideration on theoretical methods for calculating the EWF. Initially, EWF was defined as the work required to remove an electron from a metal. Over the past hundred years, this fundamental surface property has been measured for virtually all chemical elements and many conductive alloys. Initially, the EWF was measured as the ionization energy, although this is a loose definition since the ionization energy depends on the impurities present on the surface; for a monocrystal, the EWF depends on the orientation of the faces. To date, reliable methods have been developed for

determining the EWF of poly- and monocrystals [2]. One of these methods is the Kelvin probe method, which provides measuring the contact potential difference (CPD) between the surfaces of the reference and the sample under study at the macroscale and to map the CRD at the micro- and nanoscale [3]. Currently, the Kelvin probe method is widely used for nondestructive testing of the surface state and quality [3–7]. For example, in [7], a method was proposed for determining the surface energy of alloys by the magnitude of CPD and hardness, and the EWF values of 30KHGSA, R18, SHKH15 grade steels were obtained.

The contact potential difference is the difference between the electronic work functions of two metal surfaces. The electronic work function (EWF) is defined as the difference between the electrostatic potentials inside the metal φ_i and outside the metal at a certain point φ_0 and the Fermi energy of the metal E_F:

$$\varphi = (\phi_i - \phi_0) - E_F = \Delta\phi - E_F = 4\pi P_S - E_F, \quad (1)$$

where P_S is double layer dipole moment per unit surface area. The dipole moment of the double layer depends on the chemical composition of the surface layers, surface microroughness, adsorbed atoms, presence and density of defects, and crystallographic orientation of the surface. Fermi energy is sensitive to the state of the metal volume, including its chemical composition.

CPD depends on the metal state of the volume and surface, and, therefore, is a structure-sensitive value. The structure and phase composition of steel can be changed through heat treatment.

The work objective was to establish the CPD value for 107WCR5 steel after heat treatment.

Materials and Methods. The study object was alloyed tool 107WCR5 steel. Using the optical emission analysis method, the chemical composition of the samples under study was specified, which has the following average values: 1% C, 1.1% Cr, 1.4% W, 0.95% Mn, 0.25% Si, 0.35% Ni, 0.3% Mo, 0.3% Cu and less than 0.03% sulfur and phosphorus.

For the reliability of experimental data and statistical processing, the number of samples in the series was 3 units. To establish the effect of heat treatment modes on the CPD, three different modes were selected: quenching with low tempering, improvement, and normalization. The quenching temperature of the first and second series of samples was 820° C. Mineral oil was used as a cooling medium, which provided a cooling rate higher than the critical one in accordance with the diagram of the decomposition of austenite for 107WCR5 steel. Next, for the first group of samples, a low tempering was carried out at a temperature of 180° C, and additional self-cooling. For the second group of samples, tempering at temperatures of 600° C and 400° C was performed. For the third group, normalization by heating to 820° C and air cooling were carried out. The opposite ends of the samples corresponded to different preparation technologies: side A was ground after heat treatment, side B, in addition to grinding, was etched with 4% nitric acid solution in ethyl alcohol.

Hardness of the samples was measured by the Rockwell method to control the resulting structures after heat treatment.

The CPD was measured by the Kelvin probe method on a laboratory bench developed at the Research and Educational Center “Materials”, DSTU (Fig. 1)[1]. The reference electrode, taken as a standard, was made of stainless 12X18H10T steel, it was not subjected to any external actions (radiation, effect of strong electric and magnetic fields, heating and cooling, interaction with chemical reagents, etc.) and was used in all measurements. The sample was fixed on a metal table using a clamp (Fig. 1). The surface was located strictly parallel to the reference electrode. Electrical contact was provided between the clamp, the sample and the metal table.

[1] Sukiyazov AG, Zelentsov VB, Aizikovich SM, et al. Bench for measuring electronic work function from the surface of metal bodies. RF Patent 177 659, 2018. (In Russ.)

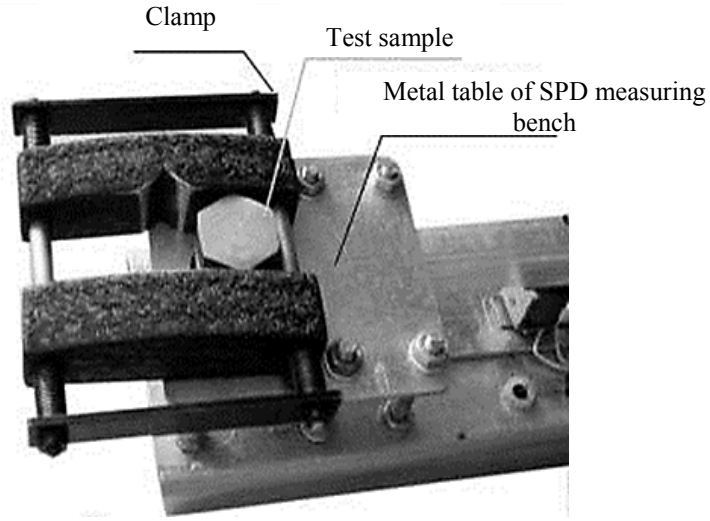

Fig. 1. Sample of 107WCR5 steel located on a metal table of measuring bench

Research Results. The CPD measurement results have good reproducibility. Statistical processing was carried out according to the Student's test method. The data obtained show that the CPD value of the samples from 12X18H10T steel changes after heat treatment (Fig. 2). As a result of normalization, a sorbitol structure (with an intermellar distance of ~ 0.4–0.2 μm) with hardness of 22 HRC, which had the minimum CPD values and hardness, was obtained. The highest CPD and hardness values are observed in the tempered martensite structure with carbides obtained as a result of quenching and low tempering at 180° C [8–10]. With an increase in the tempering temperature, the CPD value of the polished surface, as well as hardness, decreases almost linearly (Fig. 2). After processing the surface of 12X18H10T steel with a 4% solution of nitric acid, a film consisting of iron, chromium and tungsten nitrates is formed according to the ion exchange reaction. The acid action causes a significant decrease in the average CPD value for all the structures obtained, that is, the CPD values become approximately the same (Fig. 2).

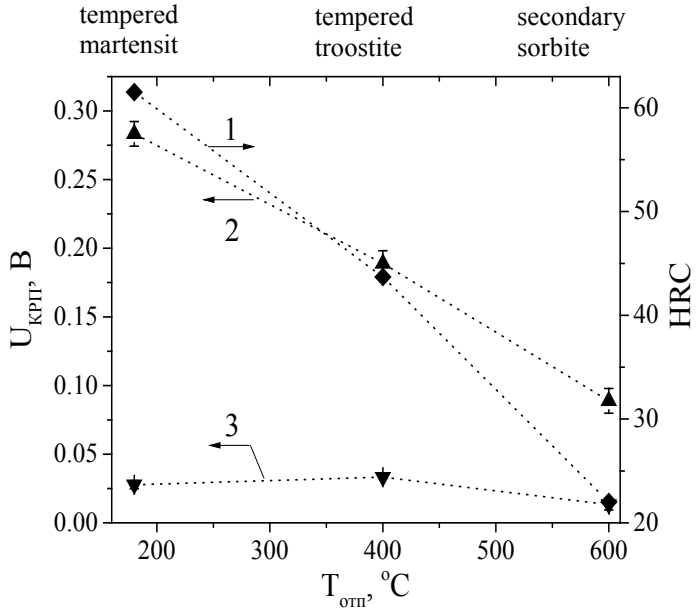

Fig. 2. Effect of tempering temperature on the contact potential difference of 107WCR5 steel: 1 — hardness, 2 — CPD of the polished surface, 3— CPD of the surface after etching

As is known, alloying elements change not only the critical temperatures of phase transformations, but also most of the steel properties [11–13]. For example, the material hardness increases. In this regard, it is advisable to analyze the influence of alloying on the steel CPD, that is, on the value of the electronic work function. The CPD data of 12X18H10T steel were compared to the results of measuring the CPD of U10 carbon tool steel with the same carbon content and a similar structural condition. Alloying steel with elements having higher electronic work function than iron causes a decrease in the CPD between the standard and the sample (Fig. 3). An exception is the structure of tempered martensite, in which there is an increase (by 0.06 V) in the CPD value, in comparison with CT105 steel tempered martensite CPD. Furthermore, different structures of alloy steel have sharper differences in the CPD values than in the

case of carbon steel. The CPD behavior when changing the steel composition strongly depends on the presence of alloying elements. The CPD dependence on the fineness of the structure is visible in both cases, however, for 12X18H10T steel, it is more pronounced.

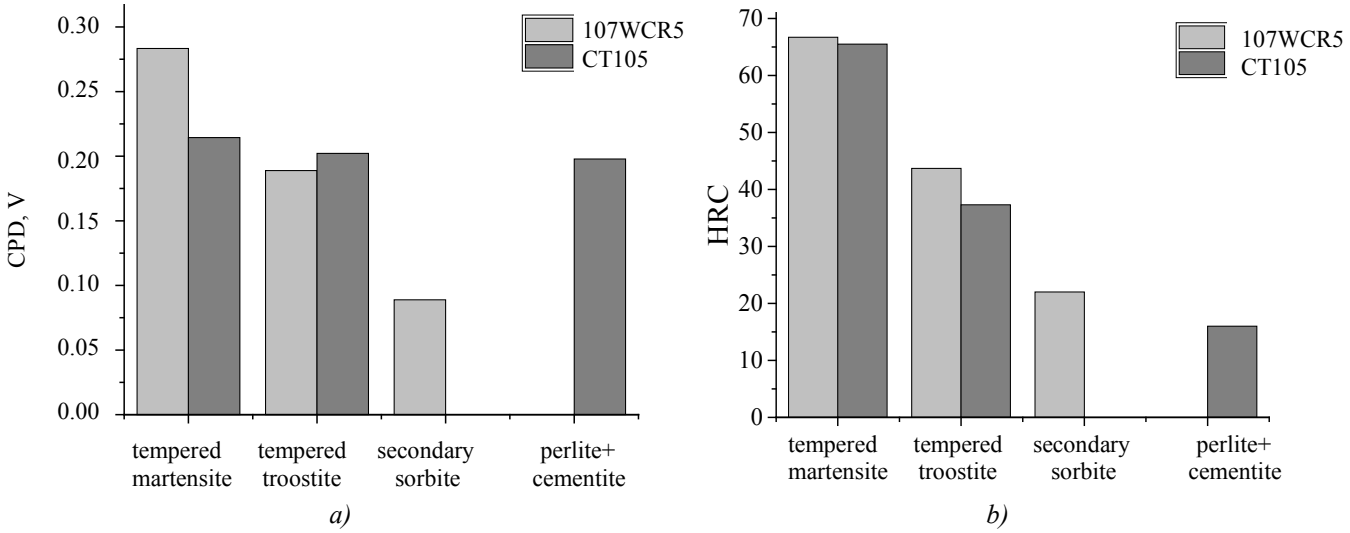

Fig. 3. Histograms of CPD values (*a*) and HRC hardness (b) for 107WCR5 and CT105 steels

According to the reference data [14], the electronic work function in stainless 12Kh18N10T steel was taken to be 3.67 eV. Based on the definition of the physical CPD value as the difference between the work functions of two parallel surfaces of different metals that form a capacitor, it is possible to write an expression for the electronic work function of the test sample in the form:

$$\varphi = \varphi_{эт} - eU_{КРП} . \quad (2)$$

According to the expression (2), the EWF value of the structures of martensite, troostite and sorbite obtained under the heat treatment of 107WCR5 and CT105 steels was estimated (Fig. 4). Since the CPD values for all investigated structures are positive, the EWF of these structures is less than the EWF of the reference sample. The dependences of the EWF value of the samples under study on the structure differ significantly. For CT105 steel, the change in the EWF value does not exceed hundredths of eV, while for 107WCR5 steel, the difference in the EWF value of sorbite and troostite structures reaches 0.1 eV, i.e., it makes up 3% of the EWF value of troostite. The EWF of tempered martensite with carbides of 107WCR5 steel is 3.45 eV. Thus, we can conclude that the following factors influence the EWF value: phase composition (different structural condition obtained under different heat treatment modes), chemical condition (dissolution of elements or formation of chemical compounds on the sample surface) and structure dispersion. Dispersion is regarded as the difference in the sizes of the plates of the tempered products (perlite, sorbite, troostite). For alloy steel, the difference between tempered structures affects significantly the EWF value (Fig. 4). At the same time, for CT105 steel, this difference is almost invisible in Fig. 4.

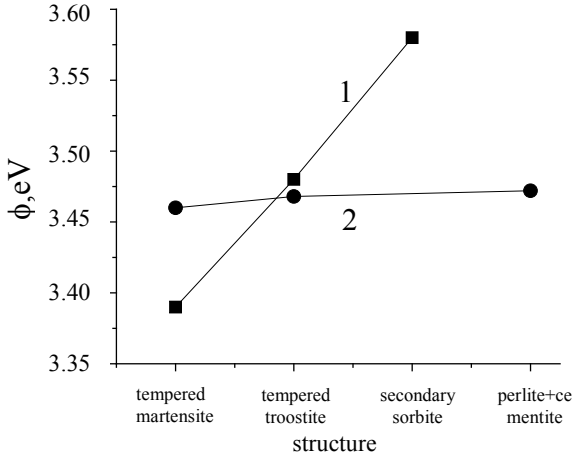

Fig. 4. Dependence of the EWF on the phase composition of steel: 1 — 107WCR5 steel; 2 —CT105 steel

Discussion and Conclusions. The dependences obtained show the correlation between the change in hardness and the CPD value. Since the CPD of all samples is positive, their EWF is less than the EWF of the standard used. The structure of tempered martensite has the highest CPD value. It is found that the CPD decreases with an increase in the tempering temperature. The addition of alloying elements with higher EWF values causes a decrease in the CPD between the studied samples with the structures of ferrite-cementite mixtures, secondary carbides, and the standard. Alloying elements increase considerably the CPD value variation under changing the structural condition of the alloy in comparison with carbon steel. The dependence of the CPD value on the structure, chemical and phase composition of steels is experimentally established. The EWF value of CT105 and 107WCR5 steels was estimated. It can be seen from the results obtained that this method is more sensitive to alloy steel samples than to carbon steel. Thus, we can conclude that the measurement of the CPD can be used as a non-destructive diagnostic express-method under monitoring surfaces exposed to active media or elevated temperatures.

References

1. Halas S. 100 years of work function. Materials Science-Poland. 2006;24(4):951−968.
2. Woodruff D, Delchar T. Sovremennye metody issledovaniya poverkhnosti [Modern techniques of surface science]. Moscow: Mir; 1989. 564 p. (In Russ.)
3. Shipitsa NA, Zharin AL, Saroka DI, et al. Issledovanie lokalizatsii deformatsii metodom zonda Kel'vina [A study of deformation localization by the Kelvin method]. Physical Mesomechanics. 2004;7(S1–1):218–221. (In Russ.)
4. Zharin AL, Gusev OK, Svistun AI, et al. Kontrol' trushcheisya poverkhnosti metodami kontaktnoi raznosti potentsialov [Friction surface monitoring using a contact potential difference technique]. Izvestiya TulGU. 2011;5(2):286–295. (In Russ.)
5. Gerasimov IV, Oleshko VS, Tkachenko DP, et al. Kontrol' prozhogov lopatok kompressora gazoturbinnogo dvigatelya metodom kontaktnoi raznosti potentsialov [Control of burn-through of blades of a gas turbine engine compressor using the contact potential difference method]. Herald of Kazan Technological University. 2012;15(17):146–149. (In Russ.)
6. Kukoz VF, Kukoz FI. Vliyanie kontaktnoi raznosti potentsialov na skorost' friktsionnoi obrabotki poverkhnostei metallov [Impact of contact potential difference on the rate of frictional processing of metal surfaces]. University News. North-Caucasian region. Technical Sciences Series. 2004;1:107–107a. (In Russ.)
7. Oleshko VS, Pigovkin IS. Operativnoe opredelenie poverkhnostnoi ehnergii metallicheskikh detalei aviatsionnoi tekhniki [The operational definition of the surface energy of metal parts of aeronautical engineering]. Naukovedenie. 2016;8(3). URL: http://naukovedenie.ru/PDF/ 131EVN316.pdf (In Russ.)
8. Pustovoit VN, Dolgachev YuV. Problemy zarozhdeniya pri martensitnom prevrashchenii v stali [Nucleation problems of the martensitic transformation in steel]. Vestnik of DSTU. 2013;13(1-2):5–24. (In Russ.)
9. Pustovoit VN, Dolgachev YuV. K voprosu o mestakh zarozhdeniya martensita [On the areas of martensite nucleation]. Izvestia VSTU. 2014;23(150:110–114. (In Russ.)
10. Pustovoit VN, Dombrovskii YuM, Dolgachev YuV. Structural identification of the phenomenon of “white zone”. Metal Science and Heat Treatment. 2017;59(1-2):3−7.
11. Popova LE, Popov AA. Diagrammy prevrashcheniya austenita v stalyakh i beta-rastvora v splavakh titana: spravochnik termista [Diagrams of the austenite transformation in steels and of beta-solution in titanium alloys]. Moscow: Metallurgiya; 1991. 503 p. (In Russ.)
12. Novikov II. Teoriya termicheskoi obrabotki metallov [Theory of heat treatment of metals]. Moscow: Metallurgiya; 1986. 480 p. (In Russ.)
13. Arzamasov VB, Smirnova EE, Stroev AA, et al. Rabota vykhoda ehlektrona splavov tugoplavkikh metallov [Electron work function of refractory metal alloys]. Izvestia MGTU MAMI. 2009;1(7):102−104 (In Russ.)
14. Rukhlyada NYa, Visheratin RK. Issledovanie izmereniya raboty vykhoda v protsesse otzhiga nerzhaveyushchei stali, obluchennoi ionami argona [Studied changes in the work function in annealing stainless steel irradiated by argon ions]. Problems of Atomic Science and Technology. Series: Nuclear and Reactor Constants. 2014;2:96–105. (In Russ.)

Submitted 29.06.2020
Scheduled in the issue 31.08.2020

About the Authors:

Aref'eva, Lyudmila P., associate professor of the Physical and Applied Materials Science Department, Don State Technical University (1, Gagarin sq., Rostov-on-Don, 344003, RF), Cand.Sci. (Phys.-Math.), associate professor, ResearcherID: J-4075-2017, ORCID: https://orcid.org/0000-0003-2431-6897, Ludmilochka529@mail.ru

Sukiyazov, Aleksandr G., professor of the Radioelectronics Department, Don State Technical University (1, Gagarin sq., Rostov-on-Don, 344003, RF), Cand.Sci. (Phys.-Math.), associate professor, ORCID: https://orcid.org/0000-0002-6117-0068, pro_suk@mail.ru

Dolgachev, Yurii V., associate professor of the Physical and Applied Materials Science Department, Don State Technical University (1, Gagarin sq., Rostov-on-Don, 344003, RF), Cand.Sci. (Eng.), associate professor, ResearcherID: B-2328-2016, ORCID: https://orcid.org/0000-0002-8558-1136, yuridol@mail.ru

Shakhova, Liliya S., student of the Physical and Applied Materials Science Department, Don State Technical University (1, Gagarin sq., Rostov-on-Don, 344003, RF), ORCID: https://orcid.org/0000-0002-9728-9909, shahowa.lilya@yandex.ru

Claimed contributorship

L. P. Aref'eva: basic concept formulation; research objectives and tasks setting; computational analysis and analysis of the research results; text preparation; formulation of conclusions. A. G. Sukiyazov: academic advising; testing; analysis of the research results; the text revision; correction of the conclusions. Yu. V. Dolgachev: analysis of the test results; text preparation; correction of the conclusions. L. S. Shakhova: sample preparation and testing; the text revision; text layout and graphical presentation of the research results.

All authors have read and approved the final manuscript.

MACHINE BUILDING AND MACHINE SCIENCE

UDC 621.7.074 https://doi.org/10.23947/2687-1653-2020-20-3-295-301

Mathematical model of shaping toothed products using volumetric tool with one motion parameter

A. A. Silich, E. M. Yusupova
Tyumen Higher Military Engineering Command School (Tyumen, Russian Federation)

Introduction. The development of a mathematical model of one-parameter shaping of a toothed product is considered. As an example, shaping of the side surface of the teeth of the Novikov gearing is studied; the mode and magnitude of the change in the shaping error heightwise the wheel tooth are shown. The work objective was to develop a mathematical model of the surface of the product teeth as a generating surface envelope of the tool. A computational and experimental study is carried out. The mathematical models obtained can be used in devices with copiers when shaping the side surface of the teeth of the Novikov gear. As an example, we consider the deviation behavior of the teeth profile of the Novikov gear with the original profile of DLZ 0.7-0.15

Materials and Methods. When building the model and studying its characteristics, the mathematical tools of the gearing theory, calculation procedure for cylindrical gears (A.A. Silich's author development) were used. The paper proposes new mathematical models of the equations of the lateral surface of the gear teeth formed with a tool whose axial profile coincides with the original one. In the model under consideration, the tool moves along the axis of the product while the latter rotates on its axis. In the course of the study, numerical modeling was carried out to determine the error value in shaping the product profile using the tool.

Results. New mathematical models and software have been developed for numerical simulation of the shaping of a toothed product using a tool with one independent motion parameter. An algorithm has also been developed to determine the deviation error of the real profile from the nominal one for the tooth of the Novikov gear. Solutions to accurately reproduce the tooth profile are provided.

Discussion and Conclusions. The parametric method of analytical description of the surface used in the work simplifies the calculation of the cutting tool displacements in the problems of numerical control. Solving the problem of synthesizing the technology of workpiece surface treatment on metal-cutting machines provides the development of a description of the entire shaping process and requires the representation of the workpiece surface in the form of a mathematical model. The results obtained can be used under creating finishing methods for processing teeth when improving the quality of gear wheels and gear drives, as well as the production efficiency.

Keywords: toothed products, mathematical model, one-parameter shaping, error of shaping.

For citation: A. A. Silich, E. M. Yusupova**.** Mathematical model of shaping toothed products using volumetric tool with one motion parameter. Advanced Engineering Research, 2020, vol. 20, no. 3, p. 295−301. https://doi.org/10.23947/2687-1653-2020-20-3-295-301

Introduction. The process of shaping the tooth flank of the Novikov gear wheel is considered using the following algorithm:

— generating surface of the tool is described in the coordinate system of this tool;

— real surface of the wheel teeth is formed as an envelope of the generating surface of the tool when the latter

moves relative to the wheel with independent parameters;

— numerical studies on the deviation of the real surface from the theoretical one and the analysis of the results obtained are carried out.

In accordance with GOST 13 755–81 for cutting tools, the standard establishes a normative number of modules and certain relationships between the dimensions of tooth components. These ratios are determined for gears by the parameters of the original rack through the parameters of its normal section — the original profile. A grinding wheel is considered as a tool in the work.

The relative motion of the gear links or the tool and the workpiece during machining can be described by one or two independent parameters. The surface of the teeth of the first link is an envelope of a one-parameter or two-parameter family of surfaces of the second link. Very often under processing, the surface of product teeth is formed as an envelope of the generating surface of the tool when the latter moves relative to the product with one independent parameter. In most cases, the angle of rotation of the product is chosen as such a parameter.

The theoretical surface of the wheel teeth in the process of its finishing with an abrasive tool is formed as an envelope of the generating surface of the tool when the latter moves relative to the wheel with independent parameters. According to GOST 16 530–83, the theoretical surface is each of two surfaces (lateral surfaces of two teeth) providing a given gear ratio during their interaction.

Having regard to the above, the task was set to determine the equations of the side surface of the product teeth. The surfaces are created with a tool whose axial profile matches the original profile. In this case, the tool moves along the axis of the product, and the wheels perform conformal eigenrotation. Since the rotation of the product and the movement of the tool are interconnected through an analytical relationship, the angle of product rotation is chosen as an independent parameter for the shaping of a toothed product $\varphi_к$.

Materials and Methods. To obtain the equation of the nominal generating surface of the tool, a coordinate system rigidly connected with the rack was used. The normal rack section is taken as the reference profile. In Fig. 1, a generalized reference profile taken from the research papers [1, 2] is exemplified. The profile is made up of circular segments that can smoothly mate with each other or intersect depending on the type of the reference profile.

In Fig. 1, the numbers in circles show the numbers of the sections (i=1,2,3,…7). The boundaries of the sections are marked with large dots. In addition, in Fig. 1 the following designations are accepted: $S_i\ (X_i;Y_i;Z_i)$ coordinate systems associated with the i-th section of the reference profile. The origin of such a system is aligned with the center of the section circle, and the direction of the axes coincides with the direction of the axes of the rack $S_p\ (X_p;Y_p;Z_p)$.

The solution to the problem is divided into two stages. At the first stage, a mathematical model of a volumetric tool in the form of a body of revolution (e.g., a disk grinding wheel or a disk cutter) is built. At the second stage, a toothed product with one independent motion parameter is formed using the tool.

Tool mathematical model

We obtain a theoretical generating surface through binding the surface of the tool to the coordinate system $S_u\ (X_u;Y_u;Z_u)$ directing the Z_u axis along the tool axis of rotation. We position the X_u axis so that it passes through the calculated point, which we take as the point of contact between the tool and the workpiece at the initial moment of time. The Y_u axis is directed so that all axes make up a right-hand Cartesian coordinate system. The reference profile is associated with its own coordinate system $S_p(X_p;Y_p)$, whose axes are located so that the Z_p axis coincides with the pitch line of the reference profile, and the X_p axis is perpendicular to it and directed towards the tool axis.

To shape the generating surface of the tool, devices are used that work with a copier, or devices that reproduce the trajectory of a dressing diamond or a sharpening tool using a NC system. For any of these cases, a mathematical description of the tool generating surface will be of the same type[1, 2] [3].

[1] Krivosheikin AV, Nurmukhamedov LKh, Perelygin SV. Mathematical modeling in instrumentation systems. St.Petersburg, 2019. 108 p. (In Russ.)
[2] Zyuz'kov VM. Mathematical logic and theory of algorithms. Tomsk, 2015. 236 p. (In Russ.)

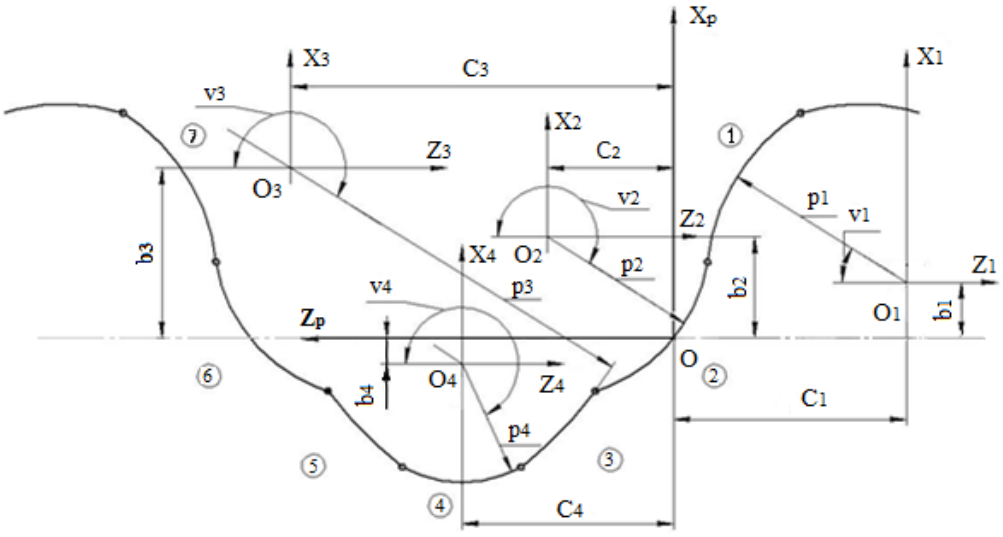

Fig. 1. Reference profile DLZ-0.7-0.15

Fig. 2 shows the relative position of the tool (1), the reference profile (2), the copier (3), the correct device diagram and the adopted coordinate systems associated with the copier and the tool.

The mathematical model of the tool generating surface will be considered as a trace of the copier contour motion when it rotates around the Z_u axis with the angular parameter of movement φ_u.

In the S_p coordinate system, the copier profile equation including sections 1, 2 and 3 can be written as follows:

$$\left.\begin{aligned} X_p &= \rho_i \cdot \sin \upsilon_i + b_i; \\ Z_p &= \rho_i \cdot \cos \upsilon_i + c_i; \end{aligned}\right\}, \tag{1}$$

where the designation of the values are taken from [4–6]: ρ_i is the radius of curvature of the i-th section of the normal profile of the rack tooth; υ_i is the curvilinear coordinate of the rack generating surface, whose origin goes clockwise from the Z_p axis; c_i is the applicate of the position of the center of curvature of the corresponding section in the S_p system; b_i is the abscissa of the center of curvature of the corresponding section in the S_p coordinate system.

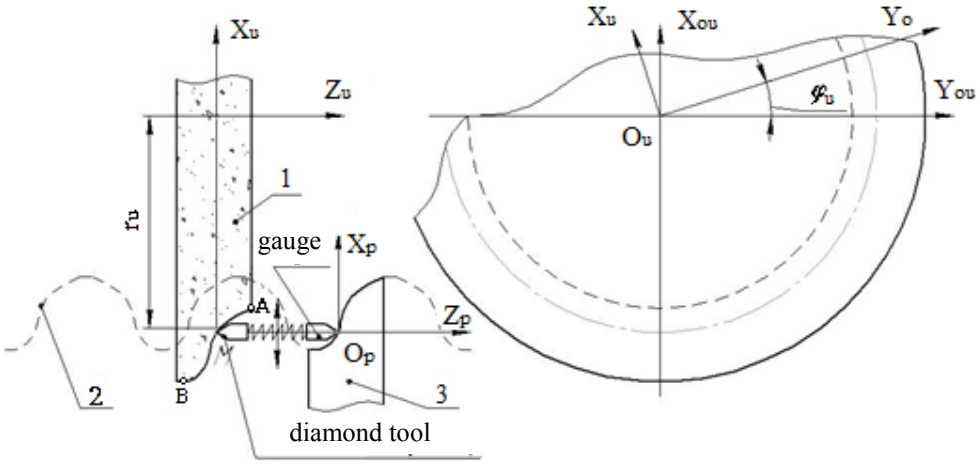

Fig. 2. Scheme of tool shaping with the adopted coordinate system

In addition, Fig. 2 indicates the calculated radius of the tool r_u.

Using the selected coordinate systems, the introduced designations and the method of shaping surfaces[3], we obtain the equation for the generating surface of the tool in projection on the coordinate axis:

$$\widetilde{r_и} = \left\{\begin{matrix} X_{ui} = cos\ \varphi_{ui} \cdot (\rho_i \cdot sin\ \upsilon_i + b_i - r_u); \\ Y_{ui} = -\ sin\ \varphi_{ui} \cdot (\rho_i \cdot sin\ \upsilon_i + b_i - r_u); \\ Z_{ui} = -\rho_i \cdot cos\ \upsilon_i - c_i. \end{matrix}\right\} \tag{2}$$

To obtain a mathematical model of the product, the equation of the normal to the generating surface of the tool

[3] Rannev GG, Tarasenko AP. Intelligent measuring instruments. Moscow, 2016. 280 p. (In Russ.)

is required. Therefore, using the well-known technique [3] and omitting the intermediate transformation, we write the equations of the unit normal vector to the generating surface in the following form:

$$\left.\begin{array}{c} e_{xui} = -\cos\varphi_u \cdot \sin\upsilon_i; \\ e_{yui} = \sin\varphi_u \cdot \sin\upsilon_i; \\ e_{zui} = \cos\upsilon_i. \end{array}\right\} \quad (3)$$

Product mathematical model

The geometrical-kinematic diagram of the shaping of the product tooth lateral surface using a tool with the appropriate coordinate systems is shown in Fig. 3. Sections of the tool generating surface are specified in the S_u (X_u; Y_u; Z_u) coordinate system rigidly connected with the tool. The coordinate system $S_к$ ($X_к$;$Y_к$;$Z_к$) is rigidly connected with the workpiece (e.g., a gear wheel). Fixed auxiliary coordinate systems of the wheel S_{ou} (X_{ou};Y_{ou};Z_{ou}) and the tool $S_{oк}$ ($X_{oк}$;$Y_{oк}$;$Z_{oк}$) associated with the rack.

As an independent parameter of the relative motion under the product processing, we take the value $\varphi_к$ numerically equal to the angle of rotation of the wheel around the $Z_к$ axis. The tool motion along the workpiece axis is denoted by S_o. The angle of inclination of the tooth line of the product is $\beta_к$. The axle spacing is $a=r_u+r_k+X_k$.

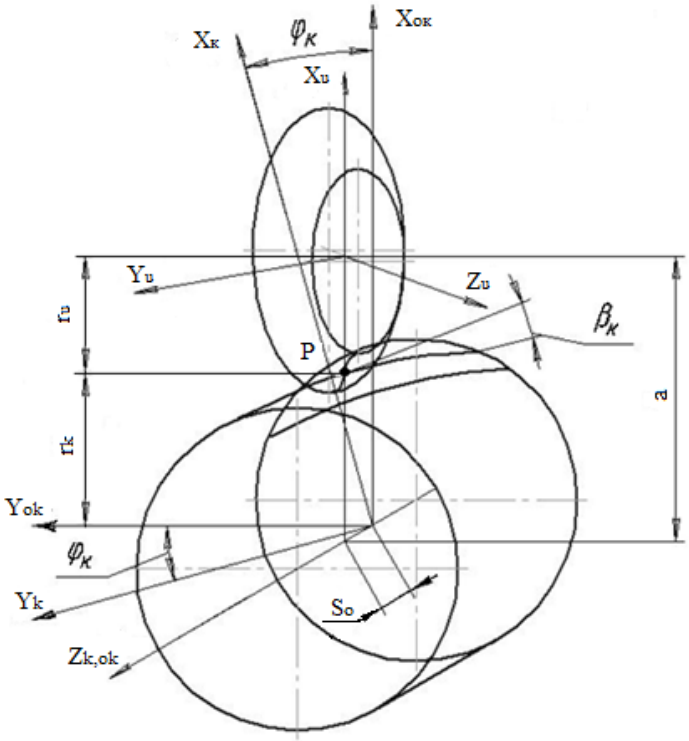

Fig. 3. Geometrical-kinematic diagram of the product tooth profile shaping by the tool

The real product tooth surface as the envelope of the one-parameter family of the tool generating surface is determined from the following equations [3]:

$$\left.\begin{array}{ll} \tilde{r}_к = \tilde{A}_{кui} \cdot \tilde{r}_u & \text{а)} \\ \bar{e}_{ui} \cdot \bar{V}_{ui} = 0 & \text{б)} \end{array}\right\}, \quad (4)$$

where $\tilde{r}_u$ is the column matrix composed of the projections of the tool generating surface recorded in the S_u coordinate system; $\tilde{A}_{кui}$ is the transition matrix from the S_u coordinate system to the $S_к$ coordinate system; $\bar{V}_{ui}$ is the prototype of the relative velocity vector by parameter φ_u; $\bar{e}_{ui}$ is the unit normal vector to the tool generating surface, whose projections in the X_u, Y_u, Z_u coordinate axes are represented by the equations (3).

We find the transition matrix $\tilde{A}_{кui}$ using the technique described in [3, 7]. Omitting intermediate transformations, we present this matrix in the following form:

$$\tilde{A}_{кui} = \begin{pmatrix} \cos\varphi_к & \sin\beta_к \cdot \sin\varphi_к & -\cos\beta_к \cdot \sin\varphi_к & a\cdot\cos\varphi_{ui} \\ -\sin\varphi_к & \sin\beta_к \cdot \cos\varphi_к & -\cos\beta_к \cdot \cos\varphi_к & -a\cdot\sin\varphi_{ui} \\ 0 & \cos\beta_к & 1 & -S_o \\ 0 & 0 & 0 & 1 \end{pmatrix} \quad (5)$$

$$S_o = \frac{\varphi_к \cdot r_к}{\tan\beta_к} = \frac{\varphi_к \cdot m \cdot z_к}{2\cdot\sin\beta_к}$$

$$a = r_к + X_к + r_u = \frac{m\cdot z_к}{2\cdot\cos\beta_к} + X_к + r_u.$$

Using the technique of one-parameter shaping of surfaces [3], adopted coordinate systems and geometrical-kinematic shaping scheme (Fig. 3), as well as omitting intermediate transformations, the equation of the real surfaces of the product teeth can be written as:

$$\left.\begin{array}{c} x_{\kappa i} = \cos\varphi_\kappa \cdot \cos\varphi_u \cdot \sin\beta_\kappa \cdot \sin\varphi_\kappa \cdot \sin\varphi_u \cdot (\rho_i \cdot \sin\upsilon_i + b_i - r_u) + \\ + \cos\beta_\kappa \cdot \sin\varphi_u \cdot (\rho_i \cdot \cos\upsilon_i + c_i) \\ y_{\kappa i} = \sin\varphi_\kappa \cdot \cos\varphi_u \cdot \sin\varphi_u \cdot \sin\beta_\kappa \cdot \cos\varphi_\kappa \cdot (\rho_i \cdot \sin\upsilon_i + b_i - r_u) + \\ + \cos\beta_\kappa \cdot \cos\varphi_\kappa \cdot (\rho_i \cdot \cos\upsilon_i + c_i) \\ z_{\kappa i} = -\cos\beta_\kappa \cdot \sin\varphi_u \cdot (\rho_i \cdot \sin\upsilon_i + b_i - r_u) - \\ - \sin\beta_\kappa \cdot (\rho_i \cdot \cos\upsilon_i + c_i) - \varphi_k \cdot r_k \cdot ctg\,\beta_\kappa \end{array}\right\} \quad (6)$$

Using the technique of obtaining the gearing equation (4 b)[4], we finally write it in the following form:

$$\cos\beta_\kappa \cdot [\sin\varphi_{ui} \cdot \sin\upsilon_i \cdot (c_i - r_k \cdot \sin\beta_\kappa + X_k \cdot \tan\beta_\kappa + r_u \cdot \tan\beta_\kappa) - \\ - \cos\upsilon_i \cdot (r_k + X_k)] = 0 \quad , \quad (7)$$

where X_κ — reference profile displacements.

Research Results

To determine the error value in shaping the product profile using the tool, the following algorithm was used:

1. The real and nominal surfaces of the product teeth were recorded in the same coordinate system. The equations of the lateral surface of the wheel teeth formed using the rack, were taken as the nominal surface of the product teeth[5] [3].

2. The current value of the independent parameter υ_j, was set, where j=1, 2, 3…n is the current point number on the wheel tooth profile.

3. Taking $Z_{\kappa i}$=*const*, the value of the second independent parameter $\varphi_{\kappa j}$ of the nominal product profile was determined.

4. A circle was drawn through the current point υ_j of the product tooth profile, its intersection with the product real tooth profile was determined.

5. The chord distance between the points of the nominal and real profile located on the same circle was taken as the shaping error.

The developed algorithm for determining the shaping error was implemented as a program in the MathCAD software environment.

As an example, Fig. 4 shows the real profile behavior in comparison with the nominal one, and the direction of reading the error Δ_{ij} of the shaping of the Novikov gear wheel tooth profile.

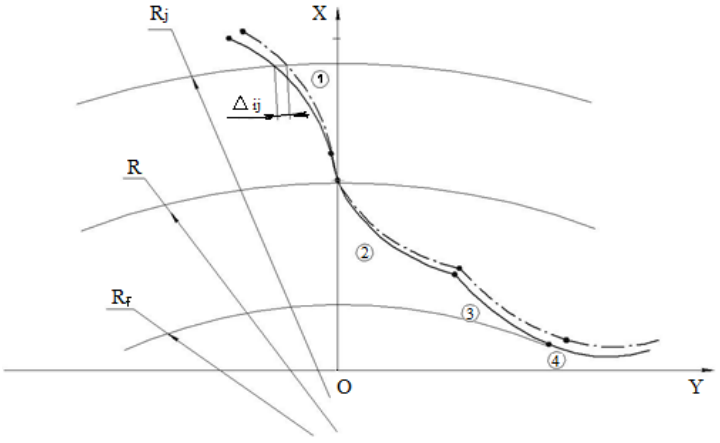

Fig. 4. Behavior of the Novikov gear wheel teeth profile:
——— — nominal profile; ——— - ——— — real profile.

Real values of the errors Δ_{ij} are shown in Fig. 5 for a Novikov gearwheel with the reference DLZ profile of 0.7–0.15 and the following geometrical parameters: gearing modulus m_n=5, number of the wheel teeth z_κ=50, angle of inclination of the tooth line β_κ=20º, displacements of the reference profile X_κ=0.

[4] Rannev GG, Tarasenko AP. Op. Cit. 280 p. (In Russ.)
[5] Zyuz'kov VM. Op. Cit. 236 p. (In Russ.)

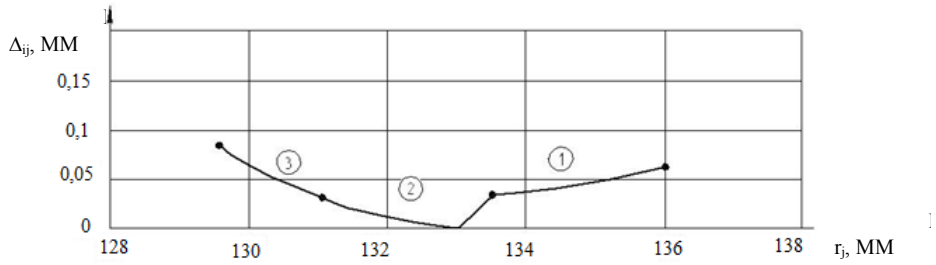

Fig. 5. Deviation of the real profile from the nominal one for the tooth of the Novikov gear wheel

As can be seen from the graph in Fig. 5, the minimum value of the deviation is in the area of the pitch radius of the wheel, and the maximum values are observed on the head and at the base of the wheel tooth. The maximum values of profile shaping depend on the type of the reference profile, the number of teeth, the angle of inclination of the tooth line, as well as on the diametrical dimensions of the tool.

Discussion and Conclusions. A mathematical model of the shaping of a toothed product using a tool with one independent motion parameter has been developed.

1. Numerical studies show that according to this processing scheme, it is impossible to theoretically accurately reproduce the product tooth profile if the generating surface of the tool is formed by the reference profile of the workpiece.

2. The maximum distortions of the profile are observed on the head and foot of the wheel tooth (at the diameter of the protrusions and depressions) and their value is the greater, the higher the reference profile, the greater the module, the smaller the number of teeth, and the greater the angle of tooth inclination.

3. For accurate reproduction of the tooth profile, it is required to correct the copier, which is used to dress and sharpen the tool.

References

1. Silich AA. Peredachi Novikova. Geometricheskii raschet tsilindricheskikh peredach Novikova [Novikov gearing. Geometric calculation of Novikov cylindrical gears]. Tyumen: Izd–vo TIU; 2016. 79 p. (In Russ.)

2. Silich AA. Tsilindricheskie peredachi Novikova. Metodika geometricheskogo rascheta [Cylindrical gears of Novikov. Geometric calculation method]. Dusseldorf: Lambert Academic Publishing; 2013. 90 p. (In Russ.)

3. Lomova OS. Matematicheskoe modelirovanie strukturnykh izmenenii v poverkhnostyakh zagotovok pri teplovykh vozmushcheniyakh v protsesse shlifovaniya [The mathematical modeling of the structural changes in the surfaces of workpieces during thermal perturbations in the grinding process]. Omsk Scientific Bulletin. 2013;120:95–98. (In Russ.)

4. Silich AA. Tekhnologiya obrabotki zubchatykh koles tsilindricheskikh peredach Novikova [Novikov cylindrical gear processing technology]. Tyumen: Izd. TyuMGNGU; 2007. 162 p. (In Russ.)

5. Litvin FL, Feng P-H, Lagutin SA. Computerized Generation and Simulation of Meshing and Contact of New Type of Novikov-Wildhaber Helical Gears. NASA Contractor Report-2000-209415 ARL-CR-428; 2000. 55 p.

6. Litvin FL. Development of Gear Technology and Theory of Gearing. NASA Reference Publication 1406, ARL-TR-1500; 1998.

7. Litvin FL. Teoriya zubchatykh zatseplenii [Gear theory]. 2nd rev. and enl. ed. Moscow: Nauka; 1968. P. 584. (In Russ.)

Submitted 08.06.2020

Scheduled in the issue 10.08.2020

About the Authors:

Silich, Aleksandr A., associate professor of the Department of Military-Technical Disciplines, Tyumen Higher Military Engineering Command School (1, Tolstogo St., Tyumen, 625001, RF), Dr.Sci. (Eng.), professor, ORCID: https://orcid.org/0000-0002-1114-4726, silichaas@gmail.com

Yusupova, Elvira M., lecturer of the Natural Sciences and General Professional Disciplines Department, Tyumen Higher Military Engineering Command School (1, Tolstogo St., Tyumen, 625001, RF), ORCID: https://orcid.org/0000-0002-0463-1067, jusupovaem@tyuiu.ru

Claimed contributorship

A. A. Silich: academic advising; analysis of the research results; basic concept formulation. E. M. Yusupova: research objective and task setting; computational analysis; text preparation; formulation of conclusions.

All authors have read and approved the final manuscript.

MACHINE BUILDING AND MACHINE SCIENCE

UDC 622.271.002.5 (06) https://doi.org/10.23947/2687-1653-2020-20-3-302-310

Bucket working bodies with conveyor bottom: systematics and design features

Yu. M. Lyashenko[1], E. A. Revyakina[2], A.Yu. Lyashenko[1]

[1] Shakhty Institute, Branch of Platov South-Russian State Polytechnic University (NPI) (Shakhty, Russian Federation)

[2] Don State Technical University (Rostov-on-Don, Russian Federation)

Introduction. The creation of new types of bucket working bodies of excavators through synthesizing technical solutions to improve the transporting functions of the bottom is considered. These solutions are based on reducing the resistance and energy consumption under digging-in and scooping due to the transition from sliding friction to rolling friction during the movement of the rock mass along the bottom of the bucket.

Materials and Methods. Analysis of the bulk materials handling processes using existing loading appliances identified design flaws that affect the efficiency of their operation. Advanced design diagrams of loading bodies were searched on the basis of the accumulated experience and the study of the morphological features of the existing equipment. Combinatorial analysis of possible combinations of elements with their various qualitative compositions, mutual arrangement, imposed links, and synthesis of new technical solutions for loading and transportation modules are carried out.

Results. The results of the morphological synthesis implementation were the systematization and development of designs of bucket working bodies with a bottom in the form of a roller surface and a closed belt, as well as with a conveyor-type drive mechanism. The application of rollers as a supporting surface of a loaded rock mass causes a decrease in friction forces and in the power capacity of the work process. In addition, rotating rollers provide uniform abrasion of the working surface, which increases significantly the time to the equipment breakdown and increases the process efficiency. Working bodies with a drive mechanism make it possible to activate the interaction of the conveyor bottom in the form of a closed belt with the rock mass and, as a result, to accelerate the process of filling the bucket container.

Discussion and Conclusions. The bucket working bodies described in the paper compare favorably with existing analogues in that they provide a reduction in the time to digging-in, scooping and unloading, a decrease in specific energy consumption, an increase in bucket filling, which ultimately contributes to an increase in productivity. A slight increase in the structural complexity and cost of the working body causes additional capital costs, which are paid back within two to four months.

***Keywords**:* bucket working bodies, loading process, working cycle operations, extraction-and-loading machines, conveyor bottom, roller surface, mechanical transmission, hydraulic cylinder, hydraulic cylinder rod, friction.

For citation: Yu. M. Lyashenko, E. A. Revyakina, A.Yu. Lyashenko. Bucket working bodies with conveyor bottom: systematics and design features. Advanced Engineering Research, 2020, vol. 20, no. 3, p. 302–310. https://doi.org/10.23947/2687-1653-2020-20-3-302-310

Introduction. The technical level of mining and conveying equipment for surface mining operations is determined by the constructive perfection of both the machine as a whole and its bucket working body[1, 2, 3]. It is possible to increase the technical and performance figures of the equipment through using, first of all, the working bodies of rational designs and parameters.

[1] Podehrni RYu. Mechanical equipment of quarries. 5th ed. Moscow, 2003. 606 p. (In Russ.)

[2] Drozdova LG, Kurbatova OA. Single-bucket excavators: design, installation and repair. Vladivostok, 2007. P. 48–56. (In Russ.)

[3] Khazanovich GSh, et al. Research directions and results of on creation of tunneling equipment of new technical level. In: Proc.Sci.-Pract. Conf. on Actual questions in scientific work and educational activities. Tambov, 2013. P. 148-152. (In Russ).

Analysis of the mechanization means of loading rock using currently operating extraction and loading machines (excavators) identified factors affecting the efficiency of their operation[4]. Fig. 1 shows a bucket of a commonly used design with a smooth bottom.

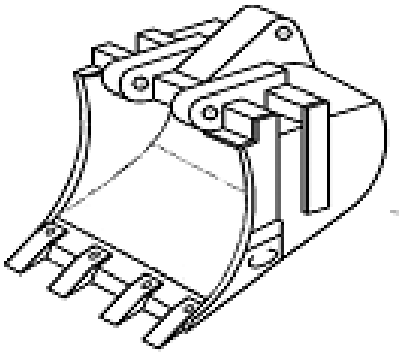

Fig. 1. Bucket working body with bottom in the form of smooth surface

It is established that the design improvement of the bucket working body is aimed mainly at reducing resistance to the bucket penetration into the pile [1]. The work objectives are to systematize new technical solutions of working bodies developed by the authors, in particular, with a conveyor bottom, to analyze their design features and improved working qualities, i.e., to consider the development trends of this class of equipment. Major tasks of the work are as follows:

– rationale for the fundamental approaches to changing the design of the bucket working body elements;

– determination of the functional and structural analysis feasibility to select directions for improving the design of the bucket;

– development of classification features characterizing excavator buckets with reduced resistance to penetration;

– preliminary qualitative assessment of new technical solutions.

Materials and Methods. According to the results of graphic-analytical and physical modeling of the "bucket — rock pile" system, it is found that the resistance to the penetration of the bucket working body into the pile depends significantly on the friction factor of the submerged material over the surfaces of the bucket [2, 3]. When synthesizing technical solutions of bucket working bodies with a constructive novelty, the problem of reducing the friction factor of rocks on the bottom of working bodies through transition from sliding friction to rolling friction was solved [4].

The creation of samples of new types of working bodies is a complex, multi-stage task. The first stage in determining promising design diagrams of bucket working bodies was the study of the accumulated experience and the establishment of morphological features of the existing equipment (Fig. 2).

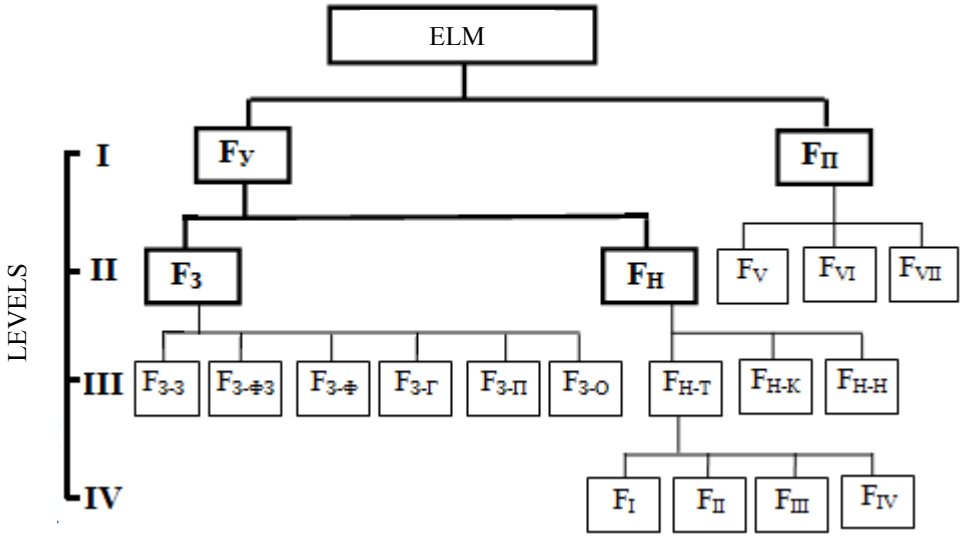

Fig. 2. Functional model of an extraction-and-loading machine (ELM)

[4] Khazanovich GSh, Lyashenko YuM, Nikitin EV. Experimental technique in study of processes of loading and transportation of lumpy rocks. Novocherkassk, 2003. 150 p. (In Russ).

The compiled functional ELM model includes the following set of actions: F_y — to remove the rock mass; F_n — to provide special motion; F_3 — to scoop up the rock mass detached from ground; $F_{3\text{-}3}$ — to form the bucket capacity; $F_{3\text{-}ф3}$ — to provide functioning of the tool for formation of the bucket capacity; $F_{3\text{-}ф}$ — to service the face line; $F_{3\text{-}г}$ — to service the face in depth; $F_{3\text{-}п}$ — to transfer the element of forming the bucket capacity to the place of release from the portion of material; $F_{3\text{-}о}$ — to provide releasing the element for forming the bucket capacity from the portion of the material; $F_н$ — to accumulate and reload the scooped rock mass; $F_{н\text{-}т}$ — to provide the transportation (displacement) of the rock mass; $F_{н\text{-}к}$ — to provide maintenance of contact with the subsequent vehicle; $F_{н\text{-}н}$ — to provide the accumulation of rock mass; F_I — to keep the rock mass in the process of transportation (displacement); F_{II} — to apply an acting force to the rock mass; F_{III} — to transfer the acting force from the drive to the final elements; F_{IV} — to transfer the bearing element with the rock mass detached from the ground; F_V — to take up crowd forces and fix the position of the system functional elements; F_{VI} — to convert the energy supplied to the drive into transition of the system kinematic condition; F_{VII} — to combine functional elements of the system for the joint operation.

The proposed differentiation of functional features enables to enter an elemental level of the structure formation of individual mechanisms of extraction-and-loading machines. The impossibility of further fragmentation of the major functions (macrofunctions) into subordinated ones (microfunctions) without a transition from the function to the objective form of their execution was a signal to complete the functional analysis.

Taking into account the developed functional model of the extraction-and-loading machine, a morphological table was worked out, with the help of which the structural and morphological features of a technical solution with a constructive novelty were formed [4] (Fig. 3).

Research Results. The result of the practical implementation of morphological synthesis was the developed design of a bucket with a bottom in the form of a conveyor [5]. The use of a closed belt as a load-carrying body and a supporting surface of the submerged rock mass provides the exclusion of spillage and jamming of the submerged material. This design is characterized by a low friction factor of the rock mass against the bottom in the form of a closed belt resting on rollers. Therefore, a decrease in the energy intensity of the working process, which will provide an increase in the productivity and reliability of the bucket working body, is expected.

The concepts of the efficiency of equipping the working bodies with roller elements when loading rocks were further developed in the novel design of the working body of the loading and transportation module with a cyclic actuator. The proposed loading and transportation module, equipped with a closed belt, differs from the existing analogues in the increased displacement rate of the rock mass; it provides the continuity of loading the material during the cyclic operation of the working body. All this contributes to an increase in productivity and efficiency of the work process while eliminating the possibility of spilling and jamming of particles between the rollers. Equipment of the transport roller in the conveyor bottom with a drive also allows increasing the efficiency of the bucket working body. This solution provides a reduction in the time of penetration, scooping and unloading operations, an increase in the filling of the bucket and, therefore, contributes to an increase in productivity [6].

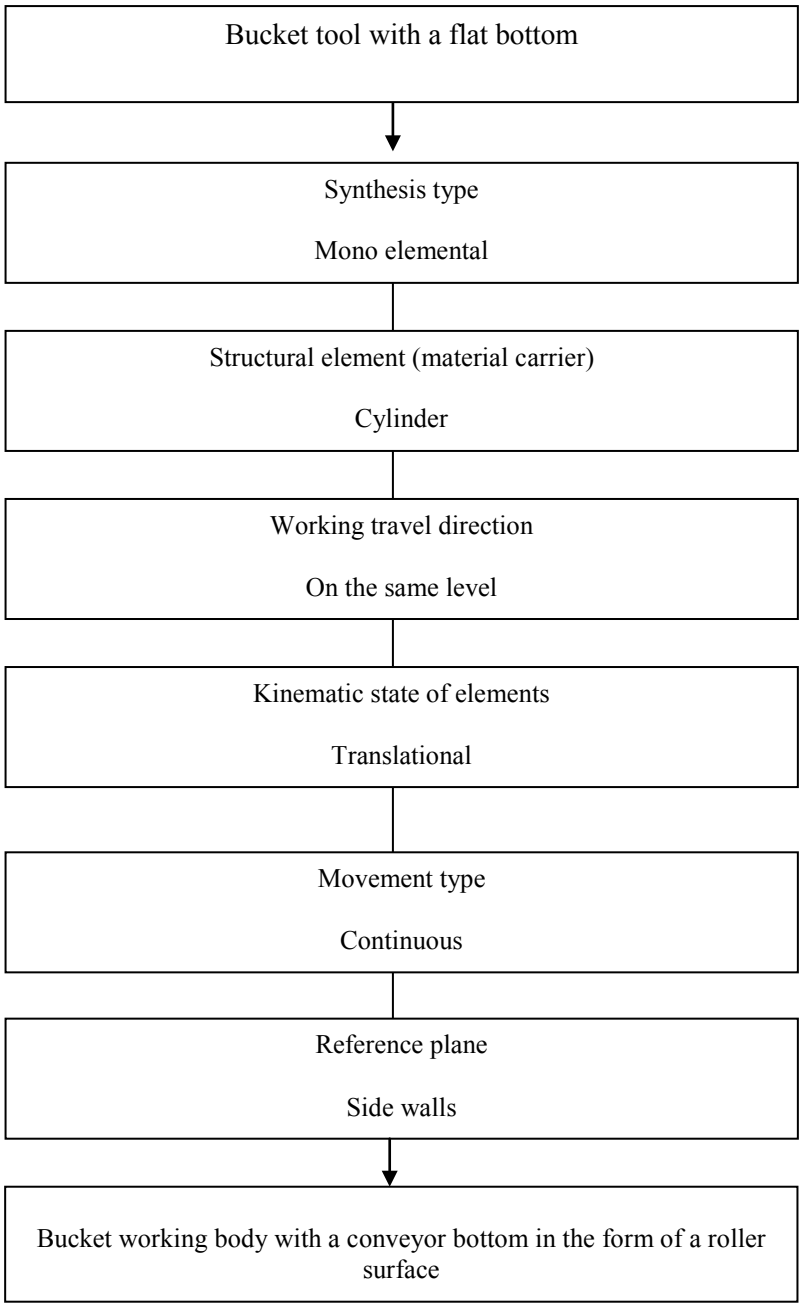

Fig. 3. Formation of structural and morphological features of a structurally novel technical solution

The models of buckets with a conveyor bottom developed on the basis of the above principles form a new constructive and technological group of loading bodies that can be used on excavators, bucket loaders and other handling equipment. Below, these technical solutions are presented through a combination of two groups of structures characterized by a bottom in the form of a roller surface and in the form of a closed belt (Fig. 4) [7]. In turn, structurally, models with a closed belt are divided into non-drive ones and with a belt drive mechanism, which can be implemented from an electric motor with a mechanical transmission and using various options for hydraulic power cylinders.

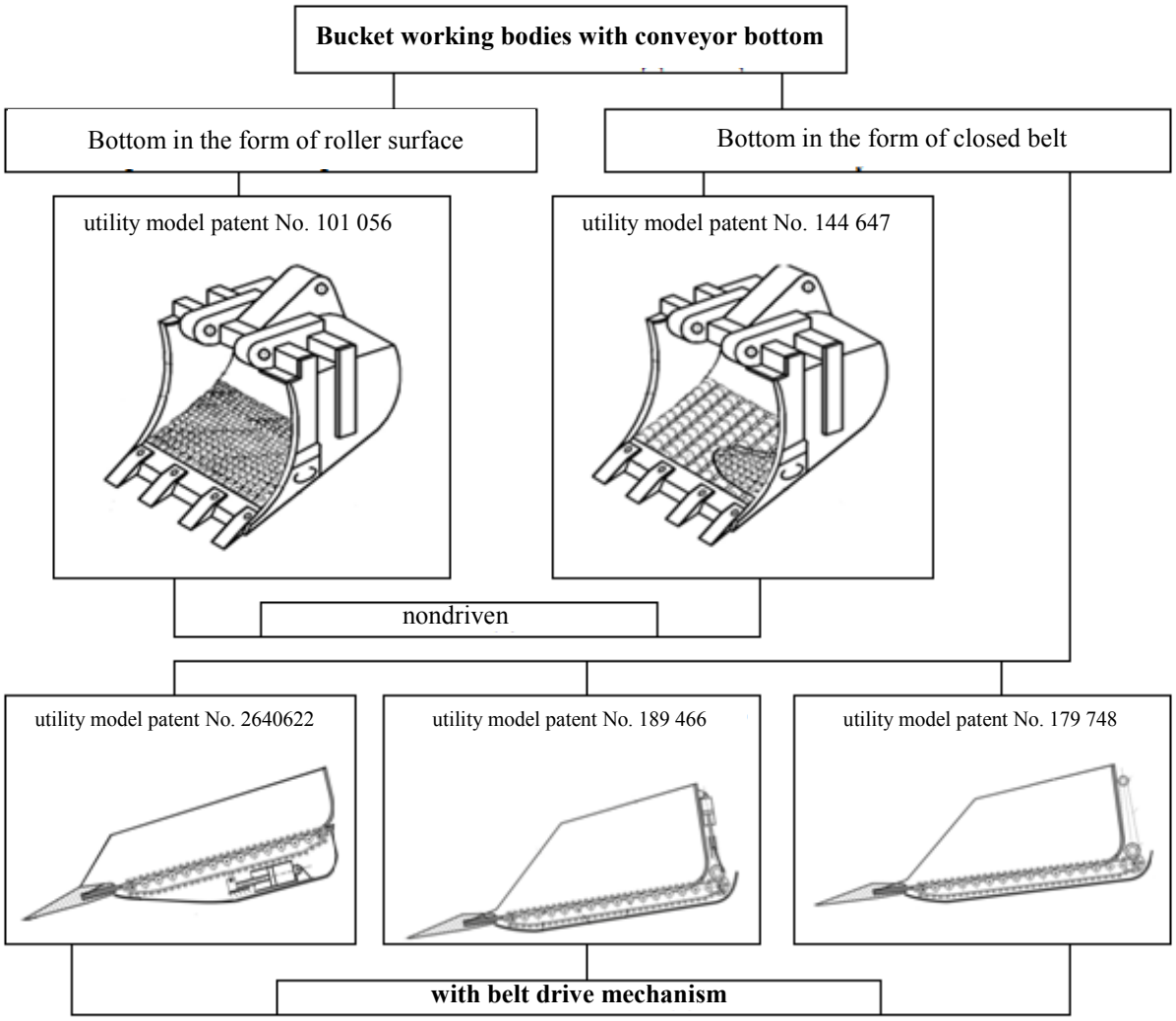

Fig. 4. Systematics of bucket working bodies with a conveyor bottom

Let us consider the design features of nondriven bucket working bodies with a conveyor bottom in the form of a roller surface, in the form of a closed belt, as well as bucket working bodies with a conveyor bottom belt drive mechanism.

Bucket working body with a conveyor bottom in the form of a roller surface [5]**.** According to the proposed design of the bucket working body (Fig. 5), the bottom (3) is made in the form of a surface consisting of a set of rollers (4), which are installed to rotate around the axes (5), fixed on the side walls(2). Before starting, when the process of rock loosening in a quarry is completed, the bucket working body is in front of the pile of lumpy rock mass in the position shown in Fig. 5 b. The filling of the bucket (1) occurs when it is forced to move in the direction of the rockpile. In this case, the cutting edge and bottom teeth (3) cut off a part of the pile material located on the face area. The loosened rock mass slides along the rollers (4) and enters the bucket (1). The rollers (4) rotate under the pressure of the rock mass relative to the axes (5) reducing the resistance to its motion relative to the bottom (3) and contributing to a more efficient filling of the bucket (1).

[5] Lyashenko YuM, Revyakina EA, Lyashenko AYu. RF Patent 101056, 2011. (In Russ.)

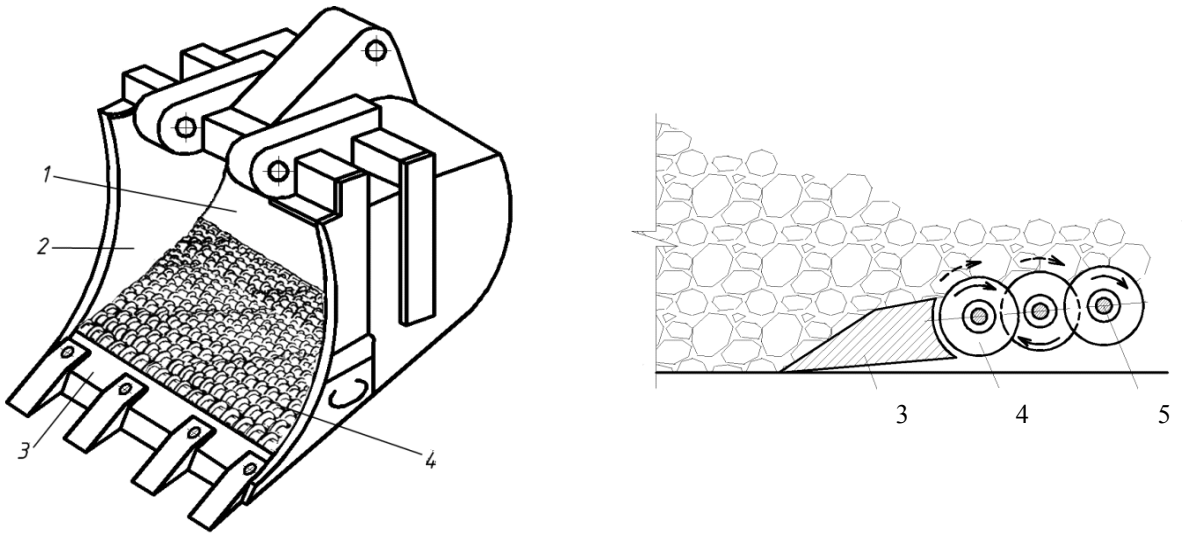

Fig. 5. Design of bucket working body with conveyor bottom in the form of roller surface (*a*) and its position in front of lumpy rockpile (*b*): 1 — bucket capacity; 2 — side walls; 3 — bottom; 4 — a set of rollers; 5 — axis of rotation

The rock mass flow to the place of unloading is carried out in the bucket (1). The bucket is unloaded when it is tilted due to the rock mass flow under the action of gravity. In this case, the sliding of the rock mass in the opposite direction along the rollers (4) rotating in the same direction helps to reduce the unloading time. The use of rollers as a supporting surface of the submerged rock mass provides the workload reduction and a decrease in the energy requirement. In addition, rotating rollers provide uniform abrasion of the working surface, which significantly reduces the risk of equipment failure and increases the process efficiency.

Bucket working body with a bottom in the form of a closed belt (Fig. 6)[6]. The design feature is that the conveyor bottom (3) is made in the form of a closed belt (6) consisting of plates (7) journaled to each other by pins (8). The belt rests on rollers (4) and bends around them. The rollers act as a guiding track during the movement of the top belt of the plate (7). Under the pressure of the belt (6) interacting with the rock mass, the rollers (4) rotate relative to the axes (5) fixed on the side walls (2). The belt (6) moves along the rollers (4). The rock mass enters the bucket (1) along the belt. The use of a closed belt as a load-carrying body and a supporting surface of the rock mass excludes spillage and jamming of the submerged material.

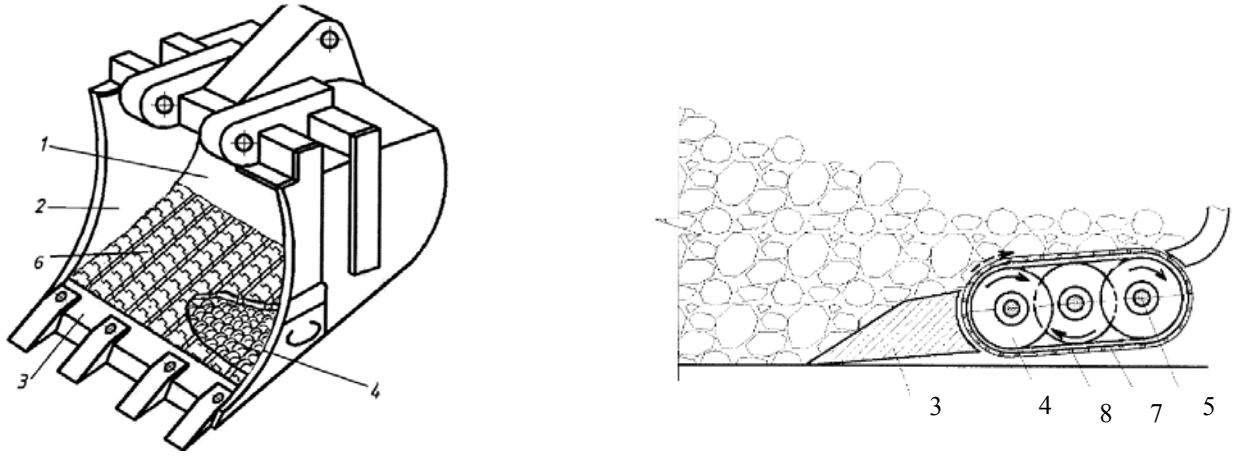

a) *b*)

Fig. 6. Bucket working body with conveyor bottom in the form of closed belt (*a*) and its position in front of lumpy rockpile (b): 1 — bucket capacity; 2 — side walls; 3 — bottom; 4 — rollers; 5 — axis of rotation; 6 — belt; 7 — plates; 8 — pins

Bucket working body with a conveyor bottom in the form of a closed belt connected to the engine through mechanical transmission[7]**.** This design, compared to the previous ones, is able to further intensify the interaction of the conveyor bottom and the rock mass, and, as a consequence, accelerate the process of filling the bucket

[6]Lyashenko YuM, et al. Bucket working body. RF Patent 144647, 2014. (In Russ.)
[7] Revyakina EA, et al. Complex of quarry equipment. RF Patent 2640622, 2018. (In Russ.)
[7] Revyakina EA, Lyashenko YuM, Sergeev VV. RF Patent 179748, 2018. (In Russ.)

(Fig. 7). Possible drive options are described in the technical solutions discussed below.

Here, the conveyor bottom (2) is made in the form of a closed belt (3) enveloping the rollers (4), whose axes of rotation are fixed on the side walls (1). One of the rollers (5) is driven and equipped with the mechanical transmission (6) connected to the engine (7) to move the closed belt.

The rock mass flow on the belt (3) geared by the rotating drive roller (5) through the mechanical transmission (6) from the engine (8), contributes to a more efficient filling of the bucket and reduces the operation time. Thus, the proposed working body compares favorably with existing analogues in that they provide a reduction in the time to digging-in, scooping and unloading; and when penetrating into a rockpile and scooping, it increases the filling capacity and, therefore, improves productivity.

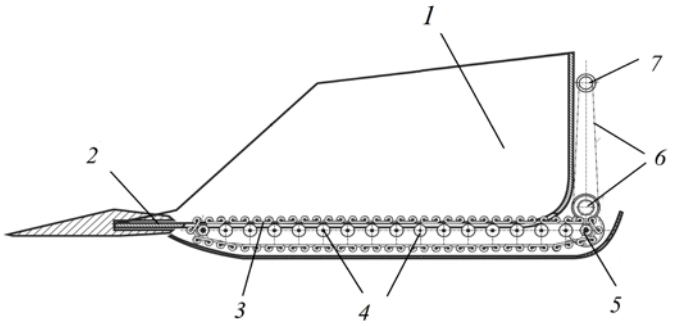

Fig. 7. Bucket working body with conveyor bottom in the form of closed belt connected to the engine through mechanical transmission: 1 — side wall; 2 — bottom; 3 — closed belt; 4 — rollers; 5 — transport (drive) roller; 6 — mechanical transmission; 7 — engine

Bucket working body with a conveyor bottom in the form of a closed belt connected with a drive from two hydraulic cylinders through transmission mechanisms [8]. A diagram of such a working body is shown in Fig. 8. Its conveyor bottom (2) is made in the form of a closed belt (3) enveloping the rollers (4), whose axes of rotation are fixed on the side walls (1). The closed belt drive consists of two hydraulic cylinders (6) and (7) with transmission mechanisms in the form of slides (8) installed in the guides, connecting rods (9) and cranks (10). The , connecting rods (9) are journaled to the slides (8), and the cranks (10) are rigidly attached to the axis of the drive roller (5) under mutually perpendicular displacement.

Equipping the bucket working body with a drive consisting of two hydraulic cylinders with transmission mechanisms of the specified design provides the rotary motion of the drive roller. Mutual displacement of the crank attachment points provides the hydraulic cylinders falling out of the dead centers in a given direction of rotation.

Through supplying the working fluid to the rod cavity of the hydraulic cylinder (6), the motion of its rod and transmission mechanisms, consisting of slides (8), cranks (9) and , connecting rods (10) installed in the guides, is provided. Thus, the drive roller (5) is set in rotation, which provides the belt (3) displacement. In this case, the hydraulic cylinder piston (7) is removed from the extreme position, after which liquid is supplied to its piston cavity, which provides the simultaneous operation of the hydraulic cylinders (6) and (7).

The bucket is filled during the period of its forced displacement towards the rockpile. In this case, the cutting edge and pins of the bottom (2) cut off a part of the material located on the face area. Loosened rock mass enters into interaction with the belt (3) and is transferred by the latter to the bottom (2) filling the bucket working body. The cycle ends in the zero-point return operation of the working body and its preparation for a new working movement and filling.

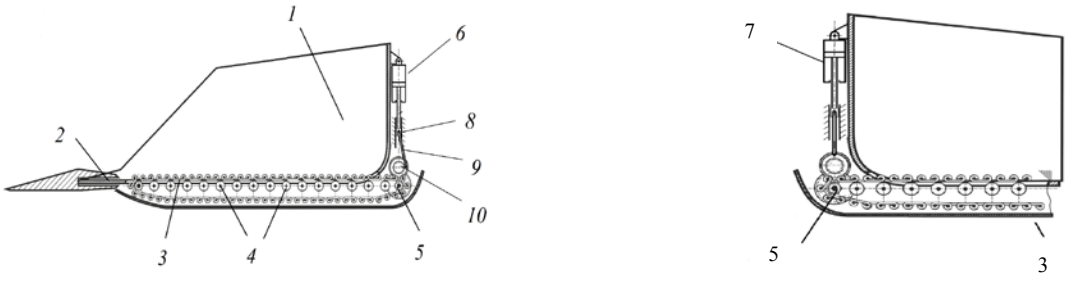

Fig. 8. Bucket working body with conveyor bottom in the form of closed belt connected with a two-hydraulic cylinder drive by transmission mechanisms: 1 — side wall; 2 — conveyor bottom; 3 — belt; 4 — supporting rollers; 5 — drive roller; 6, 7 — hydraulic cylinders; 8 — slides; 9 — connecting rods; 10 — cranks

The design of the belt drive mechanism in the form of a rotating roller driven by two hydraulic cylinders with transmission mechanisms enables to use the bucket working bodies with a conveyor bottom on hydraulic excavators that play a key role in the mechanization of extraction-and-loading operations in quarries. Such excavators account for more than 60% of the total number.

Bucket working body with conveyor bottom in the form of closed belt connected to the drive hydraulic cylinders through locking clamps[9]. The working body diagram is shown in Fig. 9. In this design, the closed belt drive (1) of the bucket working body with a conveyor bottom consists of two hydraulic cylinders (4) with spring-loaded clamps (6) mounted on the rods (5), which engage with the belt (1) under the action of the spring (7) during the forward stroke and freely move during the reverse.

In the process of loading, hydraulic fluid is supplied to the hydraulic cylinder (4). The rod (5) of the hydraulic cylinder extends, the retainer (6) under the action of the spring (7) engages with the belt (1) and sets it in motion. The belt, moving along the rollers (2), transfers the rock mass located on it. The continuity of the transportation of the rock mass is provided through the sequential operation of two hydraulic cylinders (4). Such a conveyor belt drive mechanism simplifies the design of the bucket working body, increases the reliability of the drive, while maintaining the positive effect of the belt drive discussed above in the form of a rotating roller, which is driven by two hydraulic cylinders with transmission mechanisms.

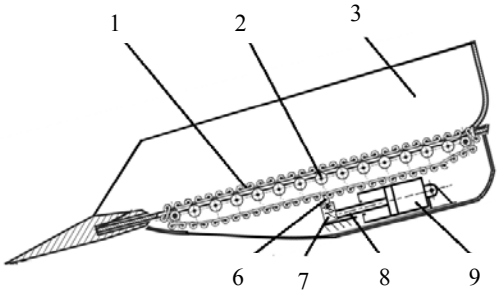

Fig. 9. Bucket working body with conveyor bottom in the form of closed belt connected to the drive hydraulic cylinders through locking clamps: 1 — closed belt; 2 — rollers; 3 — side walls; 4 — hydraulic cylinder; 5 — hydraulic cylinder rod; 6 — retainer; 7 — spring

Discussion and Conclusions. Bucket working bodies with a conveyor bottom can considerably improve the technical level of operated excavators and help to reduce the energy consumption of loading. A preliminary analysis shows that in comparison to the traditional excavator loading bodies with a bottom with a smooth surface, the proposed technical solutions have the following advantages:

— reduction of resistance to implementation;

— increasing the bucket filling ratio;

— decrease in the specific energy intensity of the process;

— increase in the resulting technical productivity.

These advantages will be more pronounced as the bucket capacity of the excavator increases. A certain structural complication of the loading unit cannot significantly affect the cost of the excavator, the estimated additional capital costs are paid off within two to four months.

The method of prioritization [8, 9] is the basis for a comprehensive expert assessment of the options of technical solutions obtained in the course of morphological synthesis. The calculation of the complex priority of bucket working bodies with a conveyor bottom and loading modules with a conveyor bottom made it possible to recognize them as promising with a representativeness of the expert panel of 0.81.

References

1. Khazanovich GSh, Luk'yanova GV. Modelirovanie rabochikh protsessov kak osnova dlya vybora ratsional'nykh variantov prokhodcheskikh pogruzochno-transportnykh modulei [Work processes simulation as a basis for the selection of rational options for tunneling loading and transport modules]. University News. North-Caucasian region. Technical Sciences Series. 2005;58:112–117. URL: https://www.elibrary.ru/contents.asp?id=41290655 (accessed 29.08.2020). (In Russ.)

2. Lyashenko YuM, Revyakina EA. Metodicheskie podkhody k modelirovaniyu sistemy «sypuchee telo — rabochii ehlement» v issledovaniyakh protsessa pogruzki gornykh porod [Methodological approaches to modeling of the system “low-body body – working element” in the investigations of the process of loading the rock]. Mining Equipment and Electromechanics. 2018;3(137):15–20. (In Russ.)

[9] Revyakina EA, Lyashenko YuM, Sergeev VV. Bucket working body. RF Patent 189466, 2019. (In Russ.)

3. Khazanovich GSh, Luk'yanova GV, Revyakina EA, et al. Modelirovanie rabochikh protsessov pogruzochno-transportnykh modulei s uchetom sluchainogo kharaktera vneshnikh vozdeistvii [Modeling the working processes of loading and transport modules taking into account random nature of external actions]. Shakhty: Izd-vo Yuzhn.-Ros. gos. un-ta ehkonom. i serv.; 2010. 177 p. (In Russ.)

4. Luskan' OA. Vliyanie rezhimnykh parametrov kachaniya ramy impul'snogo rolikovogo konveiera na protsess transportirovaniya shtuchnykh gruzov [Effects of operating parameters swing frame pulse roller conveyor for piece goods transportation process]. Transport and Technological Cars. 2011;1(32):48–63. (In Russ.)

5. Lyashenko YuM, Shurygin DN, Revyakina EA. Application of the laws of mechanics of granulated solids in studies to loader bucket interaction with bulk material stack. In: ICIE 2017. Proc. Int. Conf. on Industrial Engineering. Procedia Engineering. 2017;206:1388-1394.

6. Evstratov VA, Lyashenko YuM. Issledovaniya fizicheskoi modeli kovsha ehkskavatora s rolikovym dnishchem [Investigations of the physical model of a roller bottom excavator bucket]. Construction and Road Building Machinery. 2013;1:2–7. (In Russ.)

7. Lyashenko YuM, Revyakina EA, Lyashenko AYu. Pogruzochnye organy s rolikovoi rabochei poverkhnost'yu pogruzochno-transportnykh kompleksov kar'erov nerudnykh materialov [Machine working bodies with roller surface loading-transport complex pit aggregates]. Transport and Technological Cars. 2014;3(46):60–71. (In Russ.)

8. Moiseeva NK. Funktsional'no-stoimostnyi analiz v mashinostroenii [Functional cost analysis in Mechanical Engineering]. Moscow: Mashinostroenie; 1987. 210 p. (In Russ.)

9. Kuznetsov S. Issledovanie protsedur funktsional'no-stoimostnogo analiza sistem [Investigation of procedures for the functional cost analysis of systems]. Moscow: LAP Lambert Academic Publishing; 2018. 100 p. (In Russ.)

Submitted 16.03.2020
Scheduled in the issue 11.05.2020

About the Authors:

Lyashenko, Yurii M., professor of the Transport Safety and Road Infrastructure Management Department, Shakhty Institute, Branch of Platov South-Russian State Polytechnic University (NPI) (1, Lenin sq., Shakhty, Rostov Region, 346500, RF), Dr.Sci. (Eng.), professor, Scopus ID 6603581379, ORCID: https://orcid.org/0000-0002-6553-0163, lumdtn@yandex.ru

Revyakina, Elena A., associate professor of the Cybersecurity of IT Systems Department, Don State Technical University (1, Gagarin sq., Rostov-on-Don, 344003, RF), Cand.Sci. (Eng.), associate professor, Scopus ID 57197834319, ORCID: https://orcid.org/0000-0003-1577-2671, revyelena@yandex.ru

Lyashenko, Alena Yu., teaching assistant of the Transport Safety and Road Infrastructure Management Department, Shakhty Institute, Branch of Platov South-Russian State Polytechnic University (NPI) (1, Lenin sq., Shakhty, Rostov Region, 346500, RF), ORCID: https://orcid.org/0000-0002-2896-8043, alyona_lyashenko@mail.ru

Claimed contributorship

Yu. M. Lyashenko: academic advising; formulation of the basic concept, research objectives and tasks. E. A. Revyakina: computational analysis; text preparation; formulation of conclusions. A. Yu. Lyashenko: analysis of the research results; the text revision; correction of the conclusions.

All authors have read and approved the final manuscript.

INFORMATION TECHNOLOGY, COMPUTER SCIENCE, AND MANAGEMENT

UDC 004.771 https://doi.org/10.23947/2687-1653-2020-20-3-311-316

Modeling of information support to optimize logistics tasks in transport sector using a programmable container transformer simulator

A. A. Korotky[1], D. A. Yakovleva[2], A. A. Maslennikov[2], I. V. Golovko[2]
[1]Don State Technical University (Rostov-on-Don, Russian Federation)
[2]Platov South-Russian State Polytechnic University (Novocherkassk, Russian Federation)

Introduction. The structure of the transport logistics system for the transportation of container transformers in an urbanized environment to optimize production costs with elements of intelligent urban mobility, as well as the simulation software for modeling and testing the developed system, are described. The basic principles of the interaction between elements of the system are presented through the behavioral modeling of containers and carriers. Software is created to simulate the operation of the logistics infrastructure for transformer containers using wireless technology and the Internet of Things; and services for the rapid information exchange between participants (objects and subjects) of this process are implemented.
Materials and Methods. A general method of organizing a network with a web server and a mobile client, as well as the basic principle of interaction between the server and the client, is described. The basics of developing a simulator designed to simulate all possible states of a container transformer are specified.
Results. A common system architecture and a simulator are created for the software debugging and testing under the organization of a single space to monitor and optimize cargo transportation using "smart" container transformers while providing transport services to the population and legal entities in an urban environment.
Discussion and Conclusions. The developed simulator as part of the information system provides speeding up the creation, debugging and testing of the software for solving logistics problems in the transport sector.

Keywords: transport logistics, container transformer, web server, client, simulator, transport, route optimization.

For citation: A. A. Korotky, D. A. Yakovleva, A. A. Maslennikov, et al. Modeling of information support to optimize logistics tasks in transport sector using a programmable container transformer simulator. Advanced Engineering Research, 2020, vol. 20, no. 3, pp. 311−316. https://doi.org/10.23947/2687-1653-2020-20-3-311-316

Funding information: the research is done under contract no. 502ГРНТИС5/49457 of 11.09.2019

Introduction. There is a logistical problem associated with the transportation of cargo containers with empty crate resulting in added costs for fuel and labor, road congestion and, as a result, stress on the environment.

To solve the described logistics problem for the transportation of goods, containers-transformers SmartBoxCity are used, they are equipped with wireless technology and the Internet of Things[1]. The central element of the created product is a container equipped with IT system of remote administration and scripted control that can transform into operation condition. It is intended for large logistics companies. A container transformer provides stacking several empty containers in one vehicle, which saves logistics costs, since a specific volume of transportation is used more efficiently [1]. The proposed solution enables to reduce delivery costs, and it is a part of information system for optimizing the route of freight transport [2].

Due to the fact that the development and testing of the project components is a rather laborious and resource-intensive process, software is proposed to simulate the processes of the complex as a whole.

[1] Petrov OA, Evstratov EM, Korotkii AA, et al. Collapsible shipping container. RF Patent 2672998, 2018. (In Russ.)

The work objectives were to create a software product that provides modeling of the logistics infrastructure for transformer containers using wireless technology and the Internet of Things; and to implement services for the rapid exchange of information between participants (objects and subjects) of this process [3].

Materials and Methods. To solve the task of developing a simulator application, first of all, it was necessary to select a web server. IIS (Internet Information Services) was chosen as a web server, a proprietary set of servers for several Internet services from Microsoft, as well as an ASP.NET Core web application, because applications built on this technology are portable and easy customizable[2]. The framework uses the C # programming language and the presentation engine Razor[3].

The relational database management system Microsoft SQL Server [4] was selected as the database for storing the modeled data.

Among the components included in the software, there is a mobile application for simulating the behavior of a transformer container. With its help, the user can create a model of the container, track its possible states and sensor readings. The application consists of the following functional blocks (sections of the main menu): “Sensor readings”, “GPS coordinates”, “Container condition” and Photofixation”.

In the “Sensor readings” section of the main menu, the user can track and change the following sensor readings: temperature, cargo weight, illumination, humidity, battery charge level, network signal level. All changes made by the user are subsequently saved, and then access to the camera, which records the state of the cargo in the transformer container at the time of changing the parameters, is given (Fig. 1).

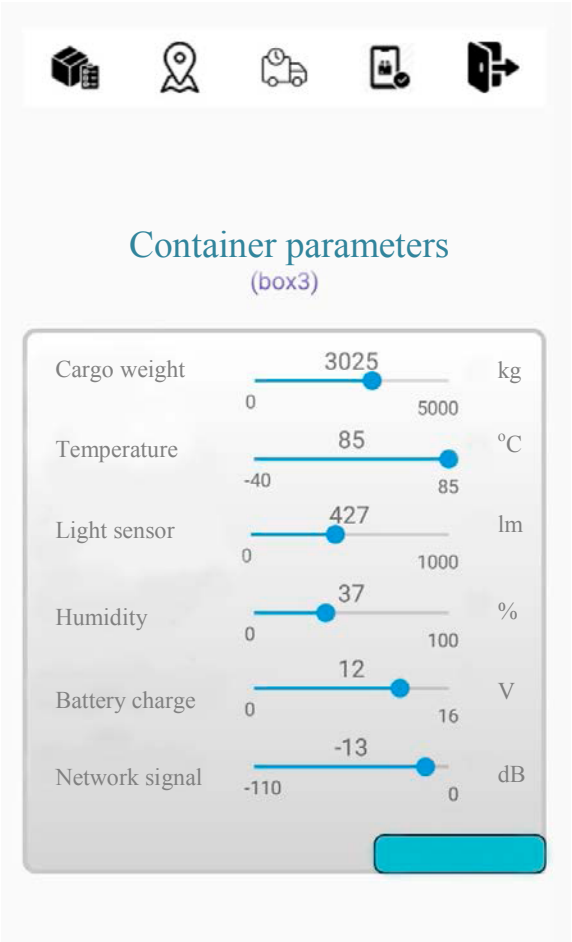

Fig. 1. Sensor readings

In the “GPS coordinates” section of the main menu, the user is presented with the real-time GPS coordinates of the container. Additionally, the date and time of coordinate change are tracked [5]. All changes at regular intervals are sent to the server and recorded in the database (Fig. 2).

[2]Internet Information Services. URL: https://ru.wikipedia.org/wiki/Internet_Information_Services (accessed: 15.04.2019) (In Russ.).

[3]Roth D, Anderson R, Luttin Sh. Introduction ASP. NET Core. URL: https://docs.microsoft.com/ru-ru/aspnet/core/introduction-to-aspnet-core?view=aspnetcore-3.1 (accessed: 13.04.2020) (In Russ.)

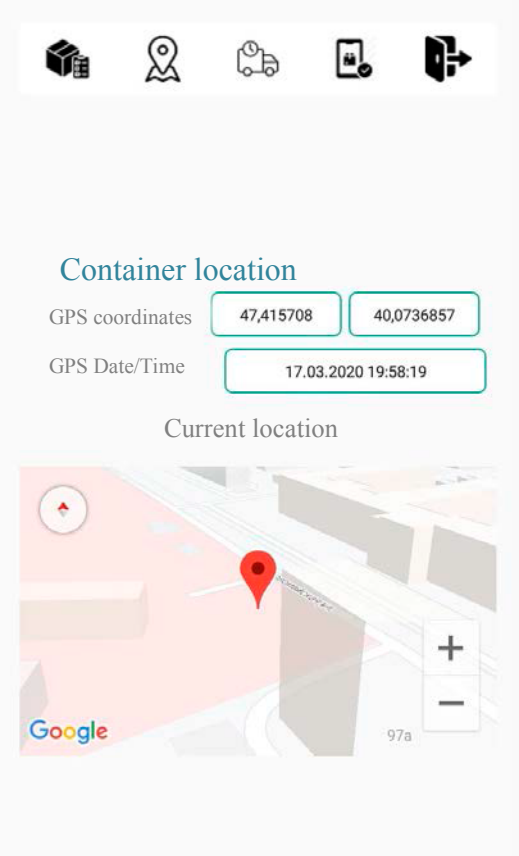

Fig. 2. GPS coordinates of the container

In the “Container condition” section of the main menu, the position of the doors (open/closed) and the container (unfolded/folded) is monitored, as well as its location: in the warehouse, by car and at the customer's [6]. As in the “Sensor readings” section of the main menu, after the user has modeled the object and clicked on the “Save changes” button, the application transfers him through the menu to the phone camera to take photographs (Fig. 3)

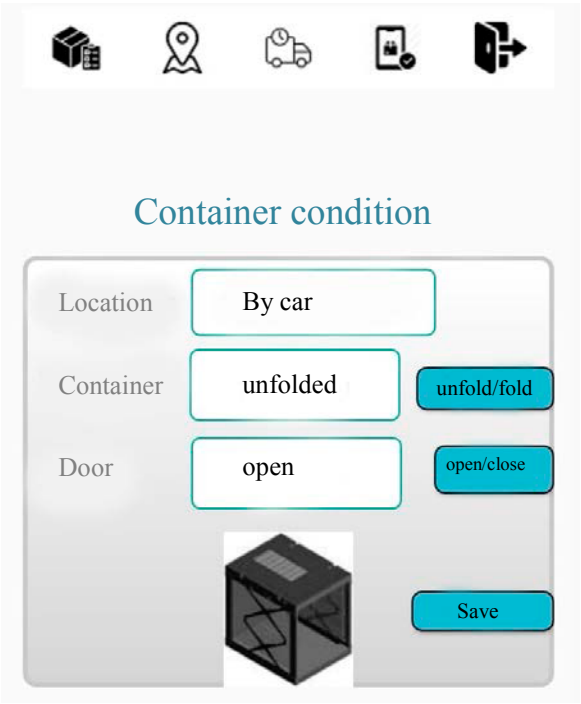

Fig. 3. Container condition

The “Photofixation” section of the main menu displays the latest readings of the transformer container sensors, as well as GPS coordinates. As a result, all simulated data is displayed in tabular form. The implementation of photofixation is a rather important component of the application since the client gets the opportunity to visually monitor the state of the cargo in the transformer container (Fig. 4).

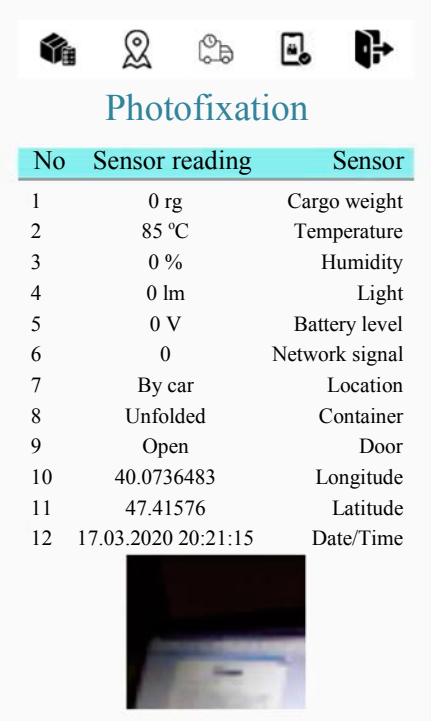

Fig. 4. Photofixation

“SmartBoxCity” mobile application that simulates transformer containers has been developed to test the functionality of software using wireless technology and the Internet of Things. Data on the parameters of the transformer containers is transmitted to the server and recorded in the database. To test the created model, it is possible to enter your personal account, and, based on a previously created account, view the condition of objects in real time, track their location using Google Maps technology [7]. It is possible to make settings that imitate the “behavior” of the transformer container through the mobile application. The data obtained by this simulator is used to solve logistics problems of the cargo transportation optimization.

Research Results. Thus, we can conclude that the user is able to exercise full control over the process of modeling the transformer container behavior through the simulator application.

The components developed as part of the simulator application are the basis for testing the future information system, which provides the implementation of the information component of the motor transportation infrastructure software to support and optimize logistics tasks.

Fig. 5 shows the developed architecture of the information system, which has been tested to support work with a variety of transformer container simulators and has shown resistance to loads and completeness of functionality for solving and optimizing logistics tasks.

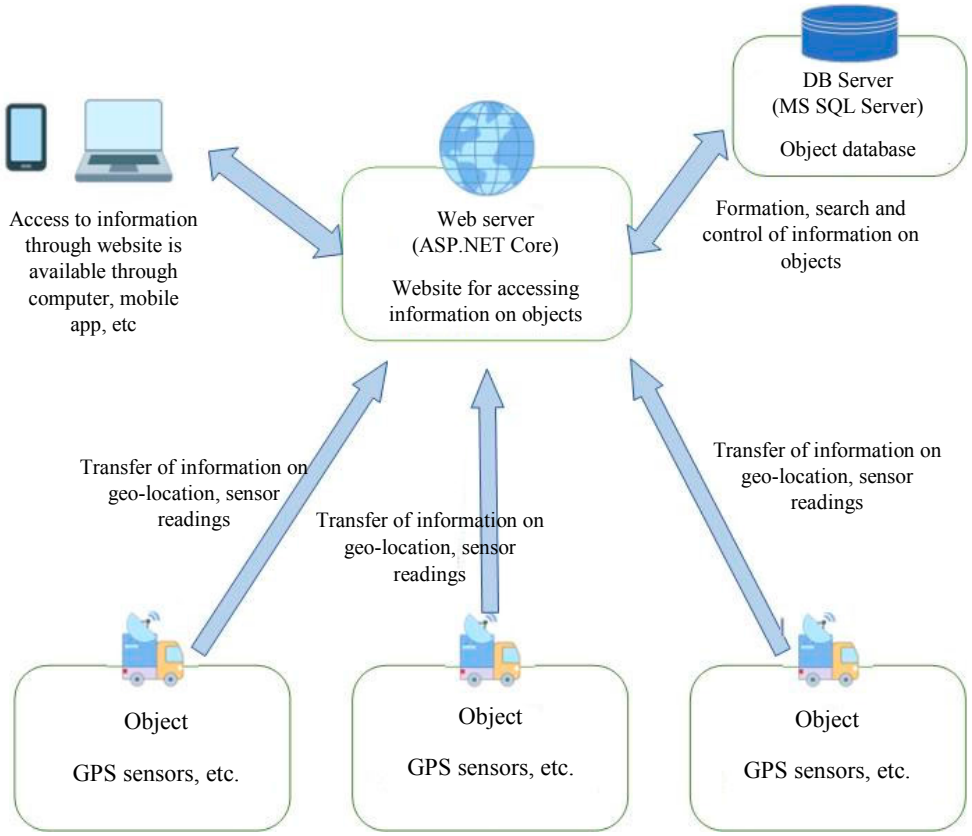

Fig. 5. Architectural scheme of the system

In the process of the software implementation, a web server that provides processing of information received from the developed mobile application, a simulator of a container transformer, and also a subsystem for interaction with real sensors that are part of the object was organized were created [8].

Discussions and Conclusions. The created simulator will provide the user with simulation of the container behavior and tracking all kinds of readings of its sensors. It is an integral part of the software for its debugging and testing when organizing a single space for monitoring and optimizing cargo transportation using “smart” transformer containers under trucking for population and legal entities in an urbanized environment.

References

1. Gal'chenko GA, Korotkii AA, Ivanov VV. Informatsionno-kommunikatsionnaya logisticheskaya sistema dlya optimizatsii transportnykh marshrutov v urbanizirovannoi srede [Information-communication logistic system for transport routers optimization in urbanization environment]. The Bryansk State University Herald. 2018;4(85):63−67. (In Russ.) DOI: https://10.30987/article_5b28d18e203e46.88731833

2. Korotkii AA, Popov SI, Gal'chenko GA, et al. Programmnyi kompleks postroeniya optimal'nogo marshruta pri karavannom dvizhenii transportnykh sredstv [Software complex for constructing the optimal route for caravan traffic of vehicles]. In:. Innovative technologies in science and education (ITNO-2019): Proc. of the VII International Sci-Pract. Conf. dedicated to 90th anniversary of DSTU (RISKhM). Rostov-on-Don; 2019. P. 68–71. (In Russ.)

3. Chambers D, Paquette D., Timms S. ASP.NET Core. Razrabotka prilozhenii [ASP.NET Core. Application Development]. St.Petersburg: Piter; 2018. 464 p. (In Russ.)

4. Petzold Ch. Creating Mobile Apps with Xamarine. Forms: Cross-platform C# programming for iOS, Android, and Windows. Redmond, WA, USA: Microsoft Press; 2016. 41 p.

5. Chernikov V. Razrabotka mobil'nykh prilozhenii na C# dlya iOS i Android. [Developing mobile applications in C# for iOS and Android]. Moscow: DMK Press; 2020. 188 p. (In Russ.)

6. Greene J, Stellman A. Izuchaem C# [Exploring C#]. St.Petersburg: Piter; 2020. 816 p. (In Russ.)

7. Freeman A. ASP.NET Core MVC c primerami na C# dlya professionalov [Pro ASP.NET Core MVC with examples in C#]. Moscow: Dialektika; 2017. 991 p. (In Russ.)

8. Phillips B, Stewart C, Marsicano K. Android. Programmirovanie dlya professionalov [Android. Programming for professionals]. St.Petersburg: Piter; 2017. 688 p. (In Russ.)

Submitted 11.05.2020
Scheduled in the issue 31.07.2020

About the Authors:

Korotky, Anatolii A., Head of the Transport Systems Operation and Logistics Department, Don State Technical University (1, Gagarin sq., Rostov-on-Don, 344003, RF), Dr.Sci. (Eng.), professor, ORCID: https://orcid.org/0000-0001-9446-4911, korot@novoch.ru

Yakovleva, Dar'ya A., student of the Computer Software Department, Platov South-Russian State Polytechnic University (NPI) (132, ul. Prosveshcheniya, Novocherkassk, Rostov Region, 346428, RF), ORCID: https://orcid.org/0000-0002-2870-657X, dasha.yakovleva.2013@list.ru

Maslennikov, Aleksei A., associate professor of the Computer Software Department, Platov South-Russian State Polytechnic University (NPI) (132, ul. Prosveshcheniya, Novocherkassk, Rostov Region, 346428, RF), Cand.Sci. (Eng.), ORCID: https://orcid.org/0000-0003-4042-314X, maslennikov@tmc-center.ru

Golovko, Il'ya V., student of the Computer Software Department, Platov South-Russian State Polytechnic University (NPI) (132, ul. Prosveshcheniya, Novocherkassk, Rostov Region, 346428, RF), ORCID: https://orcid.org/0000-0003-1426-9281, ilya.golowko2017@yandex.ru

Claimed contributorship

A. A. Korotky: basic concept formulation; the text revision. D. A. Yakovleva: text preparation; analysis of the research results; formulation of conclusions; A. A. Maslennikov: research objectives and tasks; correction of the conclusions; the text revision. description of the programmable simulator. I. V. Golovko description of the programmable simulator.

All authors have read and approved the final manuscript.

INFORMATION TECHNOLOGY, COMPUTER SCIENCE, AND MANAGEMENT

UDC 007:631.4 https://doi.org/10.23947/2687-1653-2020-20-3-317-324

Information system for assessing maturity level of an organization

I. N. Nurutdinova[1], L. A. Dimitrova[2]
Don State Technical University (Rostov-on-Don, Russian Federation)

Introduction. The paper considers problems of creating information support for solving the task of assessing the maturity level of an organization. It is proposed to use intelligent information systems, i.e. expert systems. Substantive aspects of various stages of creating such systems are briefly described; the expert system architecture, which is based on using a fuzzy expert knowledge base, is given. The work objective was to create new software to solve the problem of assessing the maturity level of an organization.

Materials and Methods. Previously performed modeling of the subject domain under consideration allowed us to create a knowledge base in the form of production memory, which is the basis of the fuzzy inference mechanism. The software is written in PHP and is suitable for embedding in complex web applications. The software system is a web application written primarily in PHP and JavaScript. The software works in all modern web browsers, which accelerates significantly the implementation and deployment based on both the parent-enterprise and its subsidiaries.

Results. New software has been created to automate the processing of questionnaires during the organization's self-assessment based on key indicators, as well as considering 6 main groups of the quality management system indicators. Application of the program will significantly speed up the process of input and processing of expert information required for self-assessment. The program provides organizations to get an adequate idea of the opportunities and prospects for improving the organization's quality management system. Some fragments of the software system interface are given.

Discussion and Conclusions. The proposed software can be used to determine the level of maturity of an organization. The application of Web-technologies improves usability, reduces software support costs. The software can be deployed in the existing network infrastructure of the customer; and the customer can use all the functionality through connecting to a remote server. The software is optimized for various screen resolutions, which allows you to use it not only at the central office, but also when analyzing the quality management system of corporate customers. The traffic generated by the web application is optimized for working with mobile devices with a low-speed Internet connection. Application of the program will significantly reduce the time for users to enter and process expert information required for the problem solving and to eliminate duplication of information.

Keywords: information support, quality management system, level of maturity of an organization, self-assessment, expert systems.

For citation: I. N. Nurutdinova, L. A. Dimitrova. Information system for assessing maturity level of an organization. Advanced Engineering Research, 2020, vol. 20, no. 3, p. 317–324. https://doi.org/10.23947/2687-1653-2020-20-3-317-324

Introduction. Achieving sustained success is an urgent task for every business entity (enterprise, organization, firm, etc.). The sustained success of the organization running presupposes providing its high operating rate and optimal balance. In this case, the interests and needs of all parties related to the enterprise should be taken into account. For example, product quality should meet customer requirements; terms, volumes of supplies and purchases — the contractual obligations with partners and suppliers; financial performance —the expectations of management and owners. The modern rapidly changing economy requires a prompt response to external influences; therefore this aspect of the analysis of activities is of particular importance. The qualitative and quantitative characteristics that affect the functioning of the organization should be balanced, which is the main criterion for providing success. Self-assessment is one of the primary tools for analyzing the functioning of an organization; it provides continuous monitoring of the state of an organization, which is a fundamental way to maintain competitiveness.

In our country, the problem of self-assessment of the organization's activities is studied in sufficient scale for certain areas of practical experience. These are the works by Eh. A. Belokorovin, V. I. Galeev, E. A. Gorbashko, T. Yu. Dvoruk, B. C. Dubinin, T. Kalita, A. I. Kochetov, D. V. Maslov, Yu. I. Mkhitaryan, I. G. Okrepilova, T. A. Salimova, M. Z. Svitkin and others[1]. Various methods and approaches to self-assessment and assessment of the organization's performance in certain industries, as well as its further improvement and increasing competitiveness were considered in foreign publications [1–5].

The urgency of the problem, covering various aspects of the organization self-assessment process based on an approach using a quality management system (QMS), is validated, first of all, by its applied significance, since the organization's maturity levels are closely related to the problem of quality assurance and control[2]. For an adequate assessment of the QMS operation, subject field professionals, experts, are used. However, a major problem accompanying the solution to the problem is the necessity of taking into account a variety of expert information, including qualitative, the subjectivity of expert assessments, as well as an insufficient number of experts. In this regard, to solve these problems, it is advisable to use intelligent decision support systems.

The application of new technology (expert systems) will provide finding the optimal solution to the problem of self-assessment of the organization. Further general automation of the enterprise will be provided through the development of a system that includes a set of hybrid expert systems and, as a consequence, will bring about an increase in the efficiency of the enterprise.

The experts' use of knowledge (heuristics) obtained during the entire period of professional activity in a specialized subject field is a specific feature of expert systems (ES).

When qualitative and quantitative assessments are ambiguous, ES are used for decision-making both in technical problems of decision-making [6] and in management, production, logistics processes [7–11], service quality assessment[3], knowledge quality assessment[4], and other humanitarian fields. To determine the level of maturity of the organization, the authors proposed a general scheme[5]. The scheme assumes using expert assessments and developing an ES [12], whose decision making is based on fuzzy inference [13–15].

The work objective is to create a computer system that automates the self-assessment process, which will significantly increase the efficiency of the decision-maker (DM) in the process of solving this problem and, in particular, in determining the level of maturity of the organization. The use of this computer system provides the

1Maslov DV, Belokorovin EhA. Small business quality management. Moscow, 2011. 192 p. (In Russ).

[2] GOST R ISO 9004-2010. Managing for the sustained success of an organization. A quality management approach. Federal Agency for Technical Regulation and Metrology. Moscow: Standartinform; 2011. 36 p. (In Russ.)

[3] Borisova LV. Features of expert quality control in the service sector. In: Proc. 5th Youth Sci.-Pract. Conf. on Product quality: control, management, enhancement, planning. Kursk. 2014;2:110-113. (In Russ.)

[4] Shumskaya NN. On approach to expert assessment of the knowledge quality. In: Proc. 8th Sci.-Pract. Conf. on State and prospects for the development of agricultural engineering. Rostov-on-Don, 2015. P. 321-324. (In Russ.)

[5]Dimitrova LA. General scheme for assessing the level of maturity of an organization based on fuzzy expert knowledge. In: Proc. Sci.-Method. Conf. on Innovative technologies in science and education "ITNO-2016". Rostov-on-Don, 2016. P. 357–360. (In Russ.)

application of the heuristics of experts, expansion of the boundaries of the solutions and recommendations being developed, and increasing their significance.

Materials and Methods. The practice of developing ES shows that the evolutionary creation method has become dominant in the field of ES. Consider the substantive aspects of the stages and features of the design of the software package (Fig. 1). The essential features of the identification stage include the determination the objectives and tasks of creating an ES; the selection of the type and breadth of the problem statement; defining the assignment of the required resources (time and "computer capacity") and participants in the development process.

Let us list the types of problems that can be solved using ES:

— systematization of the accumulated experience of self-assessment when analyzing the QMS operation;

— using the features of experience in solving problems of expert assessment;

— prompt solution to the problem of assessing the level of maturity of the organization;

— registration of specific moments in the audit of the organization and the dissemination of methods aimed at eliminating their negative impact.

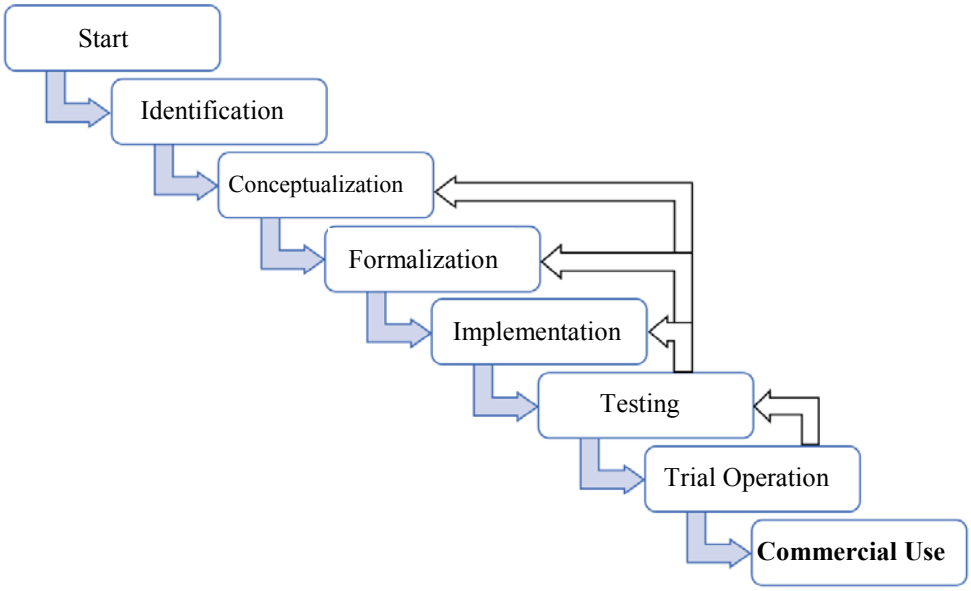

Fig. 1. Stages and content of tasks of expert system development

At the conceptualization stage, there is a delineation of the terms, relationships and management tools required to describe the methodology for the task implementation.

The content of the conceptualization stage includes the selection of concepts, relations and control mechanisms required to describe the solution to the problems under consideration. For example, the terms used to describe the current state of the organization can be defined by the standards: management for the sustainable success of the organization, strategy and policy, resource management, process management, monitoring, measurement, analysis and research, improvement, innovation and training.

At the formalization stage, structures are created for expressing knowledge, basic terms and relationships. The formal expression method in most cases is determined by the ES construction language. To construct a domain model, an approach based on the methodology of fuzzy sets was used [12–14].

The ES implementation and testing include writing a computer program, describing the rules that include knowledge, evaluating the given rules, and, ultimately, obtaining an assessment of the expert system as a whole.

To automate the solution to the self-assessment problem, a software package was created. Fig. 2 shows a block diagram of the software package created on the basis of the knowledge gained about the subject field [12–14].

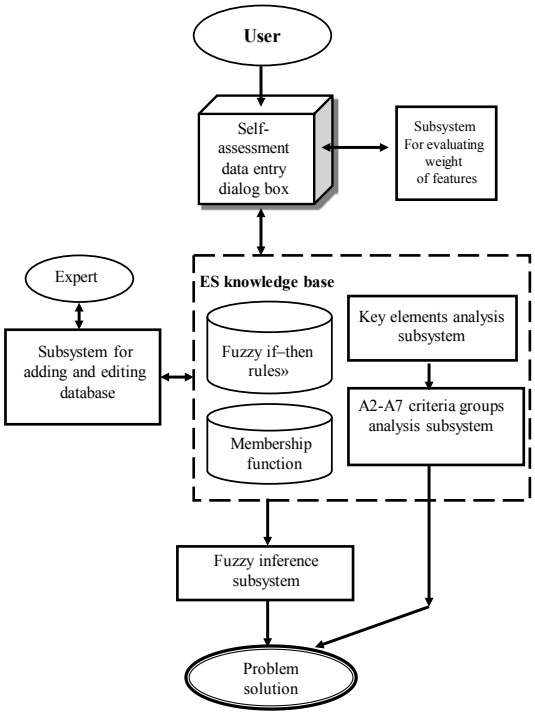

Fig. 2. Block diagram of an expert system

The ES implements the following functions:

— description of the sections of the QMS standards used in solving the problem of assessing the level of maturity of the organization;

— solving the problem of self-assessment based on 9 key criteria (according to GOST R ISO 9 004–2010);

— solution to the problem on the basis of 6 additional criteria [12-14];

— solving problems of determining the weight of the evaluation criteria[6];

— solving problems of formalizing fuzzy expert information;

— explanation of the results obtained;

— assistance to DM in the ES operation.

The set of ES components depends on the characteristic properties of the subject field and the primary requirements put forward during its development.

The mode of the system operation with knowledge plays a special role in the ES. In this mode, the user is provided with the following resources: loading the knowledge selected by the expert into the system; exclusion of the selected knowledge; changing knowledge; reading the knowledge base; conservation of knowledge.

The knowledge correction mode supports the addition of knowledge of the following types: assessment of the weight of factors, number of terms of linguistic variables, parameters of membership functions, production rules.

The ES operates in two modes: knowledge acquisition and problem solving.

The knowledge base is formed through the joint work of a knowledge engineer and a QMS expert.

The interaction of the user (DM) with the ES occurs in the mode of the problem solution. The implementation of the natural language interface with the user is realized through the dialog block for entering information.

The core component of all software products is a user interface designed for an unlimited number of users. Users (experts) can work in the system simultaneously, and their number is unlimited.

For the described ES, three types of dialogs are used: a menu-type dialog; a dialogue of the question-answer type; a dialogue based on screen forms.

Thus, the software package considered is a tool environment that enables the user to solve various problems of assessing the level of maturity of an organization in an interactive mode.

Research Results. The software product is designed as a cross-platform client-server application. All data are stored and processed on the web server; the user interacts with the web server using an Internet browser (all modern Internet browsers are supported: Mozilla Firefox, Google Chrome, Microsoft Edge, Opera, as well as their mobile versions). HTML and JS are used to implement the graphical user interface; the server logic is implemented in PHP. The user can work with the

[6] Nurutdinova IN, Shumskaya NN, Dimitrova LA. On the use of weight coefficients in the formation of expert information. In: Proc. 10th Anniversary Sci.-Pract. Conf. on State and prospects for the development of agricultural engineering. Rostov-on-Don, 2017. P. 332-334. (In Russ.)

client part of the application through a wide range of platforms (PCs, laptops, tablets, smartphones) and operating systems (Windows, MacOS X, Android, iOS).

After authorization (entering a username and password), the user goes to the start page of the application and gains access to the main menu of the system. If a survey is conducted with a specific expert for the first time, it is required to enter his attributes into the database in advance. This can be done by clicking on the link "New user registration" in the main menu of the system. In the event that the expert's data has already been entered into the system, the user can start conducting a survey both on key elements and on an extended list of questions (subsystem "detailed self-assessment, p. A2 – A7").

After the data entry completion, the user can immediately get the results of the assessment both on a simple scale and considering the previously entered weighting factors of the criteria through selecting the appropriate links in the main menu of the program. The result of solving the problem is presented in the text form, graphical, in the form of a RADAR diagram and an animated dashboard divided into sectors corresponding to each of the organizational maturity levels.

The application of this system, based on the knowledge of experienced specialists, will reduce time costs, expand the range of decisions made and improve their validity, and preserve the empirical knowledge gained under solving the self-assessment problem.

Fig. 3 shows the main menu of the system for the automated solution to the problem of assessing the level of maturity of the organization, and Fig. 4 – the user poll screen.

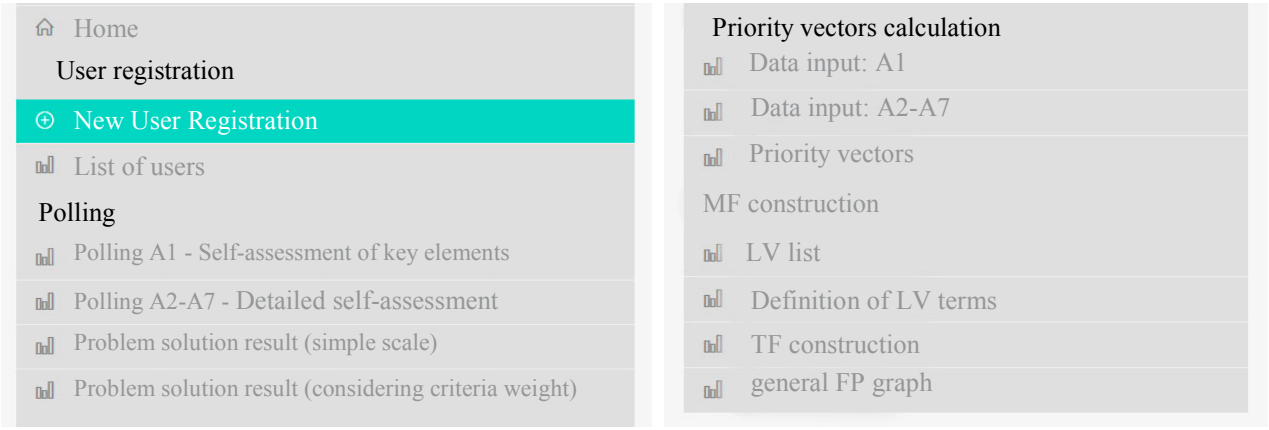

Fig. 3. Main menu of the software package

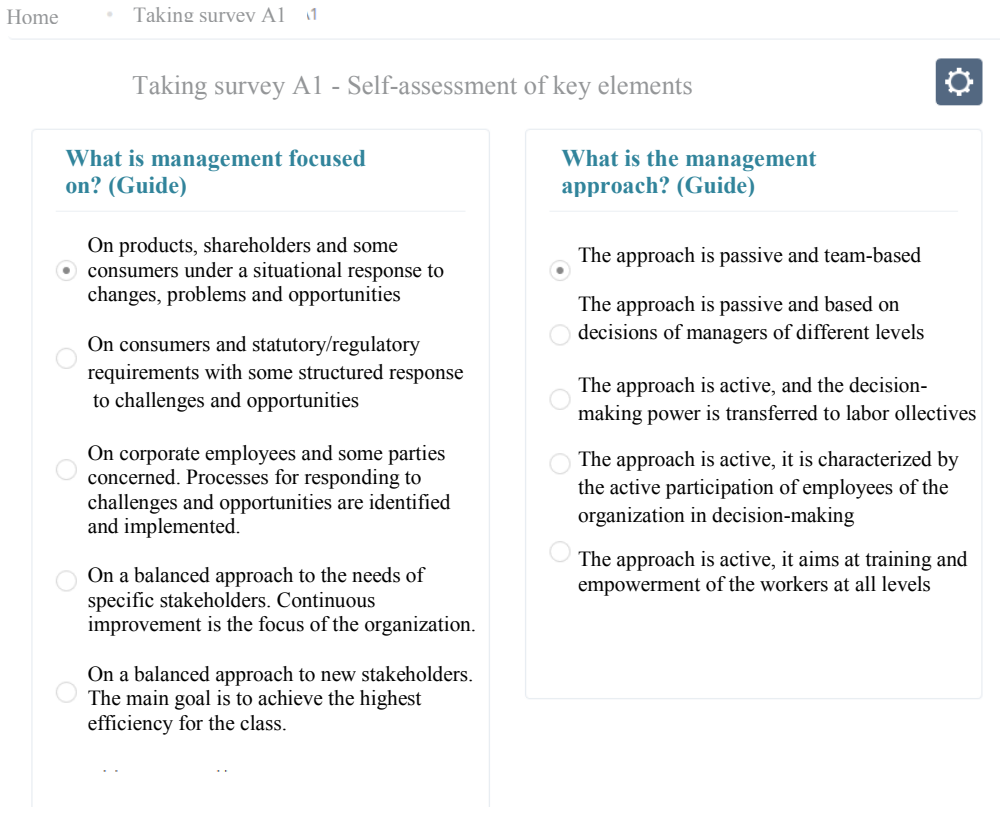

Fig. 4. User poll screen

The analysis of the survey results (based on the knowledge of the subject field entered by an expert) provides the DM with a solution to the problem (Fig. 5 and 6).

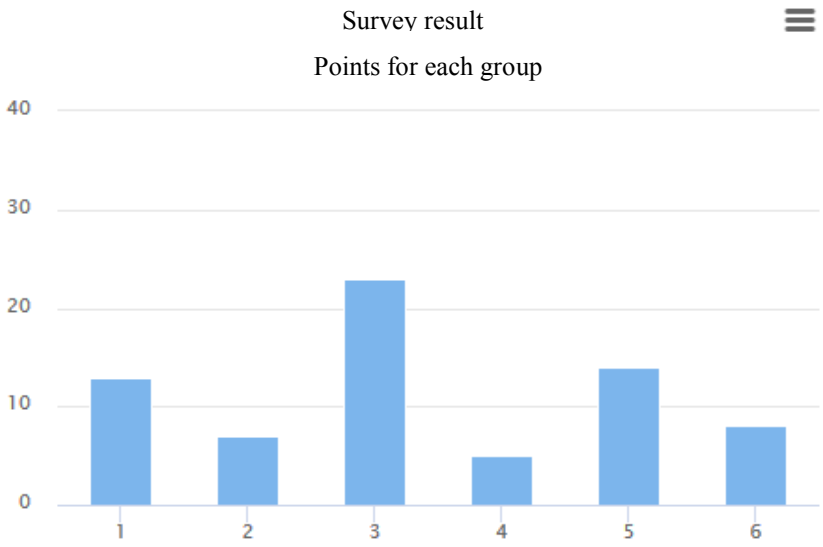

Fig. 5. General view of the user survey chart

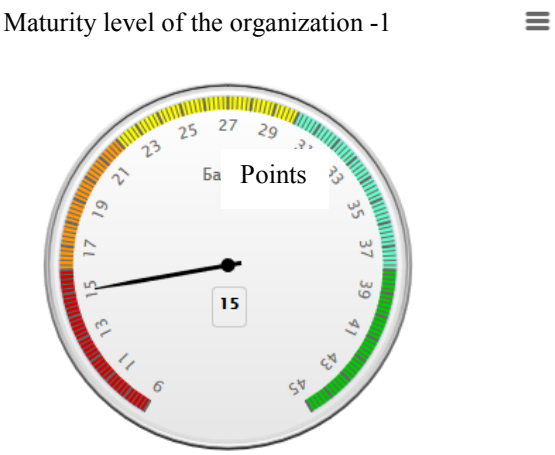

Fig. 6. Chart presentation of assessment results

The solution to the problem of assessing the level of maturity of an organization can be obtained taking into account the weight of both key indicators and the main groups of assessment criteria.

Discussion and Conclusions. The proposed software can be used to determine the level of maturity of an organization. The application of web technologies increases the usability and reduces the cost of software support. The software can be deployed in the existing network infrastructure of the customer; and the customer can use all the functionality through connecting to a remote server. The software is optimized for various screen resolutions, which allows it to be used not only in the central office, but also when analyzing the QMS of corporate customers. The traffic generated by the web application is optimized to work with mobile devices with slow Internet connections. The application of the program will significantly reduce the time for users to enter and process the expert information necessary to solve the problem, eliminate duplication of information.

An ES, which is a tool software environment, has been developed. Within the framework of ES operation, it is permissible to form the desired configurations of ES (knowledge input subsystems), which include various combinations of linguistic variables and all kinds of ways to construct membership functions. This ES is universal,

suitable for use in any business entity; it enables to classify the system by the level of maturity and to determine the potential for improvement.

The practical implementation of the developed algorithms is the creation of software for which certificates of intellectual property have been obtained (No. 2017660792 and No. 2017660791).

References

1. Andersen ES, Svein SA. Project maturity in organizations. International Journal of Project Management. 2003;21(6):457-461. DOI: 10.1016/S0263-7863(02)00088-1

2. Xu D-L, Yang J-B. Intelligent decision system for self-assessment. Journal of multi-criteria decision analysis. 2003;12(1):43-60. DOI: 1002/mcda.343.

3. Xu D-L, McCarthy G, Yang J-B. Intelligent decision system and its application in business innovation self assessment. Decision support system. 2006;42(2):664-673. DOI: 10.1016/j.dss.2005.03.004.

4. Enke J, et al. Systematic learning factory improvement based on maturity level assessment. Procedia Manufacturing. 2018;23:51–56. DOI: 10.1016/j.promfg.2018.03.160.

5. Neverauskas B, Čiutienė R. The theoretical approach to project portfolio maturity management. Economics and Management. 2011;16:845-851.

6. Makarov IM, et al. Iskusstvennyi intellekt i intellektual'nye sistemy upravleniya [Artificial intelligence and intelligent control systems]. Moscow: Nauka; 2006. 333 p. (In Russ.)

7. Hrehova S, Vagaska A. Application of fuzzy principles in evaluating quality of manufacturing process. WSEAS Transactions on Power Systems. 2012;7:50−59.

8. Biryukov AN, Kletskikh DYu. Metod otsenki zrelosti organizatsii s ispol'zovaniem modeli BPMM i ego realizatsiya [Organizational maturity appraisal method and its implementation]. Business Informatics. 2011;3(17):45–52. (In Russ.)

9. Ding J-F. Assessment of Customer Relationship Management for Global Shipping Carrier-based Logistics Service Providers in Taiwan: An Empirical Study. WSEAS Transactions on Systems. 2012;1(6):198-208.

10. Eremina EA, Vedernikov DN. Informatsionnaya sistema vybora postavshchika na osnove metoda nechetkogo logicheskogo vyvoda [Information system of the choice of the supplier on the basis of the method of the indistinct logical conclusion]. Modern Problems of Science and Education. 2013;3. URL: http://science-education.ru/ru/article/view?id=9317 (accessed 05.03.2020). (In Russ.)

11. Wang G, et al. Modelling and Analyzing Trust Conformity in E-Commerce Based on Fuzzy Logic. WSEAS Transactions on Systems. 2015;14:1−10.

12. Borisova LA, Dimitrova LA, Nurutdinova IN. Informatsionnaya podderzhka monitoringa sostoyaniya organizatsii [Information support for monitoring of the organization state]. Vestnik of DSTU. 2016;4:126–133. DOI: 10.12737/22154 (In Russ.)

13. Borisova LA, Dimitrova LA, Nurutdinova IN. Metodika otsenki urovnya zrelosti organizatsii na osnove nechetkogo modelirovaniya [Methods of evaluating maturity level of the organization based on fuzzy modeling]. Vestnik of DSTU. 2017;17(1):113–121. DOI: 10.23947/1992-5980-2017-17-1-113-121 (In Russ.)

14. Nurutdinova I, Dimitrova L. Intelligent System for Assessing Organization's Possibilities to Achieve Sustained Success. Advances in Intelligent Systems and Computing. 2019;875:379−388.

Submitted 30.04.2020

Scheduled in the issue 15.06.2020

About the Authors:

Nurutdinova, Inna N., associate professor of the Applied Mathematics Department, Don State Technical University (1, Gagarin sq., Rostov-on-Don, 344003, RF), Cand.Sci. (Phys.-Math.), associate professor, ORCID: http://orcid.org/0000-0002-3375-1295, nurut.inna@yandex.ru

Dimitrova, Lyubov' A., teaching assistant of the Quality Management Department, Don State Technical University (1, Gagarin sq., Rostov-on-Don, 344003, RF), ORCID: http://orcid.org/0000-0002-5196-5975, kaf-qm@donstu.ru

Claimed contributorship

I. N. Nurutdinova: research objectives and tasks setting; the text revision; correction of the conclusions. L. A. Dimitrova: development of the software system structure; computational analysis; software design; text preparation; formulation of conclusions.

All authors have read and approved the final manuscript.

INFORMATION TECHNOLOGY, COMPUTER SCIENCE, AND MANAGEMENT

UDC 004.852 https://doi.org/10.23947/2687-1653-2020-20-3-325-331

Overview of fuzzy vehicle routing problems

Yu. O. Chernyshev[1], V. N. Kubil[2], A. V. Trebukhin[1]

[1]Don State Technical University (Rostov-on-Don, Russian Federation

[2] Platov South-Russian State Polytechnic University (Novocherkassk, Russian Federation)

Introduction. Various algorithms for solving fuzzy vehicle routing problems are considered. The work objective was to study modern methods for the optimal solution to fuzzy, random and rough vehicle routing problems.

Materials and Methods. The paper reviews fuzzy vehicle routing problems, existing methods and approaches to their solution. The most effective features of some approaches to solving fuzzy vehicle routing problems considering their specificity, are highlighted.

Results. The Fuzzy Vehicle Routing Problem (FVRP) occurs whenever the routing data is vague, unclear, or ambiguous. In many cases, these fuzzy elements can better reflect reality. However, it is very difficult to use Vehicle Routing Problem (VRP) solving algorithms to solve FVRP since several fundamental properties of deterministic problems are no longer fulfilled in FVRP. Therefore, it is required to introduce new models and algorithms of fuzzy programming to solve such problems. Thus, the use of methods of the theory of fuzzy sets will provide successful simulation of the problems containing elements of uncertainty and subjectivity.

Discussion and conclusions. As a result of reviewing various methods and approaches to solving vehicle routing problems, it is concluded that the development and study of new solutions come into sharp focus of researchers nowadays, but the degree of elaboration of various options varies. Methods for the optimal solution of FVRP are limited, in general, to some single fuzzy variable. There is a very limited number of papers that consider a large number of fuzzy variables.

***Keywords**:* fuzzy vehicle routing problem, optimization, fuzzy methods, heuristic algorithms, hybrid algorithms.

For citation: Yu. O. Chernyshev, V. N. Kubil, A. V. Trebukhin. Overview of fuzzy vehicle routing problems. Advanced Engineering Research, 2020, vol. 20, no. 3, p. 325−331. https://doi.org/10.23947/2687-1653-2020-20-3-325-331

Funding information: the research is done with the financial support from RFFI (grants nos. 18-01-00314, 19-01-00357).

Introduction. The objective of the Vehicle Routing Problem (VRP) is to determine the optimal routes for a vehicle fleet representing an ordered sequence of passing through the loading and unloading points, satisfying some constraints. The restrictions include the demand for goods, the carrying capacity of the vehicle, the maximum time and time windows. Optimality can be assessed in different ways. The most common minimization criteria include total distance, transportation cost, size of the involved vehicle fleet. Since it was first proposed by Dantzig and Ramser in 1959 [1], VRP has attracted widespread attention of experts, academicians and managers in various fields and has

become a subject of study in the field of operations research and optimization of logistics systems. A significant number of successful studies have been conducted.

Initially, most traditional VRP research assumed that all information is deterministic, including customer demand, vehicle fleet characteristics, road conditions, and other data needed to build routes. That is, traditional research has focused on deterministic VRP. However, in a real logistics system, it is difficult to describe VRP information as deterministic due to such factors as weather effects, road conditions, vehicle speed, individual customer needs, as well as the cognitive characteristics of decision makers. Any uncertainty in such problems concentrates on demand, time, etc., and allows them to be classified as nondeterministic VRP. Compared to deterministic, nondeterministic VRPs reflect changes in time and demand, the impact of vehicle routing assignments in real time, which brings them closer to the actual production and logistics processes. The proposed algorithms and conclusions, which are valid for deterministic problems, were usually not applied to nondeterministic ones. Moreover, due to the features described above, the mathematical description of nondeterministic problems is more complicated, and the complexity of finding possible solutions also increases. Therefore, nondeterministic VRPs attract more and more attention and become one of the topical centers of modern VRP research [2].

Definition and classification of nondeterministic vehicle routing problems. Nondeterministic VRP are those in which the planner does not have complete information on the vehicle route until the start of the specified route. That is, some information may be vague, ambiguous, or even unknown. After the initial construction of the vehicle route, the destination of the vehicle route and the task can be changed [3]. Obviously, nondeterministic VRP in this regard is more general than deterministic.

In the related studies, uncertainty includes three main forms: randomness, fuzziness and inaccuracy (roughness) [2]. In some systems, the above uncertainties can coexist. Currently, VRP ambiguity is mainly caused by randomness and fuzziness, and can use fuzzy randomness or random fuzziness to describe the coexistence of randomness and fuzziness in VRP.

With the emergence of numerous generalizations and extensions of VRP, scientists began to consider them under different aspects and classify them according to different standards [4]. Based on the classification of Erbao [5] and the distinguished forms of uncertainty of problems, it is possible to divide nondeterministic VRP into singlet and double ones [6].

Singlet nondeterministic VRP include:

— Stochastic VRP (SVRP) — random vehicle routing problem;

— Fuzzy VRP (FVRP) — fuzzy routing problem;

— Rough VRP — rough vehicle routing problem.

Double nondeterministic VRPs include various pairwise combinations of singlet ones:

— Fuzzyrandom VRP (FRVRP) — fuzzy random vehicle routing problem;

— Randomfuzzy VRP (RFVRP) — random fuzzy vehicle routing problem;

— Fuzzyrough VRP — fuzzy-rough vehicle routing problem;

— Roughfuzzy VRP — rough-fuzzy vehicle routing problem;

— Randomrough VRP — random-rough vehicle routing problem;

— Roughrandom VRP — rough-random vehicle routing problem;

— Dualfuzzy VRP — dual fuzzy vehicle routing problem;

— Dualrandom VRP — double random vehicle routing problem;

— Dualrough VRP — dual rough vehicle routing problem

Random SVRP problems differ from deterministic VRP in that some of the initial data of the problem are not fully defined before the vehicle starts to execute a given route. The planner can derive statistical patterns for this data

based on previous observations or market analysis. That is, some parameters in SVRP are random, mainly such as customer demand, customer service time (time windows), customer distribution, available vehicles, service time, travel time, etc. Gendreau and Laporte [7] provided a good overview of the major variants of SVRP. Currently, research into major SVRP focuses on random demand, random travel time, random customers, and similar problems.

In fuzzy FVRP problems, as in random SVRP problems, there is uncertainty about some of the problem data. However, if randomness presupposes the existence of some well-known statistical regularities that can be used, then fuzziness excludes such regularities. This review is focused specifically on fuzzy vehicle routing problems that are currently of great interest for research.

Research results. Fuzzy vehicle routing problems. The fuzzy vehicle routing problem (FVRP) occurs whenever the routing data is vague, unclear, or ambiguous. For example, when, based on experience, the travel time of a vehicle can be described as “about half an hour”, “between 15 and 20 minutes” and so on. In many cases, such fuzzy elements can better reflect reality. In practice, it can be difficult to obtain accurate values for requests, travel time, number and location of customers, time window boundaries, and other quantities if they obey probabilistic laws. In some new systems, it is also difficult to describe parameters of the problem as random variables due to insufficient data for analyzing the distribution. However, it is very difficult to use deterministic VRP solution algorithms to solve FVRP because several fundamental properties of deterministic problems are no longer fulfilled in FVRP. Therefore, to solve such problems, it is required to introduce new models and algorithms of fuzzy programming. Thus, the use of methods of the theory of fuzzy sets will make it possible to successfully model problems containing elements of uncertainty and subjectivity.

The solution scheme is as follows: first, the information should be made fuzzy, then the idea of fuzzy reasoning to build certain fuzzy criteria and convert the fuzzy variables to their crisp equivalents using defuzzification, is used. Currently, FVRP research is mainly focused on fuzzy demand, fuzzy time windows, fuzzy travel time and fuzzy service time.

VRP with fuzzy demands (VRPFD) is the task of vehicle routing with fuzzy customer demand for goods. VRPFD assumes that the customers who need the service are identified, but their exact demand is uncertain and no statistical rule for their demand can be obtained. There is no doubt that VRPFD is the most investigated area of FVRP. Presumably, the earliest description of VRPFD was proposed by Teodorovich in 1996 [8]. Teodorovich studied VRPFD with one depot, developed fuzzy decision rules based on propensity assessment, proposed the first phase of the solution based on a heuristic sweep algorithm; then, based on the generated solution, he gradually improved it through optimizing routes. Since then, several scientists have used various heuristics to solve YRPFD with some success. Based on fuzzy possibility [3, 9–13], binary approaches [14] and fuzzy confidence [15], they applied an improved heuristic algorithm or a hybrid heuristic algorithm to solve VRPFD. The most widely used algorithm is the modified hybrid genetic algorithm [9–11]. In addition, other algorithms were applied to solve this kind of problems [3, 12–14, 15], such as modified ant colony algorithm, hybrid differential evolutionary algorithm, and improved particle swarm optimization.

VRP with fuzzy time windows (VRPFTW) is a vehicle routing task with fuzzy time windows. VRPFTW is analogous to the |soft-window vehicle routing problem. In it, violation of time windows does not necessarily entail penalties, but there is some uncertainty about long-term consequences for the service quality. For this, either the arrival time or the upper and lower boundaries of time windows is usually considered fuzzy. Wang [16] first applied such a fuzzy theory to the example of a traveling salesman problem — road inspection (Chinese postman) with time windows. Tang and others [17] proposed a VRPFTW mathematical model and a method for its solution in two stages: reduction to traditional VRP with time windows and its solution, and then, solving the problem of improving service based on the

Gomory algorithm and the subgradient optimization method. For a complex VRPFTW with multiple depots and a heterogeneous fleet, a multi-stage heuristic was proposed [18]: customer clustering, routing, vehicle type determination, route planning and improvement using simulated annealing and customer service improvement. Good results were also shown by the particle swarm optimization method [19] and the modified wolf pack algorithm [20].

VRP with fuzzy duetime (VRPFDT) is vehicle routing problem with fuzzy visit time. VRPFDT differs in that time windows are replaced by fuzzy dates. This is due to the fact that time windows in deterministic VRP cannot reflect client preferences in real time. For example, customers may want to receive a service at certain points in time; their satisfaction may be reduced if the service is offered ahead or behind time. Hence, there is fuzzy time to visit. In 1995, Cheng and others [21] first proposed the concept of VRPFDT and built a VRP model under the conditions of single export or single delivery, proposed an improved hybrid genetic algorithm for solving such a VRP model using push-bump-throw procedures. Thereafter, Teodorovich [22] investigated a fuzzy dynamic problem of constructing routes between the corresponding points of export and delivery (Dial-A-RideProblem) and additionally analyzed VRP with fuzzy visit time and fuzzy travel time. Besides, other methods, such as heuristic insertion algorithm, modified ant colony algorithm, genetic algorithm, etc., play an important role in solving VRPFDT [23, 24].

VRP withfuzzytraveltime (VRPFT) is a vehicle routing problem with fuzzy travel time. In VRPFT, the travel time of a vehicle when it is assigned a route is fuzzy, while other parameters are specified and deterministic. Research on VRPFT is currently scarce and includes only a few publications. Teodorovic first introduced fuzzy theory in VRPFT in 1991 [25] suggesting that travel times between locations are fuzzy variables. He built a VRPFT model and proposed Clarke-Wright algorithm to solve it. Based on fuzzy possibility and reliability, Chen [26] and Zheng [27] studied VRPFT with time windows and proposed an imperialist competitive algorithm and a hybrid genetic algorithm. Jia [28] used a genetic algorithm to solve VRPFT based on the I_L. measurement method. Brito [29] and Zhang [30] developed a hybrid genetic algorithm for solving VRPFT based on fuzzy logic.

VRP withfuzzyservicetime (VRPFST) is a vehicle routing problem with fuzzy service time. VRPFST occurs in companies that do not have accurate information on the service time required for each incoming order. However, decisions made should take into account the estimated service time and available resources, including working hours and the number of vehicles available. For a dynamic version of this problem, Kuo and others [31] applied successfully a fuzzy ant colony algorithm with a built-in cluster insert procedure.

In addition, some literature sources investigated VRP with fuzzy cost coefficients [32], VRP with fuzzy time windows [33], VRP with simultaneously fuzzy travel time and visit time [22, 34], and VRP with fuzzy travel time and visit time [35], etc.

In recent years, due to the concern of the world community with environmental problems, the direction of green transportation logistics is gaining popularity [36], within which a green vehicle routing problem – G-VRP [37] arose. It is aimed at finding a balance between economic benefits and environmental impact. For a fuzzy version of this problem, a hybrid genetic algorithm combined with fuzzy modeling was recently proposed [38].

Discussion and Conclusions. Based on the material presented in the review, it can be concluded that the study of fuzzy vehicle routing problems is attracting more and more attention, but the degree of development of its individual options varies. It should be noted that to date, FVRP research is mostly limited to one fuzzy variable, such as fuzzy demand or fuzzy customer visit times. There are comparatively few studies that comprehensively consider a larger number of fuzzy variables [22, 34, 35]. Another problem is that the role of the distributor experience in FVRP is rarely considered, which makes practical applicability negligible. To bridge the gap between theoretical research and practical application, it is required to enhance integrated research. It also leaves open issues on combining these studies with

some new technologies such as e-commerce, the Internet of Things and big data. In addition, a system for evaluating the algorithms for solving FVRP has not yet been developed.

References

1. Dantzig GB, Ramser JH. The Truck Dispatching Problem. Management science. 1959;6(1):80-91.

2. Liu B, Zhao R, Wang G. Uncertain programming with applications. Beijing: Chinese Tsinghua University Press; 2003. P. 43–52.

3. Erbao C, Mingyong L. The Open Vehicle Routing Problem with Fuzzy Demands. Expert Systems with Applications. 2010;37(3):2405–2411.

4. Kubil VN. Obzor obobshchenii i rasshirenii zadachi marshrutizatsii transporta [Review of the vehicle routing problem generalizations and extensions]. Vestnik RGUPS. 2018;2:97–109. (In Russ.)

5. Erbao C. Research on Vehicle Routing Problems Models and Algorithms of Logistics Distribution, Ph.D. thesis. China: Hunan University; 2008. P. 89–92

6. Chen D, Chen D, Yang Y. Nondeterministic Vehicle Routing Problem: A Review. Advances in Information Sciences and Service Sciences. 2013;5(9):485–493.

7. Gendreau M, Laporte G, Séguin R. Stochastic vehicle routing. European Journal of Operational Research. 1996;88(1):3–12.

8. Teodorović D, Pavković G. The fuzzy set theory approach to the vehicle routing problem when demand at nodes is uncertain. Fuzzy sets and systems. 1996;82(3):307–317.

9. Zhang J, Li J. A hybrid genetic algorithm to fuzzy vehicle routing problem. Journal of Industrial Engineering. 2005;19(2):23-26. DOI: 10.1109/FSKD.2014.6980823

10. Xu J, Goncalves G, Hsu T. Genetic algorithm for the vehicle routing problem with time windows and fuzzy demand. In: IEEE Congress on Evolutionary Computation; 2008. P. 4125–4129. DOI: 10.1109/CEC.2008.4631360

11. Ye X, Xu J. A fuzzy vehicle routing assignment model with connection network based on priority-based genetic algorithm. World Journal of Modelling and Simulation. 2008;4(4):257–268.

12. Peng Y, Qian Y. A particle swarm optimization to vehicle routing problem with fuzzy demands. Journal of Convergence Information Technology. 2010;5(6):112–119.

13. Tian J, Ma WZ, Wang YL, et al. Emergency supplies distributing and vehicle routes programming based on particle swarm optimization. Systems Engineering Theory & Practice. 2002;30(5):898–906.

14. Chen B, Song S, Chen X. Vehicle routing problem with fuzzy demands and its heuristic ant colony algorithm. Journal of Computer Applications. 2006;11:25–35.

15. Erbao C, Mingyong L. A hybrid differential evolution algorithm to vehicle routing problem with fuzzy demands. Journal of computational and applied mathematics. 2009;231(1):302–310.

16. Wang HF, Wen YP. Time-constrained Chinese postman problems. Comput. Math. Appl. 2002;44:375–387.

17. Tang J, Pan Z, Fung RY, et al. Vehicle routing problem with fuzzy time windows. Fuzzy sets and systems. 2009;160(5):683–695.

18. Adelzadeh M, Asl VM, Koosha M. A mathematical model and a solving procedure for multi-depot vehicle routing problem with fuzzy time window and heterogeneous vehicle. The International Journal of Advanced Manufacturing Technology. 2014;75(5-8):793–802.

19. Yan F, Wang Y. Modeling and solving the vehicle routing problem with multiple fuzzy time windows. In: Int. Conf. on Management Science and Engineering Management. Springer, Cham; 2017. P. 847–857.

20. Cao QK, Yang KW, Ren XY. Vehicle routing optimization with multiple fuzzy time windows based on improved wolf pack algorithm. Advances in Production Engineering & Management. 2017;12(4):401–411. DOI: 10.14743/apem2017.4.267

21. Cheng R, Gen M, Tozawa T. Vehicle routing problem with fuzzy due-time using genetic algorithms. Journal of Japan Society for Fuzzy Theory and Systems. 1995;7(5):1050–1061.

22. Teodorovic D, Radivojevic G. A fuzzy logic approach to dynamic dial-a-ride problem. Fuzzy sets and systems. 2000;116(1):23–33.

23. Zhang J, Li J, Guo Y. Insertion heuristic algorithm for dynamic vehicle routing problem with fuzzy due-time. Journal of Southwest Jiaotong University. 2008;43(1):107–113.

24. Gendreau M, Potvin JY, Bräumlaysy O, et al. Metaheuristics for the vehicle routing problem and its extensions: A Categorized Bibliography. In: The Vehicle Routing Problem: Latest Advances and New Challenges. Springer US. 2008;43:143–169.

25. Teodorovic D, Kikuchi S. Application of fuzzy sets theory to the saving based vehicle routing algorithm. Civil Engineering Systems. 1991;8(2):87–93.

26. Chen J, Zhang Y, Wang G. A new algorithm for a fuzzy vehicle routing and scheduling problem: imperialist competitive algorithm. JCIT: Journal of Convergence Information Technology. 2011;6(7):303–311.

27. Zheng Y, Liu B. Fuzzy vehicle routing model with credibility measure and its hybrid intelligent algorithm. Applied Mathematics and Computation. 2006;176(2):673–683.

28. Jia J, Liu N, Wang R. Genetic algorithm for fuzzy logistics distribution vehicle routing problem. In: IEEE International Conference on Service Operations and Logistics, and Informatics. 2008;1:1427–1432.

29. Brito J, Martinez FJ, Moreno JA, et al. Fuzzy approach for vehicle routing problems with fuzzy travel time. In: IEEE International Conference on Fuzzy Systems; 2010. P. 1–8.

30. Zhang J, Li J. A hybrid genetic algorithm to the vehicle routing problem with fuzzy cost coefficients. In: IEEE 11th Int. Conf. on Fuzzy Systems and Knowledge Discovery (FSKD). 2014. P. 147–152.

31. Kuo RJ, Wibowo BS, Zulvia FE. Application of a fuzzy ant colony system to solve the dynamic vehicle routing problem with uncertain service time. Applied Mathematical Modelling. 2016;40(23-24):9990–10001.

32. Zhang J, Li J, Guo Y. Modified Clark-Wright Algorithm for Vehicle Scheduling Problem with Fuzzy Cost Coefficients. Journal of Southwest Jiaotong University. 2008;39(6):281–284.

33. Tang J, Pan Z, Fung RY, et al. Vehicle routing problem with fuzzy time windows. Fuzzy Sets and Systems. 2009;160(5):683–695.

34. Lu L, Tan Q. Study Dynamic vehicle scheduling problem model under fuzzy information. Chinese Journal of Management Science. 2006;z1:156–160.

35. Jiang Z, Sheng Y, Wang D, et al. Research on Bi-objective fuzzy programming model and algorithm of logistics distribution vehicle routing problem. Chinese Journal of Enterprise Operation Research. 2008;1:19–27.

36. Abramova IO, Murtazina MSh. Zelenaya transportnaya logistika kak instrument sovershenstvovaniya khozyaistvennoi deyatel'nosti transportnykh kompanii [Green transport logistics as a tool for improving the economic activities of transport companies]. The Eurasian Scientific Journal. 2018;10(3):2–12. (In Russ.)

37. Erdoğan S, Miller-Hooks E. A green vehicle routing problem. Transportation Research Part E: Logistics and Transportation Review. 2012;48(1):100–114.

38. Wang R, Zhou J, Yi X, et al. Solving the green-fuzzy vehicle routing problem using a revised hybrid intelligent algorithm. Journal of Ambient Intelligence and Humanized Computing. 2019;10(1):321–332.

Submitted 16.04.2020
Scheduled in the issue 10.07.2020

About the Authors:

Chernyshev, Yurii O., professor of the Production Automation Department, Don State Technical University (1, Gagarin sq., Rostov-on-Don, 344003, RF), Dr.Sci. (Eng.), professor, ORCID: https://orcid.org/0000-0002-4901-1101, treandrik@yandex.ru

Kubil, Viktor N., teaching assistant of the Computer Software Department, Platov South-Russian State Polytechnic University (NPI) (132, ul. Prosveshcheniya, Novocherkassk, Rostov Region, 346428, RF), ResearcherID: AAB-8676-2020, ORCID: https://orcid.org/0000-0002-4364-4135, treandrik@yandex.ru

Trebukhin, Andrei V., postgraduate of the Production Automation Department, Don State Technical University (1, Gagarin sq., Rostov-on-Don, 344003, RF), ORCID: https://orcid.org/0000-0002-6673-706X, treandrik@yandex.ru

Claimed contributorship

Yu. O. Chernyshev: academic advising; formulation of the basic research concept and the structure of the paper. V. N. Kubil: collection and analysis of literature data; critical analysis. A. V. Trebukhin: literature analysis; participation in research; editing the text of the paper.

All authors have read and approved the final manuscript.

INFORMATION TECHNOLOGY, COMPUTER SCIENCE, AND MANAGEMENT

UDC 004.94 https://doi.org/10.23947/2687-1653-2020-20-3-332-345

Revisiting computer modeling

M. V. Yadrovskaya
Don State Technical University (Rostov-on-Don, Russian Federation)

Introduction. Modeling serves as a methodological basis for modern science and a tool for cognitive activity. It can be considered as a thinking activity mediated and optimized through information models. In this case, logical operations of cognition and simulation techniques are applied to the information.
Materials and Methods. The scientific research results on how knowledge is formed, stored and processed in a person's memory, how they interact with information representations are studied and summarized. Information models used in various subject domains are analyzed. The provisions on rational ways of presenting information under modeling are formulated, and computer tools for constructing such representations are indicated.
Results. Methods and techniques for visualizing information on the object under study are specified. Software tools and services providing visualizations and research modeling procedures are given.
Discussion and Conclusions. The results obtained can be used to optimize modeling procedures. Images, structures, relationships and connections of the object under study are visualized in special programs with the help of the described methods and techniques. They, in turn, mediate the process of mental modeling and broaden the basis for its implementation.

Keywords: modeling, model, information technologies, information model, computer model, information representation, computer simulation techniques, computer modeling environments.

For citation: M. V. Yadrovskaya. Revisiting computer modeling. Advanced Engineering Research, 2020, vol. 20, no. 3, p. 332–345. https://doi.org/10.23947/2687-1653-2020-20-3-332-345

Introduction. Modeling is used for theoretical and practical research of objects, processes, phenomena. It has a general scientific character, is an objective, universal method of cognition and is used to study animate and inanimate nature. Modeling serves as a methodological basis of modern science and a tool for cognitive activity. Development of computing and information technologies contributes to the success of information modeling. This approach involves the application of research procedures to formalized information on the object of study replacing or reproducing the object. An information model is becoming a modern tool for solving various problems using information technologies and a link connecting any subject area with informatics.

Modeling is characterized, on the one hand, by a variety of models used (Fig. 1), on the other, by a variety of means of constructing and studying them.

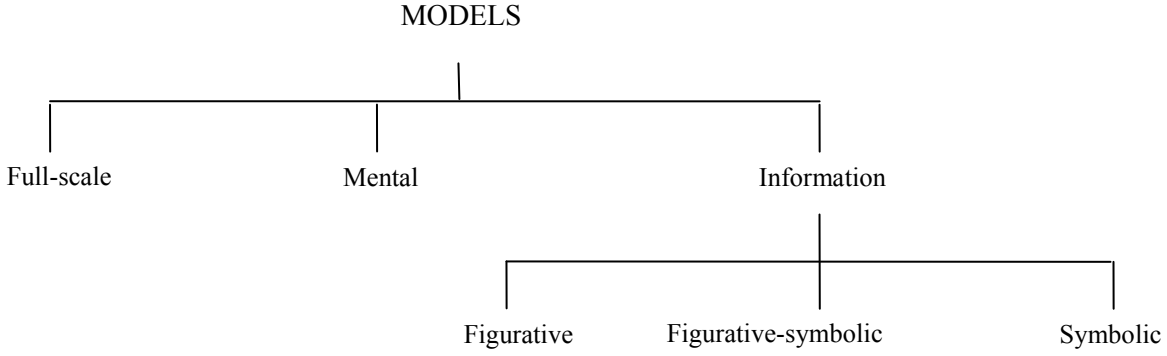

Fig. 1. Classification of models by presentation form

Summarizing many definitions, by the term "information model" [1], we mean information that describes the essential properties of an object and its links; it is formalized from the point of view of the research goal and recorded on storage medium. This definition provides clear identification of the close relationship between informatics and modeling and analyzing information technologies as modern simulation tools. Information can be presented in different forms; therefore, computer sciences [2] study various information models: verbal, graphic, mathematical, tabular, algorithmic, imitation, etc. In the cognitive theory, any model can be considered informational if it is included in the information process of cognition.

Let us consider the stages of information modeling.

The first stage is the analysis of the object and its links, which involves the execution of logical operations of cognition. These are comparison, classification, systematization, generalization, concretization, inference, idealization (construction of abstractions). Such modeling techniques as observation, analysis, synthesis, analogy, hypothesizing, formalization, are used.

The second stage is practical actions. This is actually modeling (building a model) and operations with it (rebuilding, modifying, model implementation, experimenting, interpreting, verifying, replacing). Actions with model elements include subtraction, addition, and complementation [1].

The third stage is the construction of algorithms for the implementation of the model in a specific subject domain, the involvement of information technologies to work with the model.

"These three stages reflect, on the one hand, the major stages of cognition: sensory — rational — activity; on the other hand — the classical triad of information modeling: information — model — algorithm" [3].

A computer model is built on the basis of the information model. Computer simulation is a combination of hardware and software tools and technologies for working with these models. S.A. Beshenkov emphasizes that "it is quite possible to talk about computer modeling as a special type of information modeling" [4]. Information technologies used to work with information models determine the type of the latter (figurative, figurative-symbolic and symbolic). Their classification is shown in Fig. 2.

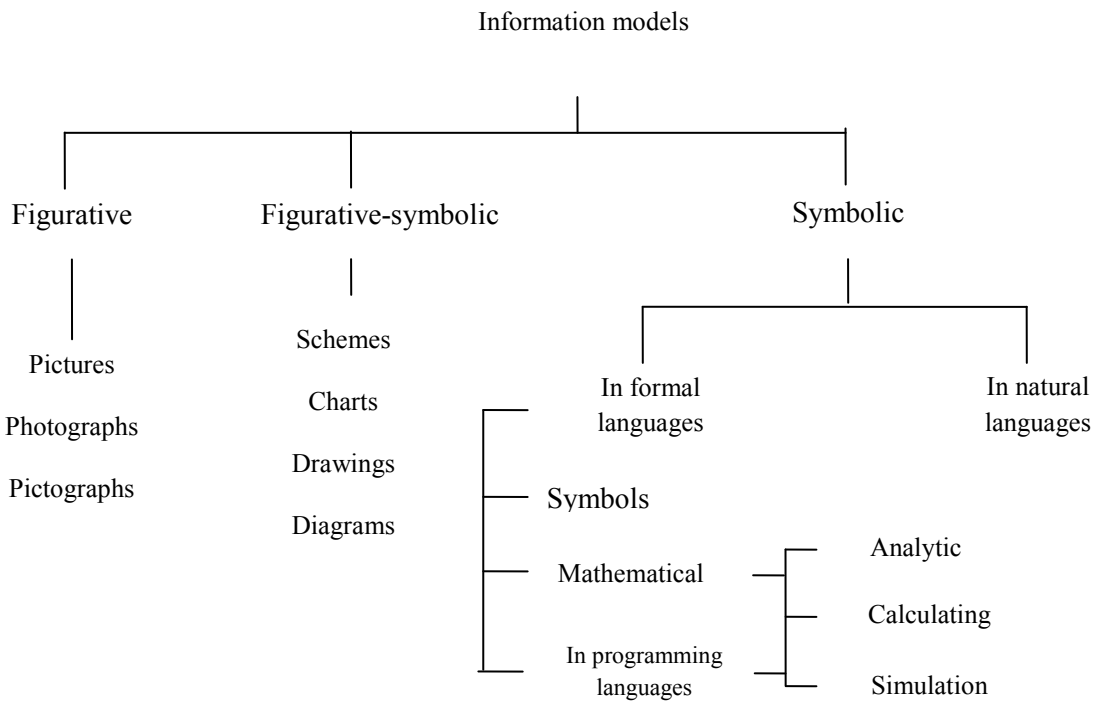

Fig. 2. Classification of information models depending on information technologies

Let us list some computer modeling tools:

— visual — hardware and software tools and technologies for working with computer graphics, video images, animation, sound, virtual reality;

— verbal — text editors and processors, optical character recognition systems, publishing systems, hypertext markup languages;

— mathematical — electronic calculators, software packages for mathematical calculations, programs for analytical transformations, calculation and information systems, virtual laboratories;

— modeling systems — visual modeling packages, simulation systems, programs for generating fractal images, spreadsheets, presentation packages, computer-aided design (CAD), geoinformation systems;

— programming languages and systems [5].

Simulation-related tasks are solved in computer simulation environments [5]. This implies specialization, interconnection of modules and modeling language, and increases the speed of research. For example, CAD is the most important means of building interconnected models within the project of the object being created. The modeling environment consists of several modules that enable to create a figure, a drawing, a 3D model of the future object, and to perform computer experiments on the model determining the possible properties of the object and predicting probable events, in the modeling environment.

According to S.I. Arkhangel'skii, modeling as a form of study provides the most clearly expressed connection between experimental data and theoretical views. This allows us to consider the model as a certain sequenced relationship of conceivable (theoretical) and experimental information based on the selection of the studied aspects and features of the object through simplification, or complication, or abstraction [6]. Here, theoretical information is information that represents the object of research, i.e., selected and formalized from the point of view of the study objective. This is the basis of mental and symbol-mediated operation. A researcher receives empirical information in the process of modeling, studying theoretical data, which are the approximate basis of his thinking activity. In other words, in the process of modeling, a chain of mental models is created. Some of them are fixed in symbolic form. Until new knowledge is obtained, logical and modeling operations based on the constructed symbolic representations are performed. When constructing a representation of the object of research, objects of operation for thinking are created; the work of thinking aimed at studying the model is stimulated. At the same time, knowledge on the object is analyzed, refined, changed and deepened.

Materials and Methods. Simulation is a multistage, cyclical procedure. It is impossible to build, study a model of an object and gain knowledge at once. In the process of modeling, it is required to repeatedly apply logical operations of cognition and modeling techniques to information. The task of this study is to highlight the techniques and methods for presenting information that support the execution of logical modeling procedures. It is also necessary to note the computer tools, the use of which activates and rationalizes the process of information modeling. To solve this problem, generalized scientific and pedagogical experience and practical knowledge of modeling are used.

For information models to effectively help to gain knowledge in the modeling process, it is required:

— to know and apply the patterns of handling ideas and knowledge;

— to use computer technologies to form representations.

At the same time, it is important to take into account scientific data on how knowledge is formed, stored and processed in a person's memory, how they interact with representations of information.

There are several hypotheses about the representation of information in memory.

According to the hypothesis of double coding, information can be encoded and stored in one of two or both systems — verbal and figurative. This position is supported by the neurological and behavioral data [7].

According to the conceptual propositional hypothesis, information is stored in an abstract propositional format that defines objects, events, and their relationships.

The radical theory of images assumes that some information is presented only in the form of images [7]. N. I. Kolodina believes that all information perceived by a person is encoded in consciousness simultaneously through sight, hearing, smell, touch, and experienced emotions, and is presented in the consciousness of an individual in the form of units of knowledge called mnemonic units of knowledge (MUK). These units are structured in consciousness according to the channels of perception and are constantly being re-formed, forming more and more new connections among themselves. N. I. Kolodina offers a model of consciousness as a structured set of units of knowledge. The formation of thought formations in this model occurs as a result of the interaction of knowledge units with the surrounding reality. Then MUK are integrated with each other according to the laws of a single logical-thinking base [7].

In the case of activating only one unit located in any zone of the structure, there is a chain activation of other units of knowledge that have stable connections with the activated unit [8]. This hypothesis has something in common with the connectionist description of the work of the speech mechanism. It is based on the research results of information processing by the brain. In this case, the forms of knowledge are represented as a network structure. The network consists of nodes and connections between them (connectionism — from the English “connect”: connection). The effective functioning of the network system provides the distribution of activation [9, 10].

N. I. Zhinkin put forward the hypothesis for the existence of a universal subject code (USC) in the human mind. USC is the language of intelligence, the basic component of thinking. It is the language of schemes, images, imprints of reality (tactile, olfactory), kinetic (motor) impulses, etc. The USC is the language in which the primary recording of personal meaning takes place [9]. USC is a code by which information turns into “primary knowledge”, sets of MUK, which can be compared to representations from cognitive linguistics: representations include

representations proper, images and concepts, as well as associated assessments and connotations. Therefore, on the one hand, representations are mental models; on the other, they are the subjective basis of objective knowledge. Representations are formed in the process of mental modeling of reality. According to G. Frege, as noted by V. V. Krasnykh, a representation is an internal image of an object that arose from memories of sensory impressions [9].

Research Results. Summarizing the above scientific judgments, it is possible to formulate provisions on the ways of representing theoretical information in models and denote the computer tools for such constructions.

Primary knowledge is actually ideas, images, concepts and evaluations. For the formation of ideas, all channels of information are important: visual, auditory, olfactory, gustatory, tactile, and kinesthetic. According to the experimental data, visual coding occurs earlier than acoustic and semantic coding [7]; therefore, under the formation of knowledge, the methods of visual modeling of information are basic and supplemented by others.

Pictures, color, representation of details are of great importance in the following ways of transmitting information: lens and the Fish Eye technique (Adobe Photoshop, Corel Draw, Inkscape, Blender), graphic simplification, maps, colored histograms (Paint, Word, Excel, Corel Draw, Inkscape, etc.), visual dictionary (Word, Excel, HTML, PHP).

a)

b)

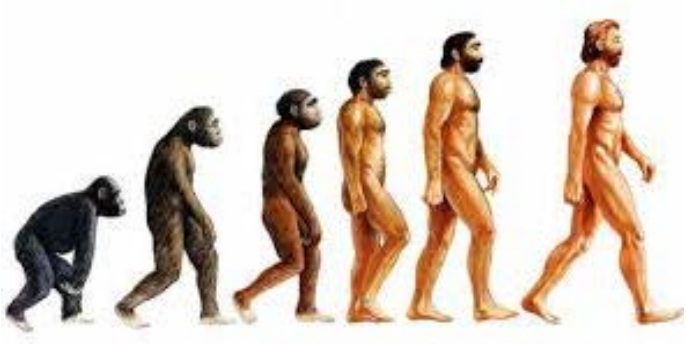

c)

d)

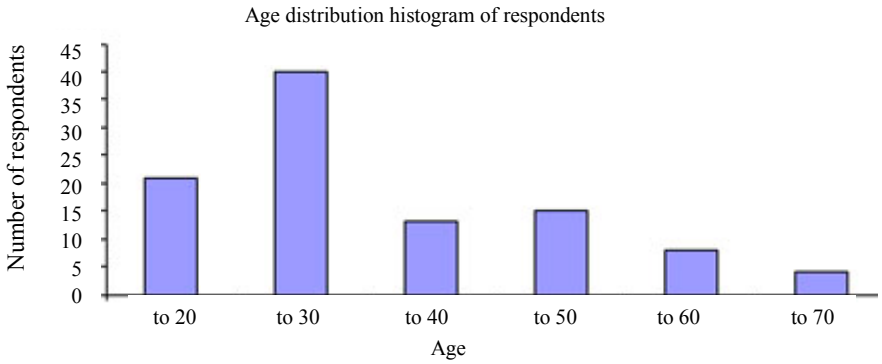

e)

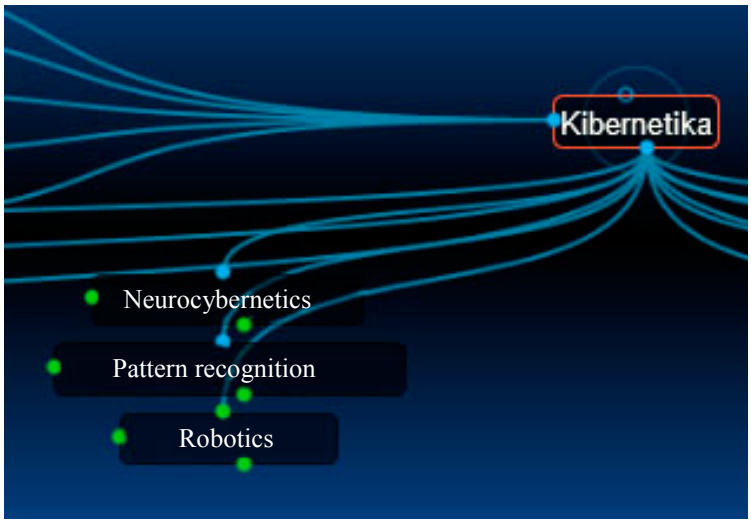

f)

Fig. 3. Examples of information presentation: lens (*a*), Fish Eye (*b*), graphic simplification (*c*, the concept of "evolution" is presented); map (*d*), histogram (*e*), visual dictionary (*f*)

The most important are the verbal and figurative coding systems; therefore, most ways of presenting information include at the same time pictures, signs, words, texts. It can be a cloud of tags, words (Wordle, Tagul, Many Eyes, Word it Out, Togxedo-Creator), mental maps (MindManager, Mindmeister, FreeMind, XMind), maps and cyclic schemes (Corel Draw, Inkscape, Excel, Word, Adobe Flash), etc.

a)

b)

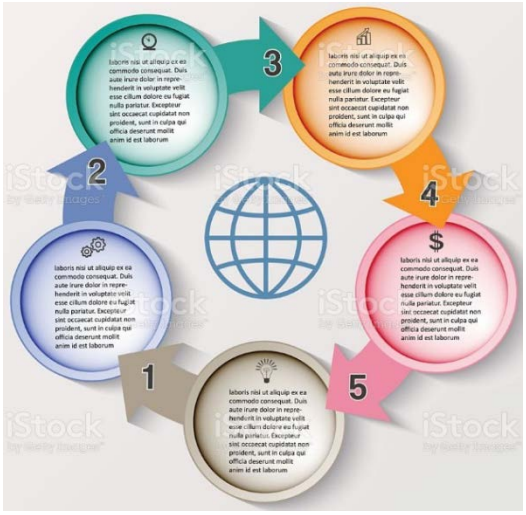

c)

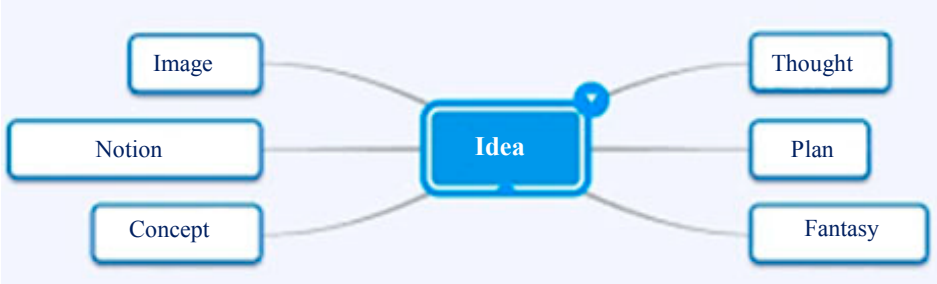

d)

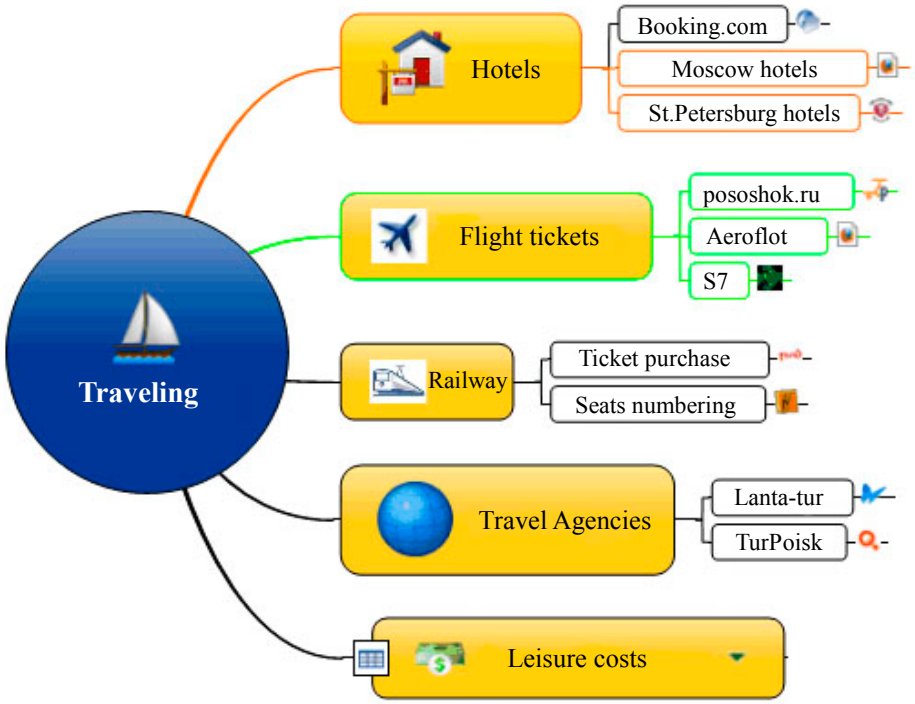

e)

Fig. 4. Examples of information presentation:
clouds of words and tags (*a, b*); cyclic scheme (*c*); mental maps (*d, e*)

Knowledge storage involves fixing data about objects, events and their relationships. The following ways of presenting data correspond to this format: timelines (Dipity, ClassTools, Timerime), causal chains (Paint, Word, Corel

Draw, Inkscape), inductive towers (Bubbl.us, Cacoo.com services), Gantt affinity diagrams (SchedRoll, Gantt Designer, Mindjet JCV Gantt Pro, Microsoft Project, Excel), Ishikawa, Venn (Corel Draw, Inkscape, Excel, Word), etc.

a)

b)

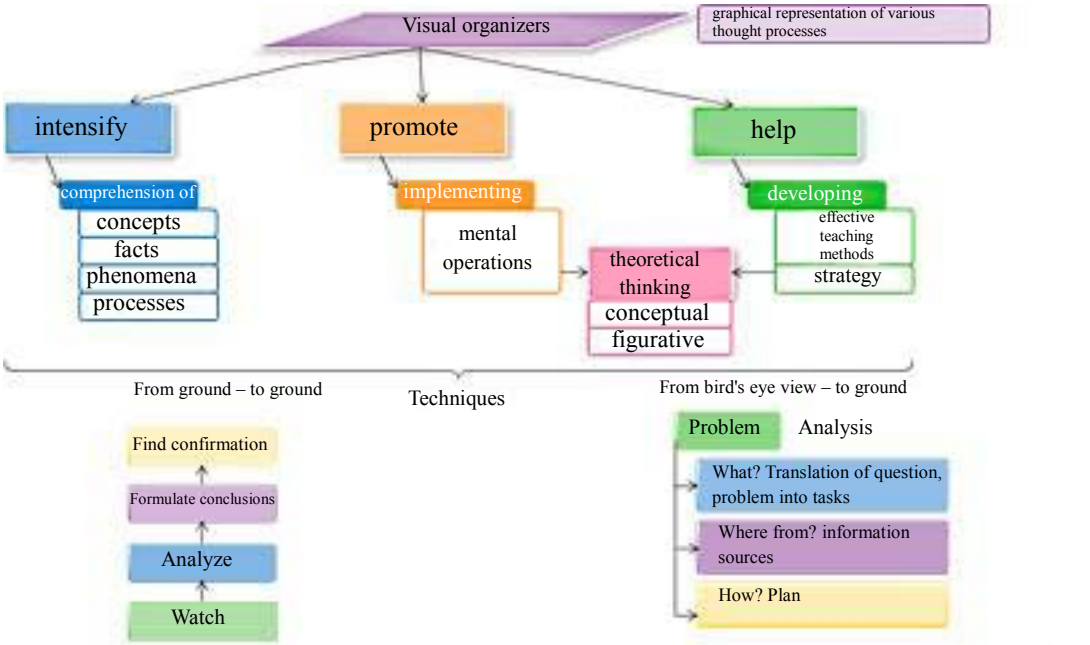

Facts - conclusions (prediction of result)
Specific – General
Scattered observations - common patterns

Application of rules, facts, experience. Comprehension of concepts, processes, rules, procedures
Problem - solution
Hypothesis - testing - confirmation/refutation

c)

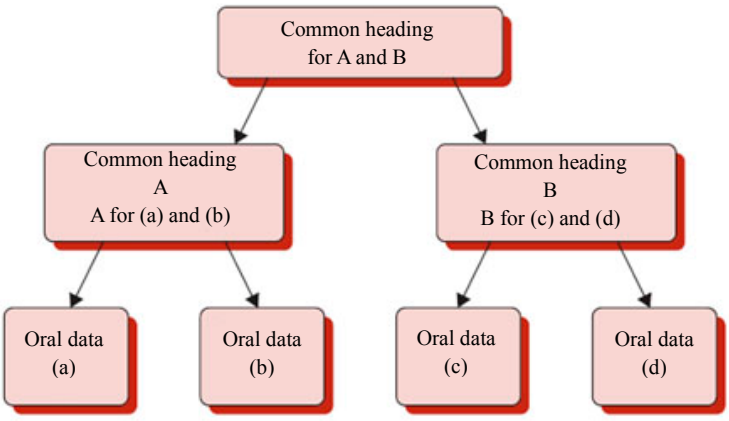

d)

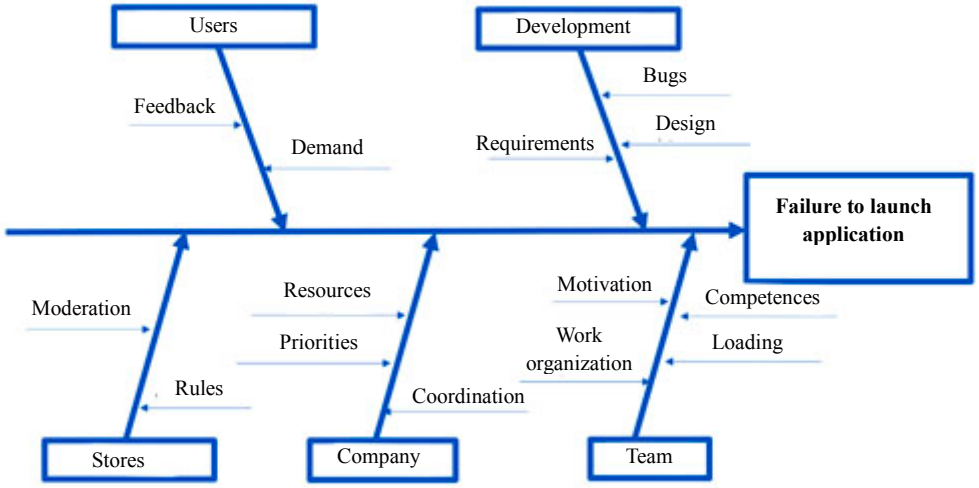

e)

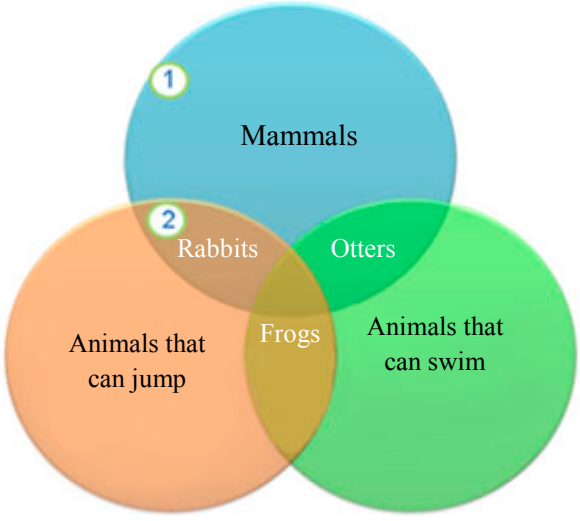

f)

Fig. 5. Examples of information presentation: timeline (*a*), causal chain (*b*),
inductive tower (*c*), affinity diagram (*d*), Ishikawa diagram (*e*), Venn diagram (*e*)

Units of knowledge in consciousness are structured in accordance with the channels of perception; they are constantly re-formed and form new relationships. Thought formations are created as a result of the interaction of units of knowledge and the surrounding reality. It is very important to rely on realistic and dynamic representations of research objects when solving complex problems. Under modeling, to present information about an object, you should use multimedia and virtual reality tools: photo, video, sound, animation (Gimp, Adobe Flash, HTML5, video players, etc.); three-dimensional representations (VRML. Blender, etc.).

All forms of knowledge appear in the form of a network structure that functions using a propagating activation mechanism: Petri nets, semantic nets, House of Quality, hyperbolic trees, pyramids (Corel Draw, Inkscape, Excel, Word), data flow diagrams (Excel, Word, MS Visio, BPwin), visual tutorial (HTML, PHP), etc.

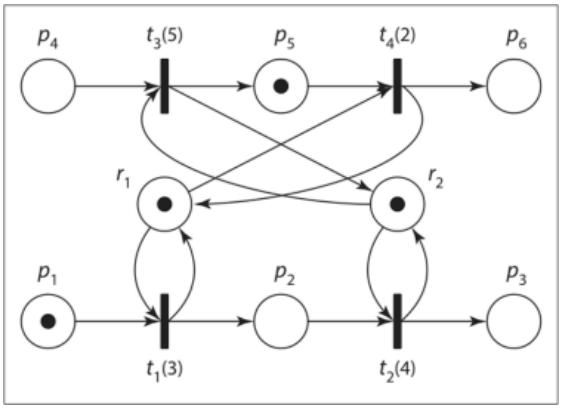

a)

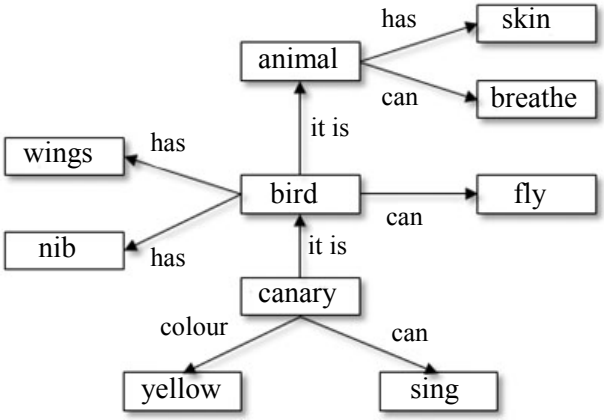

b)

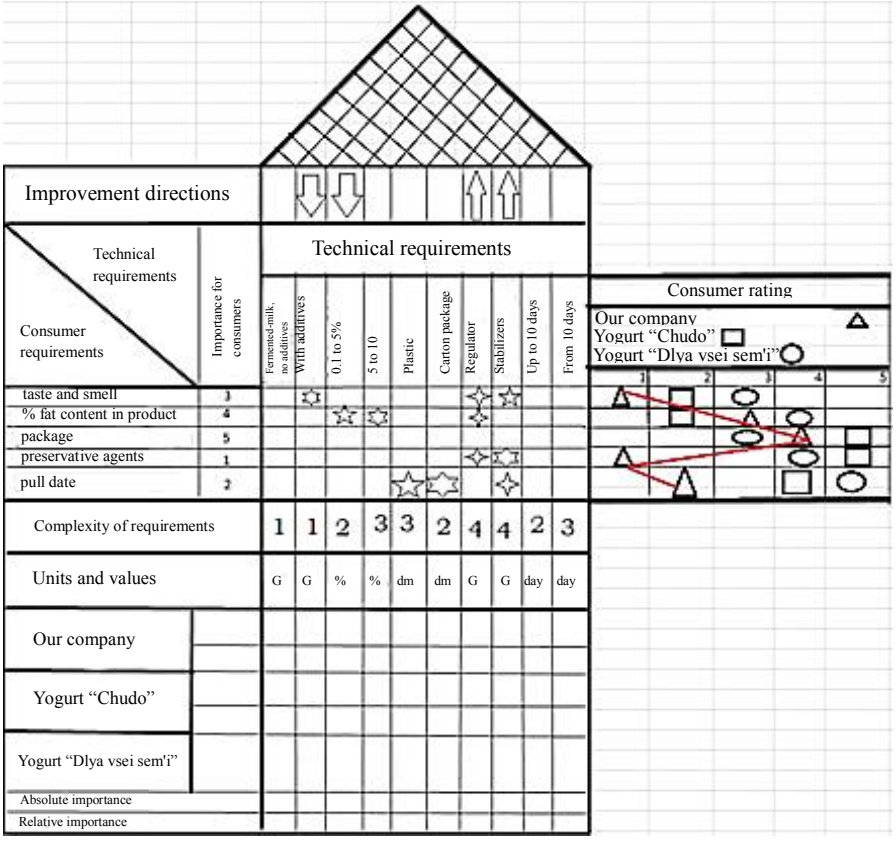

c)

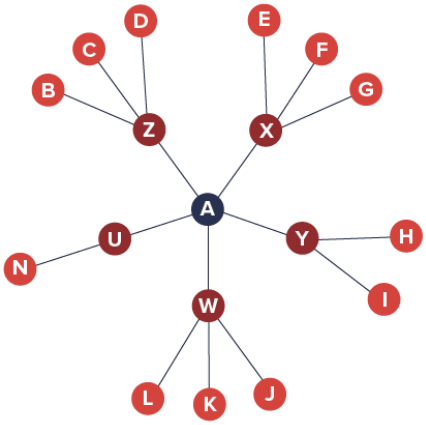

d)

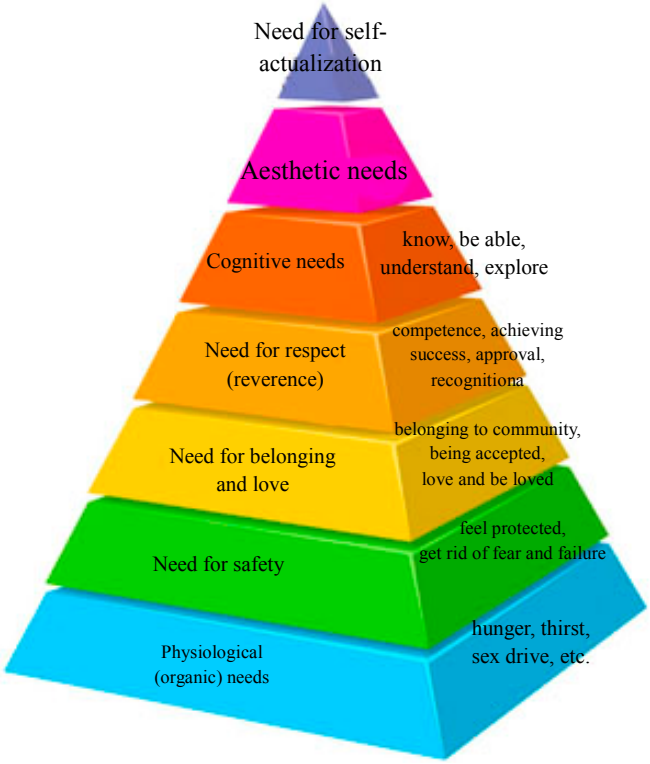

e)

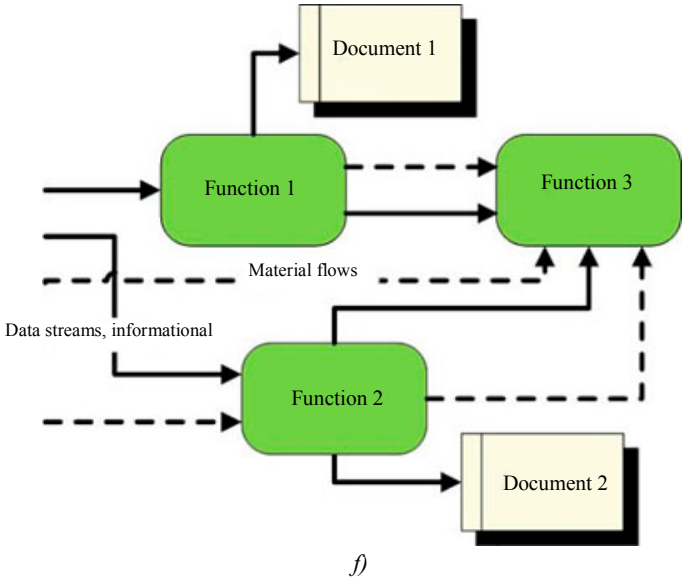

f)

Fig. 6. Examples of information presentation: Petri net (*a*), semantic net (*b*); House of Quality (*c*); hyperbolic tree (*d*), pyramid (*e*), data flow diagram (*f*)

The language of intelligence is the language of schemes, images, imprints of reality (tactile, olfactory), kinetic (motor) impulses. In this vein, decision and problem trees, life cycle and reasoning diagrams, data funnels are built (Corel Draw, Inkscape, Excel, Word), etc.

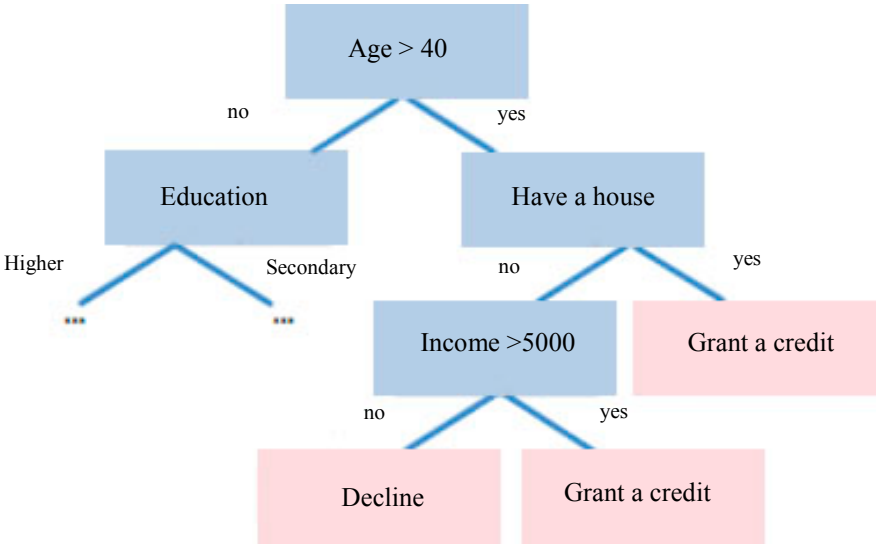

a)

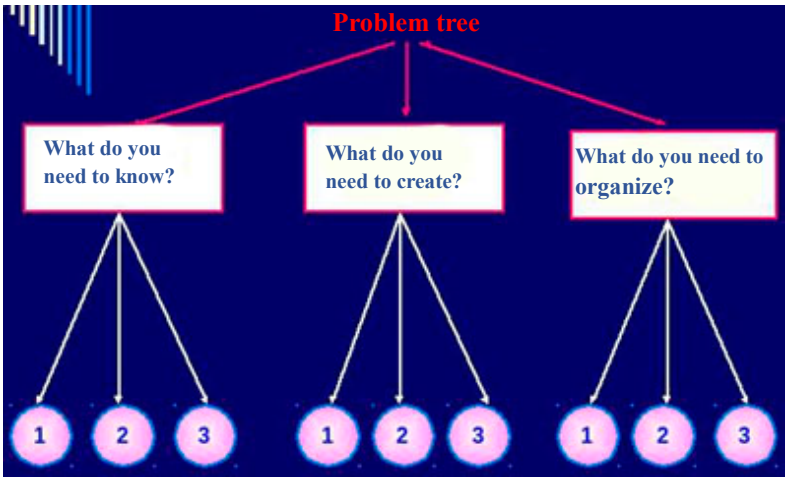

b)

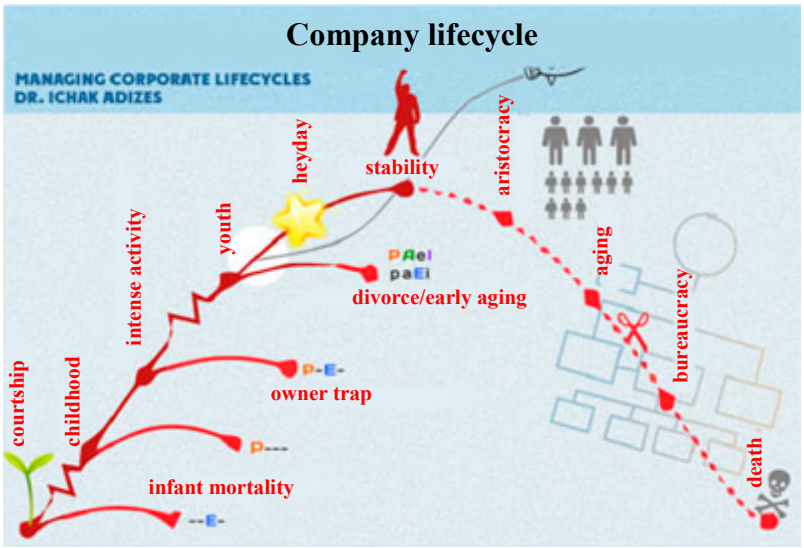

c)

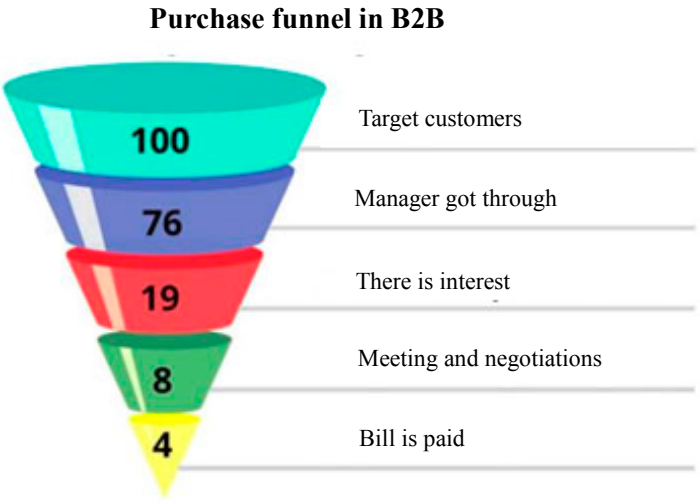

d)

e)

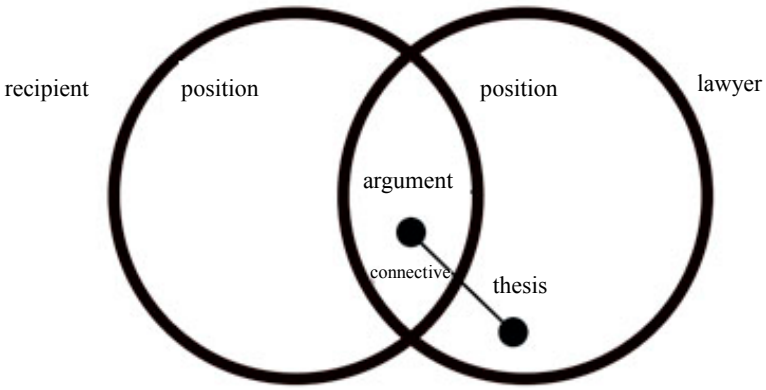

f)

Fig. 7. Examples of information presentation: decision tree (*a*), problem tree (*b*); lifecycle (*c*); funnel (*d*), argument-slide (*e*), argumentation (*f*)

So, the methods of graphical visualization of information, widely used in various subject domains, are based on scientific theses on the formation of primary knowledge, its connection and storage in human memory. These methods mediate the process of mental modeling. They help to create and save images, structure, relations, links of the studied object for modeling procedures on information medium. At the same time, it becomes possible to perform modeling actions not only individually, but also in a team using the experience of team members, which rationalizes the modeling process. At this, it is important to use software and services to create visualizations that will help in modeling research.

To increase the efficiency of modeling, graphic visualization methods adequate to the tasks, as well as IT-tools for data presentation are used: multimedia systems, computer visualization and decision support systems, expert systems, project management systems, cognitive modeling systems, simulation environments, computer games, agent-based modeling, etc.

Conclusion. The informational and logical aspects of modeling combine three key categories of cognition — information, representation, knowledge. Actions with models include search, selection, presentation and processing of available information on the object of research, on whose basis you can get new knowledge about it. For this, the means of information processes and technologies are used. Computer simulation plays a key role. Optimization is an essential function of the mental component of modeling as the fundamental basis for the model way of cognition. In mental modeling, an image is built on the basis of sensory perception, to which the operations of analysis, synthesis, comparison, abstraction, generalization, systematization, classification, and logical operations are applied. This provides transforming a sensory image into a logical model of cognition. Through mental modeling, a person first forms an information model of the object of research, and then studies it by constructing a number of interrelated mental representations and the corresponding information models.

The application of computer tools for presenting information enables to optimize mental activity. At the same time, various parameters and links of the studied object are visualized. Modern computer simulation tools complement, extend, and modify traditional simulation tools.

References

1. Yadrovskaya MV. Modeli i modelirovanie v pedagogike [Models and modeling in pedagogy]. Rostov-on-Don: DSTU Publ. House; 2014. 359 p. (In Russ.)
2. Glinskii BA. Filosofskie i sotsial'nye problemy informatiki [Philosophical and social problems of computer science]. Moscow: Nauka; 1990. 108 p. (In Russ.)
3. Filatov OK. Osnovnye podkhody k postroeniyu informatsionnoi modeli protsessa obucheniya [Basic approaches to building an information model of the learning process]. Informatika i obrazovanie. 2007;6:3−7. (In Russ.)
4. Beshenkov SA, Rakitina EA. Informatika. Sistematicheskii kurs [Informatics. Systematic course]. Moscow: Laboratoriya bazovykh znanii; 2001. 432 p. (In Russ.)
5. Yadrovskaya MV. Sredstva modelirovaniya v obuchenii [The means of modeling in education]. Vestnik of North-Eastern Federal University. 2010;7(1):89–95. (In Russ.)
6. Arkhangel'skii SI. Lektsii po nauchnoi organizatsii uchebnogo protsessa v vysshei shkole [Lectures on the scientific organization of the educational process in university]. Moscow: Vysshaya shkola; 1976. 200 p. (In Russ.)
7. Solso R. Kognitivnaya psikhologiya [Cognitive psychology]. St.Petersburg: Piter; 2002. 592 p. (In Russ.)
8. Kolodina NI. Problemy ponimaniya i interpretatsii khudozhestvennogo teksta [Problems of understanding and interpretation of literary text]. Tambov: Izd-vo TGTU; 2002. 183 p. (In Russ.)
9. Krasnykh VV. Osnovy psikholingvistiki i teorii kommunikatsii [Fundamentals of Psycholinguistics and Communication Theory]. Moscow: Gnozis; 2001. 270 p. (In Russ.)
10. Kornievskaya SI. Nekotorye issledovaniya protsessov dostupa k slovu [Lexical access research]. Herald of TvSU. Philology. 2009;3:38–49. (In Russ.)

Submitted 18.05.2020
Scheduled in the issue 10.08.2020

About the Author:

Yadrovskaya, Marina V., associate professor of the Mass Communications and Multimedia Technologies Department, Don State Technical University (1, Gagarin sq., Rostov-on-Don, 344003, RF) Cand.Sci. (Phys.-Math.), associate professor, ORCID: https://orcid.org/0000-0002-4469-1603 , marinayadrovskaia@rambler.ru

The author has read and approved the final manuscript.